Master's thesis

NTNU
Norwegian University of Science and Technology
Faculty of Natural Sciences
Department of Materials Science and Engineering

Sigurd Johannes Slåtsve Øvrelid

Carbides in Manganese Furnaces

Master's thesis in Materials Science and Engineering
Supervisor: Merete Tangstad, IMA & Eli Ringdalen, SINTEF
June 2019

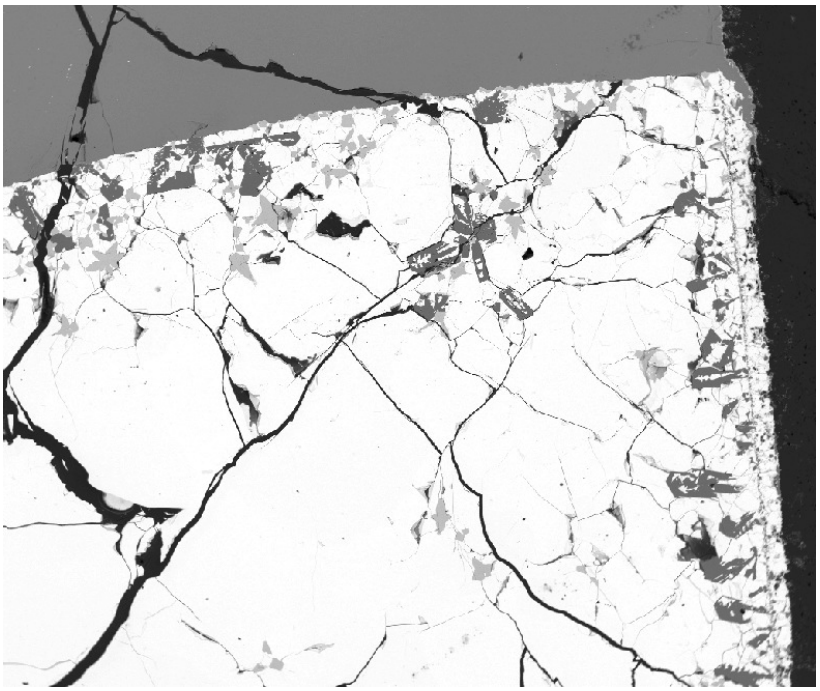

NTNU
Kunnskap for en bedre verden

Sigurd Johannes Slåtsve Øvrelid

Carbides in Manganese Furnaces

Master's thesis in Materials Science and Engineering
Supervisor: Merete Tangstad, IMA & Eli Ringdalen, SINTEF
June 2019

Norwegian University of Science and Technology
Faculty of Natural Sciences
Department of Materials Science and Engineering

NTNU
Norwegian University of
Science and Technology

Declaration

I hereby declare that this work has been carried out independently and in compliance with the examination regulations of the Norwegian University of Science and Technology, NTNU

Sigurd Johannes Slåtsve Øvrelid

Trondheim, June 2019

Preface

This thesis describes an investigation on the formation of carbides in the silicomanganese production process. The work is the master thesis of the author, and a basis for evaluation in the course TMT4920 at the Norwegian University of Science and Technology, NTNU. The work has been based on a collaboration between NTNU, Eramet Norway AS, and SINTEF, and was a part of the Controlled Tapping project.

I would first of all give my gratitude to my supervisor, Professor Merete Tangstad for allowing me to work on this project. Merete has included me in the SiManTi group and guided me with useful inputs on presentations of my project work.

An equally large thanks goes to my co-supervisor, Dr. Eli Ringdalen (SINTEF) for useful comments and ideas throughout the project. I was also included on an excavation at Eramet Kvinesdal which gave me a lot of insight in the world of manganese production, this was much appreciated.

I would also like to thank Ivar Ødegård and PhD students Arman Kermani and Didier Ngoy for help with furnace operation, Morten Raanes for the assistance with EPMA analyses and Jonas Einan for help with necessary equipment. A sincere gratitude also goes to everyone in the Controlled Tapping project and SiManTi group for social and technical support.

At last I would like to thank my fellow students at IMA for inputs on my work and social support.

Abstract

When carbon is dissolved in the silicomanganese process it can form titanium carbide, silicon carbide and graphite in the furnace. The silicon content in the alloy decides whether silicon carbide or graphite will be the stable carbon containing phase. It will also affect the solubility of carbon in the alloy. Little work is published on the formation of titanium carbide in the SiMn process. This thesis examines the formation of carbides through the reaction between slag, metal and dissolved carbon. The goal of this project was to investigate the possible origins of the carbides found in submerged arc furnaces producing silicomanganese alloys. This was done by reproducing the mechanisms of SiMn production carried out through melting experiments in a vertical tube furnace. Two types of SiMn alloy was obtained from the industry with c. 19.66 wt.% Si and 29.44 wt.% Si, named Metal 1 and 2 in the thesis. Three types of synthetic slag, Slag 1, 2 and 3 were used, containing no titanium, 1wt% TiO_2 and 10wt.% TiO_2, respectively. The produced samples were studied by EPMA to give chemical composition and structure of the phases present in the samples.

The effect of four variables in the melting experiments were investigated:

1) The effect of silicon content in the alloy

   In the experiments conducted with Std-SiMn alloy containing 20wt.% Si, SiC was observed in 2/10 experiments analyzed. In the experiments conducted with LC-SiMn alloy containing 29wt.% Si, SiC was observed in 8/9 experiments analyzed.

   When increasing the Si content in the alloy, less TiC will accumulate.

2) The effect of titanium content in the slag

   When using a slag with no TiO_2, no TiC was observed in the samples. Using a slag with higher % Ti will result in more TiC.

   When using a slag with 1wt.% TiO_2, TiC was only observed on the crucible interface and on the slag-metal interface. The crucible had to be in contact with both slag and metal to form TiC. The TiC seems to have been mostly formed by a direct reaction between dissolved carbon and dissolved TiO_2.

By increasing the TiO_2 content in the slag to 10wt.% the TiC was observed to have accumulated on the crucible interface, on the slag-metal interface and in the bulk of the slag. The TiC did not have to be in contact with both slag and metal. TiC was observed in with only graphite and slag as well as only metal and slag. The TiC seems to have been formed by a direct reaction between dissolved carbon and dissolved TiO_2.

With increased Ti content it was observed that less SiC would accumulate, and in some cases not at all. At higher Ti contents (10wt.% TiO_2 in the slag) most samples were observed to not have accumulated any SiC, or relatively small amounts.

3) The effect of temperature

Increasing the temperature will result in more carbides being precipitated by cooling in the bulk of the metal, due to increased carbon solubility at higher temperatures. Increasing the temperature will also encourage the formation of SiC as opposed to graphite, due to the increased carbon solubility.

4) The effect of hold time

The effect of hold time on TiC formation seemed to be trivial. Some increase in particle size was observed. No effect of hold time on SiC formation was observed.

From the results, formation through the graphite-slag (solid-liquid) reaction and formation through slag-metal (liquid-liquid) seemed to be the biggest contributor to TiC accumulation. Silicon saturation of the metal phase, precipitating SiC as the alloy cools, seemed to be the case for SiC formation.

Sammendrag

Når karbon løses opp i silikomangan (SiMn)-prosessen kan det dannes titankarbid (TiC), silisiumkarbid (SiC) eller grafitt i ovnen. Silisiuminnholdet i legeringen avgjør om silisiumkarbid eller grafitt vil være den stabile karbidholdige fasen. Dette vil også påvirke løseligheten av karbon i legeringen. Lite arbeid har blitt publisert på dannelsen av titankarbid i SiMn-prosessen. Denne oppgaven omhandler undersøkelse av karbiddannelse gjennom reaksjoner mellom slagg, metall og oppløst karbon fra grafittdigel.

Målet med dette arbeidet har vært å undersøke mulige opprinnelser til karbider som blir dannet i silikomanganprosessen. Dette ble gjort ved å reprodusere mekanismene i SiMn-produksjonen, utført ved smelteforsøk i en rørovn. To typer SiMn legering fra industrien har blitt brukt i smelteforsøkene, en med c. 19,66 vekt% Si og en med c. 29,44 vekt% Si. Tre syntetiske slagger ble anvendt, som inneholdt henholdsvis: 0 vekt% TiO_2, 1 vekt% TiO_2 og 10 vekt% TiO_2. De produserte prøvene ble studert ved hjelp av mikrosonde for å gi kjemisk sammensetning og struktur av fasene tilstede i de avkjølte prøvene.

Effekten av fire variabler i smelteforsøkene ble undersøkt:

1) Effekten av silisiuminnhold i legeringen

   I forsøkene utført med standard-SiMn legering, som inneholdt c. 19,66 vekt% Si, ble SiC observert i 2/10 eksperimenter analysert. I forsøkene utført med lav karbon-SiMn legering, som inneholdt c. 29,44 vekt% Si, ble SiC observert i 8/9 eksperimenter analysert.

   Når Si-innholdet økes i legeringen, vil mindre TiC akkumulere.

2) Effekten av titaninnhold i slaggen

   Ved bruk av slagg uten TiO_2 ble det ikke observert noe TiC i prøvene. Ved å bruke slagg med høyere% Ti, vil det resultere i mer TiC.

   Ved bruk av slagg med 1wt% TiO_2 ble TiC bare observert på grenseflaten til digelen og på grenseflaten mellom slagg og metall. Digelen måtte være i kontakt med både slagg og metall for å danne TiC. TiC syntes å ha hovedsakelig vært dannet av en direkte reaksjon mellom oppløst karbon og oppløst TiO_2.

Ved å øke TiO_2-innholdet i slaggen til 10 vekt% ble TiC observert å ha akkumulert på digelgrenseflaten, på slagg-metallgrenseflaten og i hoveddelen av slaggen. TiC måtte ikke være i kontakt med både slagg og metall. TiC ble observert i kontakt med bare grafitt og slagg, og i kontakt med bare metall og slagg. TiC synes å ha blitt dannet ved en direkte reaksjon mellom oppløst karbon og oppløst TiO_2.

Med økt Ti-innhold ble det observert at mindre SiC vil akkumulere, og i noen tilfeller ikke i det hele tatt. Ved høyere Ti-innhold (10 vekt% TiO_2 i slaggen) ble det observert at det ikke har akkumulert noen SiC eller relativt små mengder.

3) Effekten av temperatur

Økning av temperaturen vil resultere i at flere karbider blir utfelt ved avkjøling i hovedparten av metallet, dette på grunn av økt karbonoppløselighet ved høyere temperaturer. Ved å øke temperaturen vil dannelse av SiC i motsetning til grafitt fremmes, til på grunn av økt karbonoppløselighet.

4) Effekten av holdetid

Effekten av holdetid på TiC-formasjon synes å være lite viktig. En viss økning i partikkelstørrelse ble observert. Ingen effekt av holdetid på SiC-dannelse ble observert.

Resultatene viste at dannelse gjennom en reaksjon mellom grafitt-slagg (fast-væske) og dannelse gjennom slagg-metall (væske-væske) var den største bidragsyteren til akkumulering av TiC. Silisiummetning av metallfasen, hvor utfelling av SiC skjer når legeringen avkjøles virket å være tilfellet for SiC-dannelse.

Table of contents

1. Introduction

Silicomanganese (SiMn) alloys are produced by carbothermic reduction of oxide ores in submerged arc furnaces. The predominant method of producing standard SiMn is the simultaneous reduction of Manganese (Mn)-oxides and Silicon dioxide (SiO_2) in a blend of high-carbon ferromanganese (HC-FeMn) slag, Mn ores, quartzite and coke. Fluxes, such as dolomite and limestone are added to adjust the properties of the slag. Through the raw materials, contaminants such as titanium can be introduced.

The process temperature is dependent on the desired silicon content of the produced alloy. The limit of Si-content in standard SiMn achieved by carbothermic reduction of manganese oxides seems to be c.20%. SiO_2 is a far more stable oxide than MnO and process temperatures of 1600°C to 1650°C is needed to produce alloys containing 20% Si and at the same time discarding slag low in MnO [1]. As the carbon solubility is strongly dependent on temperature, this high temperature will cause the metal to contain more carbon than it can hold at temperatures closer to the liquidus temperature. When the metal cools, either due to tapping or by entering inactive zones of the furnace, the carbon solubility will decrease, causing considerable amounts of carbides to precipitate.

In recent years significant amounts of titanium carbide (TiC) has been observed during excavations of manganese furnaces in Norway and is believed to be caused by a buildup of Ti introduced through the raw materials. Excavations of industrial furnaces has been a valuable tool for understanding the distribution of different reaction zones and materials. From previous excavations at Eramet and Glencore, carbides have been observed: below the metal zone in the bottom of the furnace [2], SiC was observed on top of the coke bed below an electrode, in the slag [3], TiC was observed on the outer wall and in the lower part of the center of the furnace [4,5], SiC and TiC was observed around the tap holes and in the coke bed [6].

Carbides are undesirable in the production process, where an accumulation of carbides will clog and reduce the volume available for reduction in the furnace and reduce the overall efficiency of the furnace [5]. Operation has been observed to become unstable as carbides build up in the furnace [7]. To control the formation of carbides it is important to understand how it is formed and what influences the formation.

Several reports on SiC formation in the SiMn production process is available online. Davidsen [8] found that SiC can form in the reaction between silicon and dissolved carbon in an Mn-Fe-Si-C alloy. Einan [9] observed that that the SiC particle grain size increases after the solution has been exposed to

increasing number of cycles. Nordbø [10] studied SiC formation in liquid silicon in contact with graphite subjected to temperature cycles. Nordbø concluded that the initial layer of SiC is formed mostly by the direct reaction between silicon and carbon and will inhibit the formation of additional SiC from both precipitation and direct reaction. However, little work has been carried out regarding the origin and formation of both SiC and TiC in the manganese furnaces and how they will affect each other.

This work will investigate the formation of both SiC and TiC in liquid Mn-Fe-Si-C alloy and liquid MnO-SiO_2-CaO-Al_2O_3-MgO slag in contact with graphite. The main objective will be to investigate how the type, amount and appearance of carbides that are formed in the silicomanganese production process are affected by the following parameters:

- Si content in the metal
- TiO_2 content in the slag
- Temperature
- Hold time

Some consideration will also be put into the determination whether carbides are present as solid phase with liquid metal or whether they are formed during cooling. Relative shape, size and location of the carbides will also be determined.

2. Theory and literature

2.1 Silicomanganese production

The two main manganese alloys are ferromanganese (FeMn) and silicomanganese (SiMn). There are several ways to produce SiMn. In Norway, the standard industrial production process involves simultaneous carbothermic reduction of oxidic raw materials in a blend of manganese ores, quartz, coke and fluxes. Coke is the typical source of carbon, used both as a reducing agent, as well as electrical resistance. SiO_2 is used as a source of Si in the form of quartz [1].

Standard silicomanganese is often integrated with the manufacture of HC FeMn, where Mn-rich slag from the FeMn-process is used as a source of manganese in the production of SiMn. Manganese ores contain contaminants that can't be removed before they enter the production process, while the slag from the HC FeMn process is a purer source of manganese, as many contaminants already have been reduced into the metal during the production of HC FeMn [1].

Besides manganese oxides, the manganese ores will normally contain SiO_2, Al_2O_3 and sometimes CaO. SiO_2 is reduced along with MnO. As SiO_2 is far more stable than MnO, process temperatures up to

1600-1650 °C is needed to produce an alloy with c. 20% Si; while simultaneously discarding slag with lower amounts of MnO [1].

Silicomanganese is generally produced in a three-phase submerged arc furnaces (SAF) as presented in Figure 1. The furnaces are often circular with three electrodes in an equilateral triangle arrangement. The energy requirement is supplied through the electrodes, generate heat in the charge and from the C that is necessary for the reduction. Current production plants mostly use sealed, stationary furnaces with a load between 20-45 MW [1].

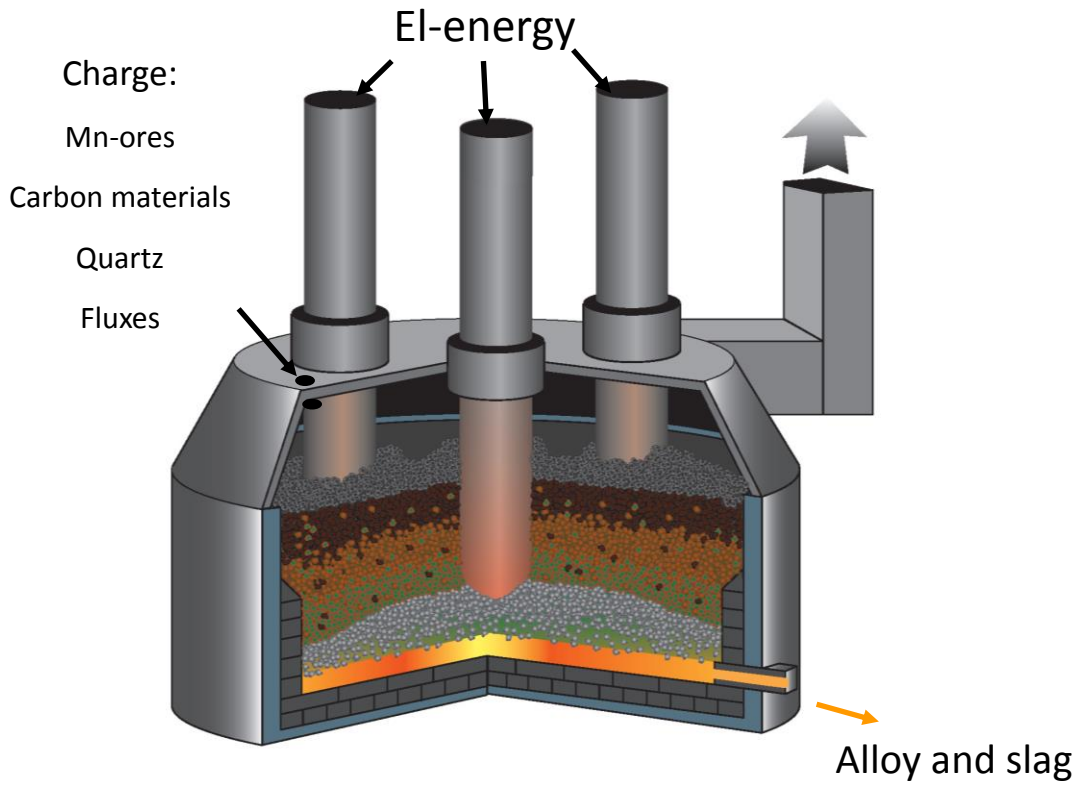

Figure 1: Schematic drawing of a closed three-phase submerged arc furnace. Reprinted from presentation by Ringdalen, E and Ksiazek, M [5]

The interior of the furnace is formed naturally but can be looked upon as two zones for the sake of convenience. The first zone is a pre-heating and pre-reduction zone where all the charge components are still solid, and the reduction takes place by gas-solid reactions. The second area is the cokebed zone where the raw material such as ore, slag and fluxes are molten, not including coke. When the metal is reduced, the metal drains down through the cokebed to the bottom of the furnace, creating a separate metal layer.

The initial slag is formed on top of the cokebed, and the reduction of the Mn-sources and melting of fluxes is started. When the viscosity of the slag is sufficiently low it will drain down into the cokebed where the final reduction of MnO and SiO_2 takes place.

The distribution of silicon and manganese between carbon-saturated Mn-Fe-Si-C alloys and Mn-Si-Ca-Al-Mg-O slags in equilibrium with CO gas is a result of simultaneous reactions taking place. The process temperatures may reach 1600°C or higher. The equilibrium composition between the slag and the metal is the driving force for the reaction that takes place in the different parts of the furnace.

The reduction of Si and Mn in SiMn production follows a series of reduction steps, assuming equilibrium at the interfaces [1]:

$$(SiO_2) + 2C = \underline{Si} + 2CO_{(g)} \quad (2.1)$$

$$(SiO_2) + 2SiC = \underline{3Si} + 2CO_{(g)} \quad (2.2)$$

The reaction (Si+C=SiC) is usually shifted to the right as soon as the solubility limit of C in the melt is reached.

$$(MnO) + C = \underline{Mn} + CO_{(g)} \quad (2.3)$$

$$(SiO_2) + \underline{2Mn} = \underline{Si} + 2(MnO) \quad (2.4)$$

$$(SiO_2) + \underline{Si} = 2SiO_{(g)} \quad (2.5)$$

$$\underline{Mn} = Mn_{(g)} \quad (2.6)$$

The parentheses indicate the species that are present in the slag, while the underscore indicates species in the alloy. C is the carbon source, that dissolves in the metal or the slag.

The manganese and silicon transfer are expressed by reactions (2.1)/(2.2), (2.3) and (2.4), although the actual reduction path of SiO_2 and MnO is more complex.

The total pressure in the furnace is assumed to be 1 atm, where the main gas components in the SiMn process are $CO_{(g)}$ and $CO_{2(g)}$ but also contains $SiO_{(g)}$, $Mn_{(g)}$. Up to 1700°C the partial pressure from SiO and Mn are modest, so the CO pressure is quite close to unit [1].

At equilibrium the expected silicon content can be derived from equation (2.1) or (2.2), depending on whether graphite or SiC is the stable carbon containing phase. The equilibrium constant is dependent on the activity of silicon, the activity of the SiO_2 in the slag, the activity of carbon and the pressure of CO as presented in equation (2.9) and (2.10).

$$Graphite\ stable: \qquad K(T) = \frac{a_{Si} * p_{CO}^2}{a_{SiO_2} * a_C^2} \tag{2.9}$$

$$SiC\ stable: \qquad K(T) = \frac{a^3{}_{Si} * p_{CO}^2}{a_{SiO_2} * a_{SiC}^2} \tag{2.10}$$

If the carbon activity is considered unity and a total pressure of 1 atm (CO pressure is close to unity) the Si-content of the alloy can be derived from:

$$Graphite\ stable: \qquad a_{Si} = K(T) * a_{SiO_2} \tag{2.11}$$

$$SiC\ stable: \qquad a_{Si} = \sqrt[3]{K(T) * a_{SiO_2}} \tag{2.12}$$

Thus, the silicon content in an SiMn alloy, for both reactions, will only be dependent on the temperature K(T) and the activity of SiO_2. The activity coefficient of SiO_2 is dependent on other species in the slag and the activity coefficient of Si is dependent on other species in the alloy.

The silicon content in an SiMn alloy is temperature dependent as illustrated by equations (2.11) and (2.12). As the temperature increases, the Si content also increases. The effect of temperature on a SiMn alloy is presented in Figure 2. The alloy is an Mn-Si-C_{sat} alloy, in equilibrium with SiO_2-CaO-Al_2O_3-MnO slag with $^{CaO}/_{Al_2O_3}$= 4. The CO pressure is 1 atm.

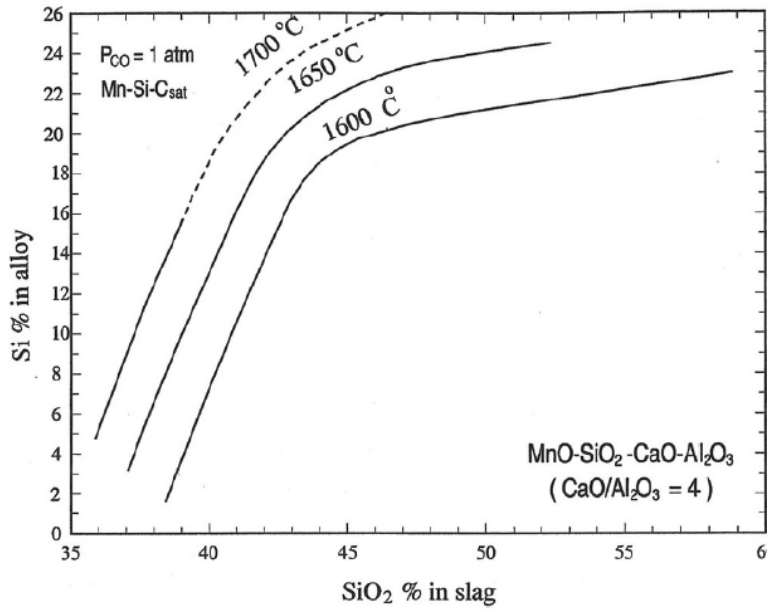

Figure 2: The effect of temperature on silicon content in an Mn-Si-C_{sat} alloy in equilibrium with a SiO_2-CaO-Al_2O_3-MnO slag [1]

The silicon content in the alloy increases fast with increasing SiO_2 in the slag up to about 18-20% Si. The slopes then follow a slow increase until silicon saturation is reached. The change in the slope is due to graphite being replaced by SiC as the stable carbon containing phase.

SiMn - alloys are usually distinguished by their silicon and carbon content. Standard SiMn contains about 1.5-2.0 wt.% C and 17-20 wt.% Si, while low carbon SiMn usually contains about 25-31 wt.% Si and carbon content ranging from 0.5% to 0.05% [1].

2.2 The Si-C system

Silicon carbide made by the Acheson process is one of the hardest materials on earth (about Mohs hardness 9.25), it is also chemically inert and does not melt [11]. SiC does however decompose at temperatures above c. 2800°C. In industrially produced SiC the main impurities are free C and SiO_2 in various degrees. SiC can also contain minor amounts of Al, Ca, N and Fe [12].

Depending on the stacking of the atomic layers, SiC can exist as many different polytypes, generally classified as either α-SiC phase or β-SiC phase. At temperatures above 2000°C the 3C (β-SiC) polymorph transforms to 6H (α-SiC) according to thermochemical data from JANAF [13]. In the SiMn production process, the β-SiC phase is assumed to be the stable polytype.

The Gibbse free energy for formation of SiC is given by [14]:

$$C + Si = SiC_{s,}, \Delta G^{\circ} = -122600 + 37T\ (J * mol^{-1}) \quad (2.13)$$

The binary Si-C phase diagram is given in Figure 3. The diagram is based on the work of Scace [15] and Dolloff [16].

The phase diagram based on the work of Scace and Dollof has gone trough many assessments. One of the latest was assessments was by Hoel [17]. It was determined that the work done by Scace was the most reliable; depicted in Figure 3 with solid lines. Scace suggested a liquidus temperature of 2834±40°C, while Dolloff suggested 2545±40°C.

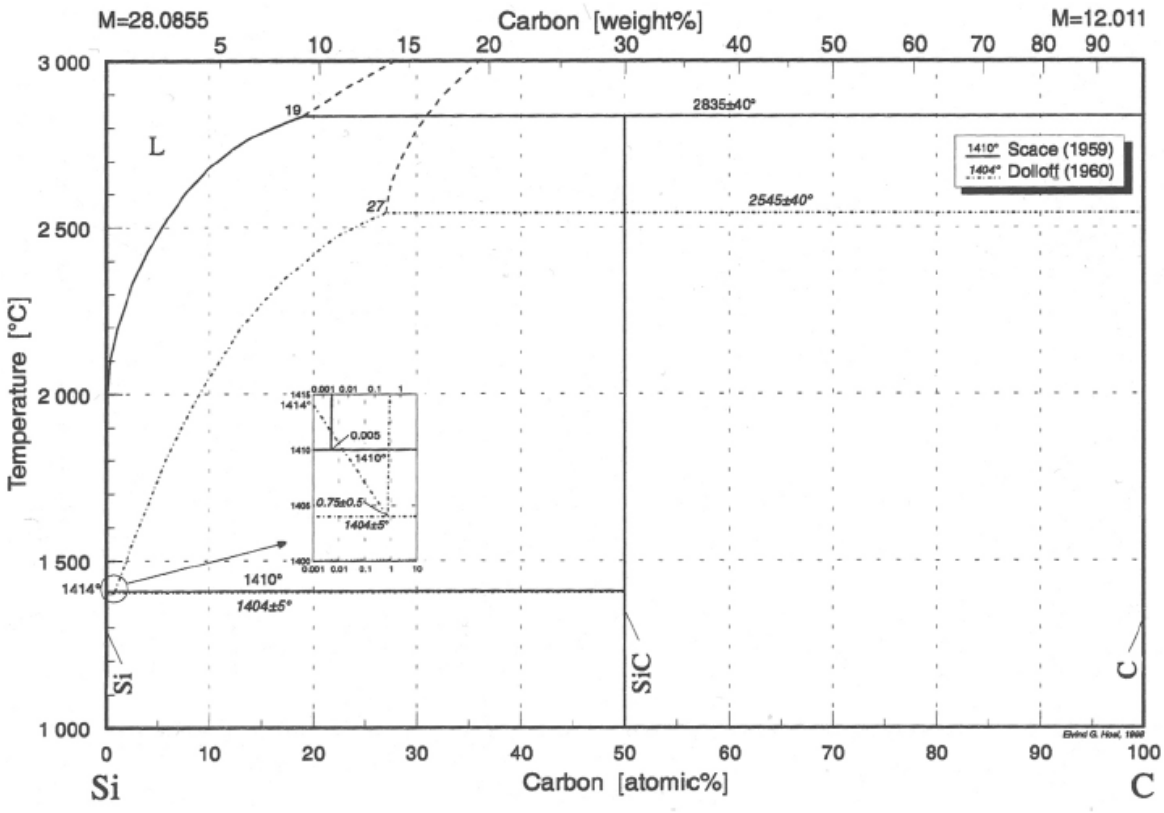

Figure 3: The binary Si-C equilibrium phase diagram. Figure is taken from Hoel [17]. Data from Scace and Dolloff [15,16]

Olsen et al. [1] reports that the maximum temperature in the SiMn process is in the area of 1600-1700°C, and thus only this part of the diagram is considered here. The diagram is a peritectic system where the only stable phases are Si, graphite and their intermediate compound SiC. The stoichiometric composition of SiC is 50 at.% C and 50 at.% Si (29.95 wt.% C and 70.05 wt. % Si). The solubility of carbon in silicon is low. Below 50 at.% C the system will mainly consist of solid or liquid Si and solid SiC, while above 50 at.% C the system will consist of solid SiC and graphite. The solubility of carbon in silicon is lower for the solid phase compared to the liquid phase, explaining why after solidification of a silicon solution saturated with carbon almost no carbon will be dissolved in the solid silicon. According to Figure 3 this will precipitate as SiC.

When pure silicon is heated into the liquid region of the Si-C phase diagram, carbon will dissolve into the liquid according to reaction (2.14).

$$C(s, graphite) = \underline{C} \tag{2.14}$$

And SiC is formed when the temperature is reduced according to the following reaction (2.15) [1].

$$Si_{(l)\beta} + \underline{C} = SiC_{(s)}, \quad \Delta G = 122\,600 - 37T \tag{2.15}$$

2.3 Thermodynamics and equilibria

2.3.1 The metal system Mn-Fe-Si-C

Commercial silicomanganese alloys can be described by the Mn-Fe-Si-C_{sat} system. Isothermal phase relations for a Mn7Fe-Si-C_{sat} alloy at 1550°C are shown in Figure 4 [1].

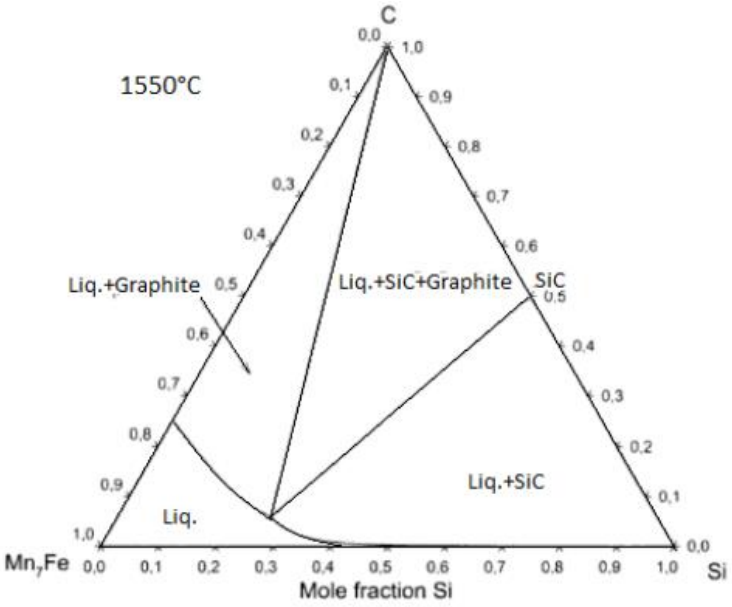

Figure 4: Calculated phase diagram showing an iso-thermal section of the Mn-Fe-Si-C system at 1550°C and Mn/Fe ratio = 7 [1].

For this alloy, graphite is the stable carbon containing phase coexisting with the liquid alloys until the silicon content exceeds approximately 16.5%. The solubility line in the phase diagram has also been calculated at both lower and higher temperatures by Tuset and Sandvik [18] as presented in Figure 5, and for different content of Mn by Tuset [18] and also Steenkamp [19]. The carbon solubility in Figure 5 was calculated for a Mn5.1Fe-Si-C_{sat} system.

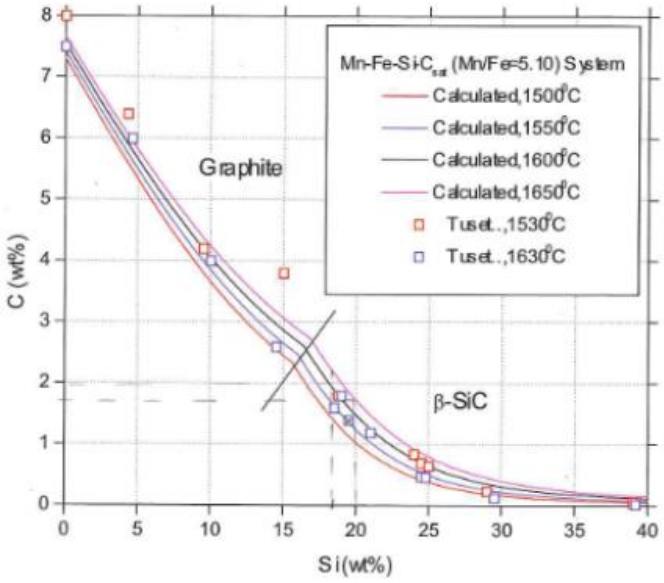

Figure 5: Calculated carbon solubility in Mn5.1Fe-Si-C_{sat} alloys. Measurements by Tuset and Sandvik, reprinted from Olsen et al. [1,18]

Tuset and Sandvik [18] found that the carbon content will increase with the temperature and the Mn/Fe ratio but decrease when the silicon content increases. When the silicon content increases from 0-20% the carbon content will rapidly decrease from 7% to 1.5%. Steenkamp found similar values, but slightly lower equilibrium content of Si and C. The silicon content will also increase with increased temperature as presented in Figure 6.

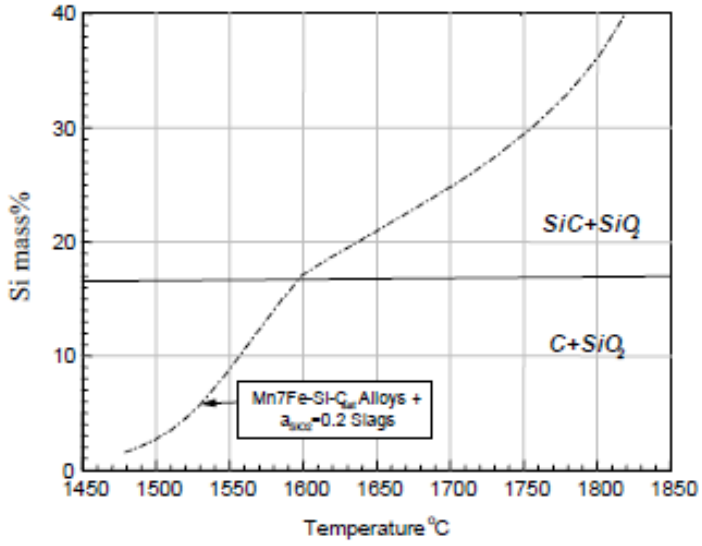

Figure 6: Temperature dependence of Si content in the alloy for a Mn7Fe-Si-C_{sat} alloy with activity of SiO_2 in the slag = 0.2 [1]

For the specific alloy in Figure 6, the Si content in the alloy will be about 16.5 wt.% at 1600°C when the stable carbon containing phase shifts from C to SiC. The Si content of the alloy increases at a higher rate until Si saturation is reached.

The calculated vertical system for standard SiMn alloys is presented in Figure 7 as a function of silicon content. The carbon content is 2% and iron content is 12%.

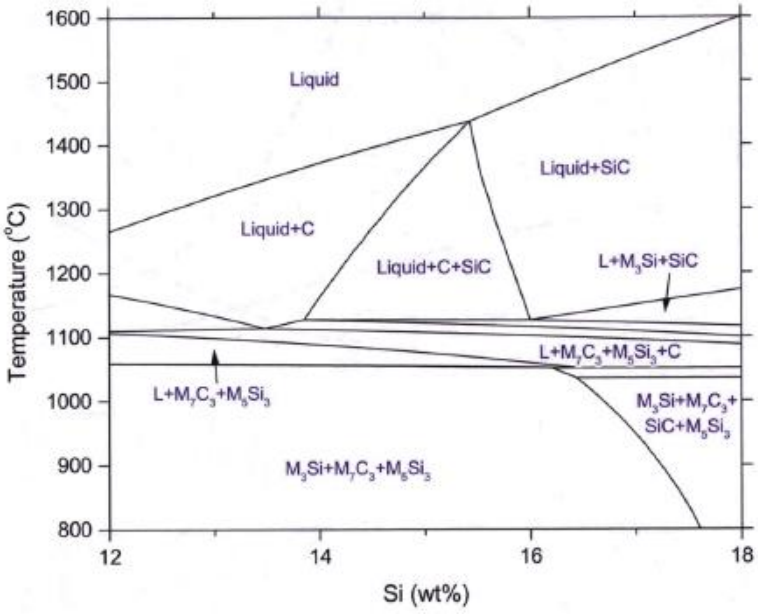

Figure 7: Calculated vertical section of the Mn-Fe-Si-C system at 2% C and 12% Fe as a function of Si content [1].

From Figure 7 it can be seen that a rapidly cooled alloy with >17.6 wt. % Si will result in $(Mn,Fe)_3Si$, $(Mn,Fe)_5Si_3$, $(Mn,Fe)_7C$, and SiC. Whereas alloys with less than 17.6 wt. % Si will result in $(Mn,Fe)_3Si$, $(Mn,Fe)_5Si_3$ and $(Mn,Fe)_7C_3$. The binary Mn-Si phase diagram determines that $(Mn,Fe)_3Si$ and $(Mn,Fe)_5Si_3$ will hold c. 14 wt% and 23 wt.% Si, respectively.

2.3.2 The slag system Mn-Si-Ca-Al-Mg-O

The main constituents of the SiMn slags are SiO_2, Al_2O_3, CaO, MgO and MnO. They are also the main oxide components in the raw materials for the production of SiMn. MnO and SiO_2 are partially reduced during the production process, whereas CaO, MgO, Al_2O_3 are regarded as unreducible and will go entirely to the slag phase. CaO, MgO, Al_2O_3 are added for the thermodynamic and physical properties they give to the slag phase [1]. A typical chemical composition of SiMn slags is presented in Table 1.

The calculated phase and liquidus relations for the MnO-CaO-SiO_2-Al_2O_3-MgO system is presented in Figure 8.

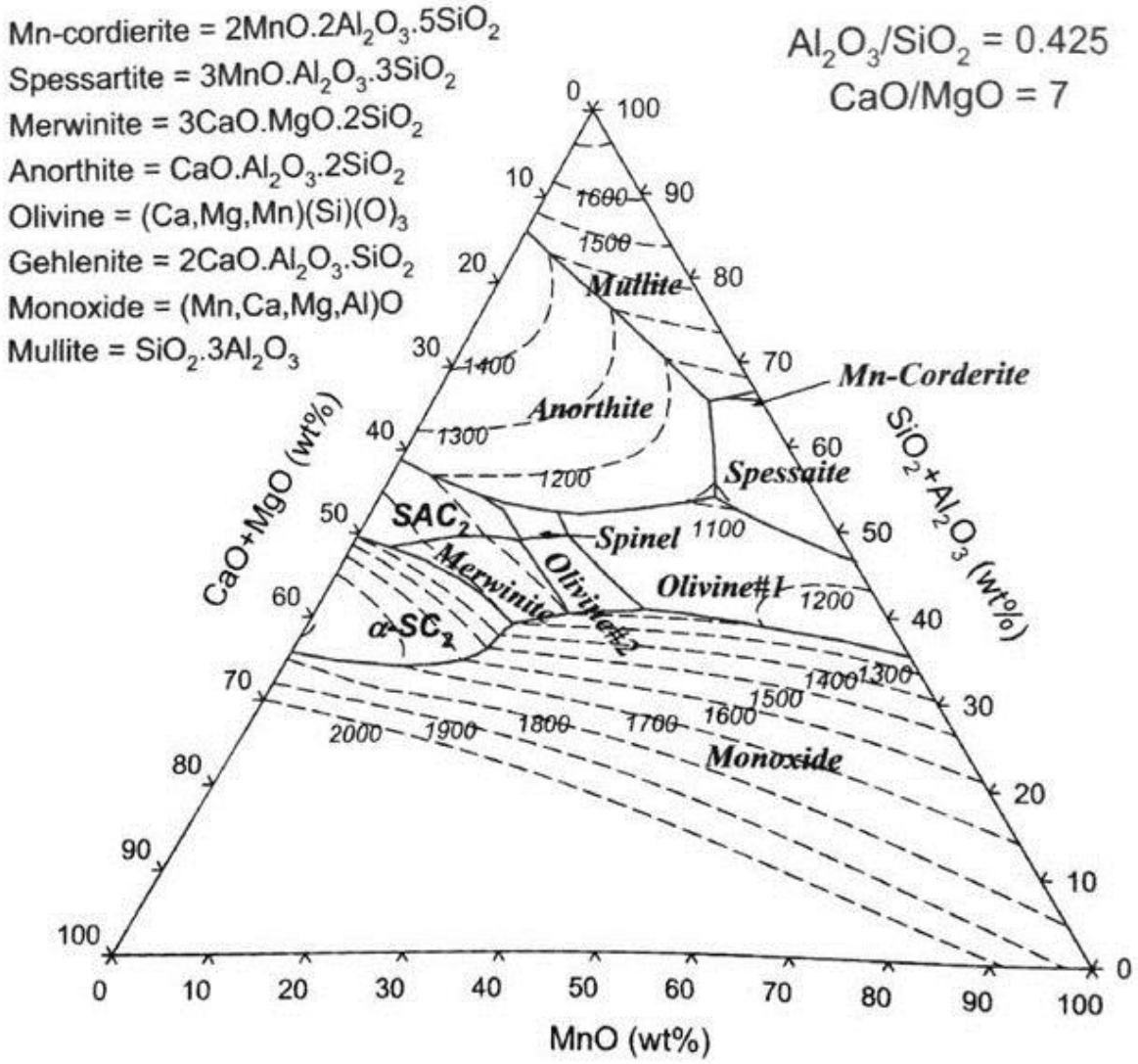

Figure 8: Calculated phase and liquidus relations for the MnO-SiO_2-CaO-Al_2O_3-MgO system [1]

SiMn slags containing for example c.10wt.% MnO, c.42wt.% SiO_2, c.17wt.% Al_2O_3, c.22wt.% CaO, 6.5wt.% MgO will have a melting temperature just above 1200°C, in the Anorthite area.

Table 1: Typical chemical composition of SiMn slags [1]

SiO_2 [wt%]	Al_2O_3 [wt%]	CaO [wt%]	MgO [wt%]	MnO [wt%]
20-35	10-25	38-44	5-15	6-12

Manganese slags are often described by the ratio between basic and acid slag constituents, the slags basicity:

$$B = \frac{CaO+MgO}{SiO_2+Al_2O_3} \tag{2.17}$$

The basicity of the slag determines the physical properties of the slag as well as the composition of the tapped metal and slag. MnO, CaO and MgO are basic oxides, whereas SiO_2 is the most important acidic oxide. The compositional ratio of these components will have an impact on the liquidus temperature of the slag. If about 6-12% of the CaO is substituted with MnO the liquidus temperature will decrease and liquid area will be extended. Replacing CaO with MgO however, will have the opposite effect. Increasing basicity ratio will also lead to an increase in liquidus temperature [1].

The SiMn slags can also be described by the R-ratio. The R-ratio does not take the SiO_2 and MnO into account, as they will be reduced out from the slag. This ratio will stay constant throughout the process as all the components are unreducible.

$$R = \frac{CaO+MgO}{Al_2O_3} \tag{2.18}$$

Similar oxides will affect each other by increasing the chemical activity while dissimilar oxides will affect each other by decreasing the chemical activity and lowering the melting point. Thus, in theory, increasing basicity will increase the activity of MnO in the slag, consequently reducing the activity of SiO_2.

Figure 9 shows how the amount of Si in the metal phase varies with the R-ratio.

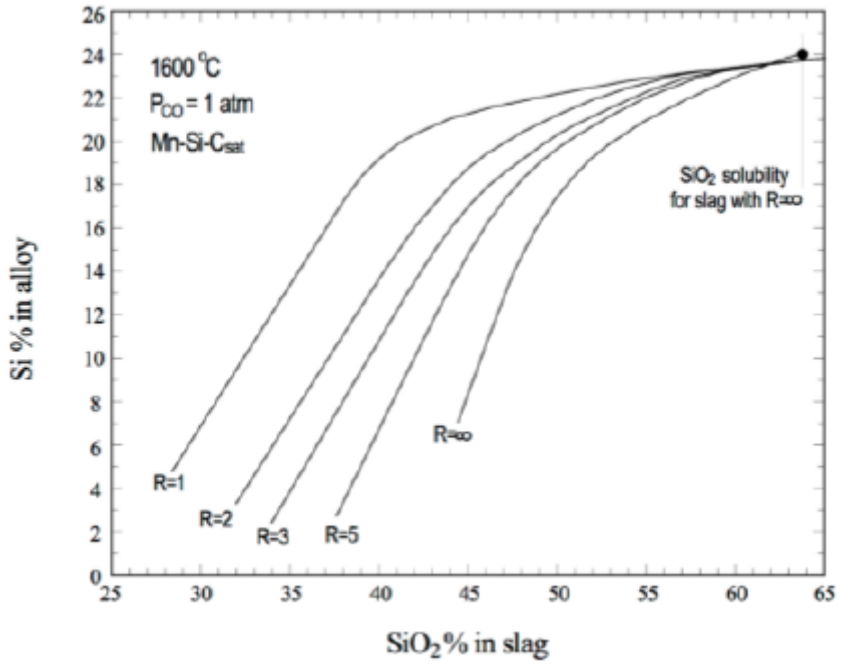

Figure 9: Distribution of Si in the metal phase as a function of SiO_2 in the slag with different R-ratios [1]

The amount of Si in the metal is observed to decrease with increasing R-ratio due to the increased content of basic oxides.

2.3.3 Mn-Fe-Si-C-Ti system

Little work has been presented on the titanium in the SiMn process. Phase relations in the Mn-Fe-Si-C-Ti alloys are the basis for understanding the TiC behavior in the silicomanganese production. In particular, this relates well to the carbon saturated alloys.

In order to define the TiC in the Mn-Fe-Si-C-Ti system, the Ti-C phase diagram is studied.

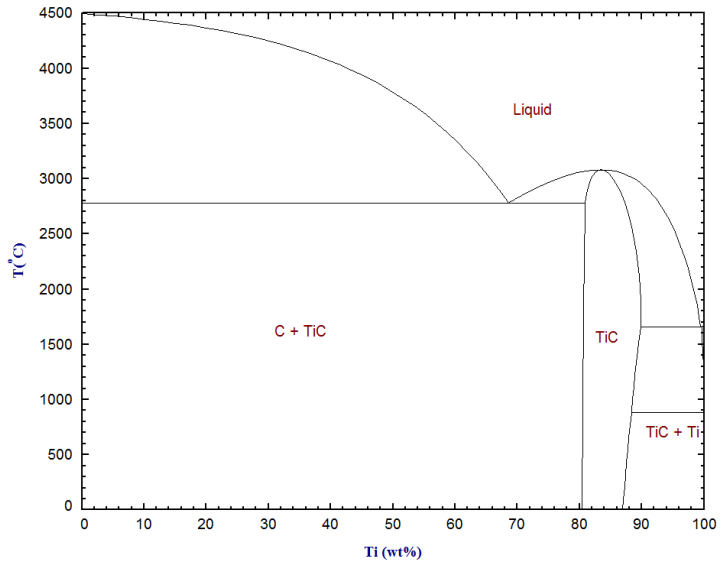

Figure 10: Ti-C phase diagram [20]

According to the Ti-C phase diagram presented in Figure 10, the titanium content in TiC varies from 80-88 wt.%.

In 2018 Tang reassessed the phase relationships in the Mn-Fe-Si-Ti-C system. He found that the calculations of the equilibrium phase relations fit industrial data well. Calculations were conducted using typical composition of 100kg Mn-ore, 20-40kg coke, and 35kg quartz [21].

The effect of temperature on the carbothermic reduction products is presented in Figure 11.

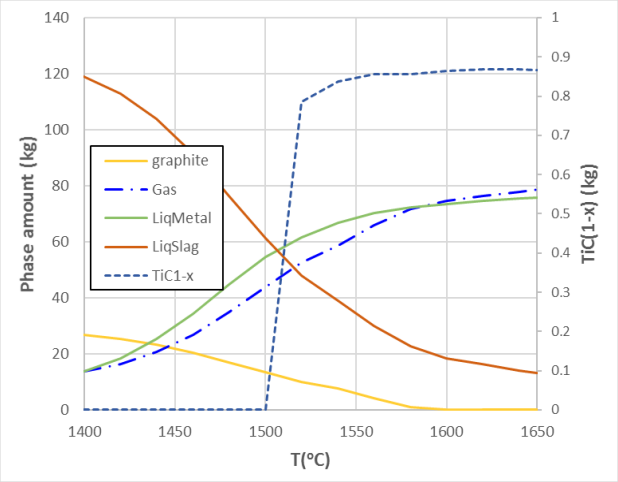

Figure 11: Effect of temperature on the carbothermic reduction products. Mix of c. 38kg coke, 35kg quartz, and 100kg Mn-ore [21]

From Figure 11 it can be seen that the TiC begins to form at 1500°C and sharply increases, then a gentle increase up to 1550°C, following the increase in the amount of metal. Further increase of the temperature will not increase the amount of TiC, indicating that the reduction of titanium oxides is finished at around 1550°C.

2.4 Carbide formation

Both TiC and SiC has previously been observed during excavations of SiMn furnaces. To better understand their behavior, some theory on TiC and SiC and their mechanisms of formation will be presented in this section.

2.4.1 Formation of SiC

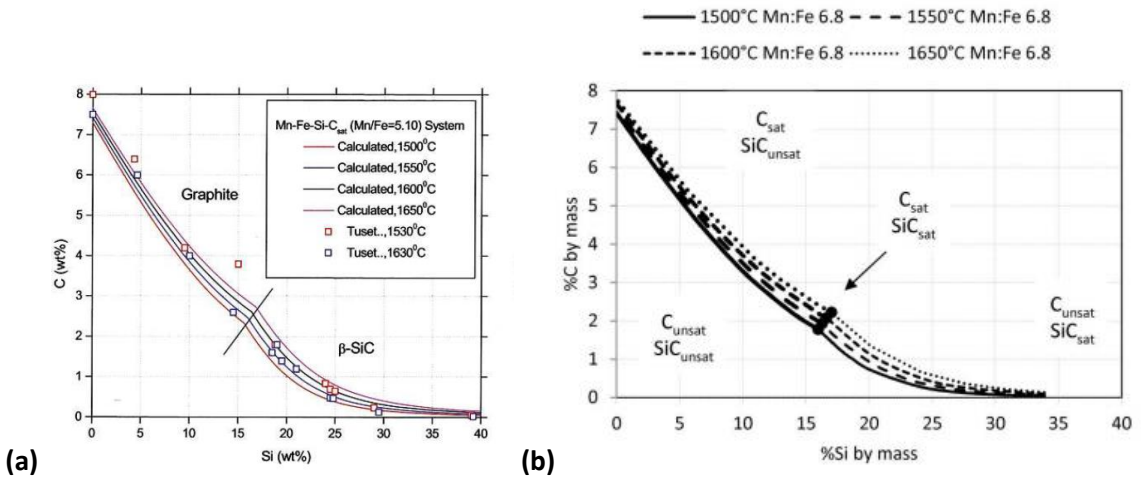

Figure 12: Calculated carbon solubility in a Mn-Fe-Si-C_{sat} alloy at 1 atm pressure with **(a)** fixed Mn/Fe ratio = 5.1 between 1500-1650°C. Measured carbon solubility by Tuset and Sandvik [18]. Reprinted from Olsen et al. [1] **(b)** fixed Mn/Fe ratio = 6.8 between 1500-1650°C, calculated in factsage [19]

The solubility lines in Figure 12 gives the equilibrium content of carbon in the liquid Mn-Fe-Si-C_{sat} alloy when SiC or graphite is present. The alloy is considered carbon saturated due to the presence of coke inside the furnace. The coexistence point is illustrated by the line between SiC and graphite in Figure 12, here both phases could be present. Above the coexistence point (in terms of Si content) SiC replaces graphite as the stable carbon containing phase.

Olsen et al. [1] found that by increasing the Mn/Fe ratio from 5.1 to 8, the solubility of Si and C increases in the vicinity of ~0.4%.

Gibb's phase rule can be utilized to analyze the multi-phase equilibria presented in Figure 12. The phase rule is defined in equation (2.19).

$$F = C - P + 2 - R \tag{2.19}$$

Where F denotes the degrees of freedom, C the number of components; in Figure 12 it is 3: Si, C Mn/Fe ratio (fixed). P denotes the number of phases; in Figure 12 it could be liquid metal, graphite and SiC. R denotes the number of independent restrictions, such as temperature and pressure, which is the case

for Figure 12; the lines indicate isothermal (1500, 1550, 1600, 1650) conditions and the system is isobaric (1 atm pressure). R is thus = 2.

By applying this phase rule to Figure 12, the number of phases present at certain conditions and the consequences thereof can be determined. At the coexistence point, when the alloy is double saturated: C = 3, P = 3 (SiC, graphite and liquid alloy), R = 2 and F = 0. There is no degree of freedom and for each temperature there is only one metal composition (fixed %C and %Si), the invariant point where SiC and C coexists.

When only C or SiC is present in the melt, the number of degrees of freedom is 2, and both the Si content and the C content can be varied independently with liquid metal as the only phase present meaning that if both C(s) and SiC is present at different C and Si compositions in the same sample on can assume that equilibrium is not reached.

Dissolved carbon will react with silicon in the liquid alloy or with slag with high SiO_2 content as presented in equations (2.19) and (2.20), respectively [1]. Reactions are presented assuming equilibrium.

$$C + Si = SiC_s \qquad \Delta G = -122\,600 + 37T \qquad [14] \tag{2.20}$$

$$C + (SiO_2) = SiC_s + 2CO_g \tag{2.21}$$

The reaction presented in (2.21) can be divided into two stages. The reduction of Si from the slag (2.22) followed by a reaction to form SiC (2.20):

$$(SiO_2) + 2C = \underline{Si} + 2CO_g \tag{2.22}$$

$$C + \underline{Si} = SiC_s \tag{2.20}$$

The temperature dependent equilibrium constant for equation (2.20) is dependent on the activity of SiC, Si and C as presented in equation (2.23).

$$K(t) = \frac{a_{SiC}}{a_{Si}a_c} \tag{2.23}$$

Below the coexisting point (equations 2.20) carbon activity will be at unity as long as the alloy is in equilibrium with pure carbon. The activity of C abow this point is given by equation (2.24)

$$a_{SiC} = K(t) * a_{Si} \tag{2.24}$$

The amount of silicon that can form SiC can be derived from equation (2.24). SiC is either present or it is not, the activity of SiC is thus 0 or 1. The wt. % Si can therefore be presented as a function of the

activity coefficient of silicon and the temperature dependent equilibrium constant as presented in equation (2.25).

$$wt.\%Si = \frac{K(T)}{\gamma_{Si}} \tag{2.25}$$

The formation of SiC is dependent on the activity coefficient of Si which is dependent on other pure elements in the SiMn melt. The formation of SiC is thus dependent on the slag composition, metal composition and temperature. When the dissolved carbon forms graphite the formation can be described by equation (2.26) and (2.27)

$$\underline{C} = C_{gr} \tag{2.26}$$

$$wt.\%C = \frac{\gamma_C}{K(t)} \tag{2.27}$$

The activity coefficient of carbon is dependent on other pure elements in the alloy such as Si, Mn and Fe [1].

2.4.2 Formation of TiC

Little work has been done on the formation of TiC in the SiMn production process, and the formation and effect of TiC build-ups are unclear. Titanium is considered an impurity in the SiMn process and is introduced through the raw materials. Since the Ti content in SiMn alloys is relatively low (<1wt%) [1] it is proposed that over time it is possible that a build-up of titanium reacting with dissolved carbon to form TiC could settle in the furnace.

$$Ti + C = TiC \qquad ,\Delta G^{\circ} = -185000 + 12.6T\ (J * mol^{-1}) \qquad [14] \tag{2.28}$$

When carbon is mixed with ores containing TiO_2 in the submerged arc furnace, a possible reaction is:

$$TiO_{2(s)} + 3C_{(s)} = TiC_{(s)} + 2CO \qquad ,\Delta G^{\circ} = 528937 - 337.23T\ (J * mol^{-1}) \tag{2.29}$$

TiO_2 in the slag could also dissolve in the metal phase and then react with the dissolved C following equations (2.30) and (2.31):

$$TiO_{2(s)} + 2C_{(s)} = Ti_{(s)} + 2CO \quad ,\Delta G^{\circ} = 170100 - 83.45T\ (J * mol^{-1}) \tag{2.30}$$

$$Ti + 2CO = TiC + CO_2 \tag{2.31}$$

Another proposed mechanism is that TiO_2 is reduced into the liquid metal. Carbon is dissolved in the alloy as the temperature is increased, and as the alloy cools TiC will precipitate, as the solubility decreases with the temperature [20].

According to the standard Gibbs free energy of reaction (2.28), TiC can be generated when the temperature is higher than 1192°C, which is lower than the real melting temperature of SiMn. From a thermodynamic perspective, the TiC is formed and will remain in the product [22], as also stated by Tang [21].

2.4.2 Equilibrium between SiC and TiC

The free energy of formation of SiC:

$$C + Si = SiC_{s,}, \Delta G^{\circ} = -122600 + 37T\ (J * mol^{-1}) \quad (2.32)$$

The free energy of formation of TiC:

$$Ti + C = TiC,\ \Delta G^{\circ} = -185000 + 12{,}6T\ (J * mol^{-1}) \quad (2.33)$$

The free energy of formation of TiC from SiC in system where both TiC and SiC coexists:

$$SiC + Ti = TiC + Si\ ,\ \Delta G^{\circ} = -62400 - 24.4\ (J * mol^{-1}) \quad (2.34)$$

Or 2.32-2.34 presented graphically (plotted in excel) :

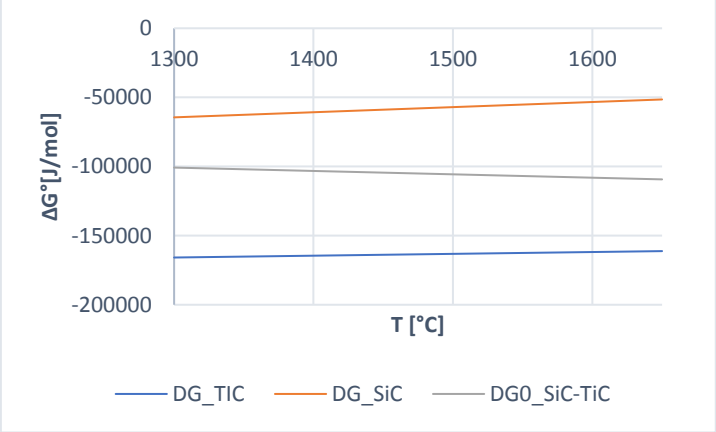

Figure 13: Gibb's energy for TiC, SiC and TiC-SiC as a function of T

We can see that for the same activity of respectively Si and Ti, TiC is more stable than SiC for the same C activity.

For the system with Si in the range of 18-26% and Ti in the range of 0.2-1.2%, we assume that the activity of Si is not affected by the Ti content and we can use the data from Li and Morris [23] evaluated by Steenkamp [19] for a similar slag metal system. The evaluation of activity data is given in Table 2 [19,23].

Table 2: Activity data [19, 23]

T(°C)	FACTSage 6.4				Li & Morris		
	aMn_FS	aSi_FS	aC_FS	aFe_FS	aMn_LM	aSi_LM	aC_LM
1550	0.202	0.042	0.757	0.03	0.172	0.031	0.685
1575	0.199	0.046	0.765	0.03	0.175	0.032	0.628
1600	0.197	0.051	0.773	0.03	0.178	0.033	0.576
1625	0.195	0.056	0.781	0.03	0.18	0.034	0.53

Activity data for Ti was not found neither for relevant slag nor alloy systems.

3. Experimental

To determine where and how carbides are formed in the SiMn process several experiments were carried out where slags and alloys were held together at different temperatures in a carbon crucible. Synthetic slag was first created, the synthetic slag and the metal obtained from the industry were then heated in graphite crucibles (along with a coke particle for some experiments) to see if carbides were formed. Three sets of slag and two types of industrial grade alloy were used. One slag was made according to a slag analysis from a previous project by Jens Davidsen [8] that received his slag from Eramet Kvinesdal. The other two slags were altered versions of the first slag, differing by the titanium content. The alloys were received from Eramet Kvinesdal, the main difference was different concentration of Si (c.20wt.% and c.29wt.% Si).

The synthetic slag was created using an induction furnace. The main constituents in a SiMn slag, CaO, MnO, MgO, Al_2O_3 and SiO_2, were mixed together in a graphite crucible and heated to about 40-50°C above the melting point. Parts of the slag was used for chemical analysis and the rest was used in the following melting experiments.

The main focus was given to slag-metal melting experiments conducted in a thermogravimetric furnace. Synthetic slag and alloy from the industry was heated together with coke and TiO_2 in graphite crucibles to investigate the formation of carbides. The mix is assumed to be carbon saturated.

The samples formed in the experiments were investigated by the use of EPMA. The carbides observed were compared with the carbides found from the industrial SiMn process and phase diagrams to find out which carbide phases are present in the system.

The following experimental work has been done during this project:

- Three synthetic slags were made (Slag: 1, 2 and 3)
- 20 experiments on slag-metal melting

- Sample preparation before analyses of the 20 experiments which included cutting with a diamond saw, epoxy casting, grounding of the surface, polishing of the sample surface and ultimately, the samples were coated with carbon
- EPMA analyses of 19 samples as well as the three original slags and the two industrial alloys
- XRF and Combustion-IR of coke particles, slag and metal used in the experiments
- Quantifications of the metal phase
- Mass balance

3.1 Materials

3.1.1 The slag

In order to create a slag similar to that from the production process of SiMn, the main constituents typically observed in these slags were used: SiO_2, CaO, MnO, MgO and Al_2O_3. TiO_2 was also added in two of the slags.

The oxides powder used to create the slag was delivered from VWR-international and Sigma-Aldrich. The particle size and purity of the oxides is displayed in Table 3.

Table 3: Particle size and purity of the chemicals used to create the slag

Chemical	**Particle size [mm]**	**Trace metals basis [%]**
SiO_2 (quartz)	<0.2-0.8	>99.9
CaO	<0.01	>99.95
MnO	<0.25	>99.5
MgO	<0.04	>99.5
Al_2O_3	<0.06	>99.5
TiO_2 (anatase)	<0.04	>99.8

3.1.2 The alloy

Two industrial grade SiMn alloys, SiMn-fines with c. 20 wt.% Si and LC SiMn-fines with c. 29 wt.% Si have been used for the experiments. These will be mentioned as “Metal 1” and “Metal 2” respectively, for the remainder of the thesis. The alloys were obtained from Eramet Kvinesdal. The alloys were analyzed by combustion-IR and XRF by SINTEF Molab; a chemical analysis of the respective alloys is presented in Table 4.

Table 4: Chemical analysis of metal 1, SiMn-fines and metal 2, LC SiMn-fines. Given in wt.%

Metal	Mn [%]	Fe [%]	Si [%]	P [%]	Ti [%]	Al [%]	S [%]	C [%]	Total
1	65.37	11.92	19.66	0.14	0.25	0.09	0.02	1.49	98.94

2	58.74	10.33	29.44	0.09	0.26	0.10	0.01	0.36	99.33

The alloys were also analyzed by Eramet, as displayed in Table 5.

Table 5: Chemical analysis of metal 1, SiMn-fines and metal 2, LC SiMn-fines. Given in wt.%. Analyzed by Eramet

Metal	Mn [%]	Fe [%]	Si [%]	P [%]	Ti [%]	Al [%]	S [%]	C [%]	Total
1	66.21	12.00	19.26	0.15	0.24	0.12	0.02	1.50	99.50
2	59.86	10.61	28.43	0.09	0.28	0.12	0.01	0.31	99.70

3.1.3 The coke

An arbitrary coke particle was used for some of the experiments. The origin of the coke is unknown, though is believed to be Polish coke. The composition of the coke is presented in Table 6.

Table 6: Chemical analysis of the coke used in some of the experiments, given in wt.%

Volatiles [wt.%]	Ash [wt.%]	FixC [wt.%]	Total [wt.%]
1.2	11.4	87.4	100

Table 7 gives the composition of the ash, given in weight percent. The exact amount of SiO_2 in the ash is not reported as it is removed prior to the analysis due to the method used, ICP-OES. The missing 52.4% from the analysis is mostly SiO_2 [24].

Table 7: Chemical composition of the ash found in the coke particles

Al_2O_3	Fe_2O_3	CaO	K_2O	TiO_2	MgO	Na_2O	P_2O_5	Total
29.0	8.6	3.9	1.4	1.4	1.3	1.1	0.9	47.6

Coke particles with a diameter of about 1.5-2.5 mm were chosen and dried at 105°C for a minimum of 24 hours to avoid moisture. Table 8 presents the size and shape coefficient of the coke particles used as well as their weight. The diameter of the coke particles was measured in four different directions. The closer the four values are, the rounder the coke particle. The roundness of the particles can be measured by a shape coefficient. An often used and simple way of determining the shape coefficient is to divide the minimum diameter with the maximum diameter [8, 25]. For a sphere the shape coefficient will be 1 and decreases as the roundness decreases.

Table 8: Weight, diameter and shape coefficient of the coke particles used. Coke particle number corresponds to which experiment it was used in. Only experiments 1, 1.2 and 2 included coke particles

Coke particle #	Weight [g]	D #1 [mm]	D #2 [mm]	D #3 [mm]	D #4 [mm]	Shape coeff.
1	7.81	1.5	1.7	1.8	1.4	0.78
1.2	3.42	2.1	2.5	2.0	2.3	0.8
2	3.20	1.9	2.35	1.6	2.4	0.67

3.1.4 Graphite crucibles

Graphite crucibles have been used to contain the samples during the experiments. The crucibles are also a source of carbon, for the formation of carbides. A sketch of the crucible used for the experiments is presented in Figure 14. To ensure free gas flow in and out of the crucible, three holes are drilled in the lid.

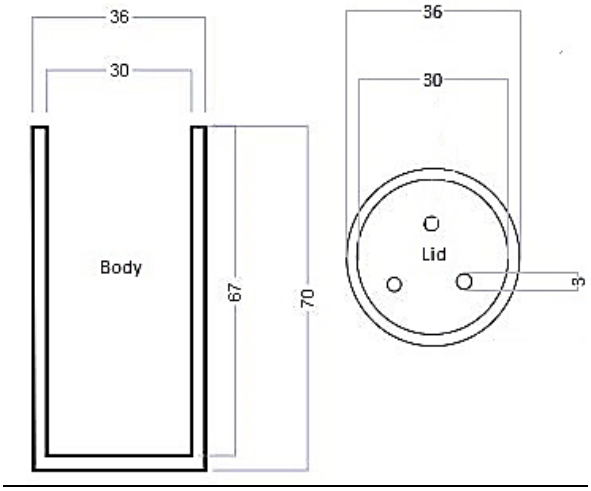

Figure 14: Technical sketch with dimensions of the graphite crucibles used in the melting experiments

The graphite crucibles are mounted in the thermogravimetric furnace by a Mo-wire. The Mo-wire is made based on the temperature profile as presented in section 3.3.

3.2 Equipment

The most central equipment used in this project are the induction furnace, the thermogravimetric furnace and the electron probe micro-analyzer. The induction furnace was used to prepare the synthetic slags. The thermogravimetric furnace was used in the slag/metal melting experiments. The electron probe micro-analyzer was used to investigate and analyze the samples produced from the experiments.

3.2.1 Induction furnace

The furnace used to produce the slag is an electrical furnace where the heat is applied by induction heating of metal, also known as an induction furnace. The furnace can handle temperatures up to 1750°C with a max power output of 7.5kW. The temperature is measured by a thermocouple connection inside the furnace and is controlled manually by increasing and decreasing the power output. The atmosphere inside the furnace is also controlled manually, where either argon or other inert gas must be used. Some CO gas must also be assumed present, coming from the trace oxygen reacting with the graphite crucible. A schematic of the furnace is illustrated in Figure 15, showing the furnace and its control system.

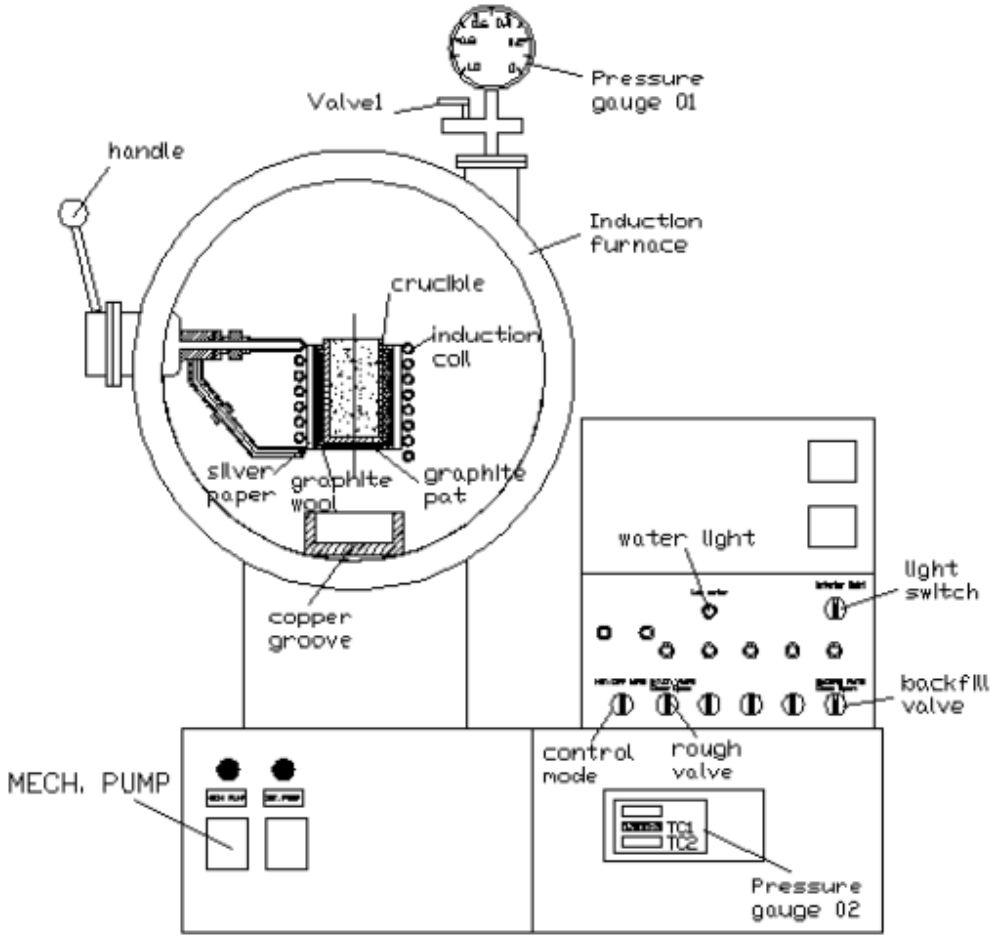

Figure 15: Schematic of the induction furnace and control system [26]

3.2.2 Thermogravimetric furnace

The furnace is a thermogravimetric graphite (vertical) tube furnace; accordingly, it measures the mass of the sample over time as the temperature changes. This measurement provides information about the physical phenomena occurring in the furnace as well as the chemical phenomena. The furnace

allows for the use of different types of atmospheres, such as argon gas and CO gas when running the experiments. It is also possible to reduce the pressure down to approximately 0.1mbar in the furnace using a vacuum pump. The furnace can handle temperatures up to 1700°C. The temperature inside the furnace is controlled by a software from LABVIEW. A schematic of the furnace is displayed in Figure 16.

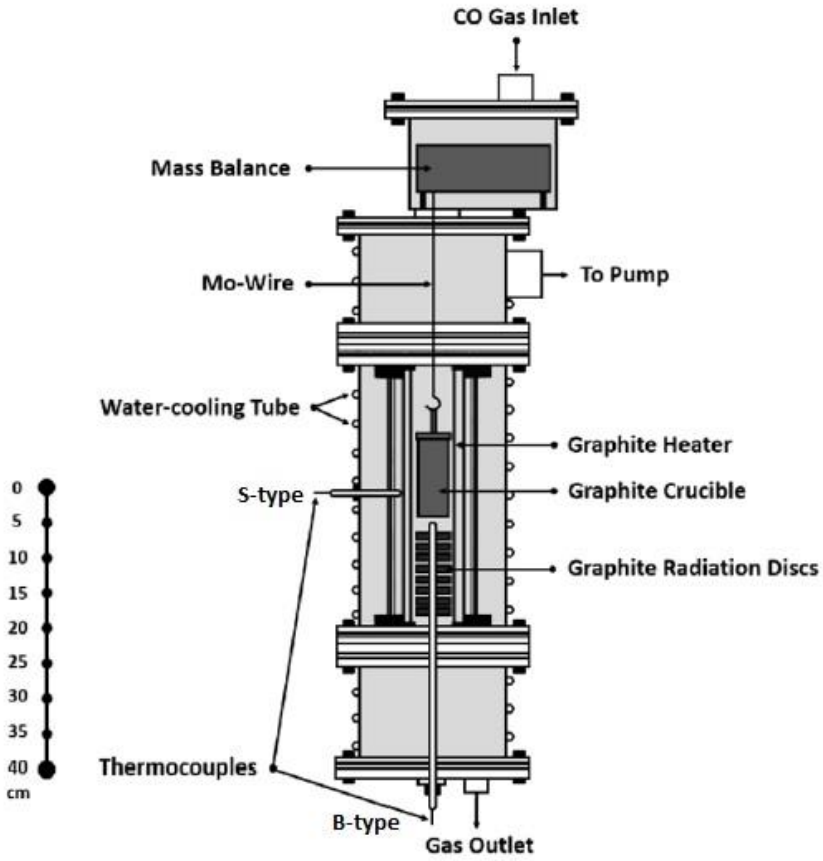

Figure 16: Schematic of furnace setup [27]

The furnace is attached to two types of thermocouples, a S-type thermocouple located close to the heating element (for temperature control) and a B-type thermocouple, located just below the sample for temperature measurements. The graphite crucible is mounted on a Mo-wire inside the furnace, by the B-type thermocouple. In the temperature range 1000-1600 °C the B-type thermocouple will be approximately 400 °C higher than the S-type. The crucible was placed with the bottom of the crucible at the highest temperature in the vertical temperature gradient that were measured prior to experiments.

Before starting any experiments, a temperature profile was conducted, showing the temperature gradient inside the furnace. The measurements were carried out at a fixed temperature setting after stabilization of the furnace. The B-type thermocouple was moved up and down inside the furnace at intervals of 1cm giving the temperature gradient of the furnace. The gradient and placement of the crucible is presented in Figure 17.

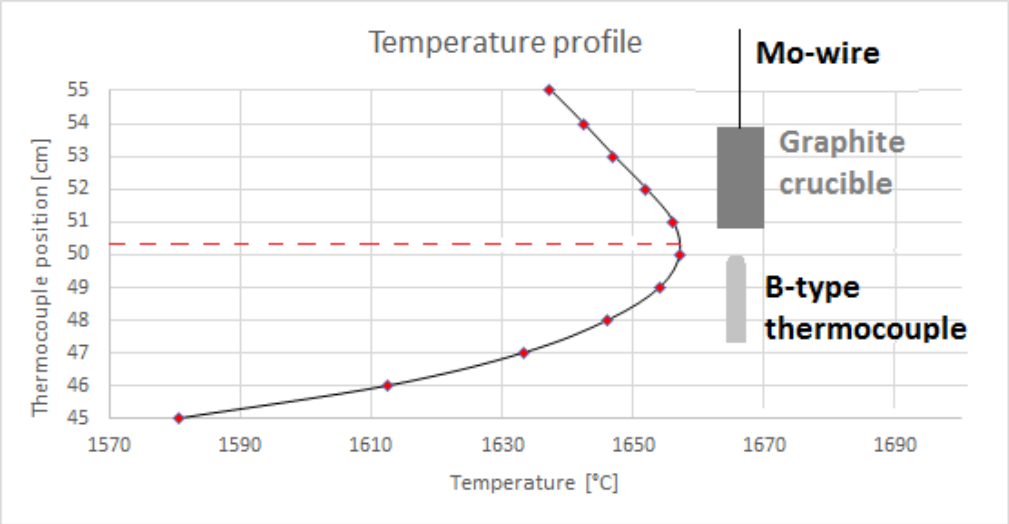

Figure 17: Temperature profile for the thermogravimetric furnace, conducted in February 2019. The size of the crucible is in fact larger.

From the Figure we read that the highest and most stable temperature gradient observed was when the thermocouple was located at approximately position 50 as marked in Figure 17 with a dotted red line. The Mo-Wire was made 20.4cm so that the crucible is positioned in this area.

Figure 18: The Mo-wire made for the melting experiments

The B-type thermocouple should also be positioned in this area, respective to the crucible, with a separation of 0.5-1 cm to ensure no contact; like Figure 17 suggests. The maximum temperature

difference from bottom of the crucible to the top will be about 30°C, not taking into account that the high effective heat transfer in the liquid could reduce the gradient. High temperature in the bottom was chosen to give maximum possible thermal convection.

3.2.3 Electron probe micro-analyzer

The electron probe micro-analyzer, EPMA, is a microbeam instrument, combining the high-resolution advantages of the scanning electron microscope (SEM); together with a high-quality chemical analysis. The EPMA uses a focused beam of high-energy electrons to generate a variation of signals at the surface of the sample. These signals give information on the sample such as external morphology, crystalline structure, chemical analysis and orientation of the materials the sample consists of.

JEOL JXA-8500F EPMA was used for analyzing the samples and operated by Morten Raanes, NTNU. This apparatus is able to detect elements in the range of beryllium to uranium [28].

3.3 Producing slag

The furnace used to produce the slag is an electrical furnace where the heat is applied by induction heating of the metal placed in a graphite crucible for melting and solidification. The furnace makes it possible to heat the samples at temperatures up to 1750°C in an inert atmosphere.

3.3.1 Procedure

The induction furnace was used to melt a mixture of oxides in graphite crucibles to create three different master slags. The difference between the slags is the amount of TiO_2 added. The constituents of the mixtures used to create slag: 1, 2 and 3 are presented in Table 9.

Table 9: Mixing ratio of the oxides used to make slag 1, 2 and 3

Slag 1 – No Ti	**SiO_2**	**MnO**	**Al_2O_3**	**CaO**	**MgO**	**TiO_2**	**Total**
Amount mixed [wt.%]	43.8	9.4	15.7	23.3	7.8	0.00	100
Amount mixed [g]	175.1	37.6	62.8	93.2	31.5	0.00	400.2
Slag 2 – Low Ti							
Amount mixed [wt.%]	43.4	9.3	15.5	23.1	7.7	1.0	100
Amount mixed [g]	86.8	18.6	31.1	46.2	15.5	2.0	200
Slag 3 – High Ti							
Amount mixed [wt.%]	39.8	8.6	14.3	21.2	7.1	10.0	100.9
Amount mixed [g]	119.5	25.7	42.8	63.6	21.3	30.0	302.8

Before starting the procedure, the furnace was cleaned, and pumped down below 0.1 mbar. To ensure extra purity in the furnace atmosphere, the furnace was vacuum pumped several times before starting.

Before mounting the crucible inside the furnace, the inside of the induction coil must be covered with graphite wool and a mica sheet to surround the graphite wool, this is to work as heat protection for the coil and avoid short circuiting. The crucible was then filled with oxides according to experimental parameters and mounted carefully into the copper coil making sure it is gripped tightly.

The voltage was then applied, starting at minimum power and increasing gradually as the temperature increased. Argon gas was inserted, and the gas flow was monitored throughout the procedure and kept at around 1040-1050mbar. The temperature and power were increased until the mix in the crucible was heated to its melting point, approximately 1455°C. The temperature was then increased to about 1500°C and held for 30 minutes. After holding, the power was shut down and after sufficient cooling the crucible was retrieved. The crucible was then crushed, and the slag was separated for further milling.

3.4 Slag-metal melting experiments

A thermogravimetric furnace was used for the melting experiments. The furnace allows for the heating of samples in an inert atmosphere. The total weight of the crucible is recorded. The heat is supplied by a resistance graphite element, and the furnace can hold temperatures up to about 1700°C.

3.4.1 Procedure

The thermogravimetric furnace was used to heat, melt and reduce the mixture of synthetic slag, metal alloy, TiO_2 and coke in a graphite crucible, deciding temperature, heat rate, hold time, atmosphere and gas flow. It is assumed to be no exchange of elements with atmosphere.

The graphite crucible was filled with crushed metal, slag and coke according to experimental parameters, as presented in Table 10. The crucible was filled layer-wise, with the metal in the bottom and the slag on top. If coke particles were included, they were put in between the layers as illustrated in Figure 19.

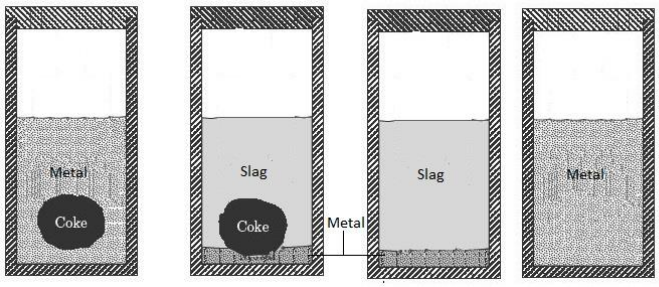

Figure 19: Illustrative drawing of the crucibles when filled with constituents.

Table 10: Experimental parameters

Experiment	Metal [g]	Wt.% Si in alloy	Slag [g]	Wt.% TiO_2 in slag	Coke-particle [g]	Temperature [°C]	Hold-time
1	101.2	20	-	-	7.8	1600	60
1.2	92.3	20	-	-	3.4	1600	60
2	10.3	20	47.4	0	3.2	1600	60
3	91.3	20	-	-	-	1600	60
4	10.4	20	45.9	0	-	1600	60
5	7.7	29	37.8	0	-	1600	60
6	7.9	20	35.5	1	-	1600	60
7	7.5	29	37.4	1	-	1600	60
8	73.0	29	-	-	-	1600	60
9	10.2	20	34.9	1	-	1650	60
10	9.8	29	34.6	1	-	1650	60
11	10.9	29	35.0	0	-	1600	90
12	7.8	20	35.5	10	-	1600	60
13	7.8	29	34.7	10	-	1600	60
14	7.8	29	34.8	10	-	1650	60
15	7.8	20	34.4	10	-	1650	60
16	7.9	20	35.2	10	-	1600	90
17	7.7	29	34.9	10	-	1600	90
18	4.5	29	20.6	1	-	1600	60
19	7.6	29	36.2	10	-	1600	60

Before each experiment, the furnace was cleaned using ethanol and a vacuum cleaner to ensure no residues were left. The furnace was then pumped down to approximately 0.1 mbar followed by filling it with argon. This step was repeated about three times to ensure no excess air in the furnace. When the cleaning was done the furnace was filled with argon gas, and the gas flow was set to 0.5l/min. The crucible was then mounted on the Mo-wire and the temperature profile according to the experiment was started. The heating rate was set to 80°C/min. When the temperature inside the furnace reached approximately 800°C, the argon gas flow was turned off and the CO gas flow was turned on. This procedure was used to avoid sooting in the furnace by the reverse Boudouard reaction. The samples were then held at a specific temperature for a specific hold time according to experimental parameters. When the experiment was done, and the furnace was cooling down the CO gas flow was turned off at approximately 800-900°C and the argon gas flow was turned on, again to avoid sooting. After cooling to room temperature, the furnace was purged using argon gas and thereafter pumped down to about 0.1mbar. This step was also repeated 2-3 times to get rid of any residual CO gas in the furnace.

3.5 Electron Probe Micro-Analyzer

Sections of samples from the slag-metal experiments were analyzed by EPMA. All samples were analyzed apart from the sample retrieved from experiment 11. Sample 11 was not analyzed at all, due to there not being any room for it in the EPMA, and no more time to use the EPMA again. The various phases present in the samples were investigated, determining their chemical composition. The EPMA combines the high-resolution advantages of a scanning electron microscope with high quality chemical analysis. The analysis from the EPMA gives a detailed overview of the phases, their chemical composition and their boundary profile.

The three main phases that will be mentioned is the slag phase, the metal phase and the carbides. Within the metal and the slag phases there is observed several distinct phases or particles, such as: dendrites, carbides and oxides. If one of the phases is heterogenous, the distinct phases will be mentioned as dark or light, which correlates to the respective gray-tone in the microstructure pictures from the EPMA analysis.

Each phase is analyzed at minimum three separate points, in order to exclude outlaying values and get more representative results. Only parts of the samples were analyzed, and thus certain uncertainties are expected. To minimize the uncertainties, point analyses of the slag have been recorded from close to the slag phase, close to the metal phase and in the bulk of the slag. Point analyses of the metal have been taken in the bulk of the metal, close to the crucible and close to the slag.

The microprobe was set to look for the following elements:

- Si, O, P, C, Mn, Mg, S, Fe, Al, Ca and Ti.

The software is not programmed to recognize carbides in the sample, the detection of carbides will only be qualitative when investigated by the EPMA.

3.5.1 Sample preparation for EPMA

In order to use the electron probe micro analyzer, the samples had to be prepared appropriately. This includes cutting the samples into the appropriate size and orientation depending on where in the sample the analysis is to be taken. Furthermore, the samples must be cast in epoxy, abraded and polished, heated and degassed as well as decarbonized.

First off, the crucibles containing the samples were cast in epoxy prior to being to prevent change in the sample during cutting. The crucibles were cut in half, length wise. This gave the possibility to observe what the sample looked like from bottom to top and in the middle. Of the two pieces, one was chosen for further analysis and was cut to fit into a holder where the sample then was cast in epoxy. The section selected for EPMA was chosen so that the sample contained all the various phases; as well as both the crucible bottom wall and one of the sidewalls as carbides were expected to accumulate by the graphite walls. For the experiments containing a coke particle, the coke/metal and coke/slag transitions were included. When the epoxy was stable, the sample was removed from the holder and abraded using Struers Tegramin-30 until the appropriate surface finish was achieved. Using the same machine, the samples were polished. Program and blades used during abrasion and polishing can be seen in Table 11. The liquid used during polishing, DiaPro, is a water-based diamond suspension, containing a mixture of diamonds and cooling lubricant. The diamond grain size in the liquid mixture corresponds to the diamond grain size in the blade used.

Table 11: Set-up for Struers Tegramin-30, used for abrasion and polishing of samples

Step	Diamond blade [µm]	Force [N]	Rotation speed [rpm]	Liquid
1	220	15-30	150-300	Water
2	9	15	150	DiaPro Largo9
3	3	15	150	DiaPro Dac3
4	1	15	150	DiaPro Nap-B1

As the samples are cast in epoxy before the analyses with EPMA, this could leave some contamination in the vacuum chamber. Residue from hydrocarbons from the preparation may also be present. After preparation a carbon layer is added to the sample surface to prevent electrons to build up and according to literature these factors combined will make up an error of up to c. 4 wt.% carbon in the

samples. According to the operator of the EPMA, a correct carbon value will only be quantitative, and comparable between the samples. A phase with known C content can be analyzed and compared to carbon content in the other phases [8,29].

3.6 Quantification of metal phase from EPMA results

Most of the metal found in the samples is a two-phased metal, distinguished as light and dark phase. The amount of each phase is quantified using the image analysis program ImageJ.

With the assumption that the images taken of the metal phase is representative for the whole sample, the average chemical composition of the metal in each sample can be calculated. For all samples an EPMA BSE image was captured of what was decided to be the most representative part of the metal phase. These images were used to find the fraction of light and dark phase in the metal. For the analyses in ImageJ the images of the representative areas were uploaded. A thresholding method was used to make the dark metal phase black and the light phase white. The now black phase could be measured by the software's "Analyze particles" function. This procedure is illustrated in Figure 20. By diving the measured area by total area, the ratio of dark and light phase can be calculated. This procedure was repeated for some of the experiments at different areas of the sample to determine the accuracy of the method.

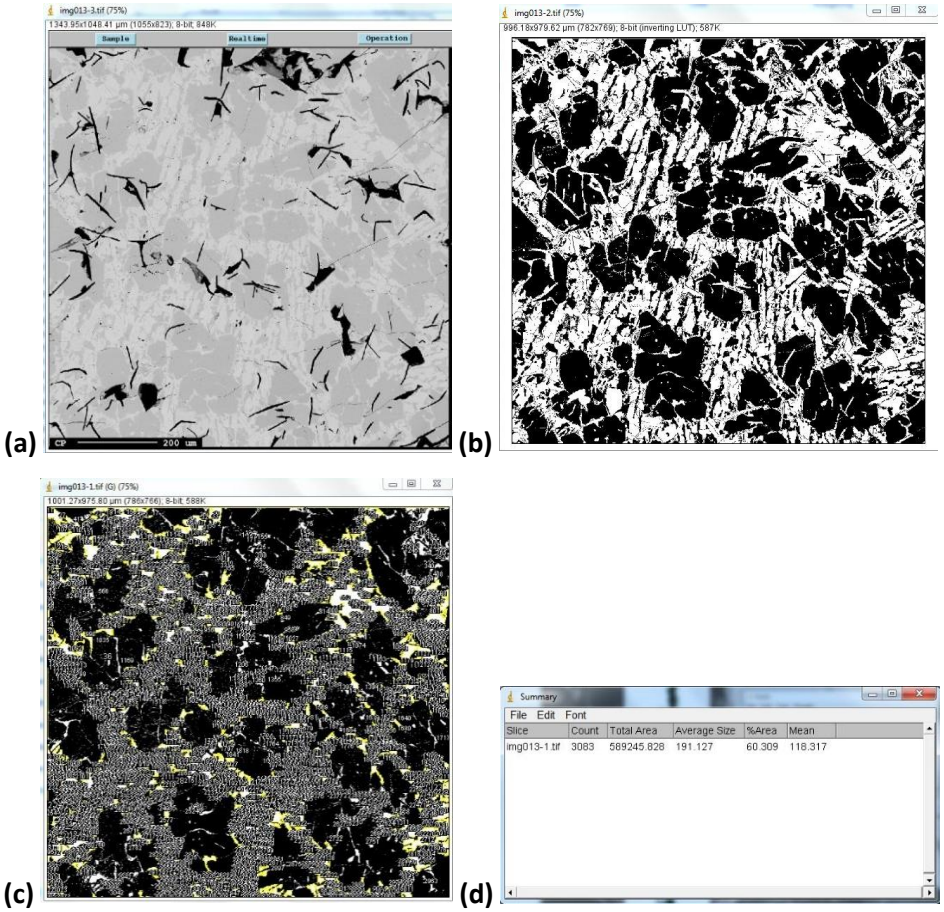

Figure 20: Procedure for quantifying the ratio between dark and light metal phase in samples **(a)** Representative image of a sample **(b)** Image after thresholding, one phase is made white, while the other dark **(c)** "Analyze particles" has counted the amount of black pixels in the image **(d)** Results

This ratio between dark and light metal was later used in the mass balance calculations to get a more accurate chemical composition of the metal phase as a whole.

3.7 Mass balance

The defined relationship between the composition of the raw materials and the slag and metal in the final sample is given by the mass balance. The raw materials in this project are a synthetic slag and industrial alloy with known chemical compositions. The amount of alloy and slag (and coke) going into the experiments is known as well. Accordingly, it is possible to calculate the exact amount of each element going into every experiment. The assumption is made that the system is semi-isolated and the only exchange of elements with atmosphere is C and O as CO gas. The amount of each element going into the experiment, remains in the sample.

The chemical composition of the slag and alloy phases in the produced samples are taken from the EPMA results and will thus carry the uncertainties linked to this process.

As stated in the theory chapter, CaO, MgO and Al_2O_3 are considered irreducible oxides and will maintain their mutual ratio in the slag during the reduction process. By using the ratio of the Ca, Mg and Al in the slag, calculating the amount of slag in the produced samples is possible following equation (3.1):

$$Slag\ out\ [g] = Slag\ in\ [g] * \frac{X\ IN\ [wt.\%]}{X\ OUT\ [wt.\%]} \quad (3.1)$$

Where X is either Ca, Mg or Al given in weight percentage. X IN represents the weight percentage of X in the original slag. X OUT represents the weight percentage of X in the produced slag. Slag out [g] represents the amount (measured in grams) of produced slag in the cooled sample following the experiments. Slag in [g] represents the amount of slag (original) added to the mix prior to the melting. If the slag in the produced sample contains a higher weight percentage of either of the oxides, it means the slag phase has decreased. The compared results from the slag calculations using Ca, Mg and Al are given in Table 12. Certain experiments are excluded due to no slag being used in the raw materials.

Table 12: Comparison of slag calculations using Ca, Al and Mg

	Ca		Al		Mg	
Experiment	Slag diff (out-in) [g]	Slag increase [%]	Slag diff (out-in) [g]	Slag increase [%]	Slag diff (out-in) [g]	Slag increase [%]
2	1,1	2,4	3,1	6,5	-16,8	-35,5
4	1,1	2,4	2,4	5,2	-16,0	-35,0
5	0,3	0,8	1,6	4,2	-13,6	-35,9
6	-1,0	-3,0	2,9	8,2	-11,0	-31,1
7	-1,5	-3,9	3,3	8,9	-11,5	-30,7
9	-2,6	-7,5	2,1	6,0	-11,2	-32,2
10	-1,8	-5,1	2,2	6,4	-11,0	-31,7
12	9,9	27,9	2,8	7,9	7,1	20,0
13	10,5	30,2	2,6	7,6	0,8	2,2
14	7,0	20,2	0,7	2,0	-9,3	-26,8
15	7,5	21,8	2,4	6,9	-11,2	-32,6
16	9,2	26,1	3,2	9,0	-9,8	-27,8
17	10,5	30,2	2,9	8,3	-1,2	-3,4
18	5,1	24,9	1,7	8,3	-4,0	-19,6
19	11,8	32,6	3,2	9,0	-2,1	-5,8

The slag calculations using Al (as the irreducible oxide) gave the most stable results. Every experiment gave an increase in slag ranging from 2-9%, as can be seen in Table 15. Calculations based on Mg and Ca gave more unstable results. An area of a representative slag was selected when choosing values for the slag calculation. Due to occasionally complex and inconsistent structure of the slag (variation between glass/crystalline), the quantification of the ratio between darker and lighter parts of the slag was not measured or calculated. The difference in Al content between the different parts of the slag is low, whereas the difference in Mg and Ca contents are higher. Mistakes during selection of values would thus be minimized by using the Al values for the following calculations. An example of the inconsistent slag structure, showing both dendrites and an amorphous phase in the same sample, is

presented in Figure 21. It is assumed that the dendrites forms during solidification of the molten slag, the structure being affected by thermal history and composition.

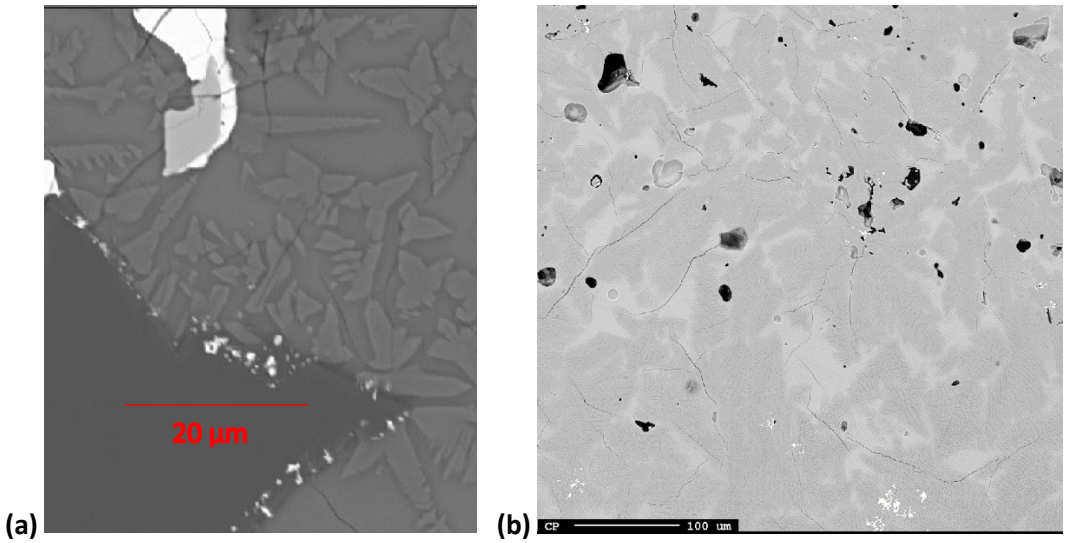

Figure 21: (a) Microstructure BSE image of metal (white), TiC (light gray), SiC (dark gray) and slag (gray and dendritic) **(b)** Slag sample with both amorphous and dendritic structure.

The amount of alloy was calculated using the amount of Mn and Fe in the samples. The manganese is distributed between the slag and alloy phase. Now that the amount and composition of the slag phase going in, and in the produced samples, is known, calculating the amount of Mn and how it is distributed is possible.

Total amount of Mn going in is equal to the amount of Mn going out.

$$Mn_{tot}(OUT) = Mn_{tot}(IN) = Mn\ from\ slag + Mn\ from\ metal \quad (3.2)$$

$$= Slag\ amount\ [g](IN) * \frac{\%Mn\ in\ slag\ (IN)}{100\%} + Alloy\ amount\ [g](IN) * \frac{\%Mn\ in\ alloy\ (IN)}{100\%} \quad (3.3)$$

By employing the same equation, with values found for the slag and alloy phase in the sample, the alloy amount is calculated.

$$Alloy\ amount\ [g](OUT) = \frac{Mn_{tot} - Mn\ from\ slag\ (OUT)}{\%Mn\ in\ alloy\ (OUT)} * 100\% \quad (3.4)$$

- Mn_{tot}(OUT)/(IN): Total amount of Mn contributed from slag and metal in the mix. IN represents the amount of Mn in the original mix prior to melting and OUT represents the amount of Mn in the cooled sample
- Mn from slag/alloy: The amount of Mn contributed from slag or alloy respectively
- %Mn in alloy/slag: Represent the weight percentage of Mn in the alloy and slag phase

Mn_{tot}(IN) is known from chemical analyses (XRD and LECO) conducted by external contributors (Eramet and Sintef molab). Mn from slag (OUT) is calculated using the results from the Al slag calculations. The chemical composition of the slag and alloy phase in the cooled sample is taken from the EPMA results. The same procedure was used when calculating the alloy amount using Fe instead of Mn. The compared results are presented in Table 13.

Table 13: Comparison of alloy calculations using Mn and Fe

	Mn		Fe	
Experiment	Alloy diff (out-in) [g]	Alloy increase [%]	Alloy diff (out-in) [g]	Alloy increase [%]
2	-0,3	-3,2	0,5	4,6
4	-0,2	-1,8	0,7	6,4
5	0,2	3,0	0,3	3,9
6	-0,3	-3,2	0,9	10,9
7	-0,1	-1,6	0,5	6,4
9	0,3	3,4	0,7	6,4
10	0,4	4,2	0,7	7,0
12	-3,5	-44,8	-0,3	-3,5
13	-1,7	-21,9	-0,7	-9,2
14	-0,5	-6,8	-0,3	-3,3
15	-1,6	-20,7	-1,2	-15,9
16	-2,1	-26,5	-1,5	-19,5
17	-2,3	-29,7	-0,5	-6,1
18	-0,1	-1,3	0,3	7,6
19	-1,9	-25,4	-0,9	-12,1

When the amount of slag and alloy in the sample is known it is possible to calculate the distribution of the titanium in the experiments. First the total amount of titanium going into the experiment was calculated using known data.

$$Ti_{tot}(OUT) = Ti_{tot}(IN) = Ti\ from\ slag + Ti\ from\ alloy =$$
$$Slag\ amount\ [g]\ (IN) * \frac{\%Ti\ in\ slag\ (IN)}{100\%} + Alloy\ amount\ [g]\ (IN) * \frac{\%Ti\ in\ alloy\ (IN)}{100\%} \quad (3.5)$$

Combining the EPMA results with the calculations of slag and alloy amount it was possible to calculate how much of the total Ti was found in the slag and alloy phase. The remaining amount of Ti is assumed to go to carbides. The % of Ti that went to TiC from the total Ti is calculated, along with the amount of TiC in the sample.

The same procedure was used to calculate the Si-distribution in the experiments.

4. Results

4.1 Production of synthetic slag

The chemical composition of the synthetic slags made in the induction furnace is presented in Table 14.

Table 14: Chemical composition of the oxides in slag 1, 2 and 3 given in weight percentage

Slag type	SiO_2	MnO	Al_2O_3	CaO	MgO	TiO_2	Total	R-ratio
Slag 1 – No Ti	42.20	9.45	17.70	23.60	6.78	0.00	99.73	1.72
Slag 2 – Low Ti	42.10	9.32	18.00	22.40	6.94	0.92	99.68	1.68
Slag 3 – High Ti	38.10	8.50	16.00	21.20	6.10	9.60	99.50	1.71

By converting the weight percentage of the compounds to atomic percentage, the atomic percentage of each element can be calculated. Furthermore, the atomic percentage can be converted back to weight percentage, thus giving the weight percentage of each element as presented in Table 15. The expected chemical composition is compared to the actual chemical composition of the slag created.

Table 15: Comparison of the expected and actual chemical composition of the three slags made

	Si	Mn	Al	Ca	Mg	Ti	O	Total
Slag 1 – No Ti								
Expected [wt.%]	20.47	7.26	8.29	16.65	4.73	0	42.58	100
Actual [wt.%]	19.79	7.33	9.37	16.91	4.13	0	42.47	100
Slag 2 – Low Ti								
Expected [wt.%]	20.27	7.19	8.21	16.49	4.68	0.60	42.56	100
Actual [wt.%]	19.73	7.24	9.53	16.06	4.26	0.55	42.63	100
Slag 3 – High Ti								
Expected [wt.%]	18.45	6.55	7.47	15.01	4.27	5.92	42.33	100
Actual [wt.%]	17.90	6.60	8.50	15.23	3.72	5.77	42.28	101

4.2 Slag-metal experiments

The results from the slag-metal experiments are grouped according to which slag type was used, either slag containing no titanium, 1wt.% TiO_2 or 10wt.% TiO_2; and according to what alloy type was used, either alloy containing c.20wt.% Si or c.29wt.% Si. Chemical analysis of the phases present and

examples of the microstructure are provided in each section. A full collection of the microstructure images can be found in the appendix.

In general nearly all of the experiments produced samples where most of the slag was homogenous but also complex at certain areas. The metal observed consisted of one light metal phase with higher content of Mn but lower content of Si and one dark metal phase with lower content of Mn but higher content of Si. This ratio between dark and light phase has been quantified. Results from the chemical composition quantifications of the liquid metal found in the experiments is provided in Table 17. The chemical composition of the slag phases, SiC and TiC for each experiment is presented in Table 19, 20 and 22, respectively.

From the mass balance regarding Si-distribution, the amount of leftover Si after distributing between the slag and metal phase has been calculated and is presented in Table 20. The amount of TiC that has accumulated, based on mass balances, is presented in Table 22. The distribution of the Ti between the slag, alloy and carbide phase is presented in Figure 22. An overview of which experiments where TiC, SiC and graphite was observed is found in Table 16.

Table 16: Observations of TiC, SiC and graphite in the experiments , x shows samples where TiC and SiC where observed.

Experiment	%Si in original alloy	%TiO_2 in original slag	Temperature [°C]	TiC	SiC	Graphite
1	19.66	-	1600	-	-	X
1.2	19.66	-	1600	-	X	X
2	19.66	0	1600	X	-	X
3	19.66	-	1600	-	-	-
4	19.66	0	1600	-	-	X
5	29.44	0	1600	-	X	-
6	19.66	1	1600	X	-	X
7	29.44	1	1600	X	X	-
8	29.44	-	1600	-	X	-
9	19.66	1	1650	X	X	-
10	29.44	1	1650	X	X	-
12	29.44	10	1600	X	-	-
13	29.44	10	1600	X	X	-

14	29.44	10	1650	X	-	X
15	19.66	10	1650	X	-	-
16	19.66	10	1600	X	-	-
17	29.44	10	1600	X	X (relatively little)	-
18	29.44	1	1600	X	X	-
19	29.44	10	1600	X	X (relatively little)	-

Table 17: Results from the chemical composition quantifications of the metal found in the samples. Original values of the light and dark metal phase are obtained by the EPMA analyses. Values are given in mass%. Mn/Fe ratio is included for all experiments and standard deviation is included for three of the experiments

Experiment	Si	C	Mn	Fe	Ti	Mn/Fe-ratio	Std. Dev.
1	17,7	0,4	66,3	16,0	N.A.	4,2	
1,2	20,1	0,4	68,3	11,5	N.A.	5,9	
2	16,0	0,5	71,7	11,4	N.A.	6,3	
3	19,3	0,4	68,5	11,5	N.A.	6,0	
4	17,7	0,5	70,4	11,2	N.A.	6,3	
5	23,1	0,4	68,0	9,9	N.A.	6,9	
6	17,4	0,4	71,1	10,7	0,4	6,6	
7	25,2	0,4	66,1	9,7	0,7	6,8	
8	28,3	0,7	62,6	10,9	0,3	5,8	
9	19,3	0,4	70,2	11,2	0,2	6,3	±0,81
10	24,2	0,3	66,7	9,7	0,6	6,9	
12	19,1	0,4	69,5	12,3	0,2	5,6	
13	25,8	0,3	63,9	11,3	1,2	5,6	
14	18,2	0,4	71,4	10,6	0,2	6,7	
15	19,5	0,4	69,7	14,2	0,1	4,9	±0,45
16	18,5	0,5	68,7	14,8	0,1	4,6	
17	24,3	0,5	66,1	11,0	1,2	6,0	
18	22,8	0,5	69,1	9,6	0,4	7,2	
19	26,1	0,5	62,9	11,8	1,0	5,3	±0,76

Table 18: Chemical composition of the slag phase from the experiments, given in mass%. Values obtained from EPMA analyses

Experiment	Si	O	C	Mn	Mg	Al	Ca	Ti
1	28,8	41,5	0,3	20,1	2,5	1,7	4,2	-
1.2	19,8	41,3	0,4	3,0	6,8	11,6	15,3	-
2	20,8	42,0	0,3	6,1	6,4	8,8	16,5	-
3	29,1	41,6	0,4	17,1	2,0	3,2	3,8	-
4	20,8	43,4	0,4	6,2	6,4	8,9	16,5	-
5	21,3	43,4	0,4	4,8	6,4	9,0	16,8	-
6	21,8	41,1	0,3	6,0	6,2	8,8	16,5	0,3
7	21,1	42,5	0,4	5,5	6,2	8,8	16,7	0,5
8	36,3	43,4	0,9	3,1	1,9	3,7	6,2	0,1
9	21,9	38,5	0,3	4,9	6,3	9,0	17,4	0,3
10	22,7	40,1	0,4	3,4	6,3	9,0	17,0	0,3
12	20,7	37,6	0,3	6,8	6,1	7,9	14,8	2,9
13	20,3	36,9	0,3	5,2	6,1	6,9	14,8	5,4
14	23,8	39,0	0,4	4,8	5,1	8,3	14,9	0,3
15	21,5	36,2	0,5	7,9	5,9	7,9	14,7	1,2
16	21,0	35,8	0,5	9,0	5,1	7,6	14,2	2,5
17	20,0	36,4	0,5	6,1	5,1	7,6	14,6	5,6
18	22,6	37,9	0,5	4,8	5,3	8,8	15,8	0,4
19	19,9	36,8	0,5	5,8	5,4	7,6	14,5	5,5

Table 19: Chemical composition of the silicon carbide observed in the samples given in mass%. Values obtained from EPMA analyses

Experiment	Si	O	C	Mn
1.2	69,4	0,6	28,9	0,2
5	69,6	0,2	29,1	0,7
7	70,4	0,1	28,0	1,1
8	68,8	0,3	5,1	0,3
9	70,5	0,2	27,2	1,3
10	69,5	0,3	28,8	0,4
17	65,2	0,8	29,5	0,4
18	66,4	0,4	29,3	0,5
19	66,5	0,4	30,4	0,7

Table 20: Amount of Si not distributed in the slag and metal phase. Calculated by mass balance, original values obtained from EPMA and XRD

Experiment	Si for carbide [g]	% of total Si
2	-0,8	-7,1
4	-0,9	-7,8
5	-0,5	-5,0
6	-1,3	-15,6
7	-1,0	-10,6
9	-1,2	-13,7
10	-1,2	-12,2
12	-1,5	-18,8
13	-0,9	-10,6
14	-1,3	-15,3
15	-1,5	-19,5
16	-1,4	-17,6
17	-0,8	-9,4
18	-0,8	-14,1
19	-0,9	-10,0

Table 21: Chemical composition of the TiC observed in the samples given in mass%. Values obtained from EPMA

Experiment	Si	O	C	Mn	Ca	Ti
6	0,7	6,5	18,9	1,0	1,2	76,6
7	0,2	1,0	19,9	3,2	0,0	76,9
9	0,5	0,6	19,0	9,5	0,0	70,3
10	0,3	3,8	18,1	1,0	0,0	78,7
12	0,3	6,3	18,0	0,4	0,5	75,6
13	0,2	0,9	19,9	1,4	0,0	77,1
14	0,3	5,5	17,5	1,0	0,4	75,9
15	1,6	7,8	17,0	1,3	1,0	73,1
16	0,4	6,5	16,8	0,8	0,8	74,9
17	0,3	6,6	17,0	0,4	0,4	77,0
18	0,2	1,7	19,6	2,1	0,1	75,3
19	0,3	4,4	18,4	1,0	0,2	76,1

Table 22: Amount of TiC formed based on mass balance and distribution of Ti. Values used for mass balance are obtained by EPMA and XRD

Experiment	Ti for carbide [g]	% of total Ti	Ti-C [g]
6	0,06	25,8	0,07
7	-0,01	-6,6	-0,02
9	0,09	40,0	0,12
10	0,07	34,7	0,10
12	1,14	55,2	1,51
13	0,47	23,1	0,61
14	1,90	93,9	2,51
15	1,58	78,6	2,16
16	1,08	52,8	1,45
17	0,26	12,6	0,33
18	0,02	17,2	0,03
19	0,09	4,5	0,12

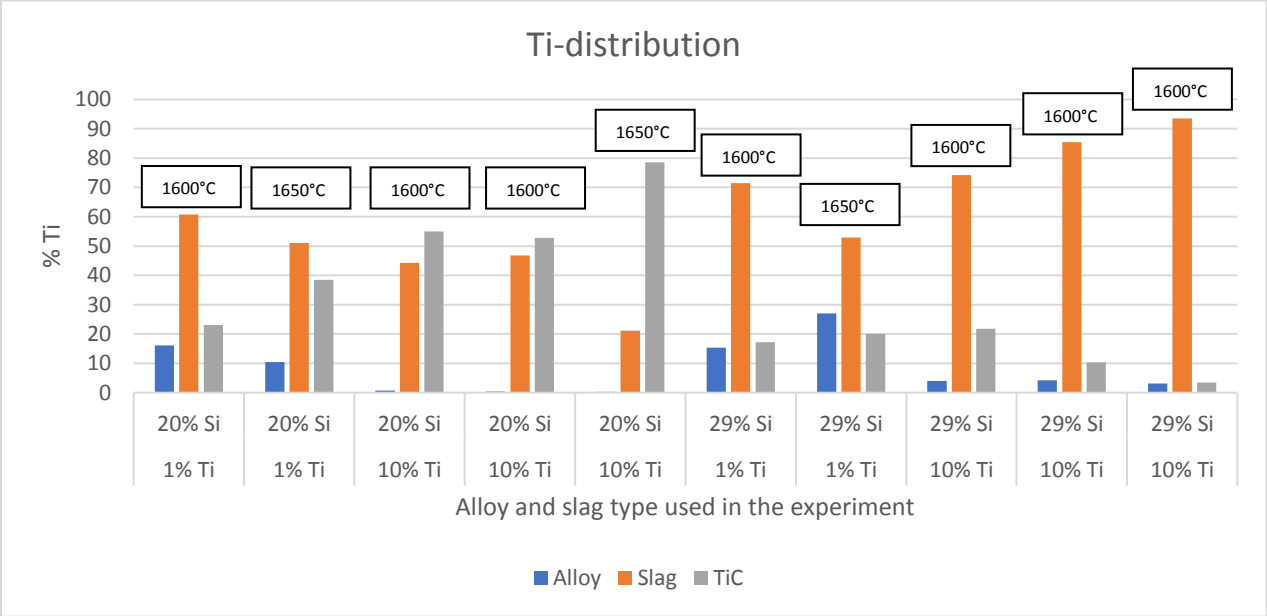

Figure 22: Graph showing the distribution of the total amount titanium in an experiment, between the slag, alloy and TiC phase. The experiments are listed after Si content in the alloy, increasing from left to right; thereafter Ti content in the slag, increasing from left to right; and lastly by temperature, increasing from left to right

Experiments 1 to 5 did not have any titanium added in the samples and the Ti content was not analyzed. The amount of Ti in the metal phases that were not analyzed is expected to be somewhere around the original Ti content of the metal, 0.2-0.3 wt.% Ti. The same applies for the slag phase and it is expected to have a Ti content close 0 – 0.1 wt.% Ti.

There was no slag in the mix to produce sample 1, 1.2, 3 and 8, initially. The slag analysis for these experiments presented in Table 19 is analysis of slag that has formed in the experiments.

The silicon carbide found in the samples is $Si_{50}C_{50}$ with equal amounts of at.% Si and at.% C, for all the experiments. From Table 19 it can be observed that some of the SiC has minor amounts of O and Mn. This is assumed to be values from underlying slag phases close to the SiC, collected by the EPMA. The SiC analyzed in experiment 8 is assumed to be $Si_{50}C_{50}$ as well. SiC was observed in experiment 13 but was for some reason not recorded in the EPMA analysis and can only be regarded as a qualitative result.

As all the values in Table 20 are negative, the results are clearly not correct. However, the difference between the experiments can be of value. Since the values are negative, the lower numbers will indicate more Si for other phases than slag or metal. SiC was observed in experiments 1.2, 5, 7, 8, 9, 10, 13, 17, 18 and 19. All with relatively lower values than the experiments where no SiC was observed. Experiment 2 and 4 has a low value compared to the other experiments, but no SiC was observed. It was however observed that the graphite formed, contained certain amounts of Si. Graphite has not been analyzed; this must thus be regarded as a qualitative result.

The titanium carbide found in the samples is $Ti_{50}C_{50}$ with equal amounts of at.% Ti and at.% C, for all the experiments. From Table 21 it can be observed that some of the TiC contains minor amounts of Si, O, Mn and Ca. This is assumed to be values from underlying slag phases close to the TiC, collected by the EPMA.

In Table 22 it can be observed that experiment 7 gives a negative value, although TiC was observed in this experiment. The mass balance obviously has some margin of error. However, the relative difference between the experiments is assumed to give an indication as to which experiments accumulated the most and least TiC. Experiment 18 was conducted with less material in the mix, and thus less TiC has accumulated.

From Figure 22 it can be deducted that most of the Ti is found in the slag or formed TiC, and only lower amounts in the alloy phase. When increasing the amount of Si in the alloy used in the experiments, from 20wt.% to 29wt.% the amount of Ti in the TiC phase decreases from an average of 50% to an average of 14.5%. For the experiments using alloy with 20wt.% Si, increasing the amount of Ti in the slag will also increase the % of Ti going to the TiC phase. This was however not observed for the experiments using alloy containing 29wt.% Si. The relative trend when increasing the temperature is that more Ti will settle in the TiC phase.

Notable observations from the results:

- The graphite crucible has reacted with both metal and slag in most experiments as seen in Figure 23.

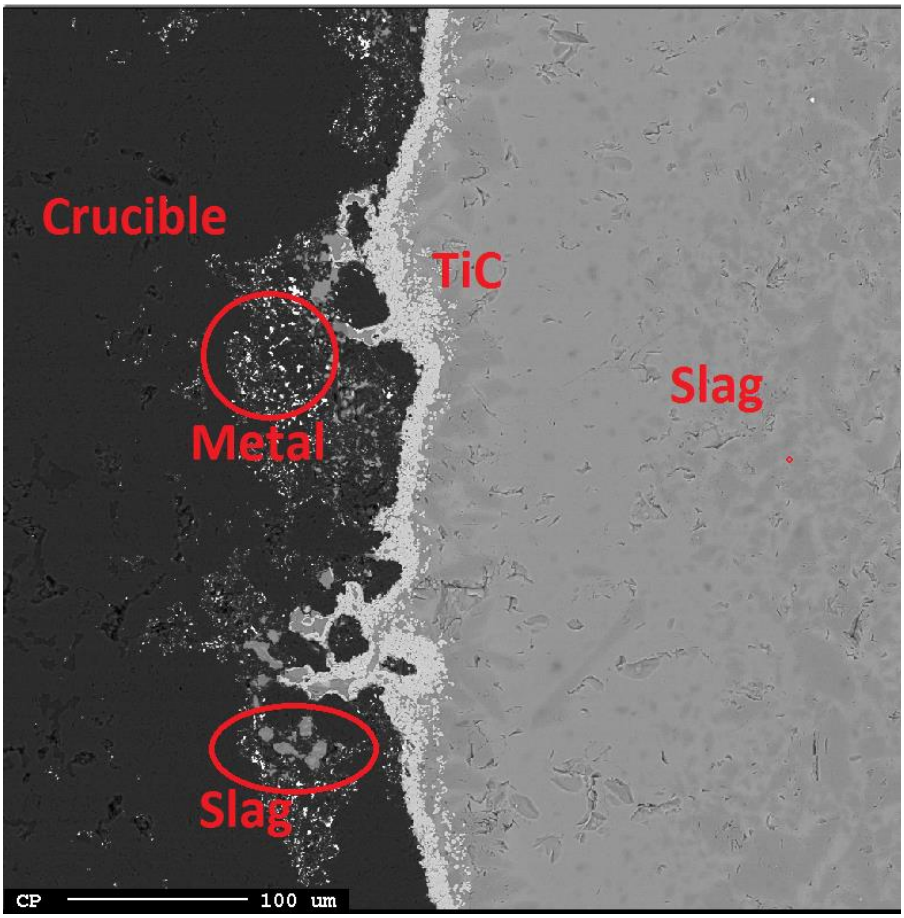

Figure 23: Illustration of metal and slag reacting with the graphite crucible

- The metal and slag in the samples have crept up the crucible walls as seen in Figure 24, indicating good wetting properties towards the graphite crucible

Figure 24: Top corner of sample from experiment 3, showing an example of metal and slag creeping up the crucible wall, indicating good wetting

- Every experiment where slag containing any amount of Ti was used has resulted in the accumulation of TiC (see Table 37)
- Higher Ti-slags will lead to more TiC and less SiC and graphite accumulating (see Table 16)
- Most of the TiC has consistently accumulated on the crucible interface and slag-metal interface, see Figure 46 and 47
    - TiC has also accumulated in the bulk of the slag and in the bulk of the metal (see Figure 51 **(c)**)
- Increasing the content of Si in the alloy increases amount of SiC accumulating, but also decreases the amount of TiC accumulating (see Table 31 and 36 for the effect on TiC amount)
    - 8/9 experiments using LC-SiMn alloy (29wt.% Si) has accumulated SiC
    - 2/10 experiments using Std-SiMn (20wt.% Si) has accumulated SiC
- Most of the SiC has accumulated on the slag-metal interface (see figure 53)
    - SiC has also accumulated on the crucible interface and in the bulk of the metal (see figure 51 **(c)** and figure 51)

- Carbide particles are larger on the slag-metal interface, than on the crucible interface (see figure 49 **(a)**)
- Increased temperature results in more carbide in the bulk of the alloy (see Table 46, experiment 9, 14 and 15 are conducted at 1650°C)

4.2.1 Thermogravimetric analysis

The recordings from the TGA revealed a weight reduction in the range of 0.1-1.2% for all samples. This was also confirmed by weighing of the crucible, before and after experiments.

4.2.2 Visual observations

Figure 25 to 44 show the crucibles after they were cooled and cut vertically. The section selected for EPMA is marked on the crucible, and the polished sample is shown to the right. All the crucibles and the sample casts are the same size.

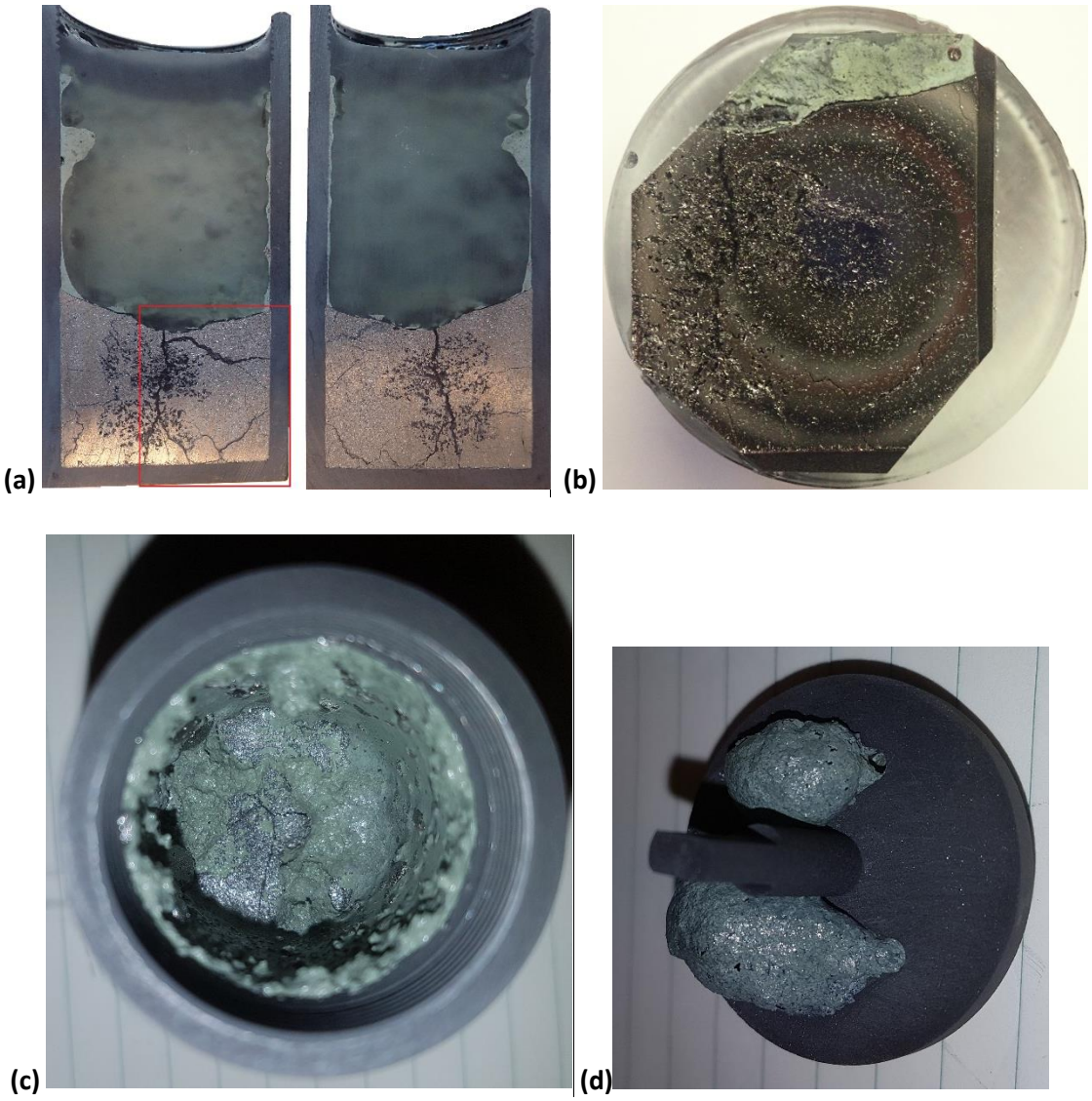

Figure 25: Sample from experiment 1 **(a)** After cutting the crucible vertically, section chosen to become the sample is indicated by a red outliner. The gray phase is metal, the dark patches in the center is porous cracking located where the coke particle was placed. Along the crucible interface, above the metal phase is a green/light gray phase, this is slag that has formed **(b)** Sample, section chosen for EPMA following sample preparation **(c)** Formed slag creeping up the crucible wall **(d)** Slag foaming out of the lid

(a) 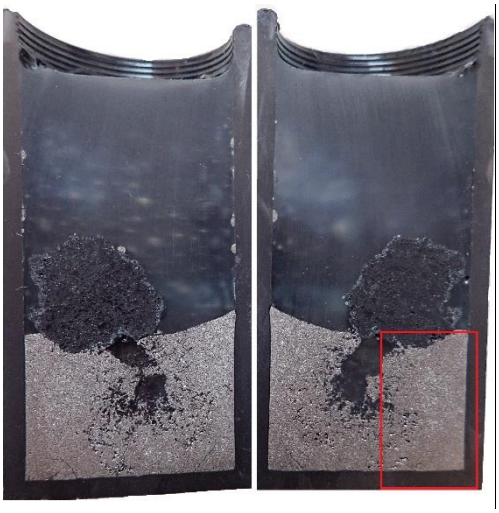 (b) 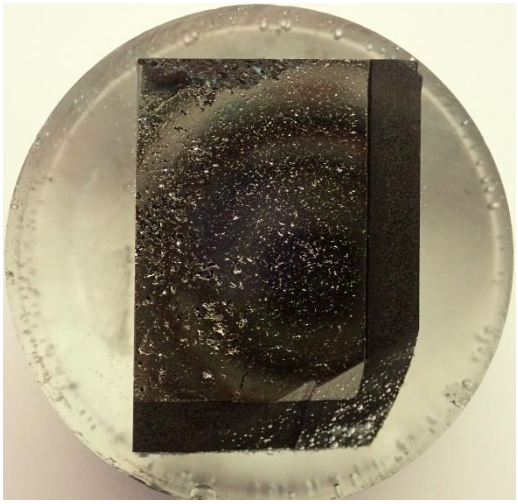

Figure 26: Sample from experiment 1.2 **(a)** Coke particle floated on top of gray metal. Section chosen to become sample is indicated by red outliner. Slag has formed on the crucible interface above the metal phase, seen as blue color behind the epofix **(b)** Section chosen for EPMA

(a) 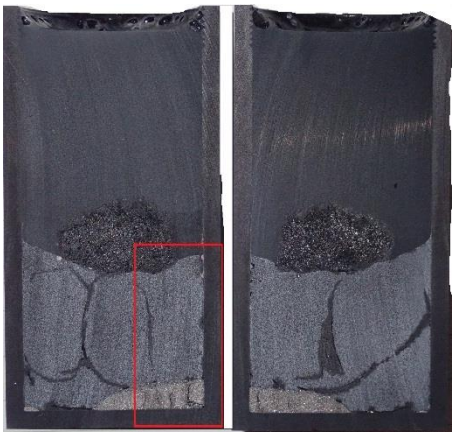 (b) 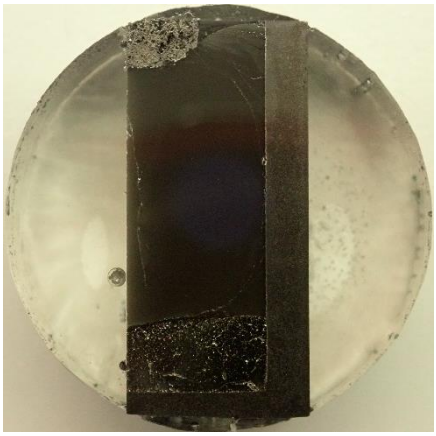

Figure 27: Sample from experiment 2 **(a)** Coke particle floated on top of gray slag. The metallic-gray metal has sunk to the bottom. The darker parts of the slag are moisture **(b)** Section chosen for EPMA

(a) 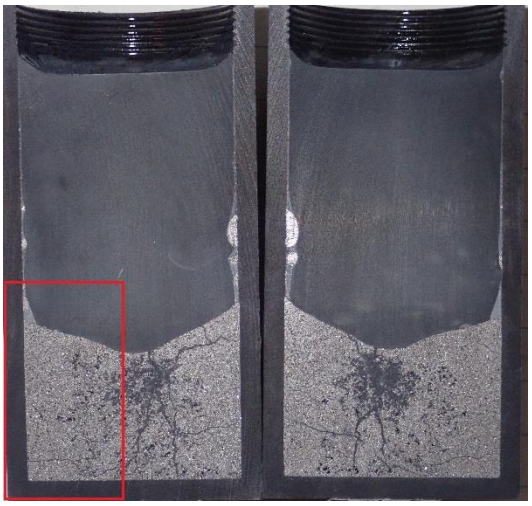 (b) 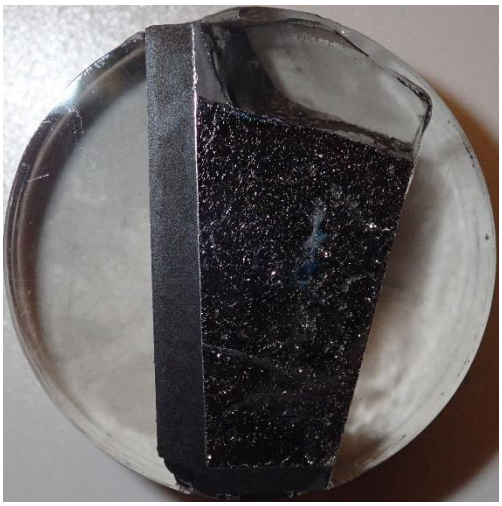

Figure 28: Sample from experiment 3 **(a)** Metallic-gray metal has solidified on the bottom while slag has solidified by the crucible interface on top of the metal. Some can be seen in the upper corners of the metal phase as a lighter gray tone. Some metal particles can also be seen to have crept up the crucible wall **(b)** Section chosen for EPMA

(a) 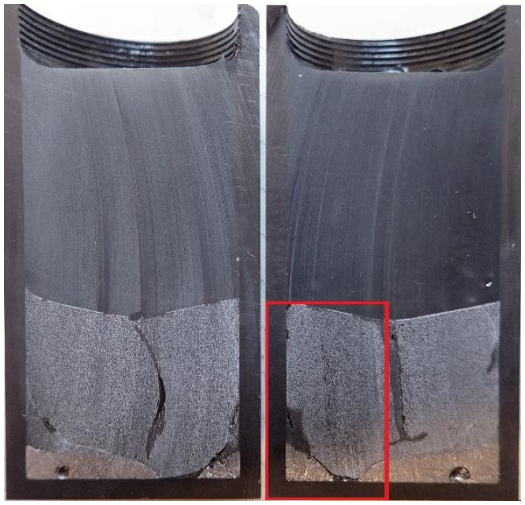 (b) 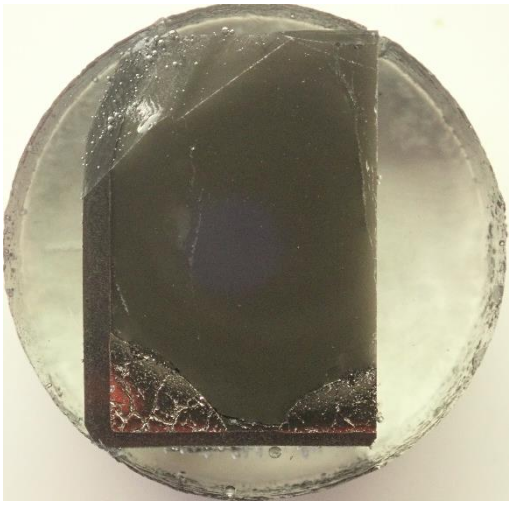

Figure 29: Sample from experiment 4 **(a)** Metal has solidified on the bottom in contact with the crucible walls, while slag has solidified on top. The darker contours in the slag phase is moisture **(b)** Section chosen for EPMA

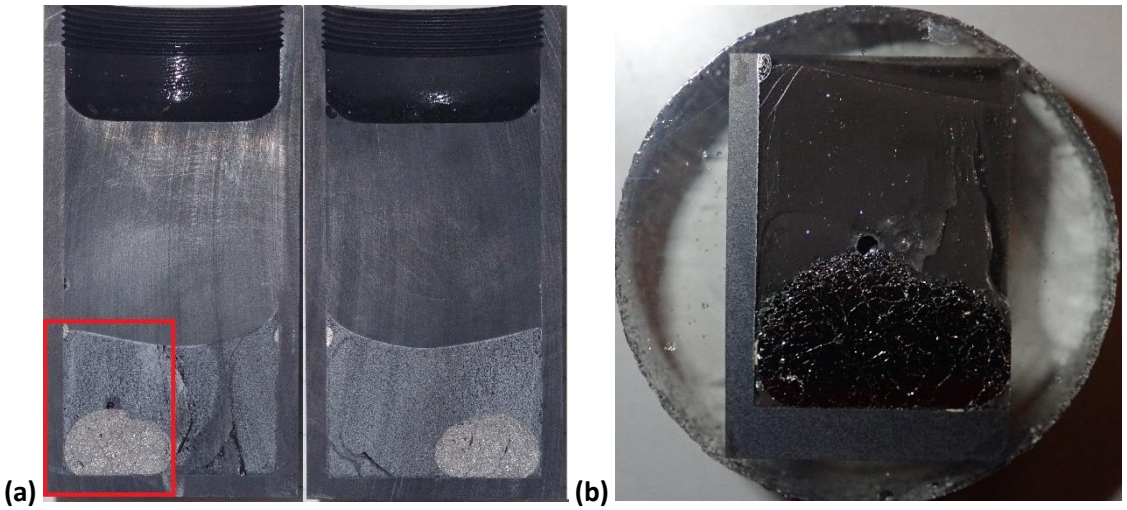

Figure 30: Sample from experiment 5 **(a)** Metal has solidified on the bottom in contact with the crucible wall, while slag has solidified on top. Droplets of metal can be seen on the top edges of the slag **(b)** Section chosen for EPMA

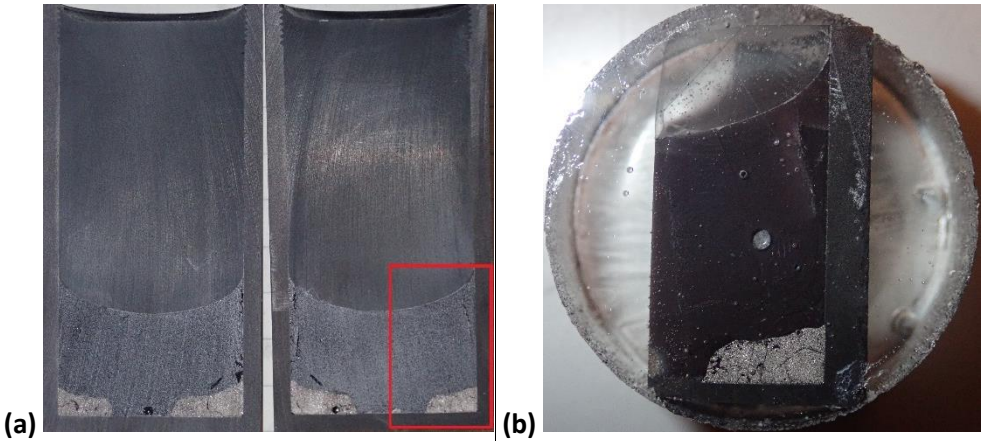

Figure 31: Sample from experiment 6 **(a)** Metal has solidified on the bottom in contact with the crucible walls and slag on top **(b)** Section chosen for EPMA

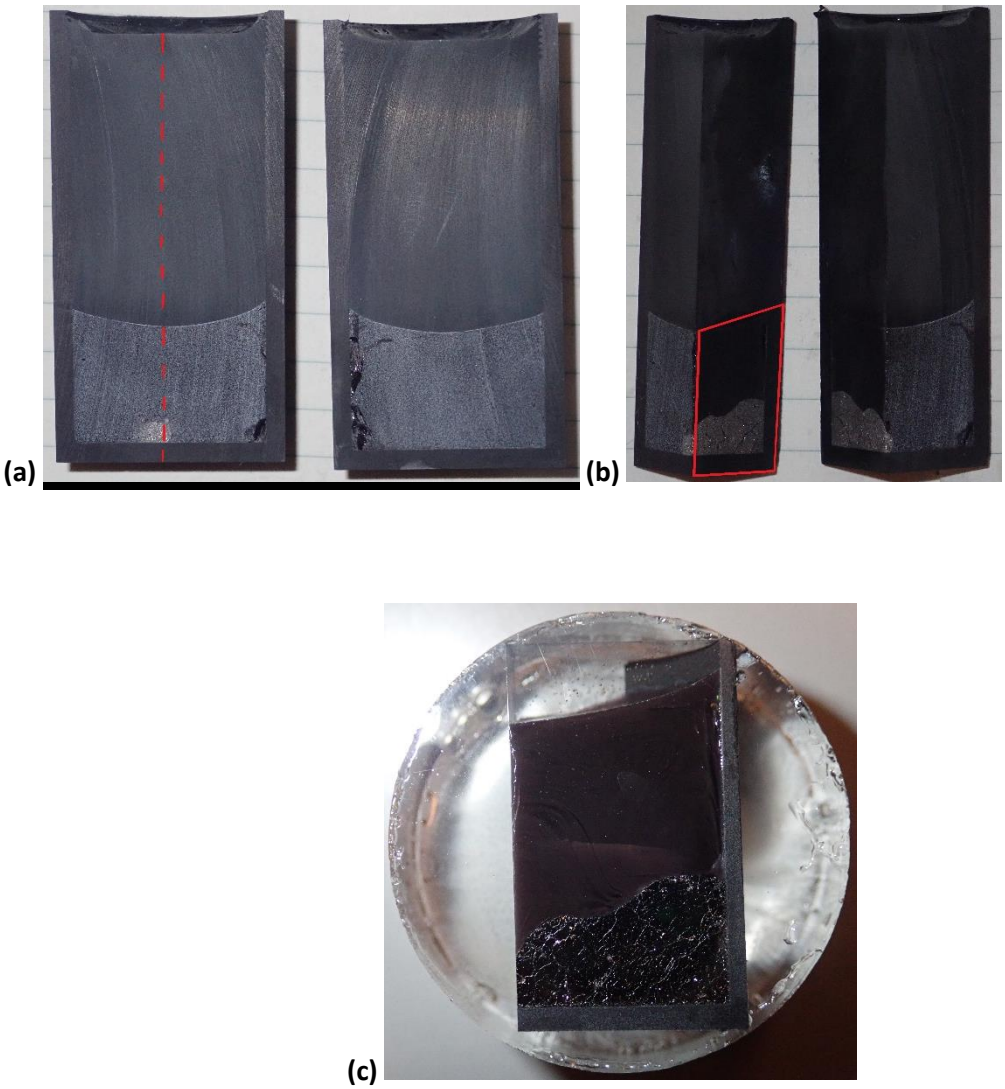

Figure 32: Sample from experiment 7 **(a)** Metal has solidified on the bottom and slag on top. Sample was cut vertically **(b)** Sample was cut vertically again to achieve the desired cross section **(c)** Section chosen for EPMA

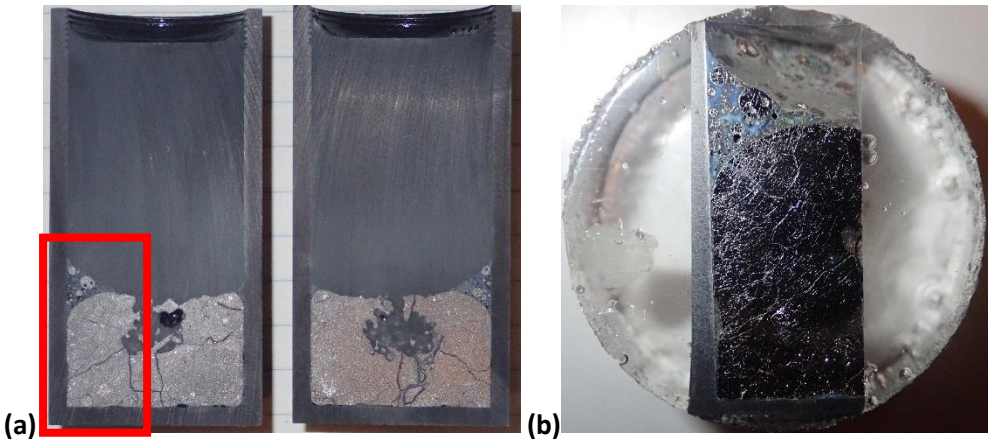

Figure 33: Sample from experiment 8 **(a)** Metal has solidified on the bottom and slag has formed on top, in the corners by the crucible wall **(b)** Section chosen for EPMA

(a) 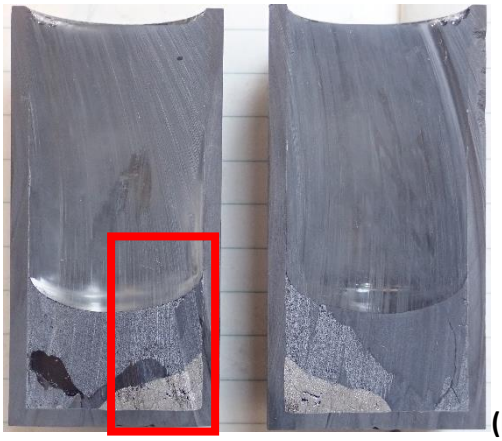 (b) 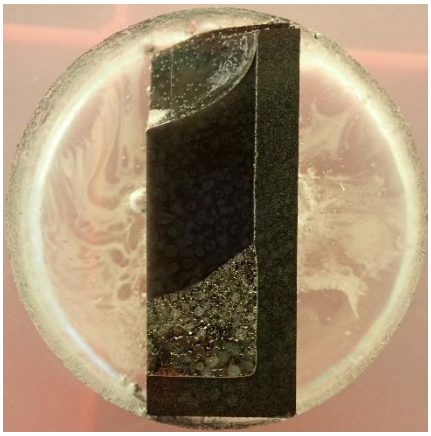

Figure 34: Sample from experiment 9 **(a)** Metal has solidified on the bottom in contact with the crucible wall and slag on top **(b)** Section chosen for EPMA

(a) 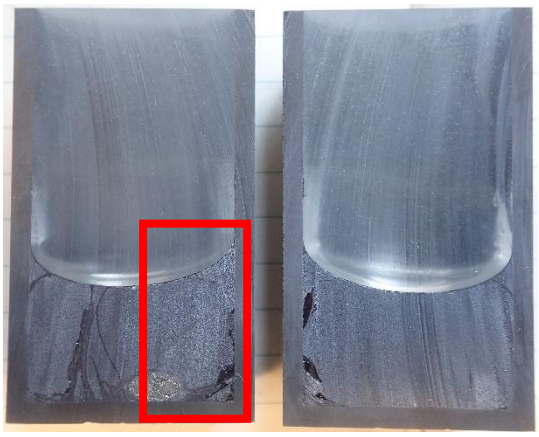 (b) 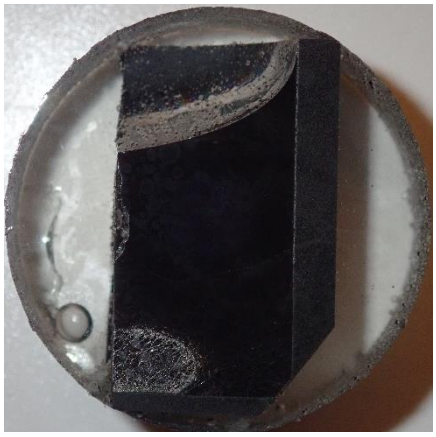

Figure 35: Sample from experiment 10 **(a)** Metal has solidified on the bottom and slag on top **(b)** Section chosen for EPMA

(a) 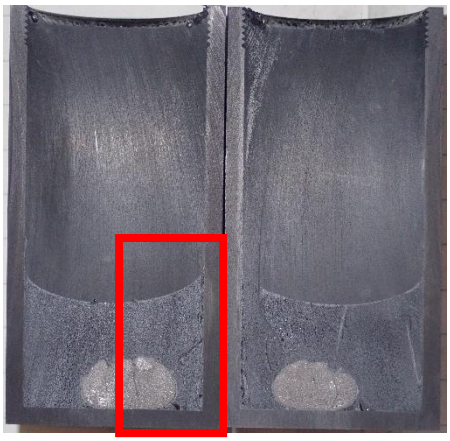 (b) 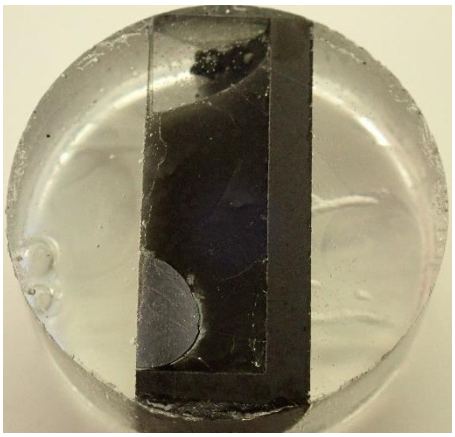

Figure 36: Sample from experiment 11 **(a)** Metal has solidified on the bottom and slag on top **(b)** Section chosen for EPMA

(a) 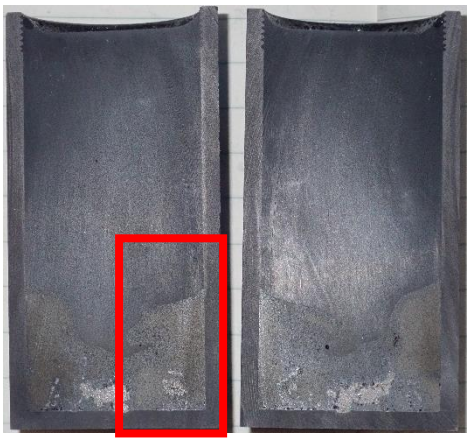 (b) 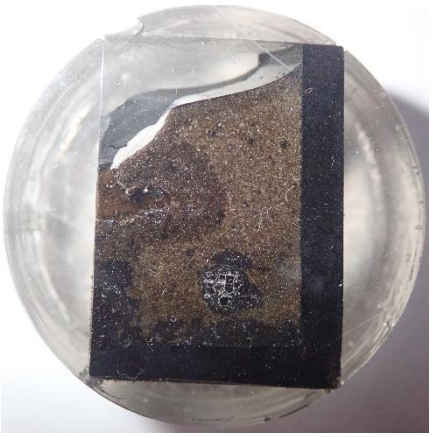

Figure 37: Sample from experiment 12 **(a)** Metal has solidified on the bottom and slag on top. Some of the metal has dispersed throughout the lower part of the slag. A large cavity has formed in the middle of the sample, with opening to the surface **(b)** Section chosen for EPMA

(a) 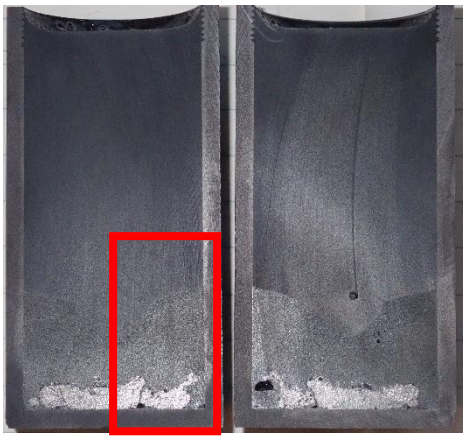 (b) 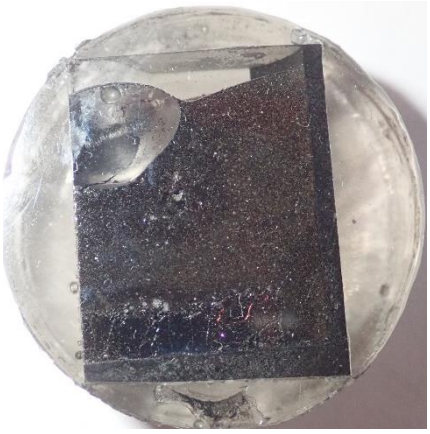

Figure 38: Sample from experiment 13 **(a)** Metal has solidified on the bottom and slag on top. A large cavity has formed in the middle of the sample, with opening to the surface **(b)** Section chosen for EPMA

(a) 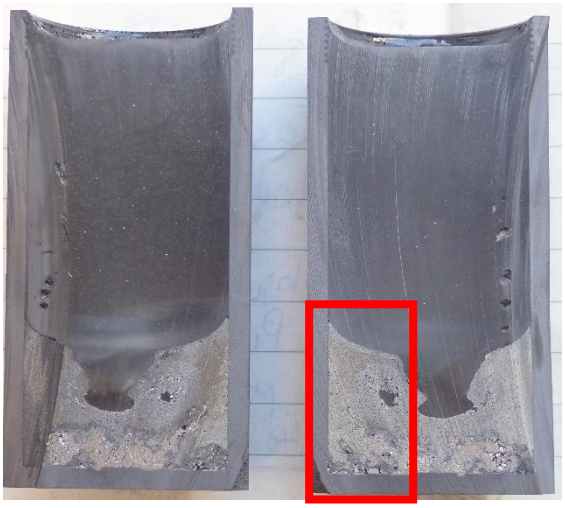 (b) 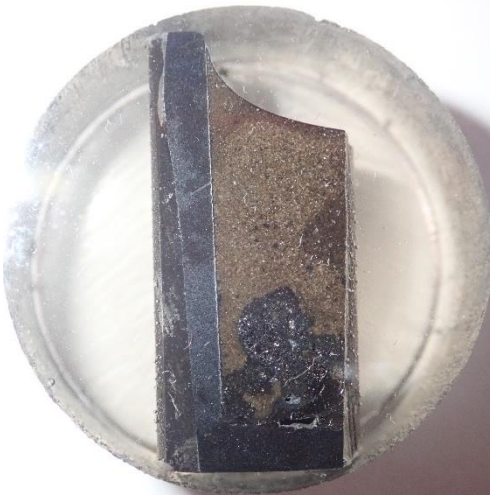

Figure 39: Sample from experiment 14 **(a)** Metal has solidified on the bottom and slag on top. A large cavity has formed in the middle of the sample, with opening to the surface **(b)** Section chosen for EPMA

(a) 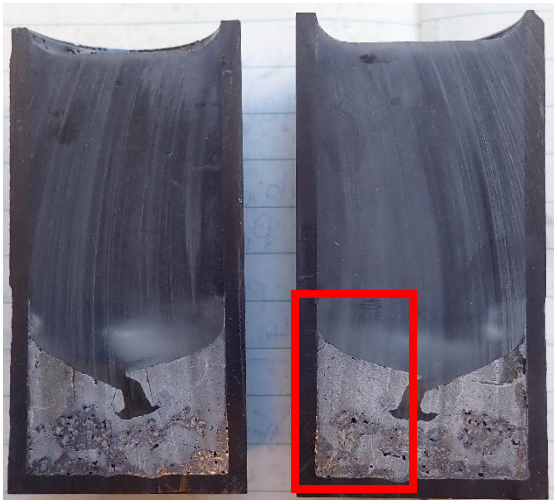 (b) 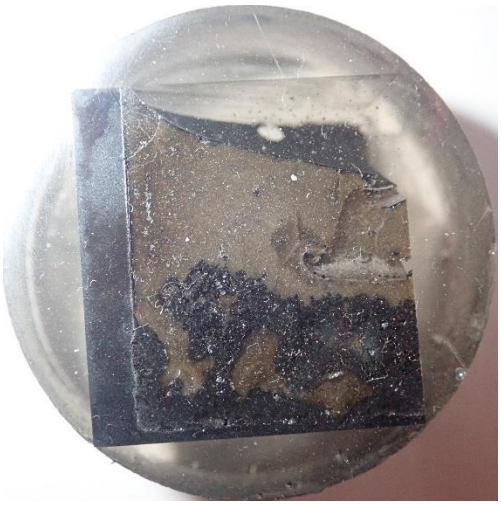

Figure 40: Sample from experiment 15 **(a)** Metal has solidified on the bottom and slag on top. The metal has dispersed throughout the bottom of the sample. A large cavity has formed in the middle of the sample, with opening to the surface **(b)** Section chosen for EPMA

(a) 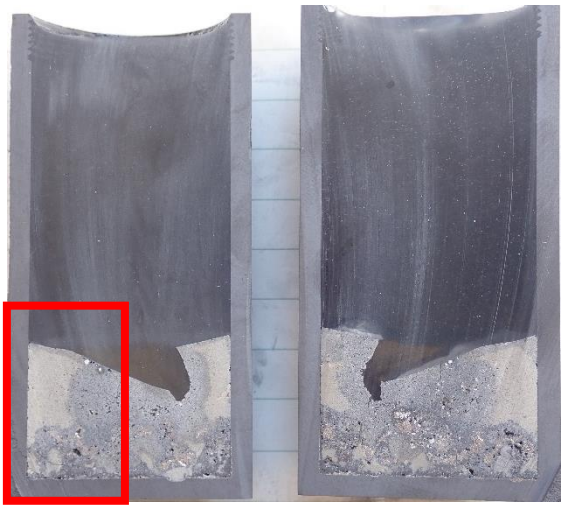 (b) 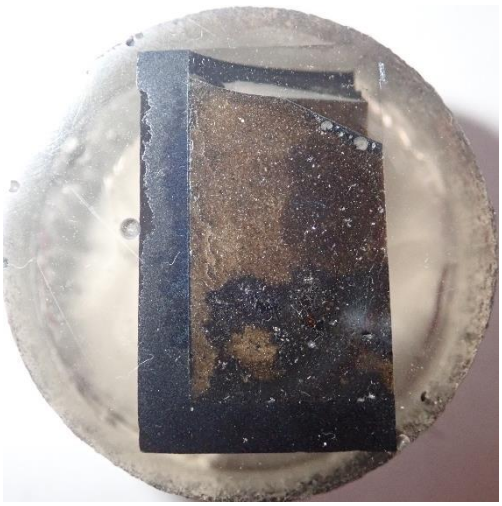

Figure 41: Sample from experiment 16 **(a)** Metal has solidified on the bottom and slag on top. The metal has dispersed throughout the bottom of the sample. A large cavity has formed in the middle of the sample, with opening to the surface **(b)** Section chosen for EPMA

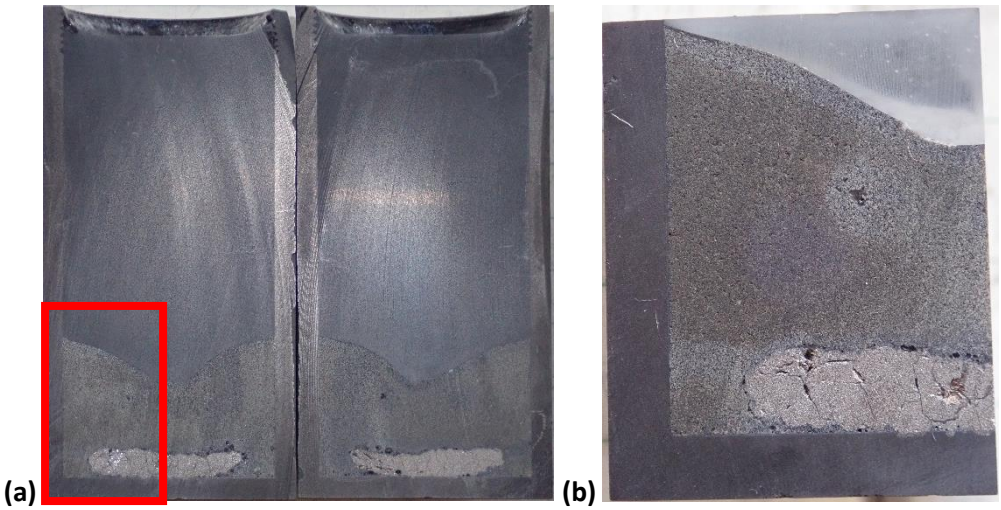

Figure 42: Sample from experiment 17 **(a)** Metal has solidified on the bottom and slag on top. A cavity has formed in the middle of the sample, with opening to the surface **(b)** Section chosen for EPMA

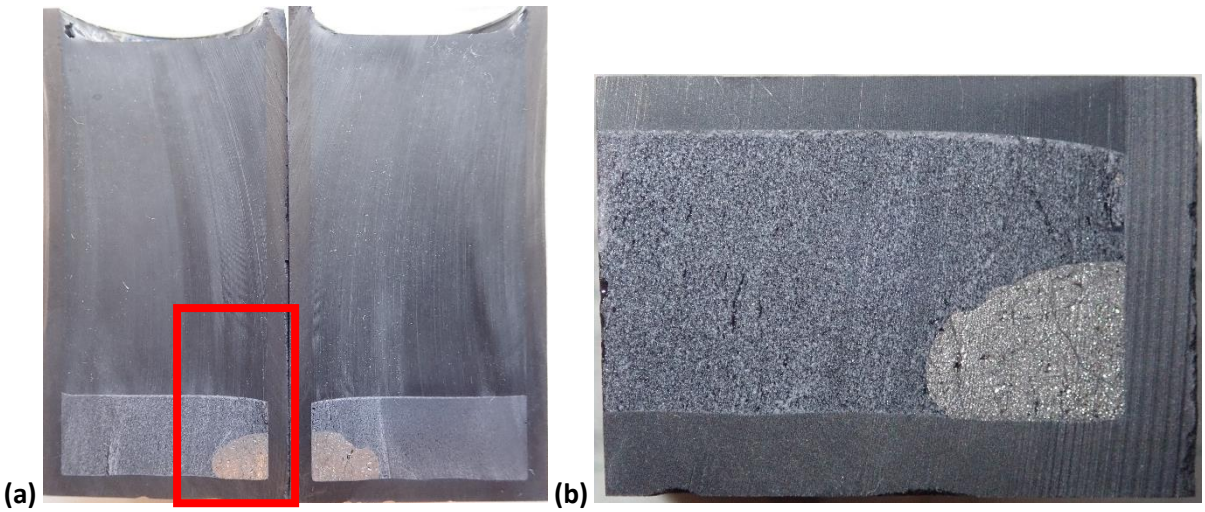

Figure 43: Sample from experiment 18 **(a)** Metal has solidified on the bottom in contact with the crucible wall and slag on top **(b)** Section chosen for EPMA

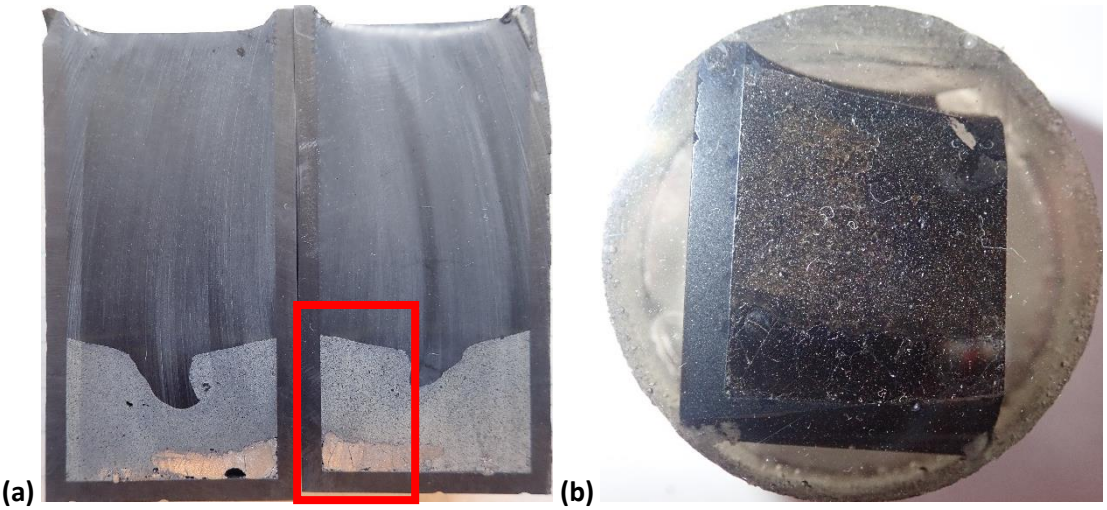

Figure 44: Sample from experiment 19 **(a)** Metal has solidified on the bottom in contact with the crucible wall and slag on top. A large cavity has formed in the middle of the sample, with opening to the surface **(b)** Section chosen for EPMA

In general, the metal has solidified in the bottom of the crucible, mostly as one large bulk which could indicate poor wetting between metal and slag. The slag has solidified on top and around the metal. Most of the slag and metal has stuck to the wall and the slag surface curves downwards towards the middle of the sample. This indicates good wetting properties towards the graphite crucible for both metal and slag. All experiments where slag containing 10wt.% TiO_2 has formed samples with larger cavities in the middle of the sample. Likely due to the change in slag properties by increased TiO_2 content.

4.2.3 Experiments using slag without titanium (Slag 1)

The results presented in this section are derived from four experiments carried out using slag containing no titanium, experiments: 2,4,5 and 11. Experiment 11 was not analyzed. An overview of the variables in the experiments is presented in Table 23and general observations in Table 24.

The main findings: No substantial amount of TiC has accumulated in the samples apart from a few particles in experiment 2. The metal and slag phases are similar in structure and composition.

Table 23: Experimental variables for experiments using slag containing no titanium

Experiment	Alloy	Slag	Temperature	Hold time
2	1 (20% Si)	1 (0% Ti)	1600	60
4	1 (20% Si)	1 (0% Ti)	1600	60
5	2 (29%Si)	1 (0% Ti)	1600	60
11	2 (29%Si)	1 (0% Ti)	1600	90

Table 24: General observations of TiC from experiments conducted with slag containing no titanium

Exp	Observations of TiC
2	A few particles of TiC were observed on the slag-metal interface
4	No TiC was observed in this sample
5	No TiC was observed in this sample
11	No TiC was observed in this sample

From the experiments using slag 1 there was observed no considerable amount of titanium carbide in the samples. There was observed insignificantly small amounts of TiC in sample 2 on the slag-metal interface, likely due to small amounts of Ti in the alloy. Only one experiment resulted in the formation of substantial amounts of carbide where silicon carbide was found in the sample from experiment 5.

Apart from the carbides observed, experiments 2, 4 and 5 were similar. The samples from these experiments contained a two-phased metal and a homogenous slag, with similar composition amongst the experiments, presented in Table 26 and 27, respectively. Figure 45 presents the structure of the metal and slag in experiment 4, this structure is similar to that found in 2 and 5.

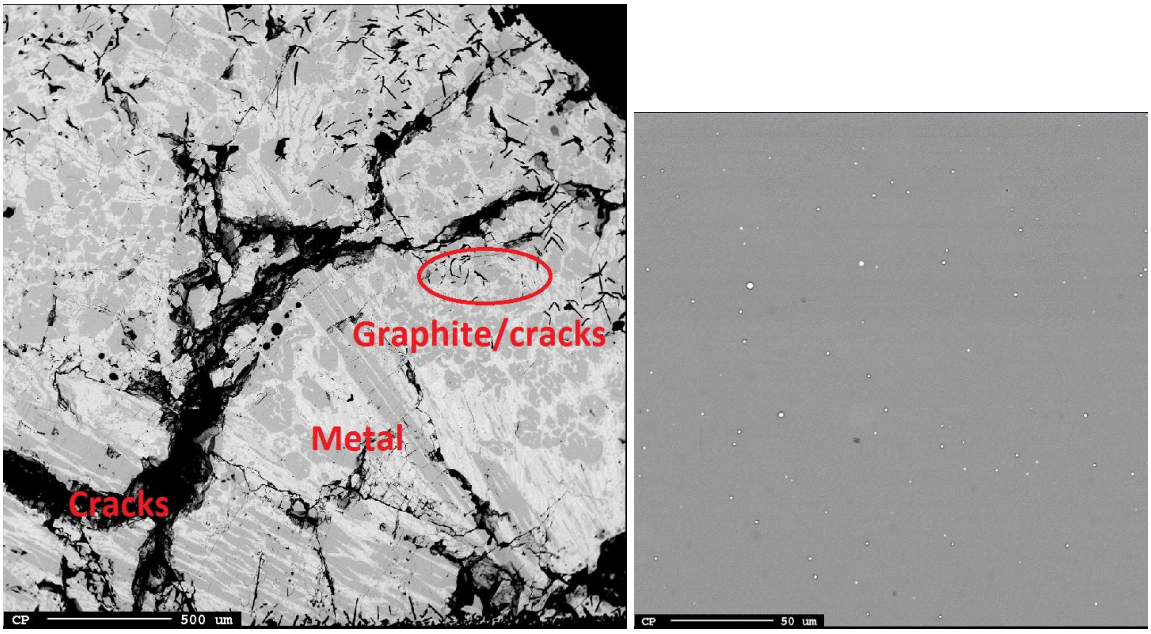

Figure 45: Sample from experiment 4 **(a)** Metal structure with a lot of cracks. The smaller cracks that are seen in the structure is a mix of graphite and cracks **(b)** The structure of the slag phase. The small white particles are metal droplets

The metal phase contains a lot of smaller and larger cracks, this can be seen in Figure 45 (a). Some of the smaller cracks are graphite flakes/needles. Which ones that are graphite and which ones are cracks

is impossible to say without analyzing each and every one of them, which was not done. This metal structure, containing both cracks and graphite was found in sample 2 as well. In sample 5 however, there was no graphite, only SiC. In Figure 45 (b) is the slag phase of sample 4. It was observed that the slag is a homogenous slag with small metal inclusions, this is also seen in sample 2 and 5.

Table 25: Chemical composition of the metal found in samples 2,4 and 5 along with the original composition of the metal used. Values are given in mass%

Experiment	Mn	Fe	Si	C
2	71,7	11,4	16,0	0,5
4	70,4	11,2	17,7	0,5
Original composition	65,4	11,9	19,7	1,5
5	68,0	9,9	23,1	0,4
Original composition	58,7	10,3	29,4	0,4

Table 26: Chemical composition of the slag found in samples 2,4 and 5 along with the original composition of the slag used. Values are given in mass%

Experiment	**Si**	**O**	**C**	**Mn**	**Mg**	**Al**	**Ca**
2	20,8	42,0	0,3	6,1	6,4	8,8	16,5
4	20,8	43,4	0,4	6,2	6,4	8,9	16,5
5	21,3	43,4	0,4	4,8	6,4	9,0	16,8
Original	19,8	42.5	0,0	7,3	4,1	9,4	16,9

From Table 25 it can be observed that the samples have increased Mn content in the metal phase, but the Si content has notably decreased. For sample 2 and 4 carbon in the original metal has reacted or precipitated. Smaller areas of graphite were observed in the metal phase of sample 2 and 4. The graphite was found in some of the cracks in the metal phase. It is important to mention that most of the cracks did not contain graphite, and graphite was hard to detect. Due to the size of the graphite particles found it was also hard to analyze, the contents were varying but certain areas contained graphite with high enough Si content to indicate the commencement of SiC formation.

The Si, C and Mg content of the slag has increased for all three samples compared to the original composition, while the Mn content of the slag has notably decreased, particularly for experiment 5. The exact values are presented in Table 27.

4.2.4 Experiments using slag containing 1wt.% TiO_2 (slag 2)

The results presented in this section are derived from five experiments carried out using slag containing 1wt.% TiO_2, experiments: 6, 7, 9, 10 and 18. An overview of the variables in the experiments is presented in Table 27 and general observations in Table 28. The composition of the metal and the slag found in the samples is presented in Table 29 and 30, respectively.

The main findings: TiC was observed in all samples, along the crucible interface and on the slag-metal interface. Metal has crept up with the belt of TiC along the crucible wall interface. More TiC was observed along the crucible interface above the slag-metal boundary, decreasing towards the bottom. TiC has penetrated the pores of the crucible for all experiments. The TiC particles found on the slag-metal interface are in general larger than the particles found by the crucible interface. In experiment 9 TiC was also found in the bulk of the metal. The amount of TiC observed has increased with temperature and decreasing Si content in the alloy.

Table 27: Experimental variables for experiments using slag containing 1wt.% TiO_2

Experiment	Alloy	Temperature	Hold time
6	1 (20% Si)	1600	60
7	2 (29% Si)	1600	60
9	1 (20% Si)	1650	60
10	2 (29% Si)	1650	60
18	2 (29% Si)	1600	60

Table 28: General observations of TiC from experiments conducted using slag containing 1wt.% TiO_2

Experiment	**Observations of TiC**
6	TiC and metal were found along the entire crucible interface, most prominent on the upper half, above the slag-metal boundary. Larger TiC particles were observed along the slag-metal interface.
7	TiC particles (1-3µm) were found in a belt of slag and metal along the entire crucible bottom interface. Larger TiC particles (~50µm) were observed by the slag-metal interface on the metal side close to the crucible, tough not very frequent.
9	TiC and metal were found along the entire crucible interface, most prominent on the upper half, above the slag-metal boundary. TiC was also observed in the bulk of the metal and along the entire slag-metal interface as larger particles.
10	TiC particles (1-3µm) were found in a belt of slag and metal along the entire crucible bottom interface. Larger TiC particles (~50µm) were observed by the slag-metal interface on the metal side close to the crucible, tough not very frequent.
18	TiC and metal were observed along the entire crucible interface. TiC was also found on the slag-metal interface, decreasing with increasing distance from the

	crucible. Some TiC was also observed in the bulk of the metal, associated to cracks and pores.

Table 29: Chemical composition of the metal found in samples 6, 7, 9, 10 and 18. Values are given in mass%

Experiment	Si	C	Mn	Fe	Ti	Mn/Fe-ratio	Std. Dev.
6	17,4	0,4	71,1	10,7	0,4	6,6	
7	25,2	0,4	66,1	9,7	0,7	6,8	
9	19,3	0,4	70,2	11,2	0,2	6,3	±0,81
10	24,2	0,3	66,7	9,7	0,6	6,9	
18	22,8	0,5	69,1	9,6	0,4	7,2	

Table 30: Chemical composition of the slag found in samples 6, 7, 9, 10 and 18 along with the original composition of the slag used. Values are given in mass%

Experiment	Si	O	C	Mn	Mg	Al	Ca	Ti
6	21,8	41,1	0,3	6,0	6,2	8,8	16,5	0,3
7	21,1	42,5	0,4	5,5	6,2	8,8	16,7	0,5
9	21,9	38,5	0,3	4,9	6,3	9,0	17,4	0,3
10	22,7	40,1	0,4	3,4	6,3	9,0	17,0	0,3
18	22,6	37,9	0,5	4,8	5,3	8,8	15,8	0,4
Original composition	19,7	42,6	0,0	7,2	4,3	9,5	16,1	0,6

TiC was observed in all the experiments using slag containing 1wt.% TiO_2. The calculated amount of TiC based on mass calculations is presented in Table 31.

Table 31: Mass TiC in experiments 6, 7, 9, 10 and 18

Experiment	Ti for carbide [g]	% of total Ti	Ti-C [g]
6	0,06	25,8	0,07
7	-0,01	-6,6	-0,02
9	0,09	40,0	0,12
10	0,07	34,7	0,10
18	0,02	17,2	0,03

From Table 32 it can be observed that the experiments conducted at 1650°C appears to have formed more TiC than the experiments conducted at 1600°C. From the 20% Si samples, the amount of TiC has

increased from 0.07 (exp. 6) to 0.12 (exp. 9) grams of TiC. From the 29% Si samples, the amount of TiC has increased from -0.02 (exp. 7) and 0.03 (exp. 18) to 0.10 grams (exp. 10) of TiC.

The slag found in the samples is a homogenous slag and the metal is two-phased, similar to what presented in Figure 45. All samples were found to have grains of TiC on the entire length of interface between the sample and the crucible. All samples also had metal creeping up the entire crucible wall interface, between the slag and crucible. Figure 46 (a) shows an example of the belt of TiC and metal along the crucible wall interface. The belt of TiC along the crucible bottom however did not include metal but was likely in contact with the metal face prior to solidification. Penetration of TiC into the crucible pores was observed along the crucible bottom as seen in Figure 46 (b). This was observed for all the low-Ti samples.

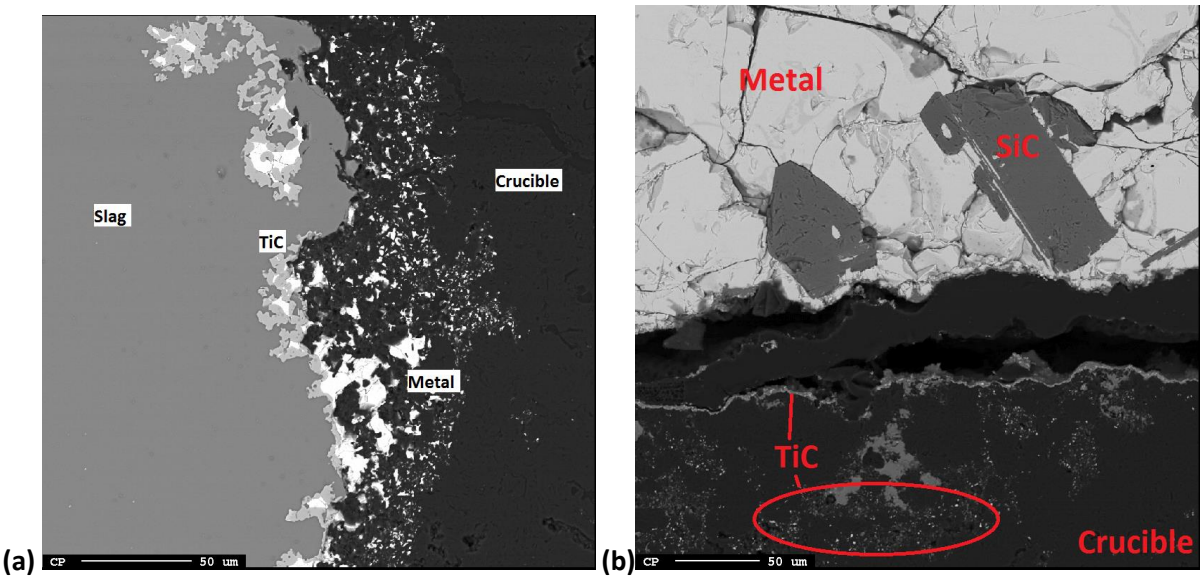

Figure 46: Example of microstructure of the low-Ti samples **(a)** Sample from experiment 6. TiC and metal can be seen as a belt along the crucible interface **(b)** Sample from experiment 10. TiC can be seen as a belt along the crucible bottom interface as well as penetrating the pores in the crucible.

The TiC in Figure 46 (b) is situated on the metal-crucible interface, the dark phase in between is epoxy that has settled in a crack between the metal and crucible caused by shrinkage during solidification. In general, more TiC has settled along the crucible wall as opposed to crucible bottom.

TiC was also found on the interface between the metal and the slag for all samples as presented in Figure 47. In terms of size, TiC particles found on the slag-metal interface are larger than the TiC found by the crucible interface, although less frequent.

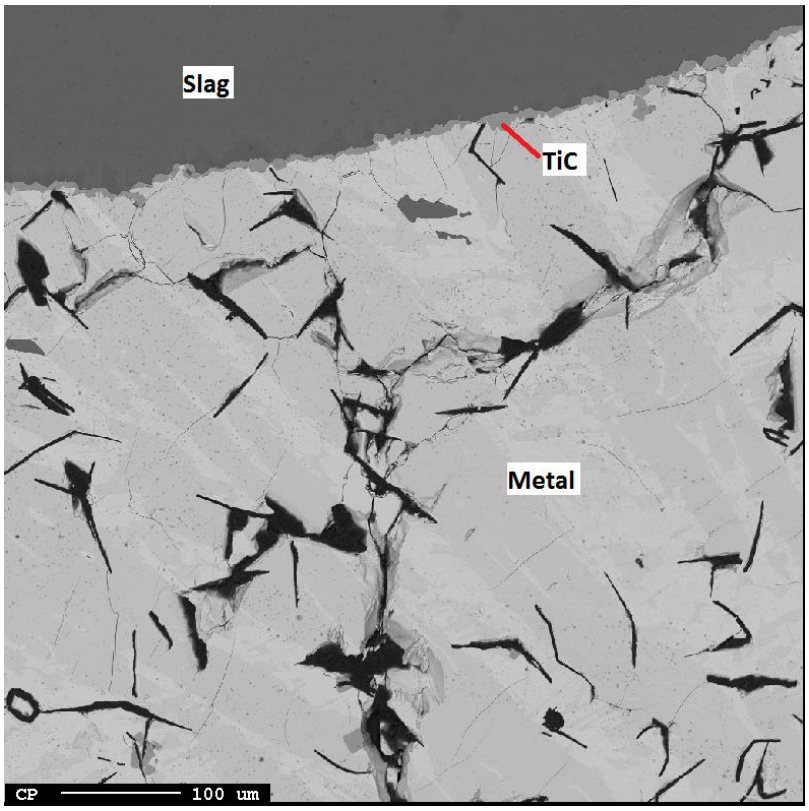

(a)

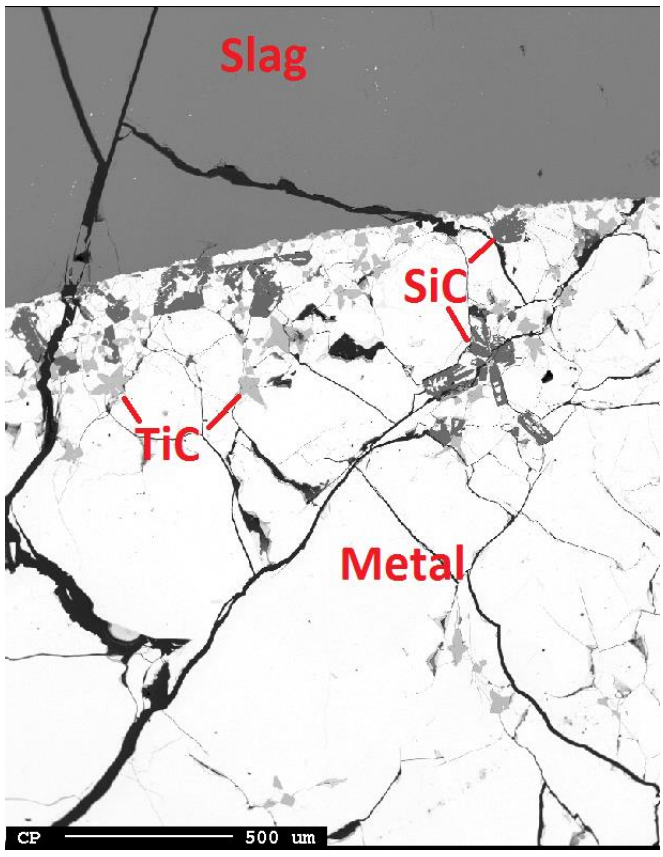

(b)

Figure 47: Example of microstructure of low-Ti samples **(a)** From experiment 6. A belt of TiC can be seen along the slag-metal interface. The cracks in the metal is a mix of cracks and graphite **(b)** From experiment 18. TiC has dispersed as particles along the slag-metal interface as opposed to a uniform belt

The TiC was either found as a belt of TiC along the interface for experiments 6 and 9 which can be seen in Figure 47 (a), or as larger dispersed particles along the interface for experiments 7, 9, 10 and 18 as seen in Figure 47 (b). TiC was also found in the bulk of the metal phase, however only for experiment 9 conducted at 1650°C. No TiC was observed in the bulk of the slag phase. The larger dispersed particles are located inside the metal phase, whereas the TiC belt is a separate phase between the slag and metal. The amount of TiC and SiC decreased with increasing distance from the crucible. TiC was observed further away from the crucible than SiC. SiC was observed for all the samples, except for sample 6. Graphite had formed in sample 6 as observed in Figure 47 (a).

4.2.5 Experiments using slag containing 10wt.% TiO_2 (slag 3)

The results presented in this section are derived from seven experiments carried out using slag containing 10wt.% TiO_2, experiments: 12, 13, 14, 15, 16, 17 and 19. An overview of the variables in the experiments is presented in Table 32 and general observations in Table 33. The chemical composition of the metal and the slag is presented in Tables 34 and 35, respectively.

The main findings: TiC was observed in all samples. More TiC was observed in samples conducted at higher temperatures and with lower Si content in the alloy. More TiC has accumulated compared to experiments at 1wt.% TiO_2 in the slag and found to a larger degree in the bulk of the metal and slag. Most of the TiC is found on or close to the slag-metal interface for these samples. It has also been observed that less SiC has accumulated compared to the experiments conducted with 1wt.% TiO_2 in the slag.

Table 32: Experimental variables for experiments using slag containing 10wt.% TiO_2

Experiment	Alloy	Temperature	Hold time
12	1 (20% Si)	1600	60
13	2 (29% Si)	1600	60
14	2 (29% Si)	1650	60
15	1 (20% Si)	1650	60
16	1 (20% Si)	1600	90
17	2 (29% Si)	1600	90
19	2 (29% Si)	1600	60

Table 33: General observations of TiC from experiments conducted with slag containing 10wt.% TiO_2

Exp	Observations of TiC

12	A belt of TiC along entire crucible interface. By the crucible bottom, the TiC has settled on the slag-metal boundary. TiC was also observed around metal particles and pores in the bulk of the slag, close to the bulk metal.
13	A belt of TiC was found along the entire crucible interface. TiC was also observed on the slag-metal interface as larger particles, as well as inside the slag phase around metal particles, close to the bulk metal.
14	A belt of TiC was found along the entire crucible interface. Some metal and slag were found in the crucible further down in the sample. TiC was also observed on the slag-metal interface as larger particles, as well as inside the metal and slag phase, close to the slag-metal interface. TiC was also found in the bulk of the metal.
15	A belt of TiC was found along the entire crucible interface. TiC was also observed on the slag-metal interface as larger particles, as well as inside the metal and slag phase, close to the slag-metal interface. TiC was also found in the bulk of the metal.
16	A belt of TiC was found along the entire crucible interface. TiC was also observed on the slag-metal interface as larger particles, as well as inside the slag phase around metal particles, close to the bulk metal.
17	TiC was found along the entire crucible interface, decreasing towards the bottom. TiC was also observed on the slag-metal interface and to a certain degree in the slag around metal particles, close to the bulk metal.
19	TiC was found along the entire crucible interface, decreasing towards the bottom. TiC was also observed on the slag-metal interface.

Table 34: Chemical composition of the metal found in samples 12, 13, 14, 15, 16, 17 and 19. Values are given in mass%

Experiment	Si	C	Mn	Fe	Ti	Mn/Fe-ratio	Std. Dev.
12	19,1	0,4	69,5	12,3	0,2	5,6	
13	25,8	0,3	63,9	11,3	1,2	5,6	
14	18,2	0,4	71,4	10,6	0,2	6,7	
15	19,5	0,4	69,7	14,2	0,1	4,9	±0,45
16	18,5	0,5	68,7	14,8	0,1	4,6	
17	24,3	0,5	66,1	11,0	1,2	6,0	
19	26,1	0,5	62,9	11,8	1,0	5,3	±0,76

Table 35: Chemical composition of the slag found in samples 12, 13, 14, 15, 16, 17 and 19 along with the original composition of the slag used. Values are given in mass%

Experiment	Si	O	C	Mn	Mg	Al	Ca	Ti
12	20,7	37,6	0,3	6,8	6,1	7,9	14,8	2,9
13	20,3	36,9	0,3	5,2	6,1	6,9	14,8	5,4
14	23,8	39,0	0,4	4,8	5,1	8,3	14,9	0,3
15	21,5	36,2	0,5	7,9	5,9	7,9	14,7	1,2
16	21,0	35,8	0,5	9,0	5,1	7,6	14,2	2,5
17	20,0	36,4	0,5	6,1	5,1	7,6	14,6	5,6
19	19,9	36,8	0,5	5,8	5,4	7,6	14,5	5,5
Original composition	17,9	42,3	0,0	6,6	3,7	8,5	15,2	5,8

All the samples had a close to homogenous slag. The samples that did not have a completely glassy slag had different phases but with similar chemical composition. All the samples also had a two-phased metal, similar to what can be seen in Figure 45 (a). TiC was observed in all the experiments using a slag containing 10wt.% TiO_2. The calculated amount of TiC based on mass calculations is presented in Table 36. It is worth to mention that the calculations of mass TiC goes over well when compared to the BSE images of the samples.

Table 36: Mass TiC in experiments 12-17 and 19

Experiment	Ti for carbide [g]	% of total Ti	Ti-C [g]
12	1,14	55,2	1,51
13	0,47	23,1	0,61
14	1,90	93,9	2,51
15	1,58	78,6	2,16
16	1,08	52,8	1,45
17	0,26	12,6	0,33
19	0,09	4,5	0,12

For the 29% Si alloy, 10% TiO_2, 1600°C experiments (13 and 19), increasing the temperature by 50°C will increase the amount of TiC in the sample considerably, based on the mass calculations presented in Table 36. Experiment 13 and 19 was calculated to have 0.12g and 0.61g of TiC, while experiment 14 to have 2.51g of TiC. The same effect was observed for the 20% Si alloy, 10% TiO_2, 1600°C experiment, where an increase in temperature by 50°C will increase the amount of TiC accumulated from 1.51g to 2.16g of TiC. The increase in hold time seems to have no effect on the amount of TiC accumulating.

As for the experiments conducted using slag containing 1wt.% Ti, the samples were found to have grains of TiC on the entire interface between the slag and the crucible, however not infused with metal particles. Compared to the experiments conducted with low-Ti slag, the belt of TiC along the interface

had become much wider and more tightly packed. A comparison of the belts of TiC from low-Ti samples and High-Ti samples is presented in Figure 48.

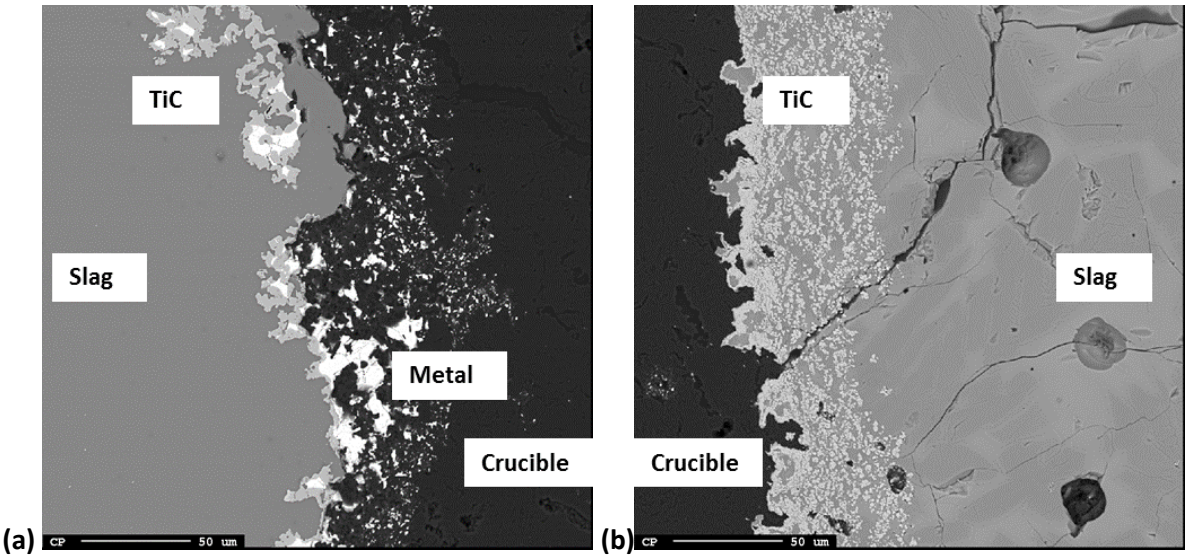

Figure 48: Comparison of microstructure of low-Ti and high-Ti samples **(a)** Microstructure of sample 6 by the crucible wall **(b)** Microstructure of sample 19 by the crucible wall

TiC was also observed in the bulk of the metal phase, and in the bulk of the slag phase along with metal particles. This can be observed in Figure 49 (a) and (b). TiC in the bulk of the metal was only observed for experiments conducted at 1650°C.

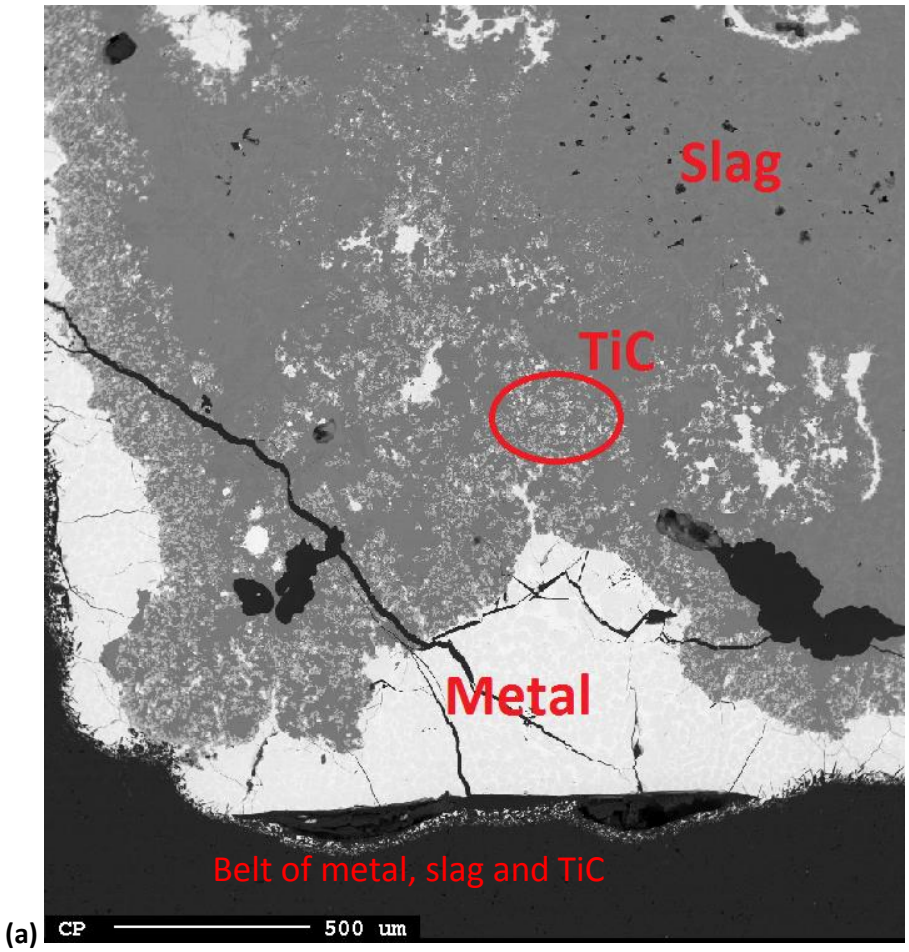

(a)

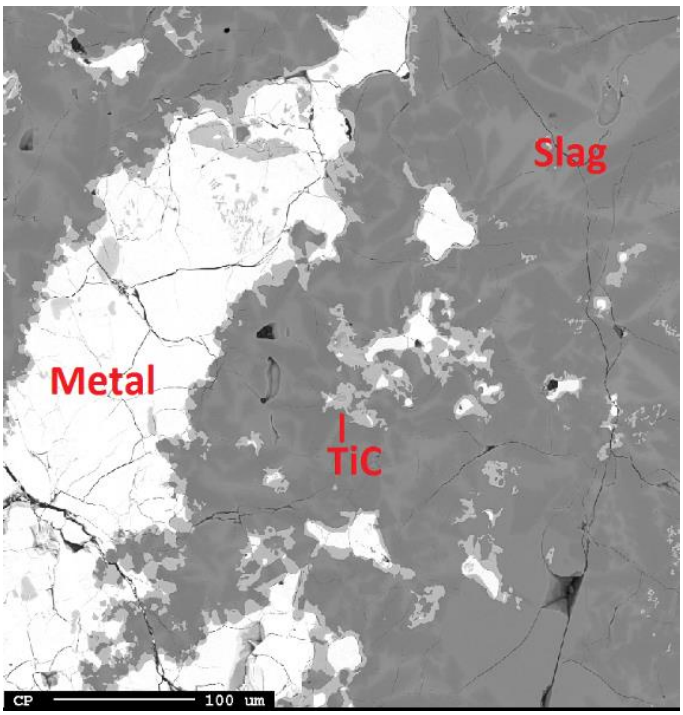

(b)

Figure 49: Example of microstructure of the high-Ti samples (a) Microstructure close to the crucible corner of sample 14. TiC (gray) can be seen in the slag phase (dark gray), around metal particles (white) and around the metal (white) by the crucible. Along the crucible bottom interface there is a TiC-metal belt (b) Microstructure

observed in the slag phase of sample 16. Metal and TiC is present, the TiC is present both inside the metal and on the periphery

The relative amount of TiC increased towards the crucible. TiC accumulation was most prominent on the slag-metal interface, with the largest amount on the bottom half. The TiC found along the crucible interface was most prominent on the top half and decreasing towards the bottom.

From the high-Ti experiments, SiC was observed in sample 13, 17 and 19 though only small amounts.

Table 37 presents a summary of where the TiC has been found in the samples.

Table 37: Location of TiC observed in the samples

Experiment	Crucible wall	Crucible bottom	Slag-metal interface	Bulk of metal	Bulk of slag (TiC+metal)
2 – No Ti	-	-	-	-	-
4 – No Ti	-	-	-	-	-
5 – No Ti	-	-	-	-	-
6 – Low Ti	X	X	X	-	-
7 – Low Ti	X	X	X	-	-
9 – Low Ti	X	X	X	X	-
10 – Low Ti	X	X	X	-	-
12 – High Ti	X	X	X	-	X
13 – High Ti	X	X	X	-	X
14 – High Ti	X	X	X	X	X
15 – High Ti	X	X	X	X	X
16 – High Ti	X	X	X	-	X
17 – High Ti	X	X	X	-	X
18 – High Ti	X	X	X	-	-
19 – High Ti	X	X	X	-	X

4.2.7 Experiments using metal containing 20wt.% Si (Std-SiMn-alloy)

The results presented in this section are derived from ten experiments carried out using an alloy containing 20wt.% Si, experiments: 1, 1.2, 2, 3, 4, 6, 9, 12, 15 and 16. An overview of the variables in the experiments is presented in Table 38. General observations of SiC and graphite is presented in Table 39. The composition of the metal and the slag found in the samples is presented in Table 40 and 41, respectively.

The main findings: SiC was only observed in experiment 1.2 and 9. With increasing Ti content, less graphite was observed. With increased temperature, SiC was observed in experiment 9, but not for experiment 15, that had a higher Ti-content.

Table 38: Experimental parameters for experiments 1, 1.2, 2, 3, 4, 6, 9, 12, 15 and 16

Experiment	Slag	Temperature	Hold time
1	-	1600	60
1.2	-	1600	60
2	1 (No Ti)	1600	60
3	-	1600	60
4	1 (No Ti)	1600	60
6	2 (Low Ti)	1600	60
9	2 (Low Ti)	1650	60
12	3 (High Ti)	1600	60
15	3 (High Ti)	1650	60
16	3 (High Ti)	1600	90

Table 39: General observations of SiC and graphite from experiments conducted with alloy containing 20wt.% Si

Exp	Observations of SiC and graphite
1	Graphite was observed in the bulk of the metal, no SiC was observed in the sample
1.2	SiC on coke-metal and coke-slag interface. Graphite was observed in the bulk of the metal
2	Graphite was observed in the bulk of the metal, no SiC was observed in the sample
3	No graphite or SiC was observed in the sample
4	Graphite was observed in the bulk of the metal containing smaller amounts of Si, no SiC was observed in the sample
6	Graphite was observed in the bulk of the metal, no SiC was observed in the sample
9	SiC was observed in the metal phase, close to the slag interface. No graphite was observed in the sample

12	No graphite or SiC was observed in the sample
15	No graphite or SiC was observed in the sample
16	No graphite or SiC was observed in the sample

Table 40: Chemical composition of the metal found in samples 1, 1.2, 2, 3, 4, 6, 9, 12, 15 and 16. Values are given in mass%

Experiment	Si	C	Mn	Fe	Ti	Mn/Fe-ratio	Std. Dev.
1	17,7	0,4	66,3	16,0	N.A.	4,2	
1,2	20,1	0,4	68,3	11,5	N.A.	5,9	
2	16,0	0,5	71,7	11,4	N.A.	6,3	
3	19,3	0,4	68,5	11,5	N.A.	6,0	
4	17,7	0,5	70,4	11,2	N.A.	6,3	
6	17,4	0,4	71,1	10,7	0,4	6,6	
9	19,3	0,4	70,2	11,2	0,2	6,3	±0,81
12	19,1	0,4	69,5	12,3	0,2	5,6	
15	19,5	0,4	69,7	14,2	0,1	4,9	±0,45
16	18,5	0,5	68,7	14,8	0,1	4,6	
Original Composition	19,7	1,5	65,4	11,9	0,3	5,5	

Table 41: Chemical composition of the slag found in samples 1, 1.2, 2, 3, 4, 6, 9, 12, 15 and 16. Values are given in mass%

Experiment	Si	O	C	Mn	Mg	Al	Ca	Ti
1	28,8	41,5	0,3	20,1	2,5	1,7	4,2	-
1,2	19,8	41,3	0,4	3,0	6,8	11,6	15,3	-
2	20,8	42,0	0,3	6,1	6,4	8,8	16,5	-
3	29,1	41,6	0,4	17,1	2,0	3,2	3,8	-
4	20,8	43,4	0,4	6,2	6,4	8,9	16,5	-
6	21,8	41,1	0,3	6,0	6,2	8,8	16,5	0,3
9	21,9	38,5	0,3	4,9	6,3	9,0	17,4	0,3
12	20,7	37,6	0,3	6,8	6,1	7,9	14,8	2,9
15	21,5	36,2	0,5	7,9	5,9	7,9	14,7	1,2
16	21,0	35,8	0,5	9,0	5,1	7,6	14,2	2,5

The graphite has reacted with the metal and/or slag for all the experiments. However, the formation of SiC was only observed in experiments 1.2 and 9. On the sample from experiment 1.2 SiC was found on the coke-slag interface and on the coke-metal interface as presented in Figure 50 (b) and (c) respectively. The sample from experiment 9 contains minor amounts of SiC, but mostly TiC, accumulating on the whole crucible interface as well as on the whole slag-metal interface. The SiC was only observed in the metal phase, close to the slag interface as presented in Figure 51 (c). Needles of graphite is also seen to penetrate the metal phase along the crucible bottom as presented in Figure 51 (b).

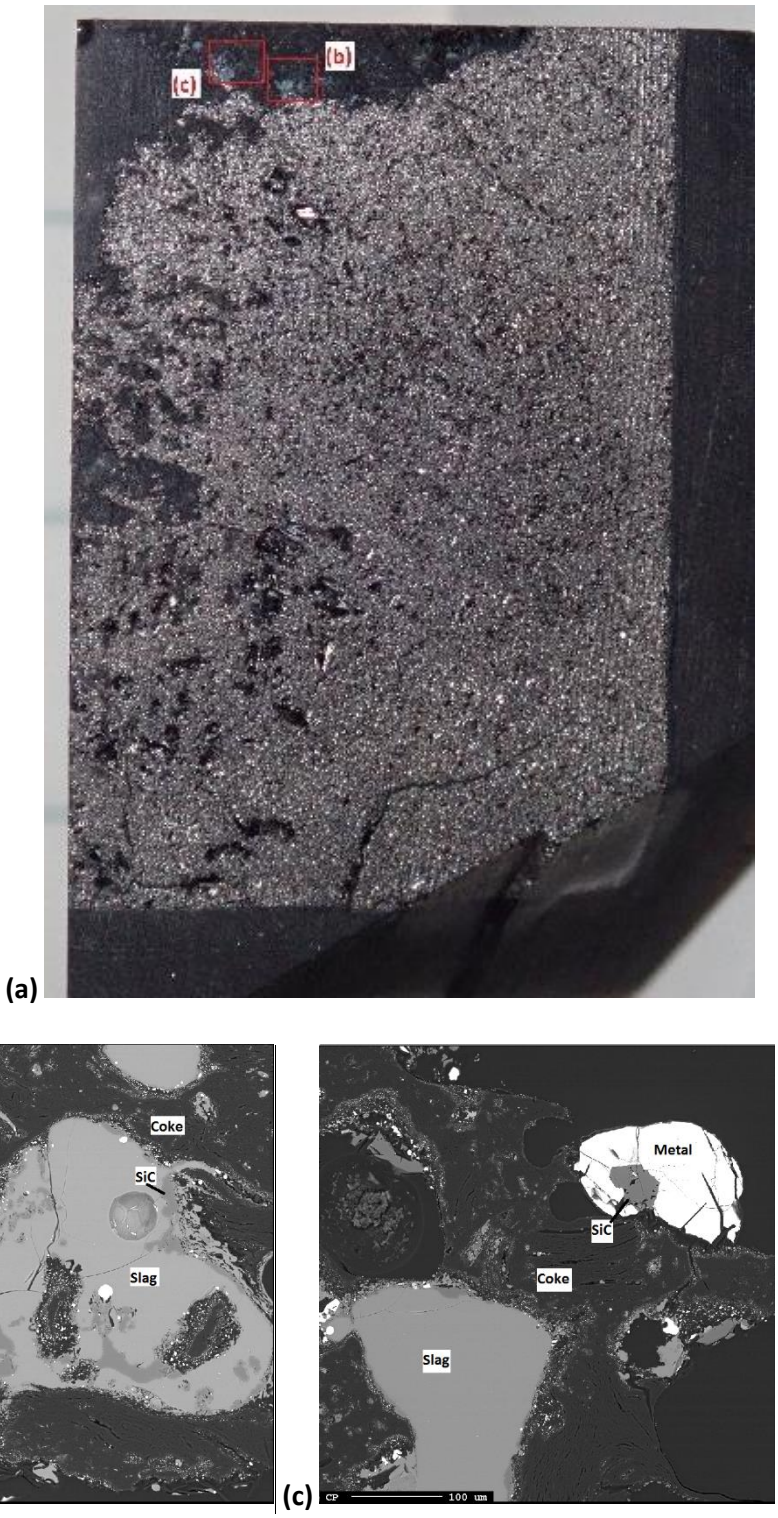

Figure 50: Sample from experiment 1.2: (a) Position of image (b) and (c) in the sample. **(b)** SiC found on the coke-slag interface. **(c)** SiC particle found on the metal-coke interface

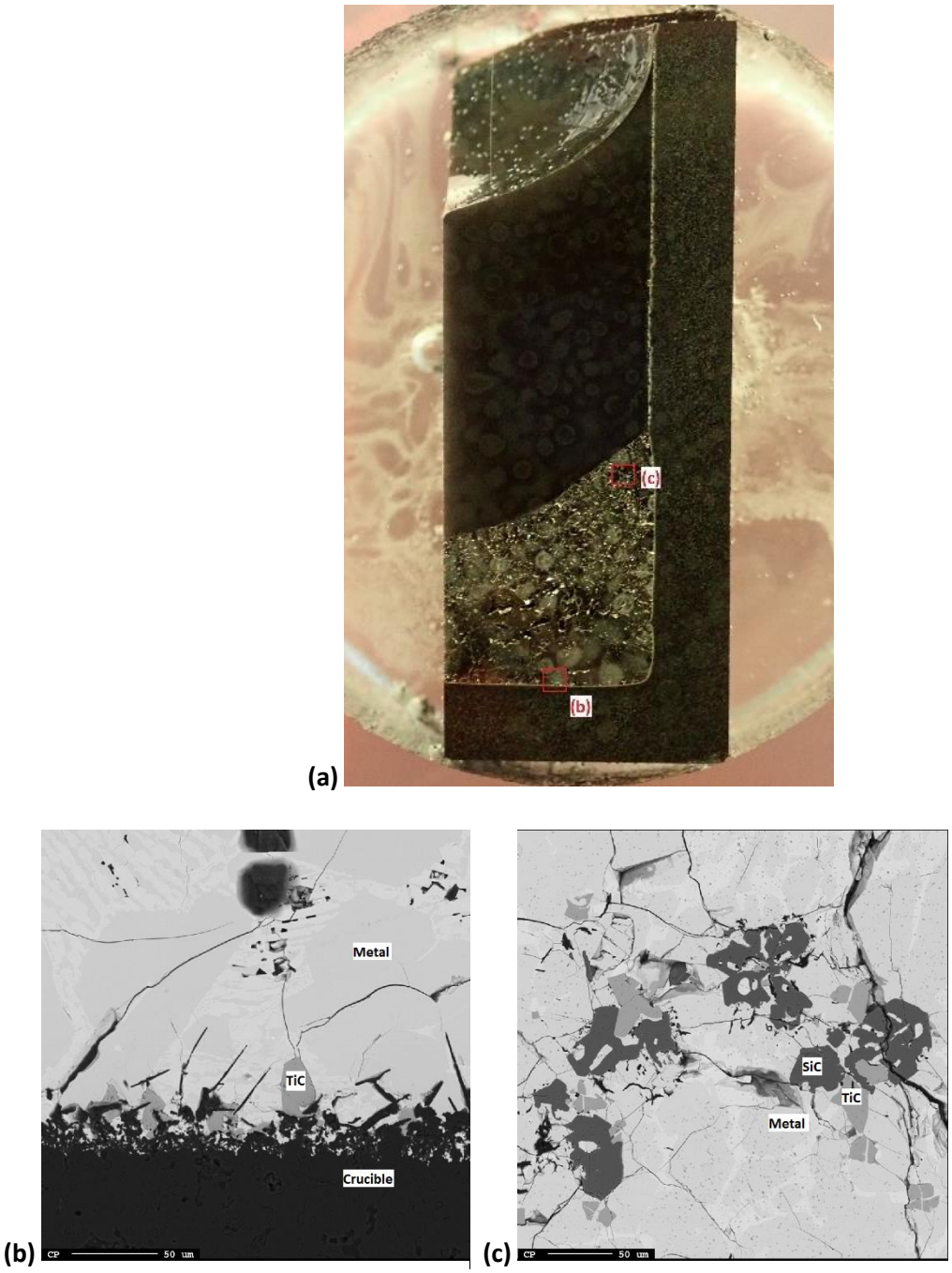

Figure 51: Sample from experiment 9: (a) Position of image (b) and (c) in the sample **(b)** The crucible bottom is seen to propagate into the metal phase as needle-shaped graphite, and TiC has accumulated on the interface **(c)** SiC and TiC found in the bulk of the metal phase, close to the slag interface in sample 9

Experiments 1, 1.2 and 3 was run without the addition of any slag. A slag phase had still formed in the samples. The slag found in experiment 1 consisted of SiO_2 dendrites and a slag matrix consisting mainly of SiO_2 and MnO with minor amounts of CaO, Al_2O_3 and MgO. The slag found in experiment 1.2 was a homogenous slag consisting mainly of SiO_2, Al_2O_3 and CaO with lesser amounts of MgO and MnO. Whereas the slag found in experiment 3 consisted mainly of SiO_2 and MnO with minor amounts of

MgO, CaO and Al_2O_3. The slag found in experiment 1 and 3 contained about 10wt.% more Si than the slag found in experiment 1.2 where SiC was found.

4.2.8 Experiments using metal containing 29wt.% Si (LC-SiMn-alloy)

The results presented in this section are derived from ten experiments carried out using an alloy containing 29wt.% Si, experiments: 5, 7, 8, 10, 13, 14, 17, 18 and 19. An overview of the variables in the experiments is presented in Table 42. General observations of SiC and graphite is presented in Table 43. The composition of the metal and the slag found in the samples is presented in Table 44 and 46, respectively.

The main findings: SiC was observed in all experiments apart from experiment 14. Graphite was only observed in experiment 14. The samples either accumulated graphite, or SiC. With the increased content of Si in the alloy, SiC was observed in the samples as opposed to graphite. With increased content of titanium in the samples, less graphite and less SiC has formed.

Table 42: Experimental parameters for experiments 5, 7, 8, 10, 13, 14, 17, 18 and 19

Experiment	Slag	Temperature	Hold time
5	1 (No Ti)	1600	60
7	2 (Low Ti)	1600	60
8	-	1600	60
10	2 (Low Ti)	1660	60
13	3 (High Ti)	1600	60
14	3 (High Ti)	1650	60
17	3 (High Ti)	1600	90
18	2 (Low Ti)	1600	60
19	3 (High Ti)	1600	60

Table 43: General observations of SiC and graphite from experiments conducted with alloy containing 29wt.% Si

Exp	Observations of SiC and graphite
5	SiC is located: Crucible bottom (slag-crucible, metal-crucible & slag-metal interface). On the slag-crucible, the SiC is almost always in contact with metal. The particles/clusters are relatively large (about 60-80µm length)

7	SiC is located: Bulk of the metal, close to the crucible wall or crucible bottom. Accumulated as relatively large clusters (about 50x50µm). Slightly larger particles have accumulated in the metal by the slag-metal interface (close to the crucible).
8	Slag has been formed in the upper part of the crucible. The metal particles inside the slag are encircled by SiC particles, on the slag-metal interface. The SiC is also found in the slag phase as well as inside the metal phase (close to crucible or slag). Some slag has also been formed in between the whole crucible bottom- and metal-interface. Large (285*450µm) clusters of SiC are propagating from the crucible bottom (and slag) out into the metal phase.
10	SiC has accumulated on the slag-metal interface and on the metal-crucible bottom interface. SiC has accumulated as large particles in the metal side.
13	Smaller amounts of SiC was observed in the bottom of the crucible, on the slag-metal interface close to the crucible
14	No SiC was observed, but graphite needles were found in the bulk of the metal
17	Little SiC was found. A few particles were found on the slag-metal interface
18	SiC is found inside the metal phase, close to either the crucible or the slag phase. More on the crucible-interface than the slag-metal interface. As the distance from the crucible increases, the amount of SiC decreases on the slag-metal interface. SiC was also found inside the bulk of the metal in contact with pores or cracks.
19	SiC is only found in the bottom of the crucible along with TiC and slag, on the slag-metal interface close to the crucible.

Table 44: Chemical composition of the metal found in samples 5, 7, 8, 10, 13, 14, 17, 18 and 19, compared to the original metal. Values are given in mass%

Experiment	Si	C	Mn	Fe	Ti	Mn/Fe-ratio	Std. Dev.
5	23,1	0,4	68,0	9,9	N.A.	6,9	
7	25,2	0,4	66,1	9,7	0,7	6,8	
8	28,3	0,7	62,6	10,9	0,3	5,8	
10	24,2	0,3	66,7	9,7	0,6	6,9	
13	25,8	0,3	63,9	11,3	1,2	5,6	
14	18,2	0,4	71,4	10,6	0,2	6,7	
17	24,3	0,5	66,1	11,0	1,2	6,0	
18	22,8	0,5	69,1	9,6	0,4	7,2	
19	26,1	0,5	62,9	11,8	1,0	5,3	±0,76
Original composition	29,4	0,4	58,7	10,3	0,3	5,7	

Table 45: Chemical composition of the slag found in samples 5, 7, 8, 10, 13, 14, 17, 18 and 19. Values are given in mass%

Experiment	Si	O	C	Mn	Mg	Al	Ca	Ti
5	21,3	43,4	0,4	4,8	6,4	9,0	16,8	-
7	21,1	42,5	0,4	5,5	6,2	8,8	16,7	0,5
8	36,3	43,4	0,9	3,1	1,9	3,7	6,2	0,1
10	22,7	40,1	0,4	3,4	6,3	9,0	17,0	0,3
13	20,3	36,9	0,3	5,2	6,1	6,9	14,8	5,4
14	23,8	39,0	0,4	4,8	5,1	8,3	14,9	0,3
17	20,0	36,4	0,5	6,1	5,1	7,6	14,6	5,6
18	22,6	37,9	0,5	4,8	5,3	8,8	15,8	0,4
19	19,9	36,8	0,5	5,8	5,4	7,6	14,5	5,5

From the experiments analyzed, SiC was observed in the samples from all the experiments apart from experiment 14. Graphite needles as presented in Figure 52 was found in bulk of the metal.

SiC was found on the slag-crucible interface, slag-metal interface and metal-crucible interface as presented in figure 53. SiC was also found in the bulk of the metal for experiments 8 and 18 as presented in figure 54.

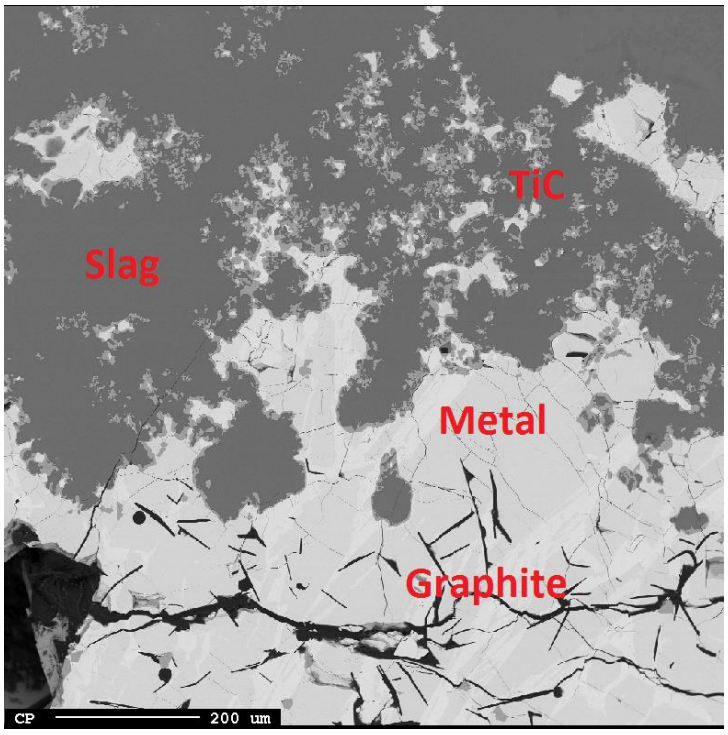

Figure 52: Sample from experiment 14. Graphite needles can be seen in the bulk of the metal

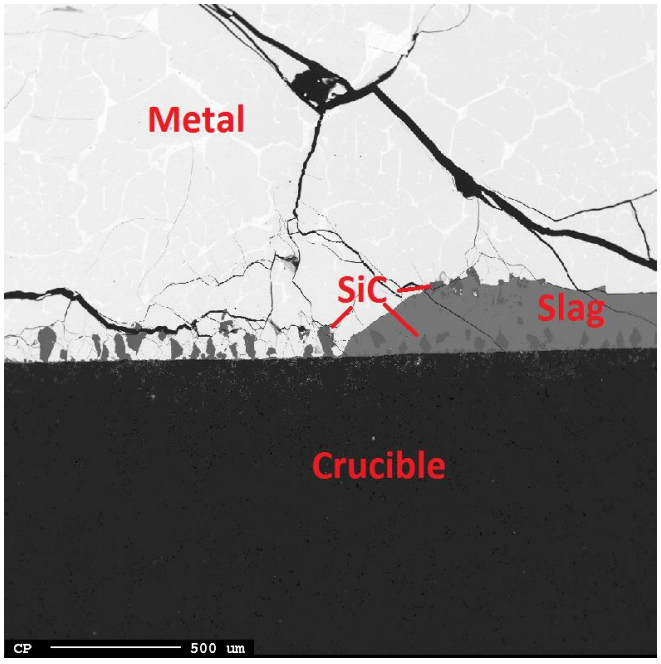

Figure 53: Sample from experiment 5. Metal is depicted as white, crucible as black, slag as gray and SiC as darker gray. SiC has accumulated on the metal-crucible, slag-crucible and slag-metal interface

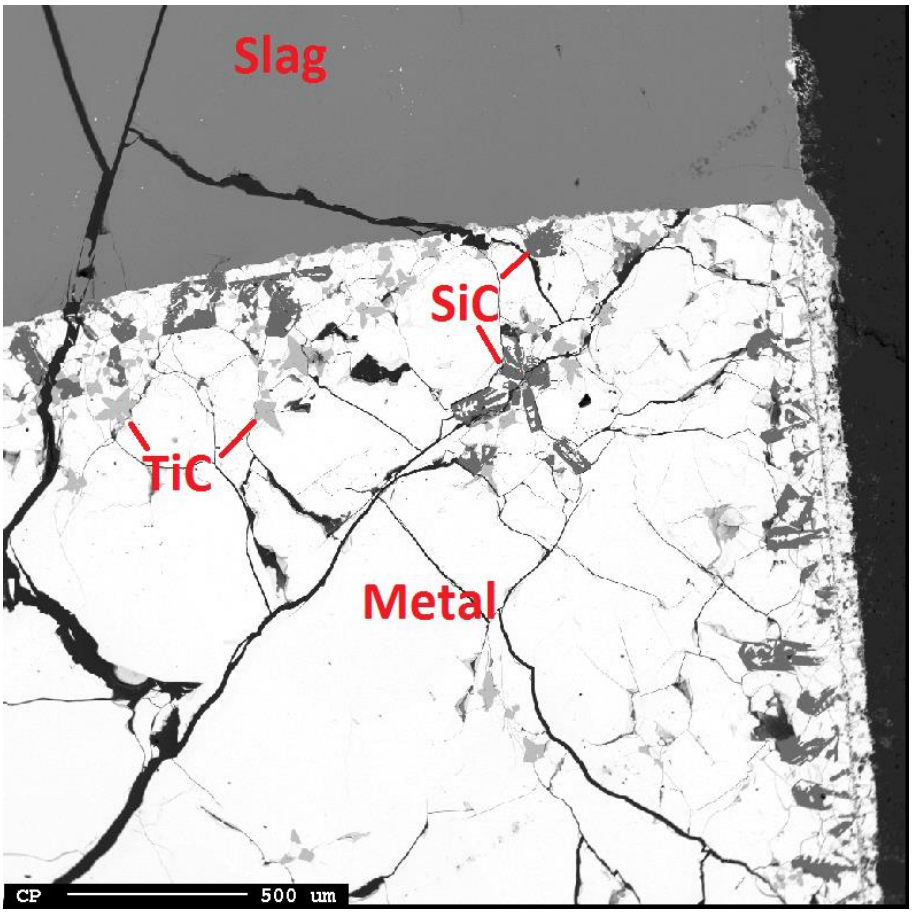

Figure 54: Sample from experiment 18. SiC can be seen in the bulk of the sample, along the interface of slag-metal and along the interface of metal-crucible

Table 46 presents a summary of where the SiC and graphite has accumulated in the samples.

Table 46: Location of SiC and graphite found for all experiments

Experiment	Crucible wall interface	Crucible bottom interface	Slag-metal interface	Bulk of metal	Graphite in bulk metal
1	-	-	-	-	X
1.2	-	-	-	-	X
2	-	-	-	-	X
3	-	-	-	-	-
4	-	-	-	-	X
5	-	X	X	-	-
6	-	-	-	-	X
7	X	X	X	-	-
8	-	X	X	X	-

9	-	-	X	X	-
10	-	X	X	-	-
12	-	-	-	-	-
13	-	-	-	-	-
14	-	-	-	-	X
15	-	-	-	-	-
16	-	-	-	-	-
17	-	-	X	-	-
18	X	X	X	X	-
19	-	-	X	-	-

4.2.10 Experiments using coke particle

The coke particles remained intact in experiment 1.2 and 2. In experiment 1, the coke particle had reacted completely and only left cracks in the metal where it was previously positioned.

BSE Images of the coke particle and the coke boundary for experiments 1, 1.2 and 2 are presented in Figure 55, 56 and 57, respectively.

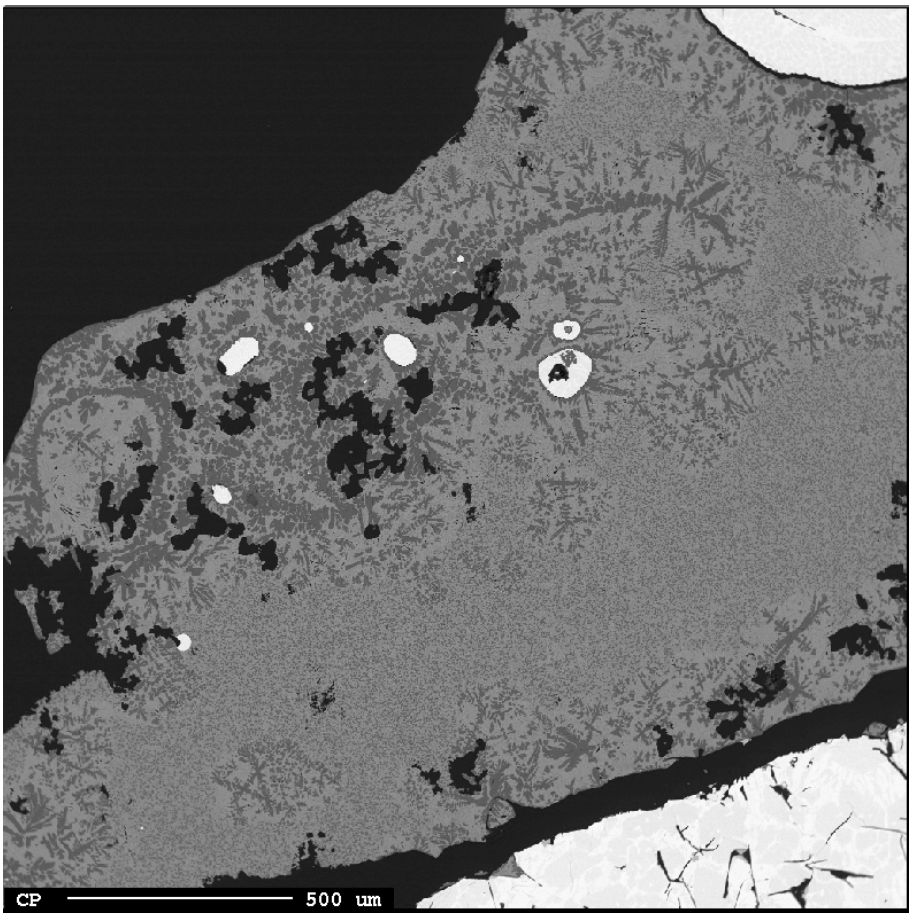

Figure 55: Coke boundary of sample in experiment 1

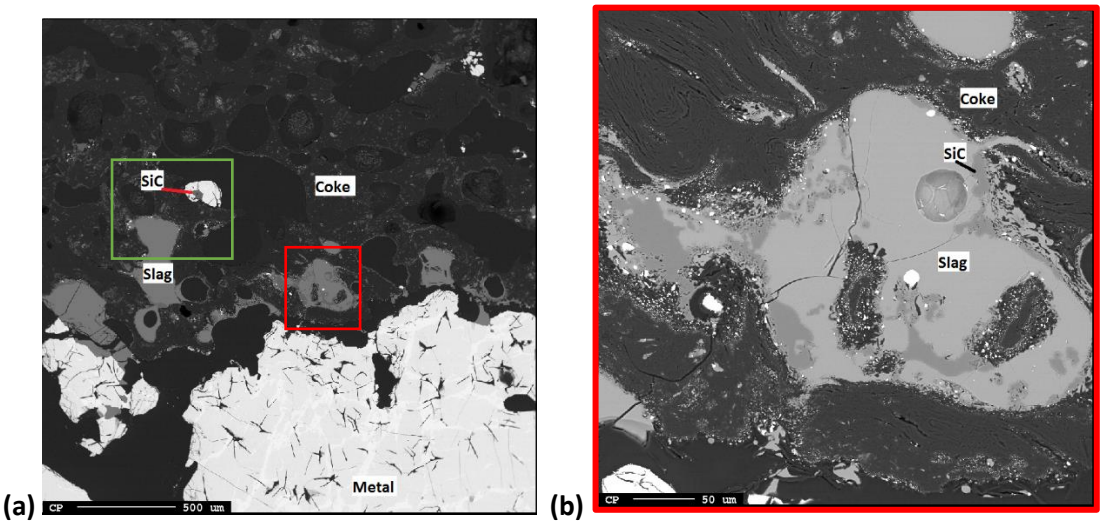

(c)

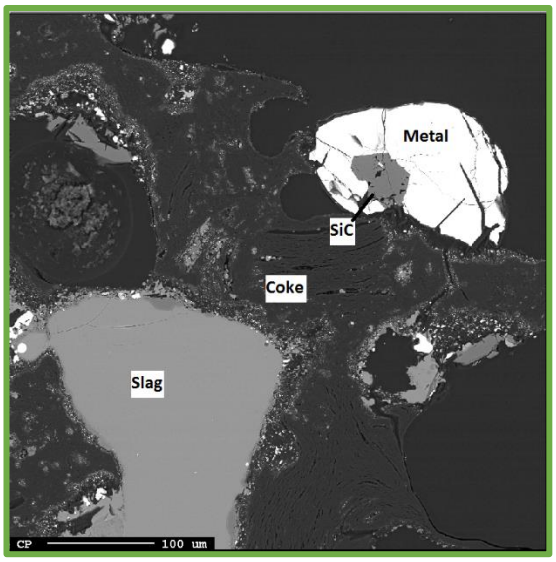

Figure 56: Coke particle in the sample from experiment 1.2 **(a)** Coke boundary, positions of (b) and (c) marked as red and green respectively **(b)** Slag in the coke particle containing SiC **(c)** Metal with higher Si-content, in the coke particle containing SiC

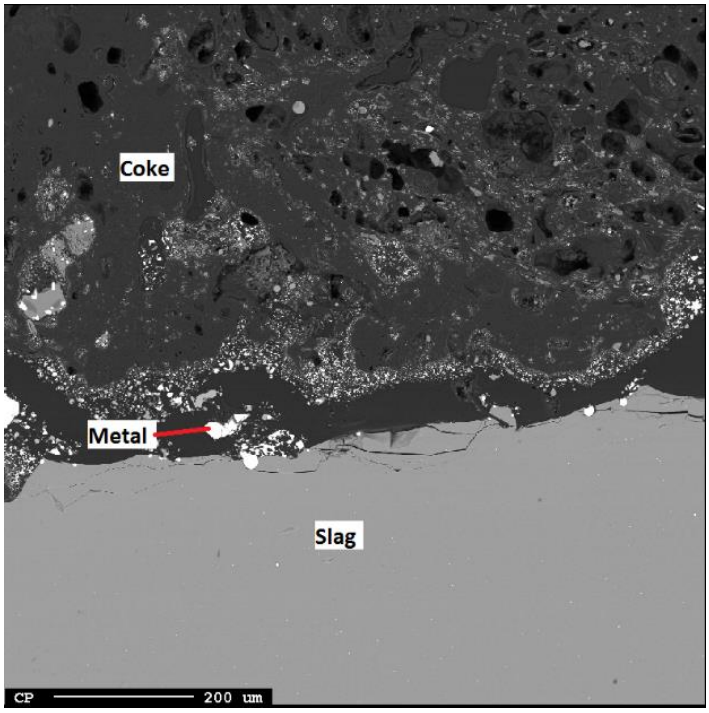

Figure 57: Coke boundary from experiment 2

SiC was observed inside the coke particle for experiment 1.2. On the coke-metal and on the coke-slag interface. The chemical composition of the metal in Figure 56 (c) deviated from the bulk metal. This metal was found to have elevated values of Si as presented in Table 47.

Table 47: Chemical composition of the metal particle where SiC had accumulated, from sample 1.2. The metal was situated inside the coke particle

	Si	C	Mn	Fe
Metal particle	20,9	0,6	70,0	8,9
Bulk metal	20.1	0.4	68.3	11.5

4.3 Original alloy and slag

The original alloys and slags used for the slag-metal melting experiments were also investigated by the use of EPMA, mostly due to unexpected formation of slag and oxides in the samples. The results will also be used to compare with the produced slag and alloy phases.

BSE Images of the microstructure of the slag and LC-SiMn alloy is presented in Figure 58 and 59 respectively.

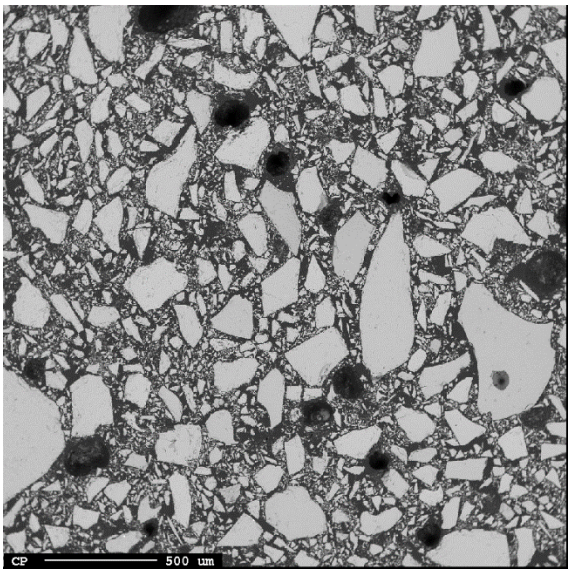

Figure 58: Microstructure of slag 3 (high Ti) with particles ranging from 1 to 500µm

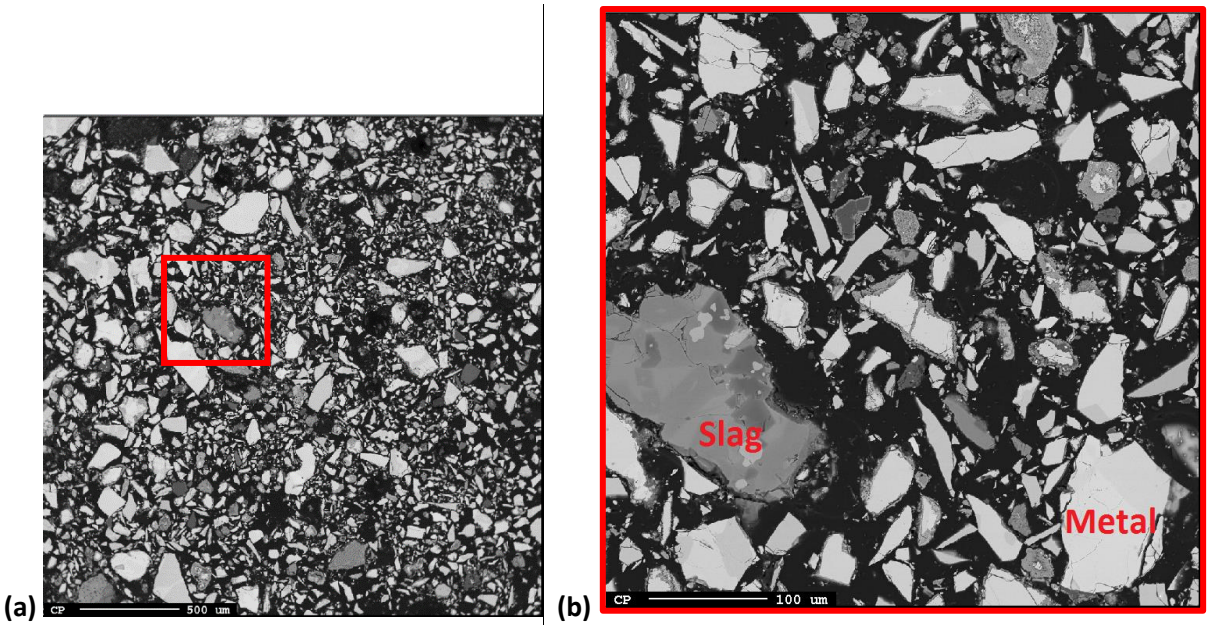

Figure 59: BSE image of the microstructure of the LC-SiMn alloy **(a)** Overview of the structure **(b)** Slag and metal found inside the alloy

The structure and particle size were the same for all three slags. The three slags were all amorphous slag only, consisting of particles ranging from 1µm to 500 µm as imaged in Figure 58. The microstructure of the alloys are similar. In Figure 59 (b) dark particles infused in the metal can be seen, these are slag particles. Some metal particles can also be seen to have dark outlines, this is also oxides. The slag in the Std-SiMn is found to be MnO and SiO_2 whereas the slag found in the LC-SiMn includes SiO_2, CaO, MgO, MnO and Al_2O_3. The chemical composition of the slag found in the Std-SiMn and LC-SiMn alloy is presented in Table 48.

Table 48: Chemical composition of the slag particles infused in the two original alloys

Std-SiMn (wt.%)		LC-SiMn (wt.%)				
SiO_2	MnO	SiO_2	Al_2O_3	MnO	CaO	MgO
44	55	44	21	20	10	6

5. Discussion

The experiments were designed to be a qualitative test in order investigate at which conditions carbides could would form in the Mn furnace. It was chosen to use multicomponent slags and metals in the experiments to be as close to industrial case as possible. Also temperature and holding time was varied. This gives a lot of results that can be used for screening but difficult for quantification.

The methods used will be discussed and thereafter the findings.

5.1 Sources of error and uncertainties

5.1.1 Carbon content

The carbon content in the analyses will be affected by the carbon coating on the metallographic samples prepared for the EPMA. Hydrocarbons and contaminations in the vacuum chamber could also be present to various degrees, due to the samples being cast in epoxy. The exact impact the carbon coating has on the carbon content in the analyses is hard to say; according to Davidsen [14] these factors combined represents c. 4 % relative error in the carbon measurement.

The EPMA did not have standards for Carbon analyzes (private communication with Morten Raanes) meaning that the absolute value is uncertain.

The amount of carbon found as SiC, TiC or graphite in the experiments exceeds the amount of carbon put into the experiments through the alloy. This confirms that carbon has dissolved into the alloy, from the graphite crucible.

5.1.2 Selection of sample for analysis

The samples were cut in half, to expose the area of interest after solidification. Due to the high resolution in the EPMA (Scanning Electron Microscope) only a limited area could be selected for further investigation. The analyses are taken from the surface. The microprobe analyses are spot analyses covering 1µm cross section volume. In conclusion, only a small portion of the original sample from each experiment has been analyzed. The parts that have not been analyzed could contain phases not present in the part that was chosen for analysis and some of the analyses could contain particles resulting in too high values.

To select representative spots for the EPMA, the BackScattered Electron (BSE) image (showing different gray scales depending on atomic number of the material) was used to get an overview of the sample and first impression of the content. The BSE image was also used later to estimate the fraction of the different phases in the solidified sample. As seen from the metallographic images, the samples contain several phases and the interfaces ranges from a clear metal droplet in slag to more complex

formations. The selection of sample affects the qualitative assessment as well as the accuracy in the chemical composition as discussed in the next section.

5.1.3 Chemical composition of phases

The error in the phase distribution is mainly due to the selection of the sample for image processing but also due to the fact that a 2D cross section does not give an accurate description of the 3D structure with varying shape size of the different phases.

The observations of phase distribution are used to calculate the average chemical composition of either the slag or metal phases considered as one. The margin of error is not quantified but some uncertainty must be considered when comparing the results. The level of uncertainty has been estimated for some of the results by calculation of standard deviations has been included in the results. (table 18) To reduce the error, aluminum was chosen to calculate the amount of slag after heat treatment, since aluminum was almost evenly distributed between the different phases in the slag compared with the other irreducible elements. For the metal, the images showed better contrast gave higher accuracy in the image processing.

The EPMA analyzes a droplet shaped area in the sample, this interaction volume could intersect with several phases, thus the phase being analyzed could receive data from underlying phases, or phases nearby. As only the surface of the sample is visible, it is hard to know what elements could be laying below the surface of the phase being analyzed, giving secondary fluorescence. Errors such as these can yield high “total” values. A good indication on whether the EPMA results are done properly is to check the “total” values of the wt.% analyses and the stoichiometry. High “total” values were not observed in the EPMA results, but this does not mean there is no peak interference present; it is just used as an indication. The total values ranged from c.91wt.% at lowest to 107wt.% at highest. However, the interference from other elements has to be considered when comparing the results, nonetheless. Below the results and standard deviation of three EPMD point measurements showing examples of the analysis from sample #17 and 18#. Especially the standard deviation of Ti is interesting to compare between the metal sample #17 and #18. (table 49,50 and 51)

Table 49: Standard deviation of the EPMA analyses of slag in experiment 17

Element	Si	Mn	Mg	Fe	Al	Ca	Ti
Value	20.8	12.7	1.7	0	8.3	12.4	3.0
STDV	0.04	0.37	0.05	-	0.04	0.1	0.16
STD%	0.2	2.9	2.7	-	0.4	0.8	5.3

Table 50: Standard deviation of the EPMA analyses of metal (light) in experiment 17

Element	Si	Mn	Mg	Fe	Al	Ca	Ti
Value	23.3	67.3	0	10.5	0	0	1.3
STDV	0.1	0.3	-	0.9	-	-	0.6
STD%	0.5	0.4	-	8.2	-	-	48.4

Table 51: Standard deviation of the EPMA analyses of metal (light) in experiment 18

Element	Si	Mn	Mg	Fe	Al	Ca	Ti
Value	22.8	69.1	0	9.6	0	0	0.4
STDV	0.2	0.01	-	0	-	-	0.07
STD%	0.8	0.01	-	0	-	-	18

In general Ti has a higher standard deviation probably due to segregation in the solidified structures. The standard deviation shows us that the metal analysis in experiment 17 had a higher standard deviation, compared to experiment 18.

The effect of the variations Ti analyzes on the mass balance discussed further in the next section.

5.1.4 Mass balance

In this section the method for estimating Ti in the TiC by combining chemical analysis of slag and metal combined with image processing to estimate the fraction of dark and light metal will be discussed.

The first step off the mass balance is to determine the final distribution of slag and metal. The approach was to use the unreducible oxides (Ca, Al, Mg) where the amount in the slag would be the same before and after reduction. Then the initial weight and concentration combined with the final concentration would give the final weight of the slag phase. For most of the samples only one phase was observed, but for some samples the structure consisted of several phases with different composition.

After the initial analyses of the slag, Al gave the most stable results. An indication that the assumption of no exchange of Ca, Al and Mg was correct, is that no Ca Al or Mg increase in the metal phase was detected by the EPMA.

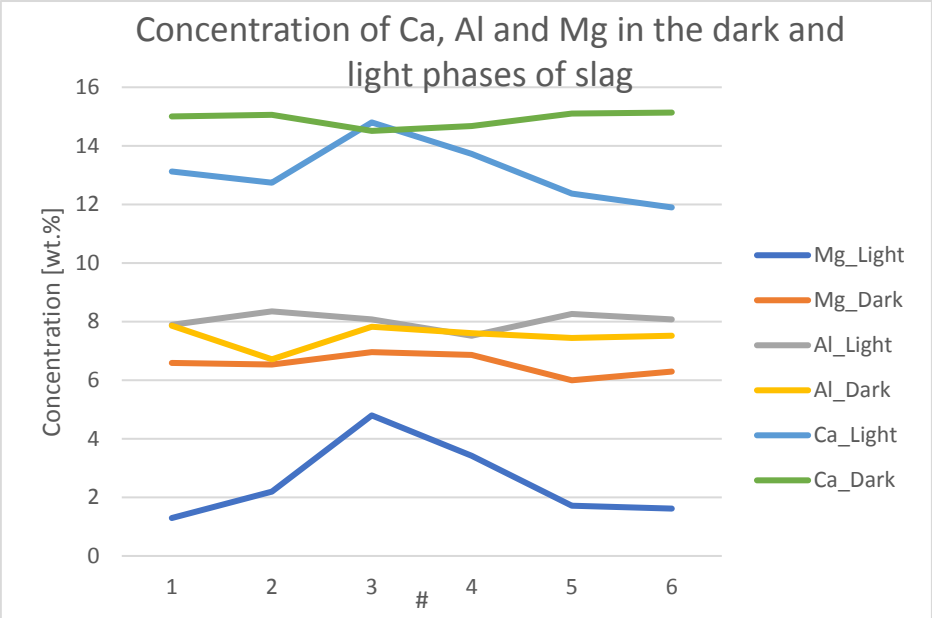

Figure 60 Concentration of Ca, Al and Mg in the different slag phases

The aluminum content was the most stable between the two different phases, giving the most stable and correct results by minimizing the uncertainties linked to measuring amount of each phase.

The final result for the mass balance of Ti taken from Appendix 1 is presented in Figure 60 the calculated distribution of Ti between the different phases has been plotted. We can see that the trends are relatively linear indicating that the method is good for most of the experience. The R^2 values shows how well the relationship is described by a straight line. For instance, the relationship between the amount of Ti in TiC vs Ti in the slag is 99,5% described by a straight line. For the metal at 1600°C ,only 6.84 % follows a linear relationship. However, removing some of the outliers gives us a linear relationship of 95% and the slope becomes the same as for the metal at 1650°C (indicated with a transparent blue broken line).

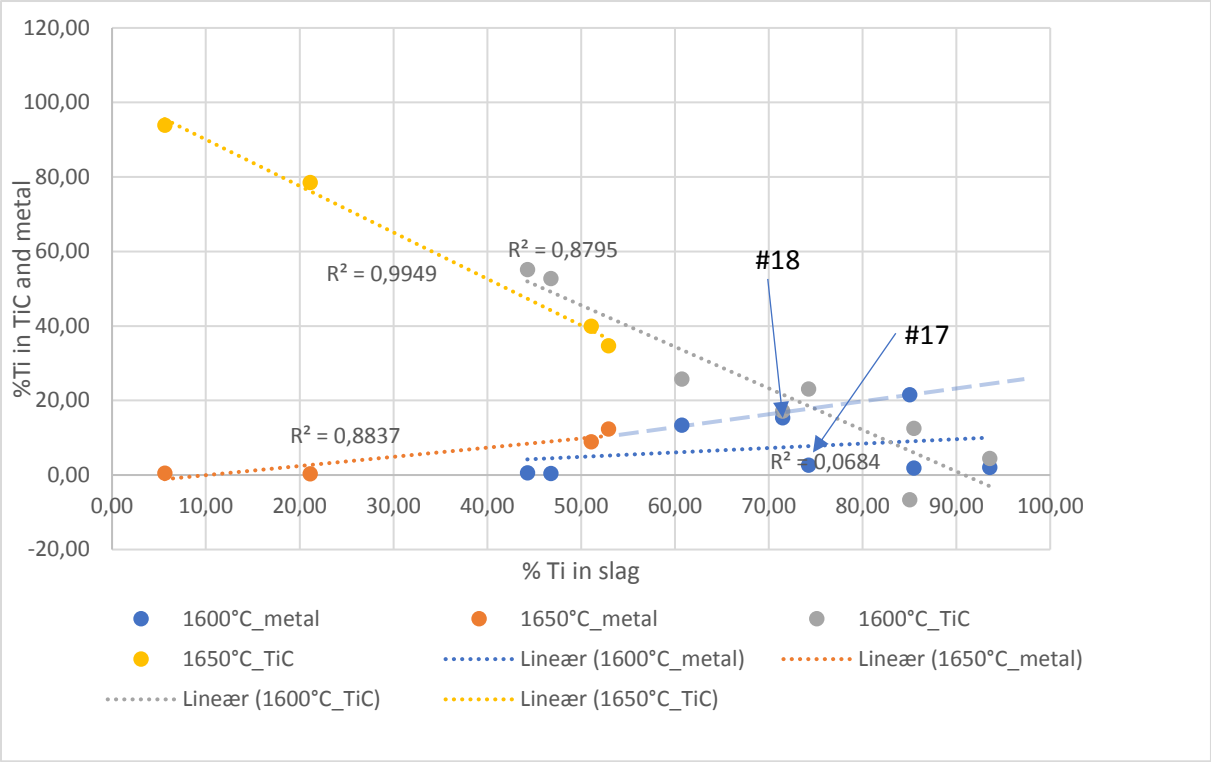

Figure 61 Distribution of Ti in TiC and metal plotted against amount of Ti in slag

The accuracy of the EPMA is in the range of 10-50ppm meaning that variation in the analyzes of Ti in the metal primarily comes from particles or macro/micro segregations in the sample. The conclusion is that this is the major source of errors in the mass balance for Ti.

The errors in the mass balance also have an effect on the Si content in the final results.

From the Si calculations it was observed that the total amount of Si in the sample increased during all experiments. There is no supply of Si into the experiments and thus the calculations are obviously not that accurate. However, the relative trend between the numbers achieved are valuable.

5.2 Effect of silicon content in the alloy

As observed from the results, by increasing the Si content from 20wt.% Si to 29wt.% Si, SiC was observed to form in a much higher degree. This clearly indicates that by increasing the Si content in the alloy, more SiC will form, in agreement with the results presented by Tuset [18].

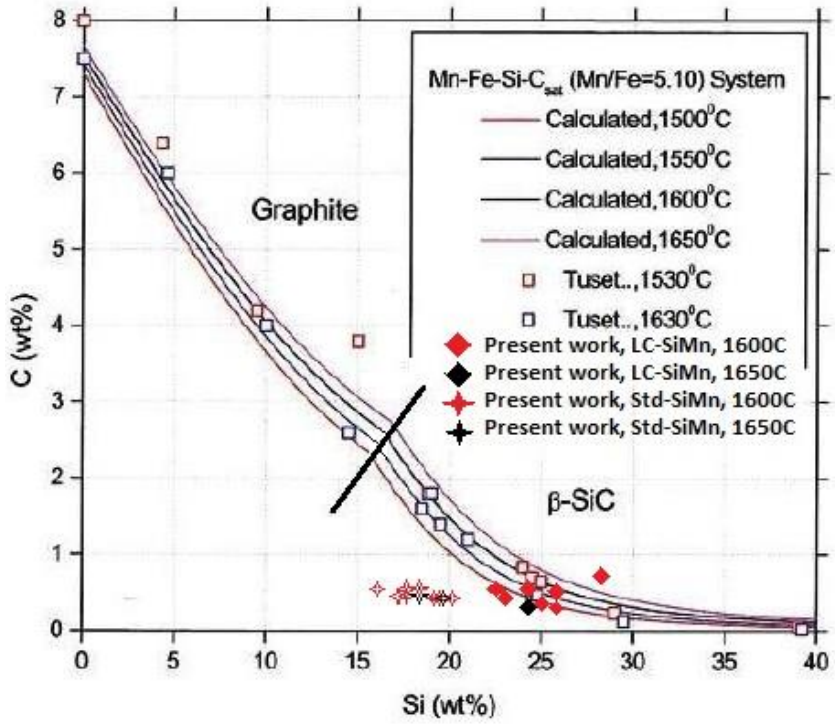

Figure 62: Calculated carbon solubility in a Mn-Fe-Si-C_{sat} alloy with fixed Mn/Fe ratio = 5.1 between 1500-1650°C. Measured carbon solubility by Tuset and Sandvik [18]. Reprinted from Olsen et al. [1] Present work has been included as indicated on the figure

Results (from EPMA analyses and quantifications of metal phase) from present work is presented in Figure 62 as red and black stars for the Std-SiMn experiments at 1600°C and 1650°C, respectively, and as red and black squares for the LC-SiMn experiments at 1600°C and 1650°C, respectively. According to the figure only one experiment from the LC-SiMn experiments has reached equilibrium, and one experiment is supersaturated; whereas all the other experiments are considered unsaturated in carbon. This would indicate that there should be no formation of either SiC or graphite in the latter. With the recorded Si content in the alloys, the C content would have to be c.1.5wt.% and c.2wt.% for Std-SiMn alloys to reach equilibrium and about 0.6 and 0.8wt.% for the LC-SiMn alloys.

The original alloys that were used in this project had a Mn/Fe ratio of 5.5 and 5.7. The liquid alloy in the experiments had a Mn/Fe ratio ranging from 4.6 to 6.9. A somewhat lower or higher Mn/Fe ratio will have a slight effect on the carbon solubility. The change in the coexistence point in the diagram will be in the vicinity of ±0.3% for the C (wt.%) and ±0.4% Si (wt.%), depending on if there is an increase or decrease in Mn/Fe ratio in the range 4.6-6.9. All experiments apart from experiment 1, 15 and 16 were observed to have a Mn/Fe ratio larger than 5.1 (Table 17), slightly increasing the equilibrium content of Si and C, moving the samples from present work further away from equilibrium and

saturation of both Si and C. The impact from a lower Mn/Fe ratio in experiments 1, 15 and 16 would still not indicate saturation by either Si or C.

Deviations from the calculated carbon solubility could be explained by several reasons:

1. Due to irregularities in the metal phase, certain areas of the liquid alloy could contain higher amounts of Si compared to other areas. The areas with elevated content of Si could have a high enough content for the alloy to be saturated in Si and for the stable carbon containing phase to be SiC.
2. The average concentration of the metal phase has been calculated by image processing of a 2D cross-section. This 2D cross-section only covered a minor part of the entire sample. The std. deviation was calculated for three of the experiments, ranging from ± 0.45 to ±0.81. More accurate analysis of the material produced can provide better information. For a representative sample, ICP can provide better accuracy. It can be argued that within the boundaries of the method I have used to analyze, the results match well with what Tuset has found.
3. The measured carbon content could be wrong. As explained by the operator of the EPMA [29], the C content could vary by 3-4% of the recorded value. The samples furthest away from equilibrium would need an increase in 1.5wt.% C in the alloy to reach SiC saturation.

As mentioned, the Std-SiMn (c.20wt.% Si) experiments did not produce a lot of SiC. SiC was only observed in two experiments, one where only metal and coke was mixed at a temperature of 1600°C and a hold time of 60 minutes; the other where metal and low-Ti (1wt.%) slag was mixed at a temperature of 1650°C and a hold time of 60 minutes. Experiments 1.2 and 9, respectively.

In experiment 1.2 the few particles of SiC observed were only found by the coke particle. A reason for SiC accumulating on the coke particle and not by the crucible walls could be that the reduction rates of SiO_2 might be higher at the interface of natural carbon materials as opposed to graphite (crucibles). This was observed by Djis and Smith [30]. In the bulk of the metal, graphite was formed, as opposed to SiC. This could indicate that a direct reaction between the dissolved C from the coke particle and Si from the alloy has formed SiC on the coke interface and the graphite has precipitated by cooling, in the bulk of the alloy.

The chemical composition of the coke particle shows that it contains about 6wt.% SiO_2. It is also observed that the coke particles have dissolved or partly dissolved in the alloy. Most of the oxides from the coke and the metal has formed a layer of slag in the coke particle. However, some of the SiO_2 could have reduced in the alloy, increasing the silicon content to silicon saturation, resulting in the formation of SiC in the coke particle. This was partly confirmed by analyses of the metal close to the coke particle.

The metal by the coke particle had a higher Si and C content than the average of the sample, about 21wt.% Si. This strengthens the indication that certain areas of the samples could experience elevated levels of Si resulting in the formation of SiC. However, 21wt.% Si and 0.6wt.% C would still leave it in the unsaturated (C and Si) zone of the carbon solubility graph.

In the other experiment using Std-SiMn alloy (20wt.% Si) where SiC was detected, experiment 9, the SiC particles were found in the bulk of the metal phase, close to the slag-metal interface and metal-crucible interface. The formation of SiC would indicate that the liquid alloy in this sample has reached silicon saturation, although this is contradicted by the other experiments which puts the silicon saturation at a higher Si content. Needle-shaped graphite was also found on the interface between the metal and crucible seen in Figure 63.

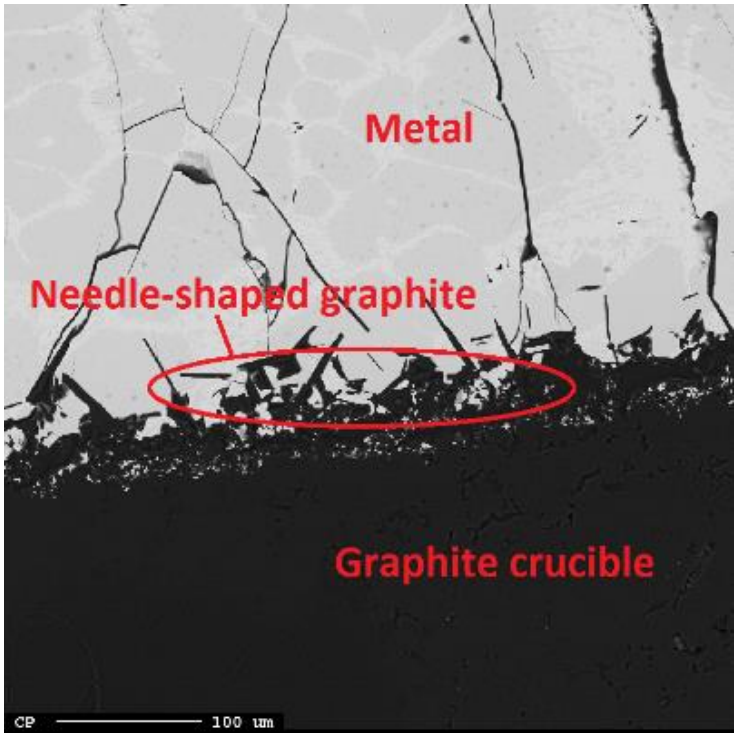

Figure 63: Needle-shaped graphite found in sample 9

Most likely the graphite has not been formed in this sample but are parts of the graphite crucible. The graphite is still attached to the graphite crucible and some reaction between the crucible and the metal could have occurred. However, they do not appear to have formed by precipitation or direct reaction as the structure and composition of the graphite needles is identical to the graphite crucible. The graphite could have been introduced through cracks and voids in the alloy due to cracking of the metal during cooling or from mechanical wear during preparation of the sample. The metal has most likely dissolved the crucible, and what we see in figure 63 is parts of the reacted crucible with metal inclusions.

Large amounts of SiC was observed in the bulk of the alloy, this could indicate that it has formed due to precipitation during cooling. The metal phase in this sample was quantified to contain about 18.5% Si. However the metal found surrounding the SiC particles was observed to have higher (+2.5%) silicon concentration than in the bulk metal. Indicating that the real values could be higher than quantified, or that the certain areas of the metal phase is silicon saturated.

The silicon content in the experiments also affected the formation of TiC. More TiC would accumulate in the experiments using alloy containing 20wt.% Si. A graph illustrating the distribution of Ti to the slag, metal and TiC phase is presented in Figure 64.

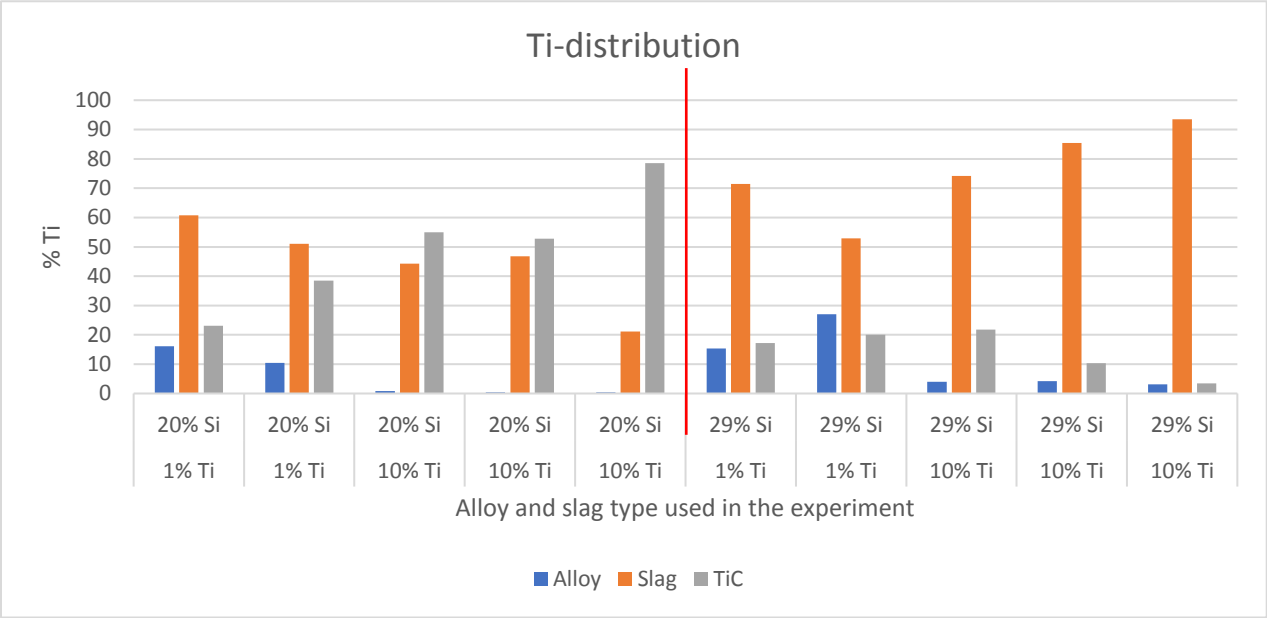

Figure 64: Graph illustrating the distribution of titanium between the slag, alloy and TiC phase. The experiments are listed after Si content in the alloy, increasing from left to right; thereafter Ti content in the slag, increasing from left to right; and lastly by temperature, increasing from left to right

Most of the Ti has ended up in the slag or TiC, and only lower amounts in the alloy phase. When increasing the amount of Si in the alloy used in the experiments, from 20wt.% to 29wt.% the amount of Ti in the TiC phase decreases from an average of 50% to an average of 14.5%. For the experiments using alloy with 20wt.% Si, increasing the amount of Ti in the slag will also increase the % of Ti going to the TiC phase. This was however not observed for the experiments using alloy containing 29wt.% Si. This is due to the alloys containing 29wt.% Si formed SiC in the samples and thus less Ti would react with the dissolved carbon as some Si did instead. Another reason could be that with increased Si-content in the alloy, the solubility of carbon decreases, resulting in less carbon being dissolved in the alloy and thus less TiC being formed through the metal phase.

5.3 Effect of titanium content in the slag

It was observed that the relative effect of adding more titanium in the slag is that more TiC accumulates in the samples. This was observed for all experiments. From the experiments using the slag with no titanium it was observed that no TiC had accumulated, apart from experiment 1. The amount was very little, and the particles were small. This is likely produced from the Ti introduced from the original alloy containing c. 0.25wt.% Ti. This would be indicating that even at very low concentrations of Ti, TiC can accumulate. This was also observed by Sahoo and Koczak [31].

The general difference in using slag containing 1wt.% TiO_2 or 10wt.% TiO_2 has been illustrated in a drawing in Figure 65. The amount and consistency of TiC in the drawing is not entirely representative to the amount of TiC formed in the experiments. The purpose of the drawing is only for a quantitative comparison between the use of the two different slags.

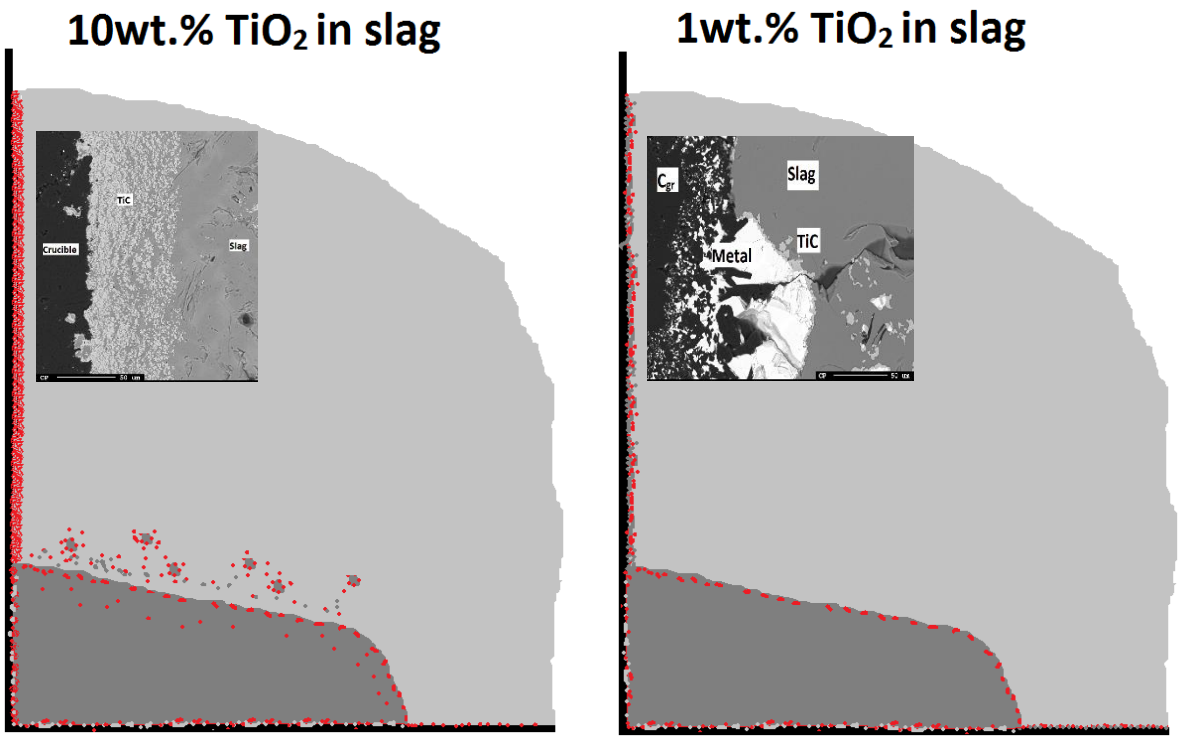

Figure 65: Drawing used for comparison of where the TiC has formed in 1 and 10wt.% TiO_2 slag experiments. The amount and consistency of TiC are not representative, but the difference between the experiments is. Carbide is depicted as red color, crucible as black, metal as dark gray and slag as light gray **(a)** TiC has accumulated on the entirety of the crucible interface, on the slag-metal interface and in the bulk of the slag and the metal. TiC has accumulated when both metal and slag is present, as well as when only slag is present **(b)** TiC has accumulated on the entirety of the crucible interface and on the slag-metal interface. TiC has only formed when both metal and slag is present

When using a slag with 1wt.% TiO_2, TiC was only observed on the crucible interface and on the slag-metal interface. Both slag and metal needed to be present for TiC to form. This can be seen in Figure 65 (b). Figure 65 (a) demonstrates that when increasing the Ti content to 10wt.% TiO_2, the layer of TiC along the crucible interface became wider and more tightly packed. By the crucible wall the presence of metal was not necessary to form TiC. More TiC had also formed in the bulk of the slag (surrounding metal particles) and in metal phase (close to the slag-metal interface) and not only on the slag-metal interface. TiC in the bulk of the metal was only observed for experiments conducted at 1650°C.

Prior to the experiments it was expected that the TiC would form from a direct reaction between dissolved C in equilibrium with the crucible and dissolved TiO_2 in equilibrium with the slag following the reaction (2.29):

$$TiO_{2(s)} + 3C_{(s)} = TiC_{(s)} + 2CO_{(s)} \quad (2.29)$$

Another proposed reaction mechanism was that TiO_2 in the slag would dissolve in the metal phase and then react with the dissolved C following equations (2.30) and (2.31):

$$TiO_2 + 2C = Ti + 2CO \quad (2.30)$$

$$Ti + 2CO = TiC + CO_2 \quad (2.31)$$

TiC could also form by precipitation during cooling where Ti dissolved in the metal will react with C dissolved in the metal to form TiC following reaction (2.28)

$$Ti + C = TiC \quad (2.28)$$

For the 1wt.% TiO_2 experiments the TiC seems to have been formed by a direct reaction between reduced Ti from the slag with dissolved C from the graphite crucible introduced through the metal, as the TiC has settled mostly on the metal-slag interface, but close to the crucible. The experiment using 10wt.% TiO_2 in the slag shows a direct reaction between reduced Ti from the slag and dissolved C straight from the crucible as there is no metal present. TiC was also observed in the bulk of the metal. Indicating that some TiC has precipitated during cooling of the sample; as the temperature decreases, the solubility of carbon decreases and will be precipitated out as TiC when the alloy is saturated in Ti. The main increase in TiC formation from increased TiO_2 content in the slag is seen on the slag-metal interface and in the bulk of the slag and metal, close to the interface. This could be explained by the layer of TiC along the crucible interface, that will act as a barrier layer, reducing the amount of dissolved carbon and inhibiting further reactions between the Ti and C along the crucible interface.

With increased Ti content it was observed that less SiC would accumulate, and in some cases not at all. At higher Ti contents (10wt.% TiO_2 in the slag) almost no SiC was observed to have accumulated. The dissolved carbon seems to favor binding to the Ti as opposed to the Si, in fair agreement with what was found on the equilibrium between SiC and TiC, where TiC is more stable than SiC for the same carbon solubility. When TiC forms, the amount of dissolved C available to react with Si to form SiC is reduced, resulting in less SiC being formed. The formation of TiC could also affect the rate of reduction from SiO_2 in the slag to Si in metal.

A small impact could also come from the driving force and kinetics of this reduction process will be determined by the SiO pressure generated, which in turn is dependent on the CO_2 pressure at the slag/gas interface. This CO_2 pressure may be controlled by the rate at which CO_2 reacts with C and forms CO. In other words, the reaction of CO_2 with carbon has a big influence on the kinetics of silica reduction. When lower amounts of SiO_2 is reduced to the alloy phase it could result in the metal not being saturated in silicon or reaching equilibrium. However, since the samples are produced with an alloy already containing a given Si content, it is the equilibrium between the Si content of the slag and the metal that has the most impact on the formation of SiC.

5.4 Effect of temperature

Comparing Figure 5 and Figure 6, we can see that increasing temperature will also increase the silicon content, and the stable carbon containing phase will shift from carbon to SiC at approximately 1600°C. The largest contribution by increased temperature is the solubility of carbon, silicon and titanium. As shown in Figure 6 by Olsen & Tangstad, the effect of temperature on the silicon content (in a similar alloy system) shows that there is a change in stable carbon containing phase When the temperature increases, more Si/Ti could be reduced into the metal phase. By increasing the temperature it was observed for one experiment that SiC would form instead of graphite. In another experiment it was observed that by increasing the temperature more SiC would precipitate in the bulk of the alloy, confirming the impact of the temperature. As the solubility of carbon strongly depends on the temperature, metal at high temperatures contains more carbon than it can hold at temperatures closer to the liquidus. Hence, during cooling and solidification a considerable amount of carbides will precipitate. A strong indication of the temperature increasing the solubility of titanium is that TiC was only found in the bulk of the metal at 1650°C, indicating that it has precipitated during cooling. An explanation could be that the increased temperature would increase the super saturation to a higher extent and during cooling the TiC would precipitate.

According to Olsen and Tangstad, the effect of temperature on the silicon distribution is significant and would increase by 6% for every 50°C, until saturation is reached, then it follows a slow increase. The

impact of temperature was bigger on the experiments conducted with the alloy containing 20wt.% Si as opposed to 29wt.% Si. This goes over well with the expected theory of increasing the temperature.

It can also be assumed that with higher temperatures the amount of carbides forming would increase, as the reaction rates will be higher. However, this was not explicitly confirmed from the results. Since most of the SiC had not accumulated on the crucible walls, it was hard to decide how much SiC had accumulated in the samples. If I had managed to record the amount of SiC formed in the experiments the impact of temperature on the amount of SiC formed would be more easily deduced.

5.5 Effect of hold time

There was no observed impact on the formation of carbides due to an increase in hold time which is supported by Dalaker and Tangstad's [32] results from their investigation of the time dependence of the solubility of carbon in liquid silicon equilibrated with silicon carbide. From their results it was detected no time dependence of the solubility limit and it was concluded that equilibrium is rapidly established as observed in this project.

The effect of hold time on TiC was observed to be very small. TiC is likely formed quickly as found in previous experiments conducted by Øvrelid [6] and confirmed by Sahoo and Koczak [31]. Sahoo and Koczak found that longer hold times will not have any effect on the number of particles formed but tends to increase the size of the TiC particles. However, even the increase in particle size is not very substantial which corroborates the theory of TiC forming quickly in the experiments.

5.6 Additional observations

5.6.1 Formation of slag in experiments where no slag was added

The slag crept up the crucible walls and foamed out through the holes of the lid as presented in Figure 25. The formed slag consisted mostly of SiO_2 and MnO and smaller amounts of MgO, CaO and Al_2O_3. The high content of Si in the slag could explain why the slag crept out of the crucible. Acidic slags tend to climb high up along the crucible wall, as experienced by Olsen & Ding [33]. In order to form slag, oxides are required. There could be several reasons as to why the slag was produced. It was believed the oxides must have been introduced either through the coke particle or the alloy.

The moisture content of a bulk sample of the alloys was calculated to be 1.02% by weight for the SiMn-fines and 0.81% for the LC-SiMn-fines. 101.15g of SiMn was used in experiment 1, resulting in 1.03 grams of liquid. This alone could not be the reason for the slag production, as the slag was in higher quantity. The alloys were heated at 105°C for 48 hours after the first experiment, to evaporate some moisture. Slag was still formed during the experiments where no additional slag was added, although the amount of slag formed decreased.

Alloys with higher amounts of Si could contain substantial amounts of SiO_2 [34]. It was believed the alloy used in the experiment could contain particles infused with slag, and was analyzed in the SEM. Image of the microstructure is presented in Figure X.

From Figure 59 it can be observed that the alloy contains substantial amounts of slag infused in the metal, ranging in particle size from 1 to 500µm. The slag found fused in the metal, and the slag that has formed in the experiments, has been compared in Table 52.

Table 52: Chemical composition of the slag that has formed in the experiments that were conducted without the addition of any synthetic slag

Experiment	Si	Mn	Al	Ca	Mg	O
1	28.8	20.1	1.7	4.2	2.5	41.5
1.2	19.8	3.0	11.6	15.3	6.8	41.3
3	29.1	17.1	3.2	3.8	2.0	41.6
Std-SiMn	20.80	42.98	-	-	-	36.22
8	36.3	3.1	3.7	6.2	1.9	43.4
LC-SiMn	20.37	15.31	10.99	7.08	3.61	42.64

The values are necessarily not very similar, and the Std-SiMn was not observed to contain any Al, Ca or Mg. However, only three different slag particles infused in the metal was analyzed for each alloy. The slag particles not analyzed could contain any ratio of the oxides observed in the formed slag. The slag particles analyzed in the LC-SiMn metal gave three very different values, whereas the slag particles in the Std-SiMn gave three similar values. The oxygen from the slag inclusions could also have oxidized some of the Ca, Al and Mg in the coke and the metal. In conclusion, the slag has most likely formed due to slag inclusions in the metal and to a minor degree parts of the metal or coke. This has most likely impacted the mass balance to a certain degree, as slag will probably have formed without it being noticed in the other experiments as well. The mass of slag formed has not been analyzed and thus it is hard to say how much of an impact this has on the results.

5.6.2 Formation of cavities

All samples containing slag with 10wt.% TiO_2 had cavities on the center-top of the sample. The cavities may have been formed due to:

- Gas formation
- Shrinkage of metal during solidification
- Wetting to graphite crucible

All the cavities observed had openings towards the surface, however no gas channels, formed due to escaping gas, was observed. Both the slag and the metal were observed to have good wetting properties towards the crucible, and they both clearly crept up the crucible wall during the experiments. This could explain why the metal and slag is found at a higher level of the crucible when in contact with the graphite walls. A proposed mechanism of the cavity formation is presented in Figure 65.

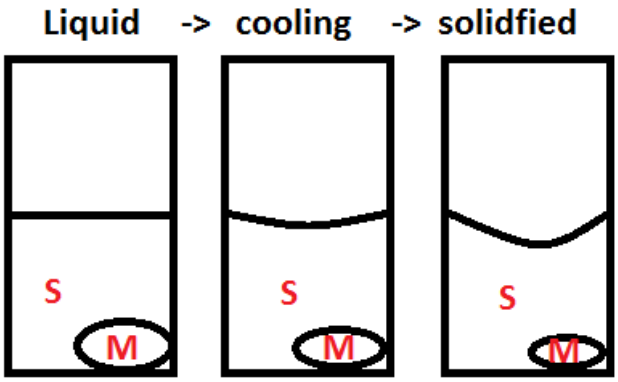

Figure 66: Proposed mechanism of cavity formation

When the metal in the sample cools down and solidifies, it will shrink, this will reduce the level of the mass in the crucible. The metal and slag that is in contact with the graphite will hold onto the crucible due to the good wetting properties, increasing the level difference, forming cavities.

5.6.3 Formation of cracks between crucible and sample

Several samples experienced several cracks in the alloy and between the crucible interface and the sample. This apparent void between the alloy and crucible only occurred when a belt of TiC had formed on the crucible interface. The cracks may have been formed due to:

- Shrinkage of metal during solidification
- Wetting to graphite crucible
- Wetting to TiC

The metal shrank during solidification creating cracks in the sample but due to good wetting properties towards the crucible, no void was formed between the alloy and the crucible. When there was a TiC layer between the crucible interface and the metal, these zones experienced cracks and brittleness, suggesting that the TiC and metal was non-wetting.

5.7 Mechanism of carbide formation

Both silicon carbide, titanium carbide and graphite has formed in the experiments. As shown in Table 19, there is samples with SiC, C or TiC particles present but also samples with C +SiC , C + TiC and SiC+TiC.

In Table 37 and 46 the locations of the particles are given. The particles could be found close to the interfaces both in slag metal and the crucible. Another finding is that the concentration of C and Ti was relatively constant in the different phases with no measurable gradients from bulk to the interfaces.

In the crucible, we know that the transport is only by diffusion. In the slag and metal the transport of elements can be by diffusion and convection if the slag is not to viscous. The particles can also be transported by convection or due to surface forces.

It was observed that the experiments using high Ti slag gave a decrease in the amount of metal.

Apart from metal 1 containing 1.49% C, metal 2 containing 0.36% C and a coke particle for some of the experiments, the graphite crucible is the sole source of carbon in the experiments. Carbon from the graphite crucible has dissolved into the liquid alloy, as the amount of carbon found as carbides or in the alloy exceeds the amount of carbon put into the experiments.

The results indicate that particles are nucleated in zones close to the interfaces probably with local high concentration of C and Ti respectively for formation of SiC and TiC. Then C and Ti is transported by diffusion or convection to allow for the particles to grow.

Another mechanism could be that the particles would grow in the bulk of slag and metal and then transported to the interfaces by convection and due to the wetting conditions.

6. Conclusion

The goal of this project was to investigate the possible origins of the carbides found in submerged arc furnaces producing silicomanganese alloys. This was done by reproducing the mechanisms of SiMn production carried out through melting experiments in a vertical tube furnace. The effect of four variables in the melting experiments were investigated:

1. The effect of silicon content in the alloy

   In the experiments conducted with Std-SiMn alloy containing 20wt.% Si, SiC was observed in 2/10 experiments analyzed. In the experiments conducted with LC-SiMn alloy containing 29wt.% Si, SiC was observed in 8/9 experiments analyzed.

   When increasing the Si content in the alloy, less TiC will accumulate.

2. The effect of titanium content in the slag

When using a slag with no TiO_2, no TiC was observed in the samples. Using a slag with higher % Ti will result in more TiC.

When using a slag with 1wt.% TiO_2, TiC was only observed on the crucible interface and on the slag-metal interface. The crucible had to be in contact with both slag and metal to form TiC. The TiC seems to have been mostly formed by a direct reaction between dissolved carbon and dissolved TiO_2.

By increasing the TiO_2 content in the slag to 10wt.% the TiC was observed to have accumulated on the crucible interface, on the slag-metal interface and in the bulk of the slag. Contradictory to the 1% Ti , for 10% Ti, TiC was observed in the areas with only graphite and slag as well as only metal and slag. The TiC seems to have been formed by a direct reaction between dissolved carbon and dissolved TiO_2.

With increased Ti content it was observed that less SiC would accumulate, and in some cases not at all. At higher Ti contents (10wt.% TiO_2 in the slag) most samples were observed to not have accumulated any SiC, or very little.

3. The effect of temperature

Increasing the temperature will result in more carbides being precipitated by cooling in the bulk of the metal, due to increased carbon solubility at higher temperatures. Increasing the temperature will also encourage the formation of SiC as opposed to graphite, due to the increased carbon solubility.

4. The effect of hold time

The effect of hold time on TiC formation seemed to be trivial. Some increase in particle size was observed. No effect of hold time on SiC formation was observed.

From the results, formation through the graphite-slag (solid-liquid) reaction and formation through slag-metal (liquid-liquid) seemed to be the biggest contributor to TiC accumulation. Silicon saturation of the metal phase, precipitating SiC as the alloy cools, seemed to be the case for SiC formation.

The results indicate that particles are nucleated in zones close to the interfaces probably with local high concentration of C and Ti respectively for formation of SiC and TiC. Then C and Ti is transported by diffusion or convection to allow the particles to grow.

Another mechanism could be that the particles would grow in the bulk of the slag and metal and then be transported to the interfaces by convection and due to the wetting conditions.

References

1. Olsen, S.E., Tangstad, M., % Lindstad, T. (2007). *Production of manganese ferroalloys.* Trondheim: Tapir Akademiske Forlag.
2. Olsen, S.E. & Tangstad, M. (2004). *Silicomanganese Production – Process Understanding*. www.researchgate.net/publication/250156250 Accessed: December 2018
3. Davidsen, J.E. (2010) *Reaction Mechanisms in the SiMn Process*. Project thesis, NTNU.
4. Haukali, M. (2017). Excavation of SiMn furnace: Examination of phases in SEM. Report 2017:00287. Sintef, Trondheim, Norway.
5. Ringdalen, E. and Ksiazek, M. (2018), "Excavation of a SiMn-Furnace", Furnace Tapping 2018, Edited by J.D. Steenkamp & A. Cowey, Southern African Institute of Mining and Metallurgy, Kruger National Park, 14-17 October 2018
6. Øvrelid, S. (2018) *Carbide Accumulation in Manganese Furnaces*. Project thesis. NTNU.
7. Tangstad, M. (2013) *Metal Production in Norway.* Akademika Publishing, Oslo, 2013.
8. Davidsen, J.E. (2011) *Formation of Silicon Carbide in the Silicomanganese Process*. Master's thesis, NTNU.
9. Einan, J. (2012) *Formation of Silicon Carbide and Graphite in the Silicomanganese Process.* Master's thesis, NTNU.
10. Nordbø, E (2018) *The formation of SiC in liquid silicon in contact with graphite during temperature cycles*. Project thesis, NTNU.
11. Lindstad, L. H. (2002) *Recrystallization of Silicon Carbide. PhD Thesis, NTH Trondheim*
12. Washington Mills (2010). Carborex. http://www.washingtonmills.no. Datasheet no.1, Accessed by [8]: May 28th, 2011.
13. Chase, M.W. (1998). NIST-JANAF *thermochemical tables,* volume no.9 of *Journal of physical and chemical reference data, Monograph.* Washington, D.C.: American Chemical Society and the American Institute of Physics for the National Institute of Standard and Technology. 4th ed.
14. Thorvald Abel Engh, *Principles of Metal Refining*, Oxford Science Publications, NTNU Norway
15. Scace, R. I. and Slack, G. A. (1959) *Solubility of carbon in silicon and germanium*. Journal of Chemical Physics, 30(6):1551-1555.
16. Dollof, R.T. (1960) Research study to determine the phase equilibrium reactions of selected carbides at high temperatures. Technical report, Research Laboratory of National Carbon Company, Parma, Ohio.
17. Hoel, E.G. (1998) *Structures and phase relations in silicomanganese alloys.* PhD thesis, NTH, Trondheim.

18. Tuset, J.K. and Sandvik, J. (1970) *The solubility of Carbon in Ferrosilicomanganese at 1330-1630°C,* Technical report, SINTEF.
19. Steenkamp, J.D. (2012) *Chemical Wear of Carbon-based Refractory Materials in a Silicomanganese Furnace Tap-hole.* PhD thesis, University of Pretoria
20. Tang, K. (2017), Equilibria among MnSi alloys, Ti carbides and Slags. Memo, PROJECT NO 102015386, SINTEF
21. Tang, K. (2018), Titanium Behaviour in the Manganese Ferroalloy Furnaces, Technical report, SINTEF, PROJECT NO 102015386-3
22. Chu, S. J., Chen, P. X. and Zeng, S. L. (2015) RESEARCH ON DE-TITANIUM OF SILICOMANGANESE FERROALLOY BY BLOWING N2, Journal Article, University of Science and Technology Beijing, 100083, Beijing, China
23. Li, H. and Morris, A. (1997). *Evaluation of unified interaction parameter model parameters for calculating activities of ferromanganese alloys: Mn-Fe-C, Mn-Fe-Si, Mn-C-Si, Mn-Fe-Si-C systems*. Metall. Mater. Trans. B, Vol. 28B, pp. 553-562.
24. Private communications with Dag Håland, Eramet Kvinesdal
25. Sandvik, K. L., Digre, M., & Malvik, T. (1999). *Oppredning av primære og sekundære råstoffer.* Trondheim: Tapir.
26. Krystad (2011), Schematic of the induction furnace and control system, NTNU, Trondheim, Norway
27. Larssen, T. A. (2017), Reduction of MnO and SiO_2 from Assmang and Comilog based slags. Technical report, Department of Material Science and Engineering, NTNU
28. JEOL AB (2008). Jeol JXA-8500F electron probe microanalyzer (EPMA). Datasheet
29. Private communications with operator of EPMA, Morten Raanes, NTNU
30. Djis, H. M. and Smith, D. J. (1980) *Factors effecting the resistivity and reactivity of carbonaceous reducing agents for the electric-smelting industry.* J. South African Inst. Min. Metallurgy, pages 286-296.
31. Sahoo, P. and Koczak, M. J. (1991) *Analysis of in situ formation of titanium carbide in aluminum alloys*
32. Dalaker, H. and Tangstad, M (2009) *Time and Temperature Dependence of the Solubility of Carbon in Liquid Silicon Equilibrated with Silicon Carbide and Its Dependence on Boron Levels*. NTNU.
33. Olsen, S. E. and Ding, W. (2000) *Manganese and Silicon Distribution between Slag and Metal in Silicomanganese Production. ISIJJ International.*
34. Private communication with Merete Tangstad, Professor at NTNU

Appendices

A BSE Images

A.1 Sample 1

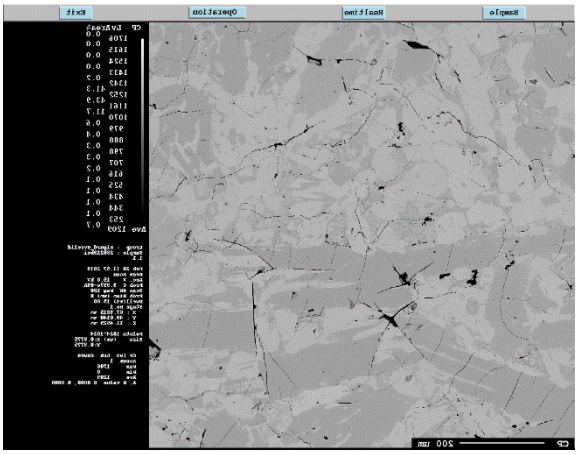

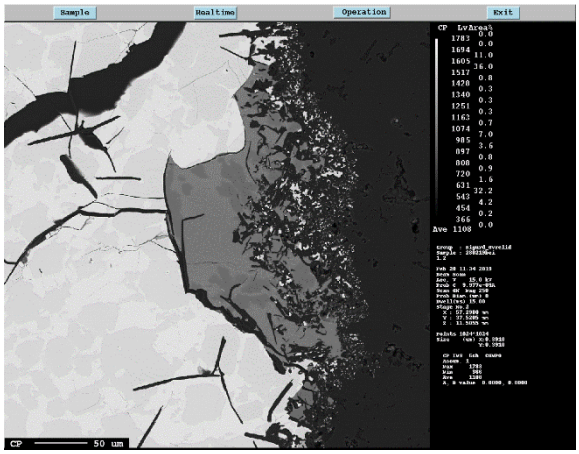

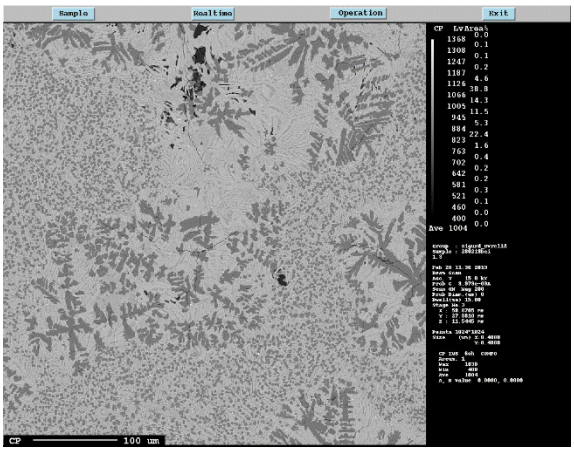

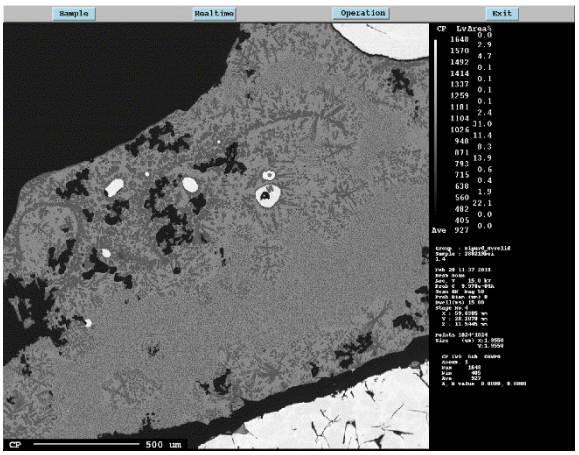

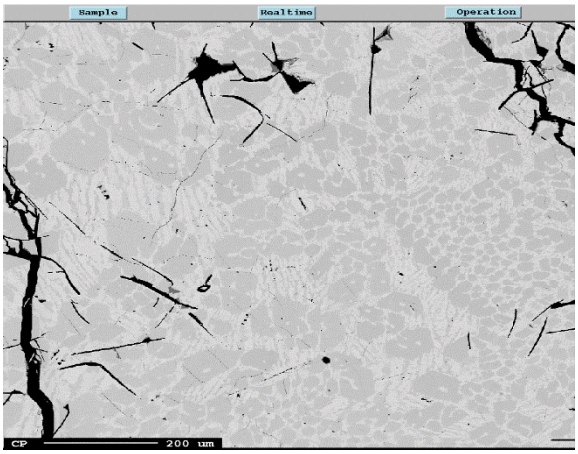

A.2 Sample 1.2

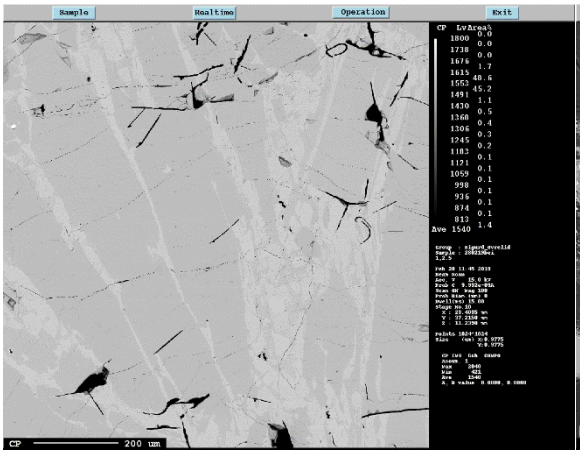
Sample
Realtime
Operation
Exit
200 um

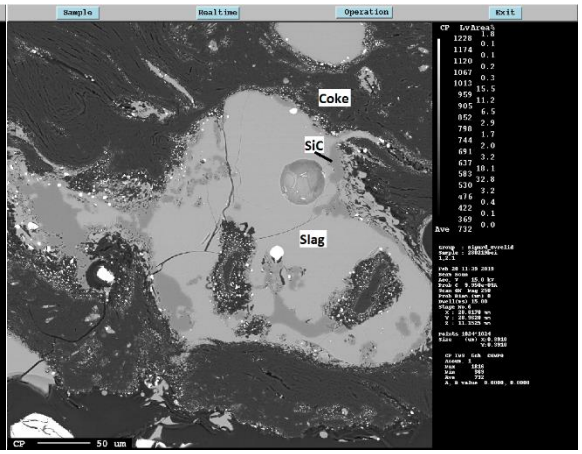
Sample
Realtime
Operation
Exit
Coke
SiC
Slag
50 um

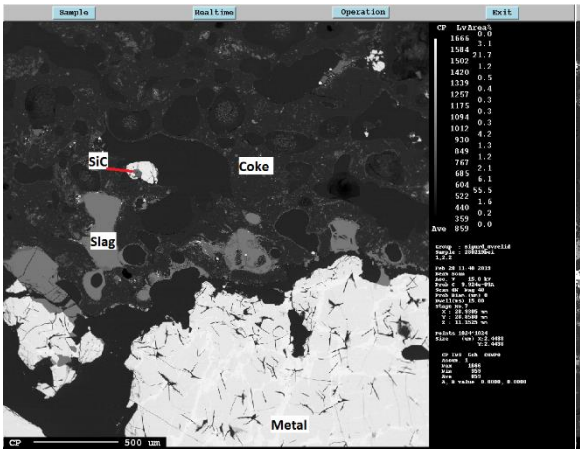
Sample
Realtime
Operation
Exit
SiC
Coke
Slag
Metal
500 um

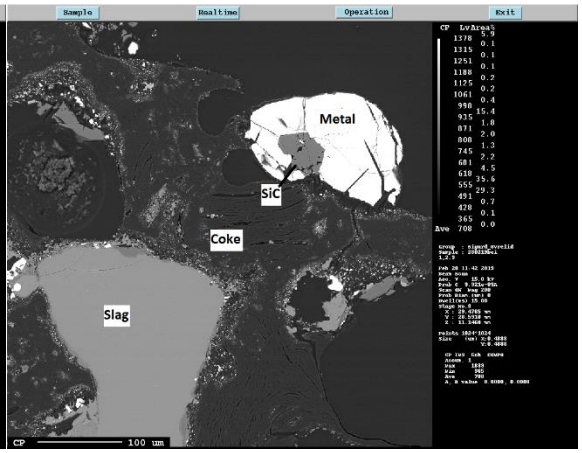
Sample
Realtime
Operation
Exit
Metal
SiC
Coke
Slag
100 um

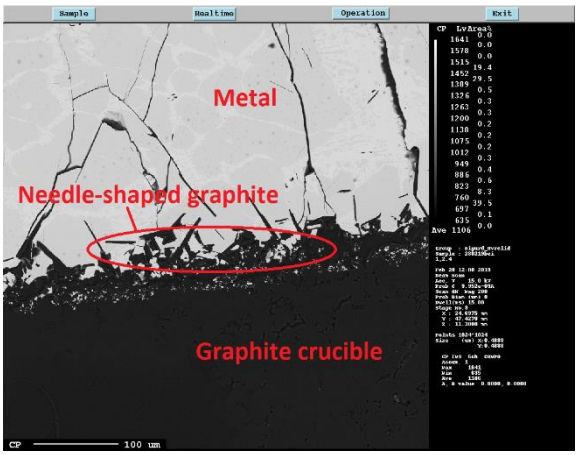
Sample
Realtime
Operation
Exit
Metal
Needle-shaped graphite
Graphite crucible
100 um

A.3 Sample 2

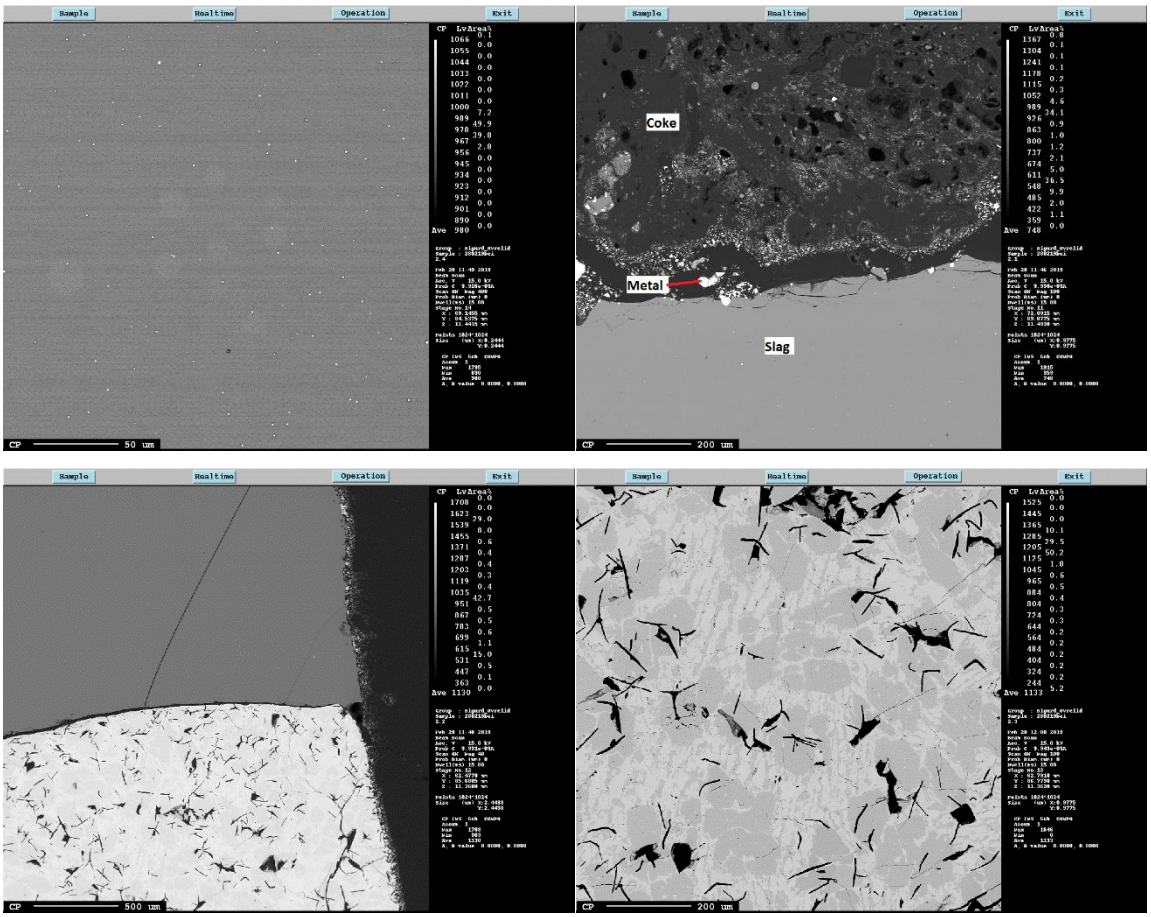

A.4 Sample 3

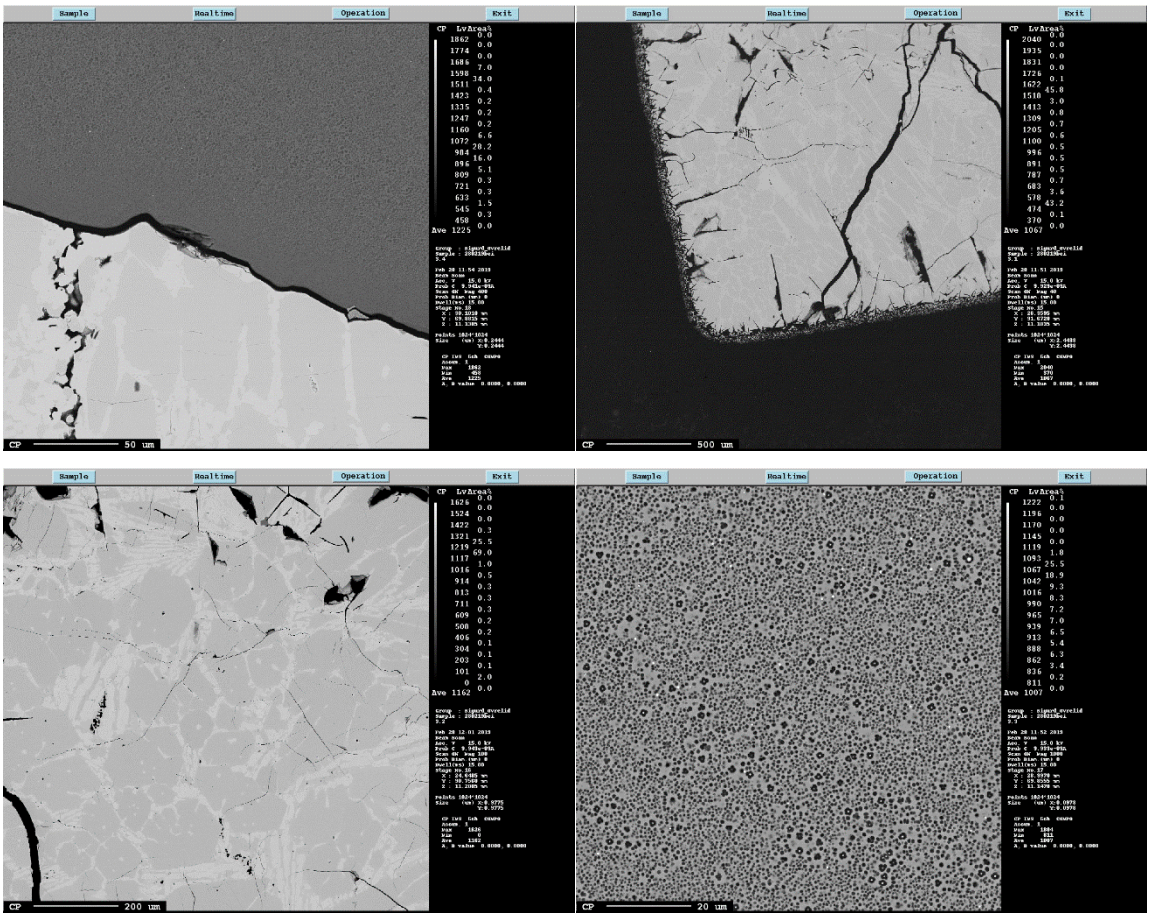

A.5 Sample 4

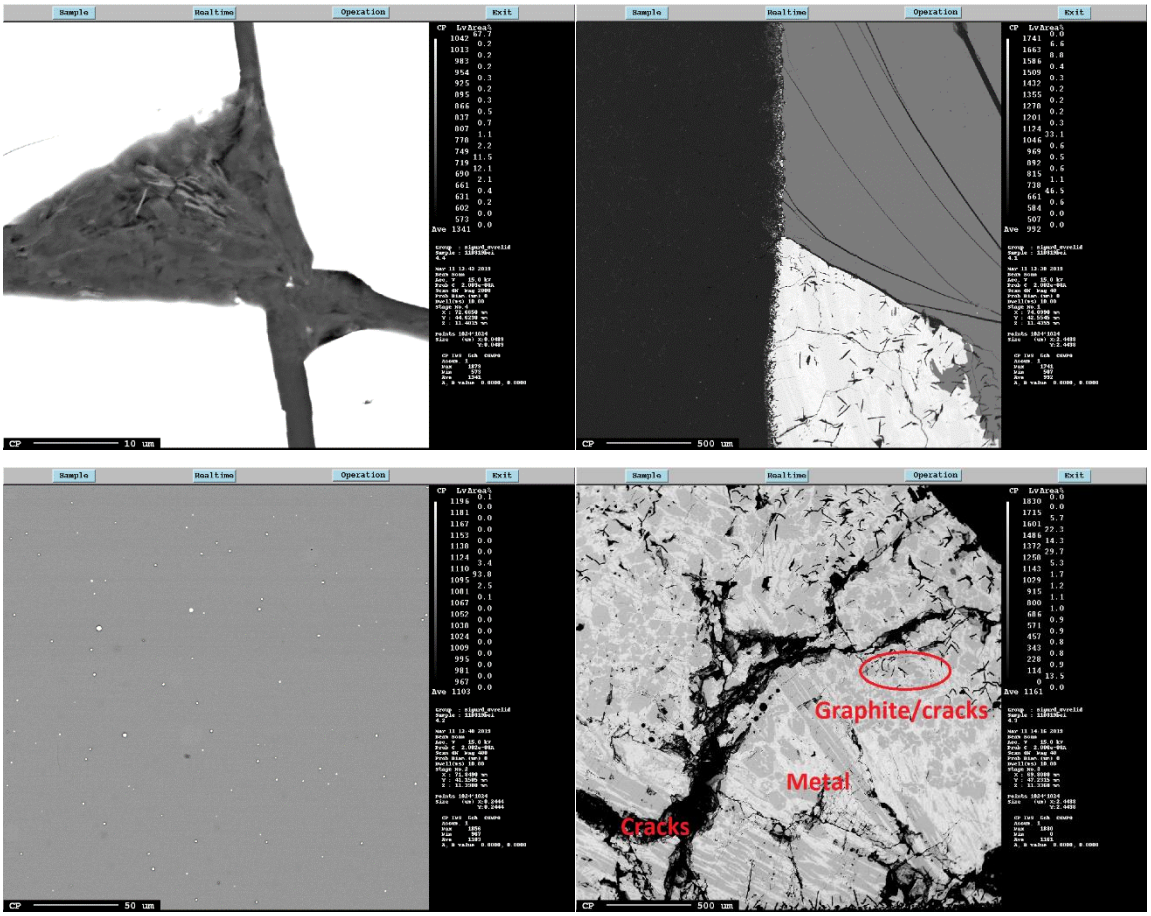

A.6 Sample 5

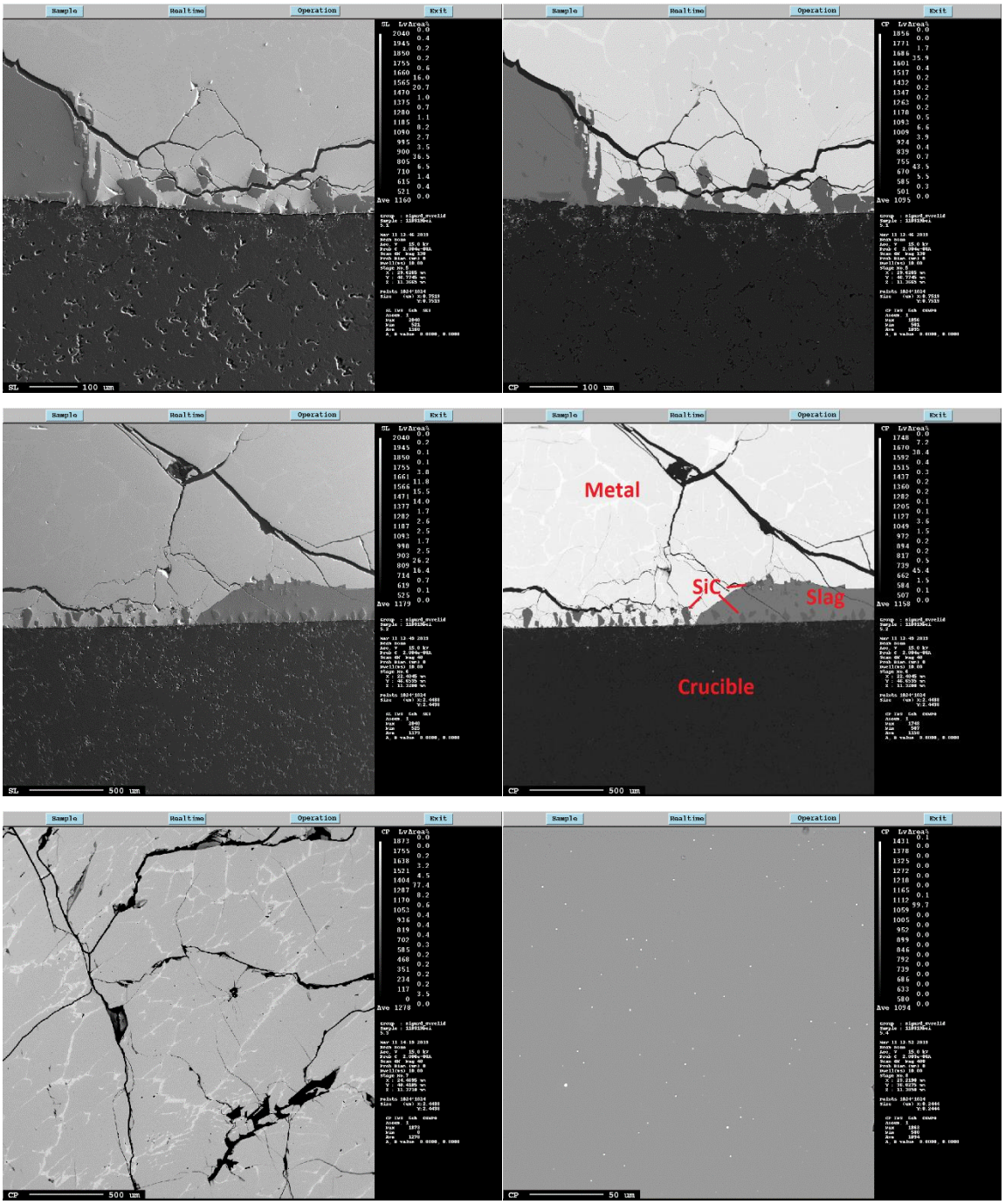

A.7 Sample 6

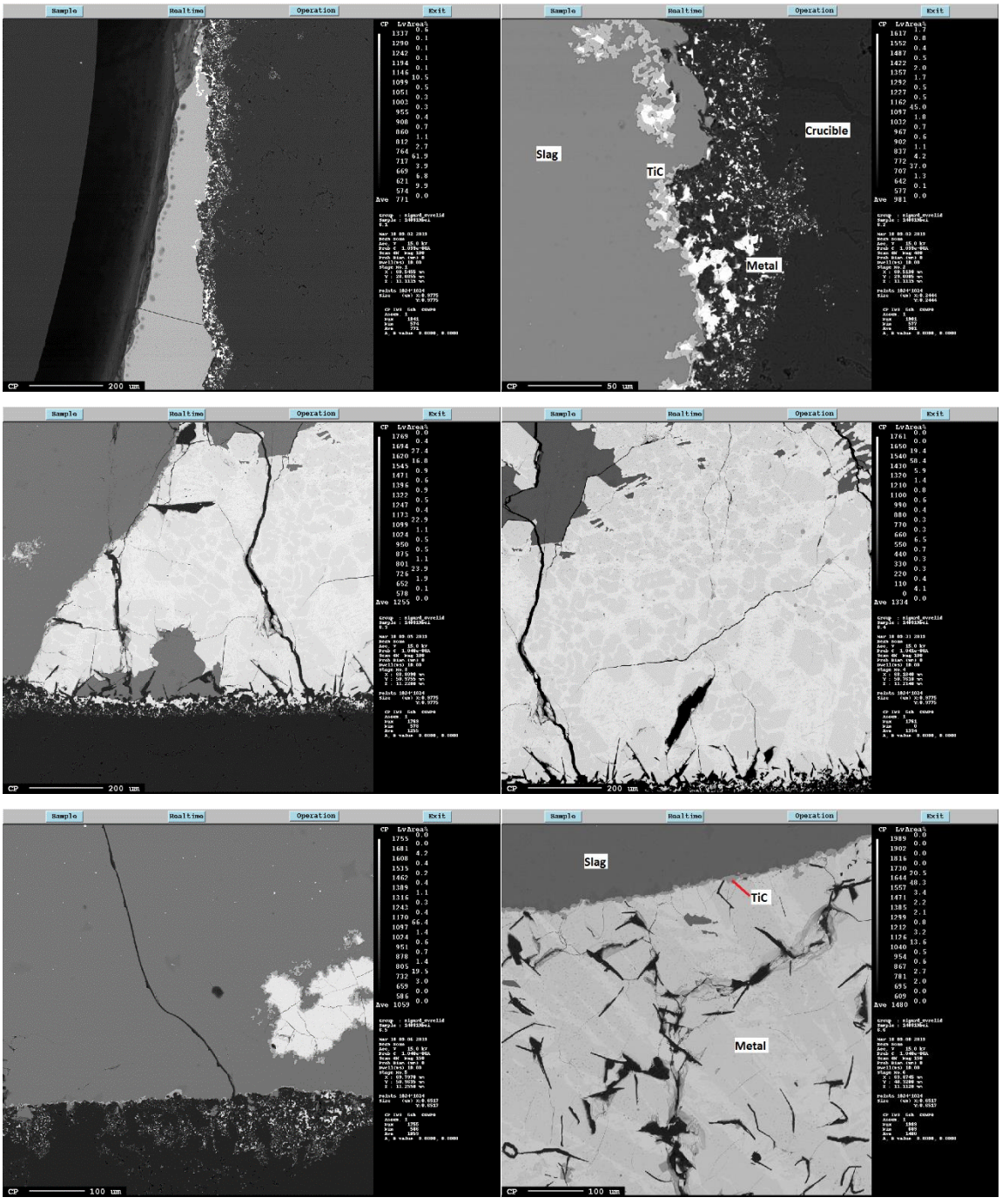

A.8 Sample 7

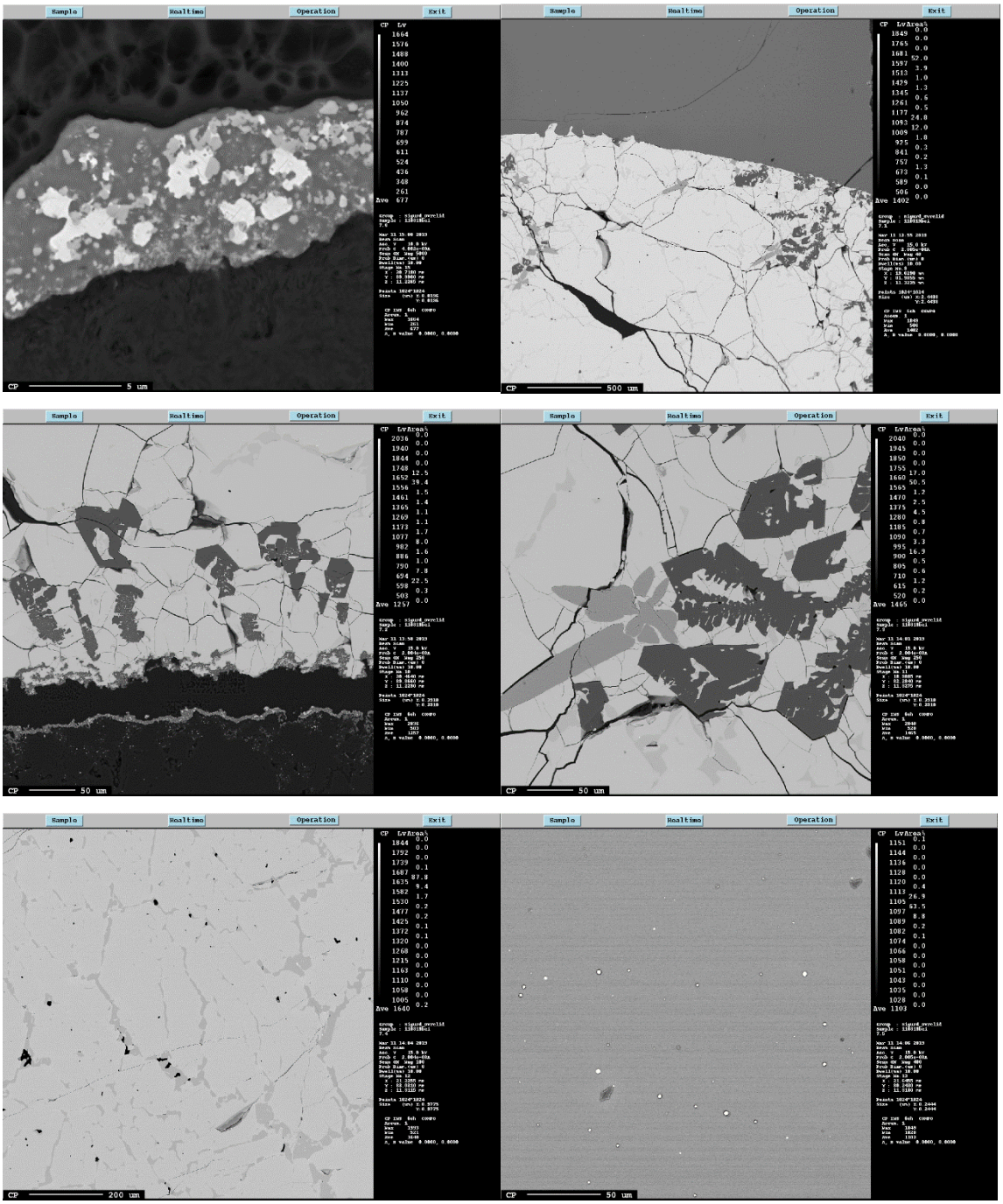
Sample
Realtime
Operation
Exit
5 um
500 um
50 um
50 um
200 um
50 um

A.9 Sample 8

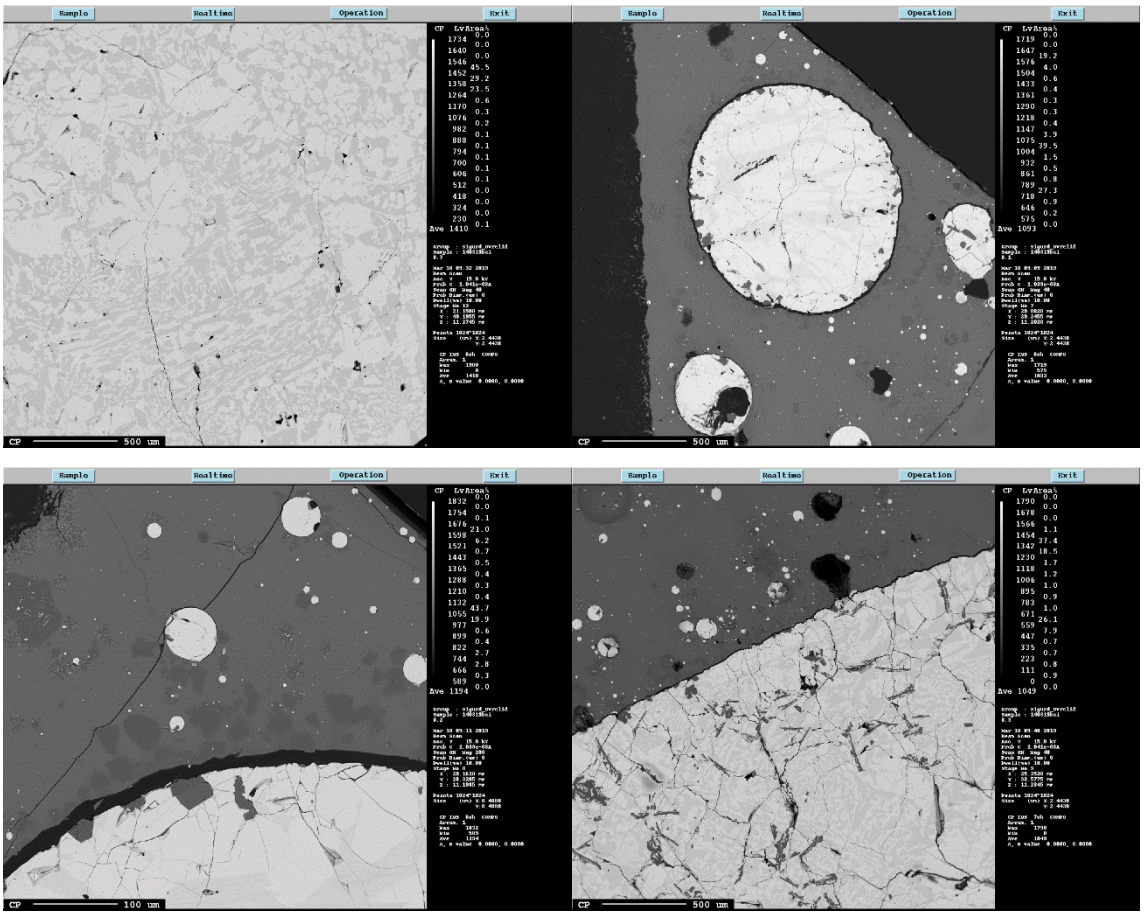

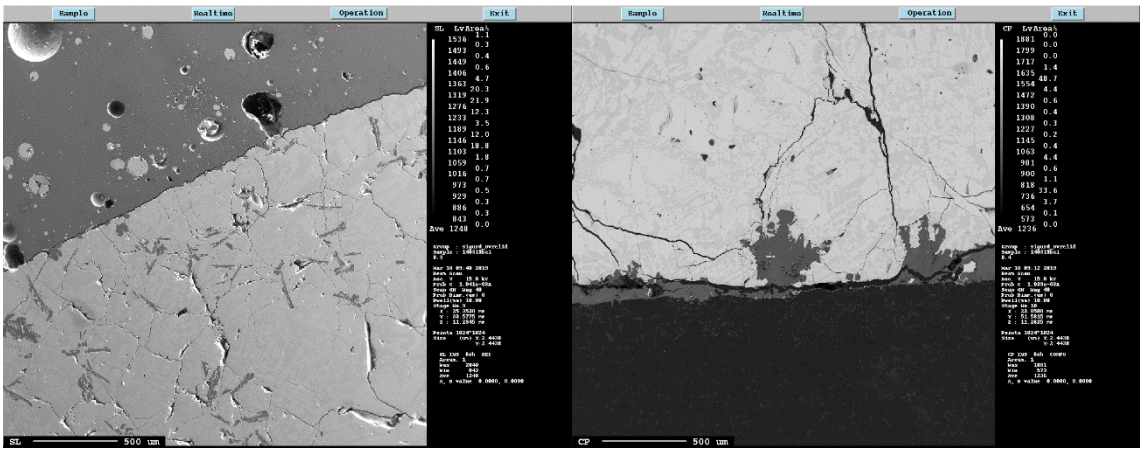
Sample
Realtime
Operation
Exit
500 um
Sample
Realtime
Operation
Exit
500 um

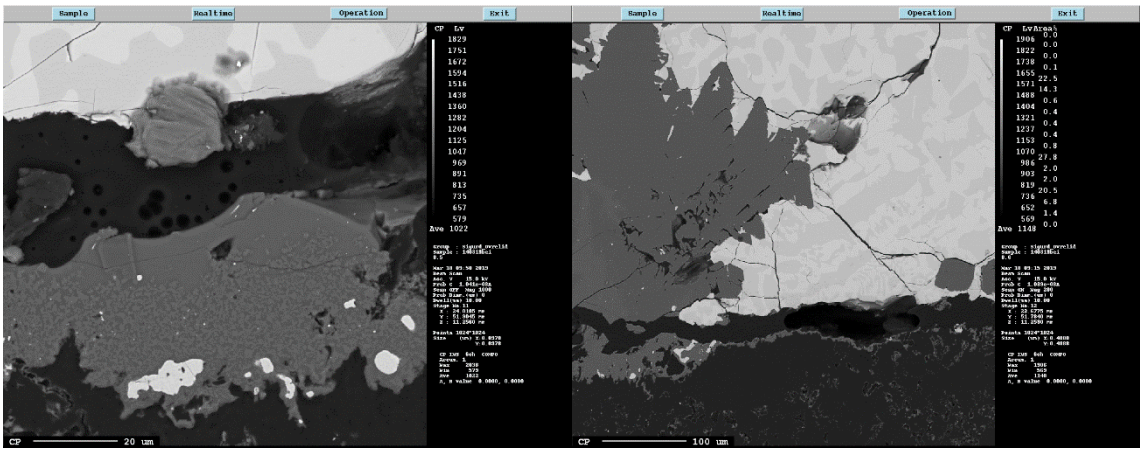
Sample
Realtime
Operation
Exit
20 um
Sample
Realtime
Operation
Exit
100 um

A.10 Sample 9

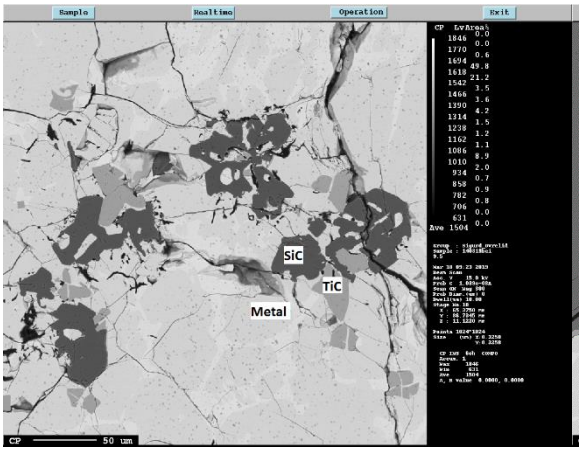

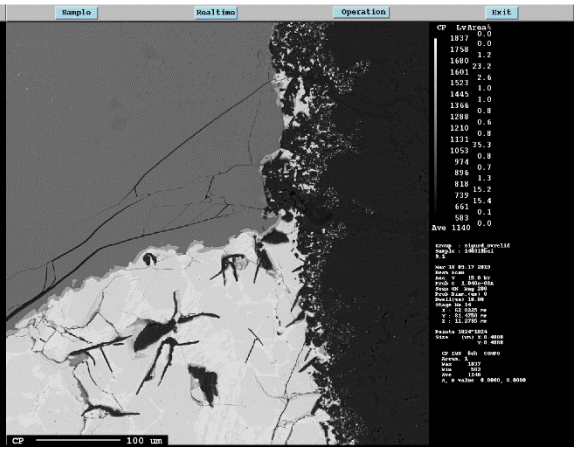

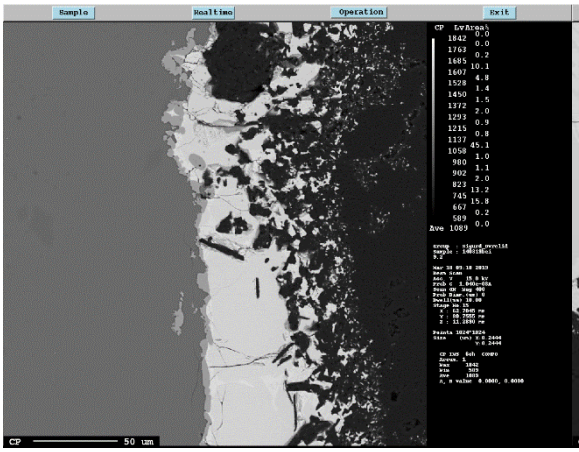

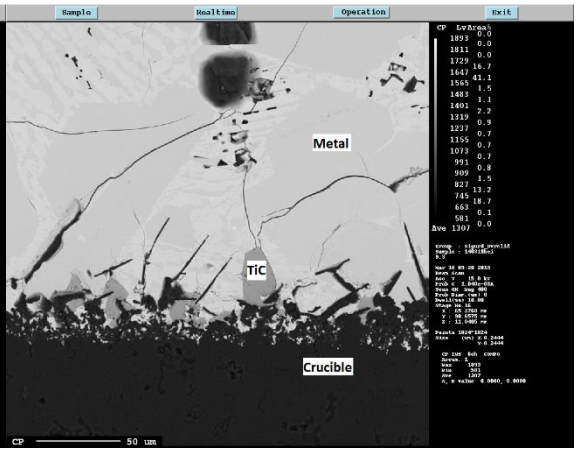

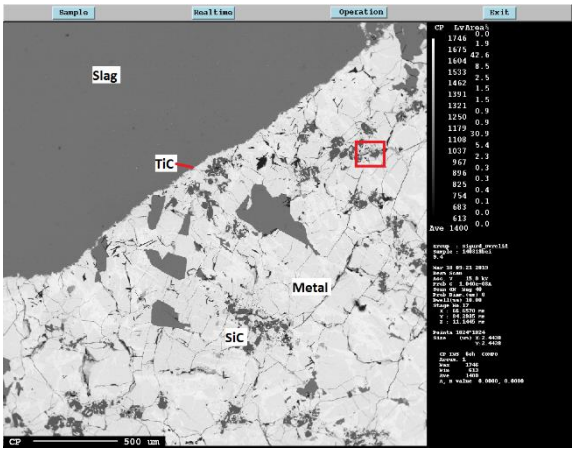

A.11 Sample 10

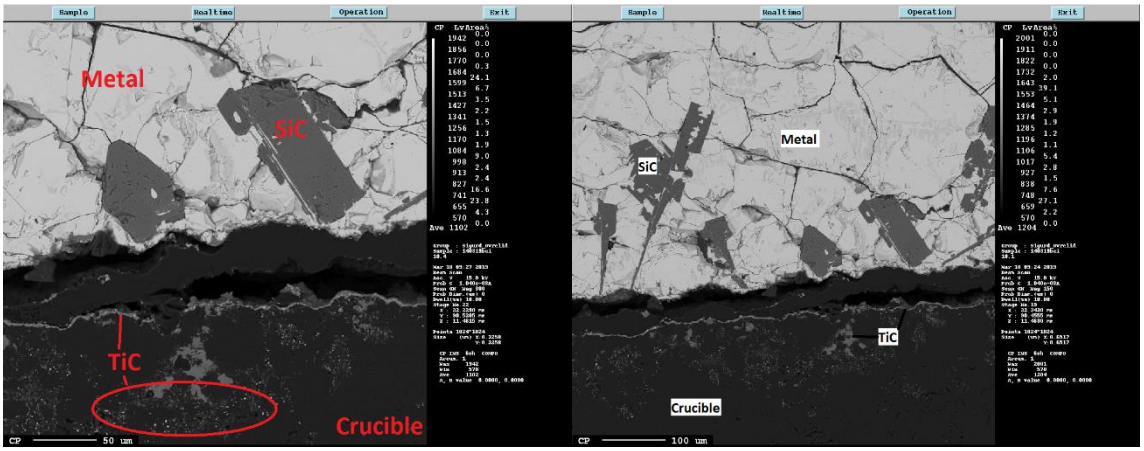

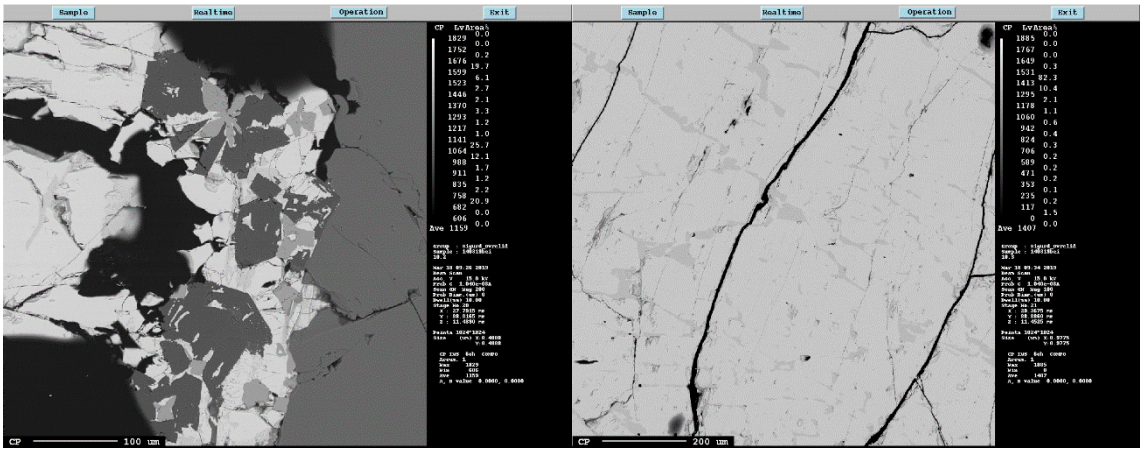

A.12 Sample 12

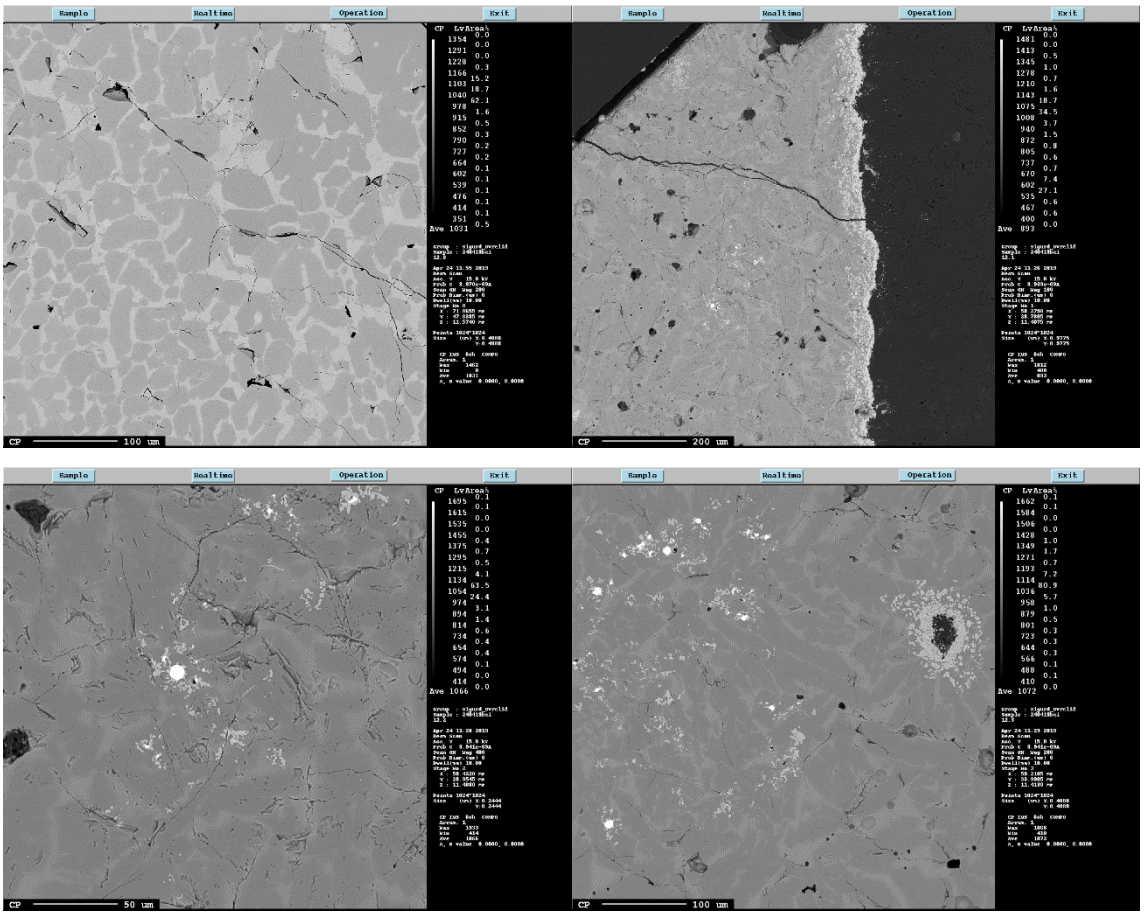

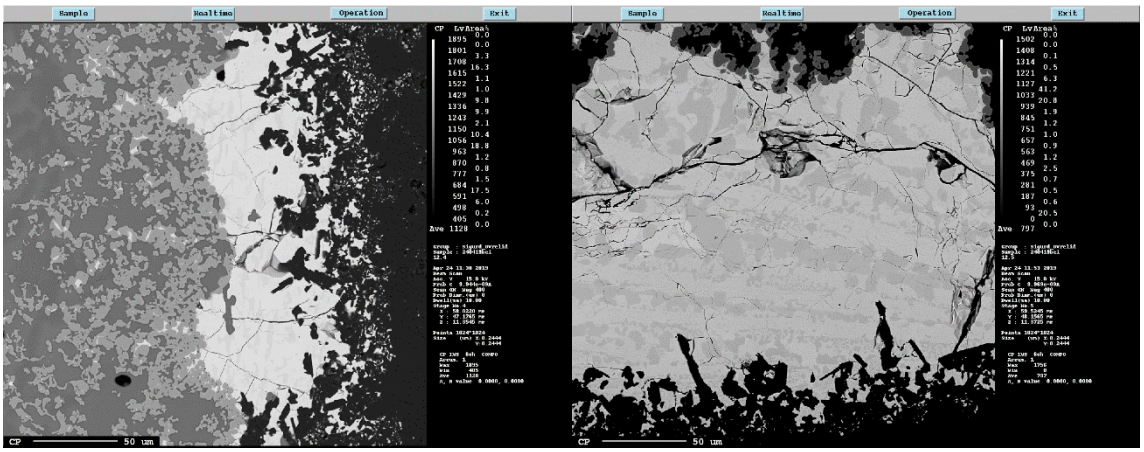
Sample
Realtime
Operation
Exit
50 um
50 um

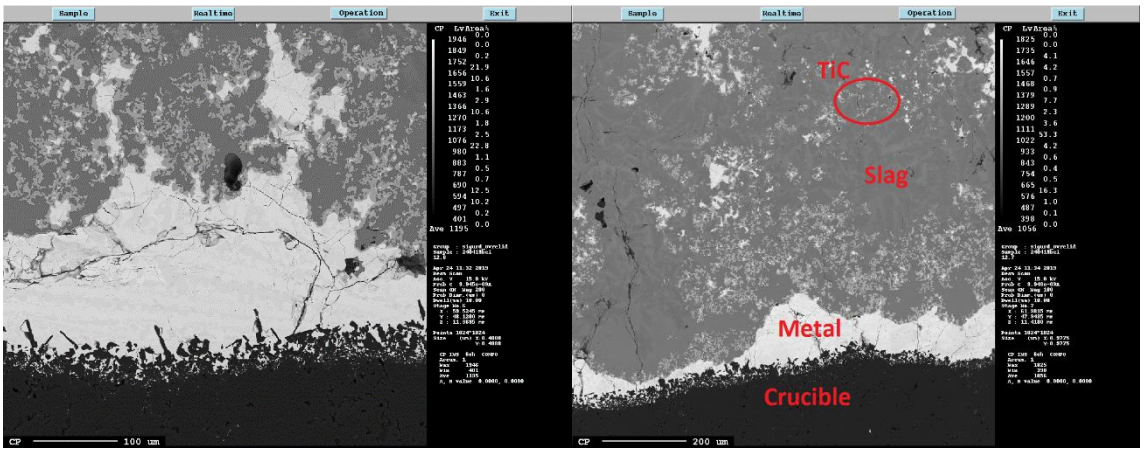
Sample
Realtime
Operation
Exit
100 um
TIC
Slag
Metal
Crucible
200 um

A.13 Sample 13

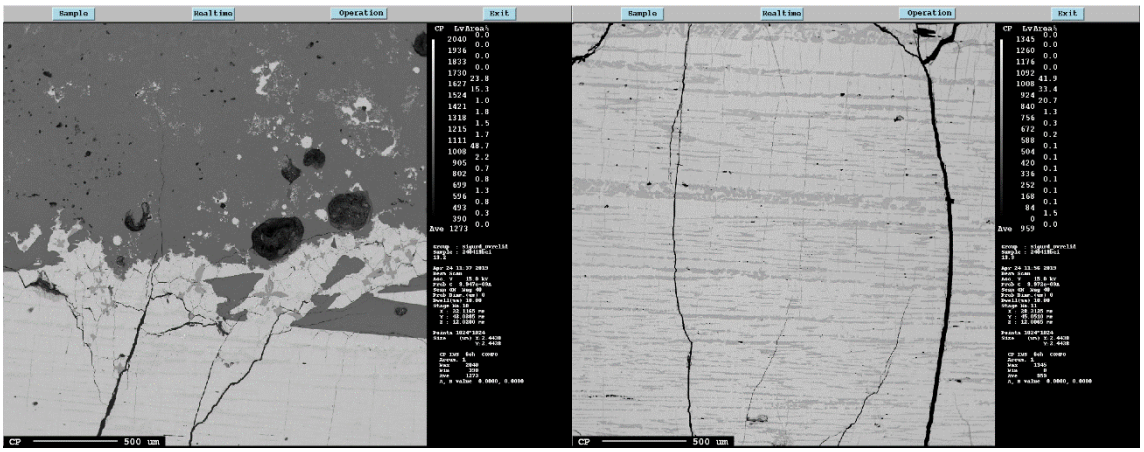

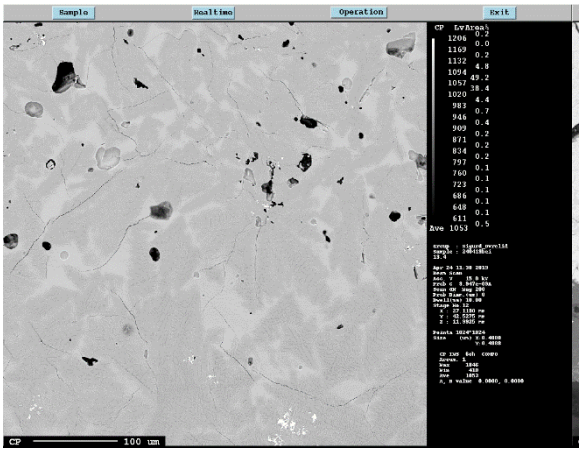

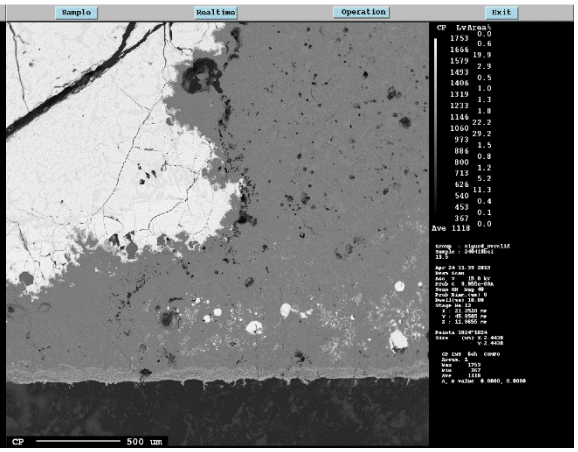

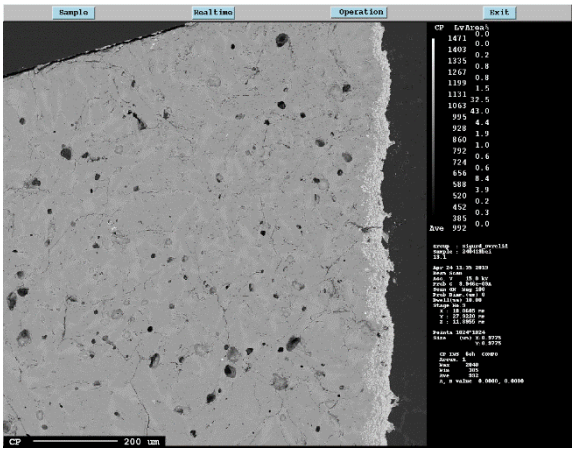

A.14 Sample 14

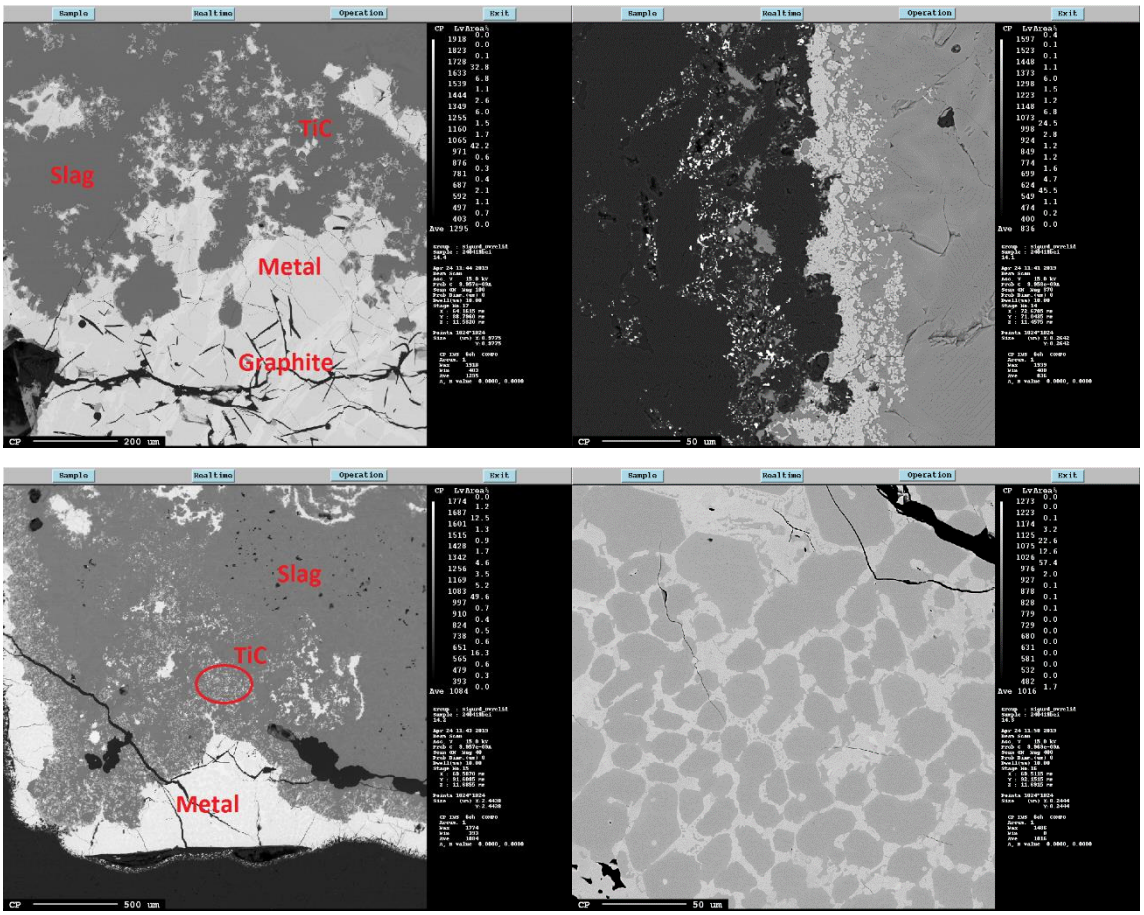

A.15 Sample 15

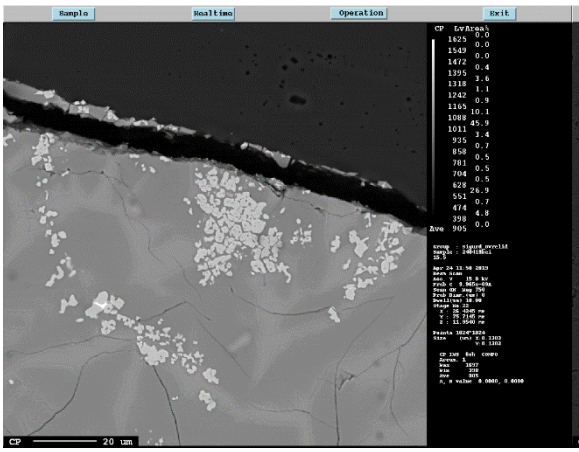

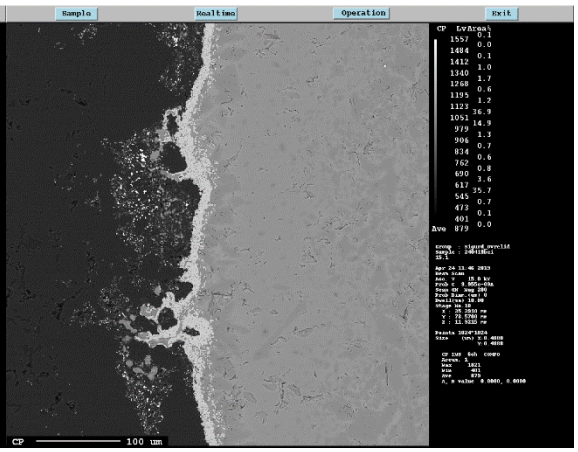

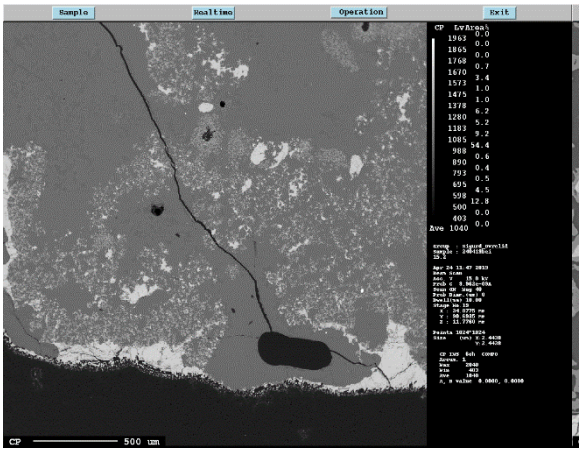

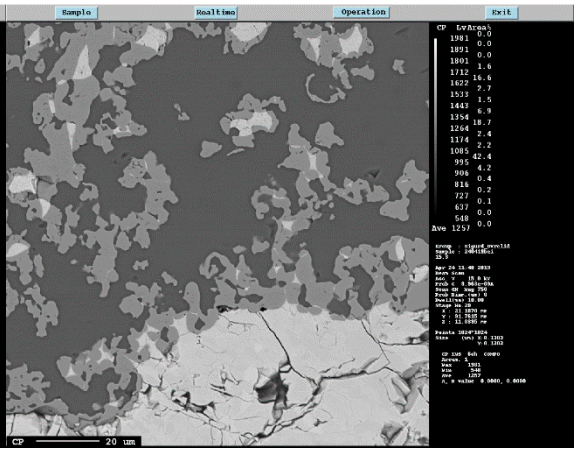

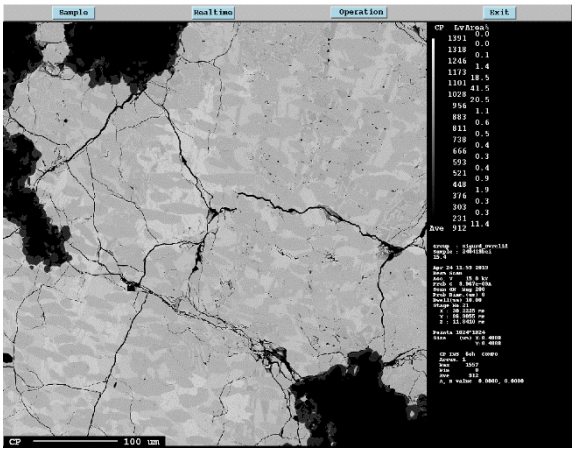

A.16 Sample 16

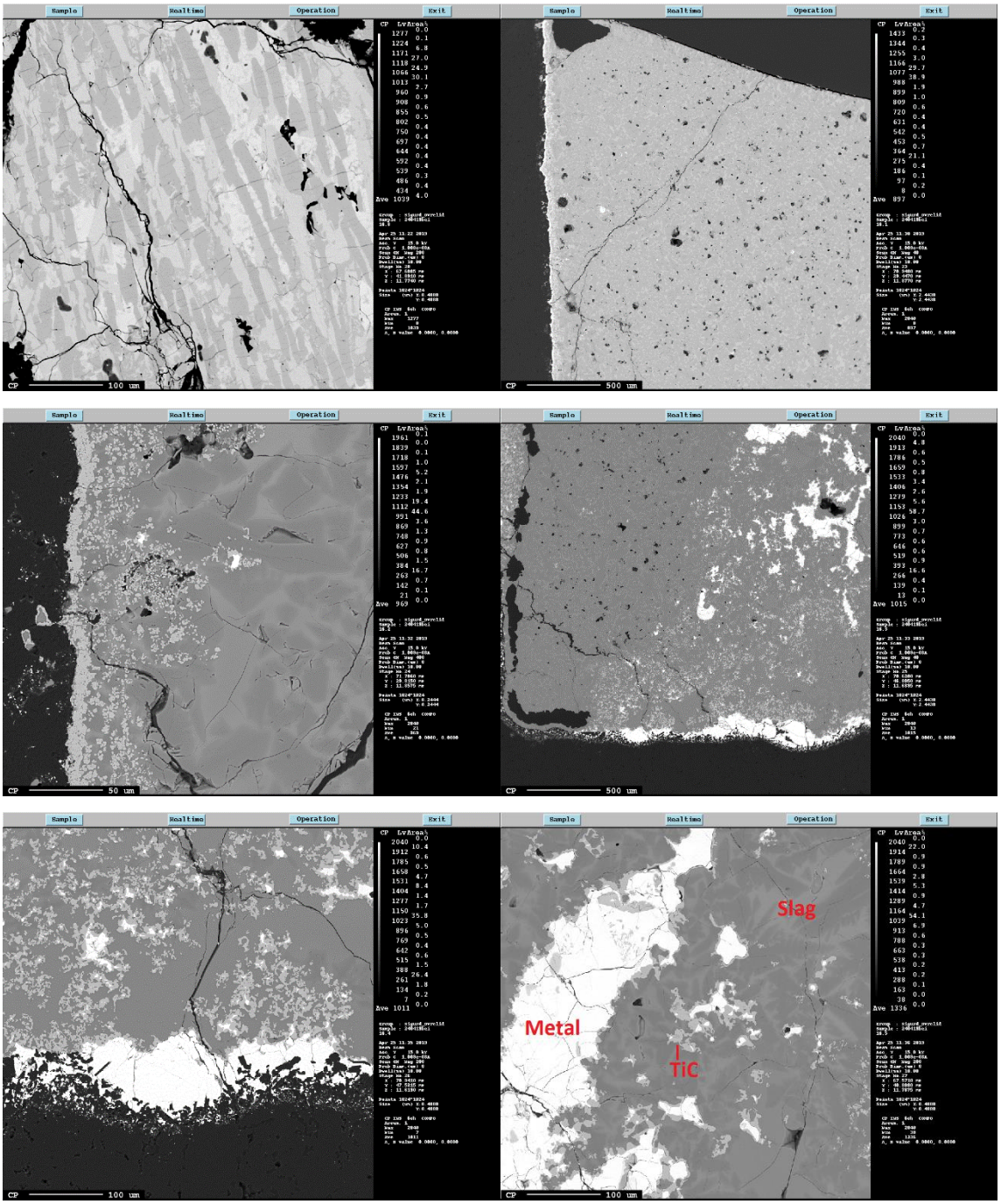

A.17 Sample 17

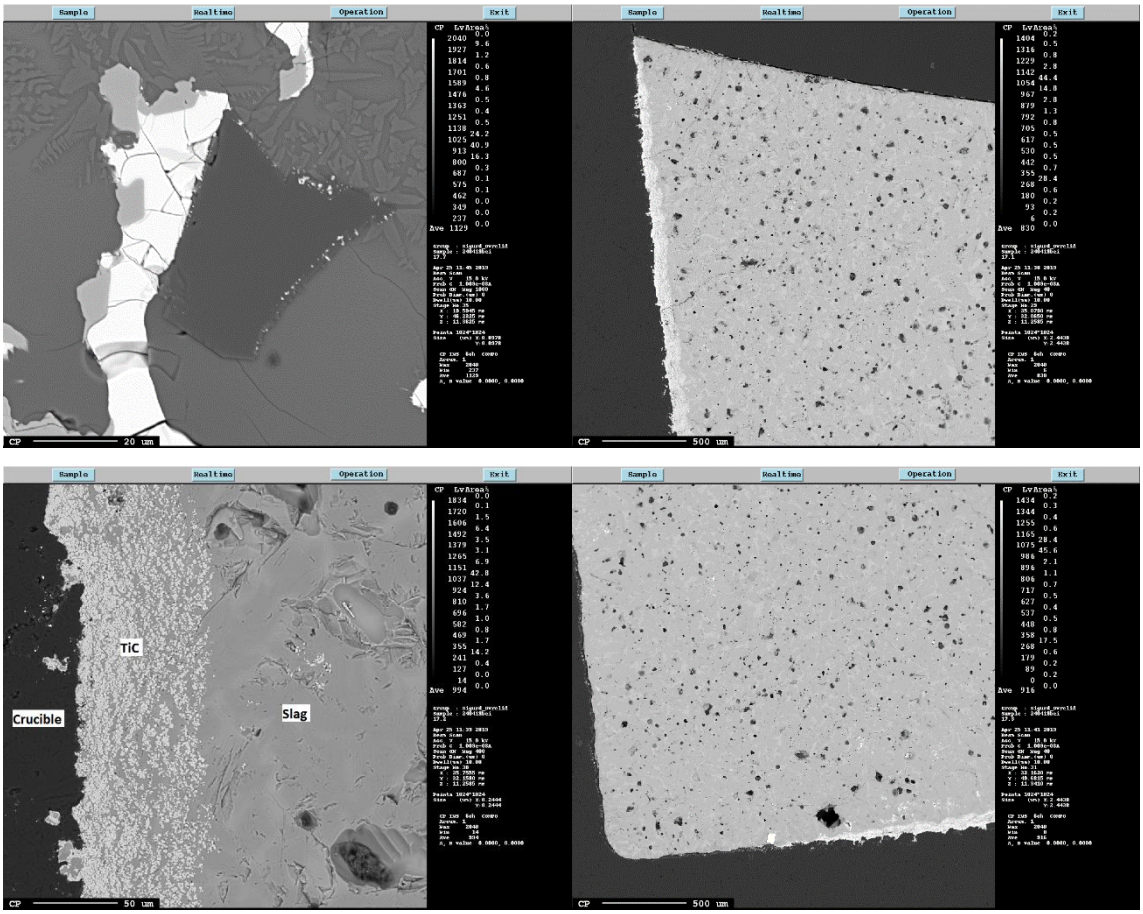

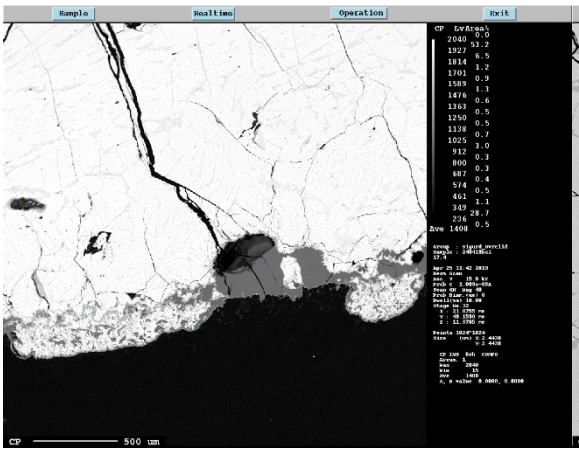
Sample
Realtime
Operation
Exit
CP
500 um

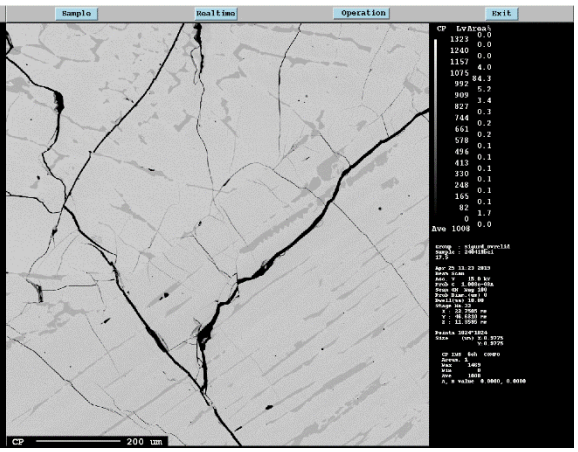
Sample
Realtime
Operation
Exit
CP
200 um

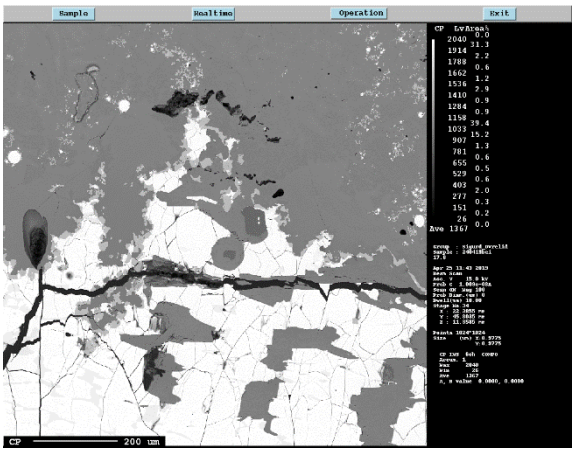
Sample
Realtime
Operation
Exit
CP
200 um

A.18 Sample 18

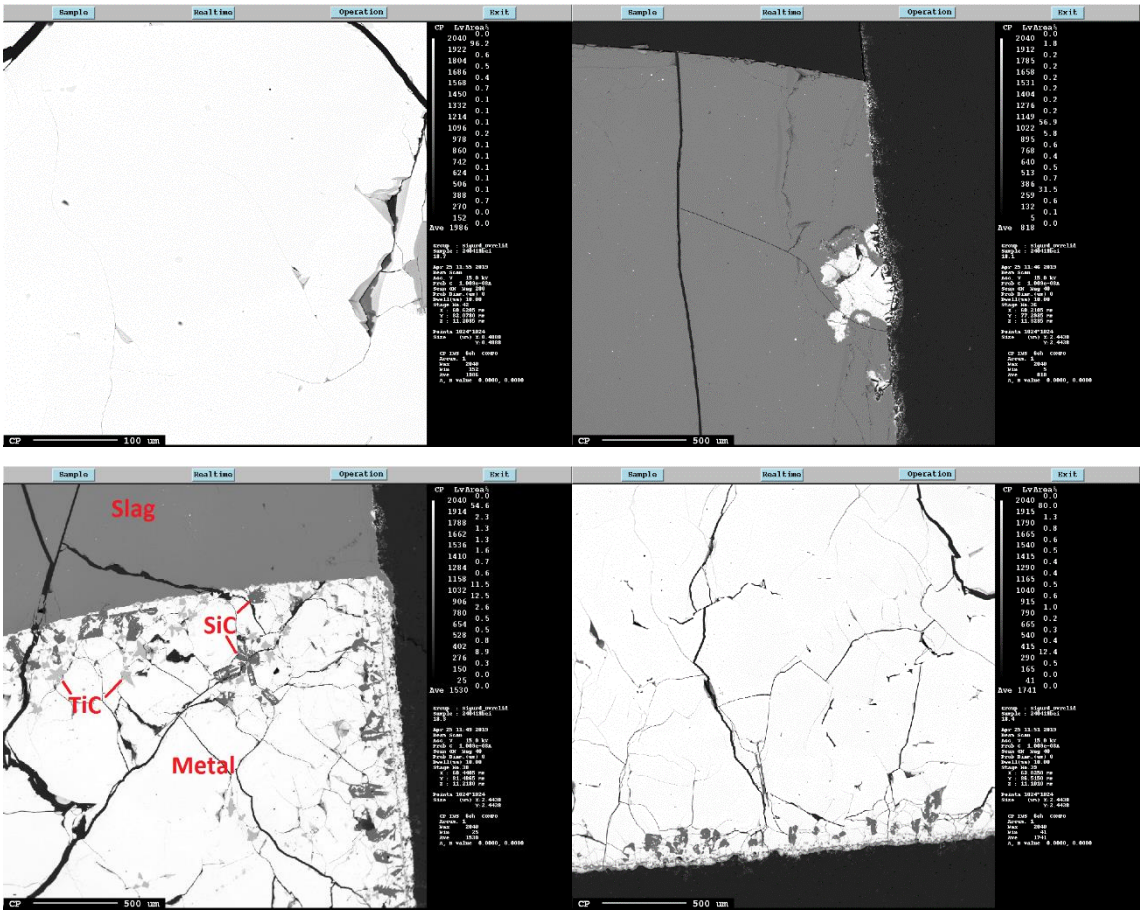

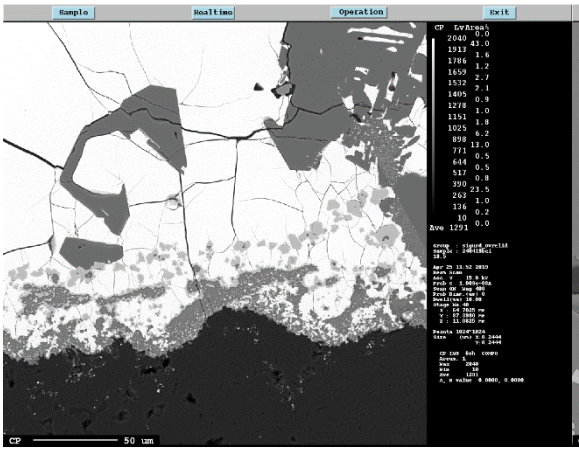
Sample
Realtime
Operation
Exit
CP
50 um

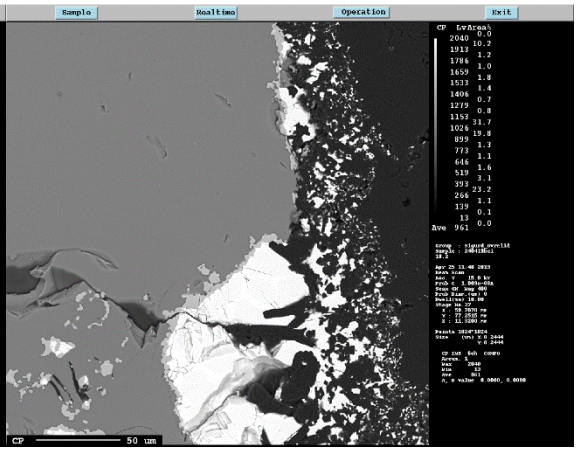
Sample
Realtime
Operation
Exit
CP
50 um

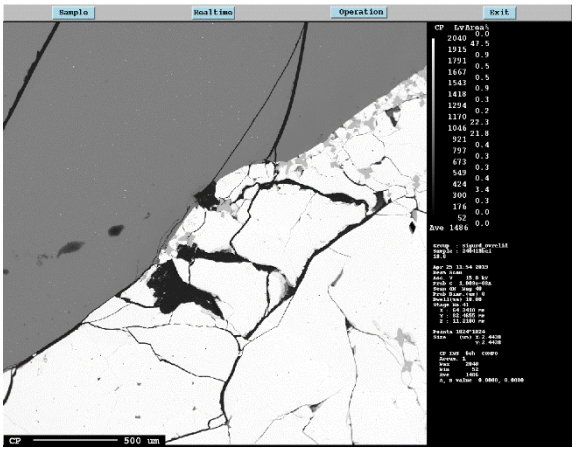
Sample
Realtime
Operation
Exit
CP
500 um

A.19 Sample 19

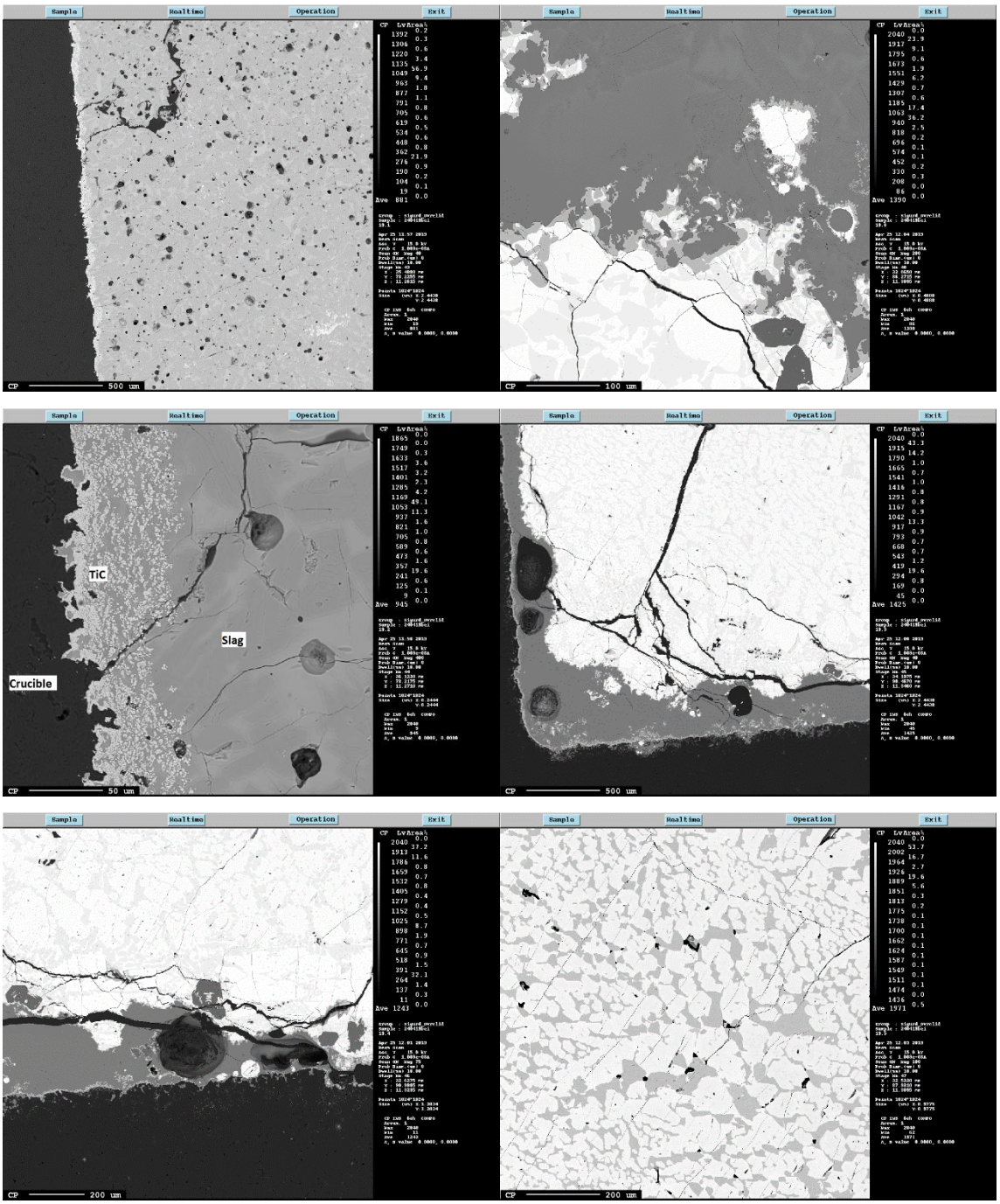

B Raw Data From EPMA Analyses

B.1 Samples 1-3

Mass percen	Group : Si	Sample : 28	Page	1									
No.	Si	O	P	C	Mn	Mg	S	Fe	Al	Ca	Ti	Total	Comment
1	10,261	0,106	0	0,524	74,122	0	0,026	15,648	0,033	0	0,108	100,828	1
2	10,151	0,186	0	0,514	71,449	0	0,001	16,164	0	0	0,096	98,561	1
3	10,268	0,062	0	0,524	71,786	0	0,008	16,37	0,006	0	0,084	99,108	1
4	24,244	0,03	0	0,365	60,656	0	0,004	16,659	0	0	0,244	102,202	1
5	24,329	0,054	0	0,365	60,62	0	0,005	16,75	0,001	0	0,249	102,373	1
6	24,123	0,061	0	0,37	60,62	0,014	0,003	16,976	0,011	0	0,205	102,383	1
7	29,103	41,711	0	0,352	19,139	1,791	0,475	0,027	1,965	4,47	0,643	99,676	1
8	28,508	41,447	0	0,338	20,778	3,402	0,318	0,076	1,35	3,924	0,609	100,75	1
9	28,659	41,445	0	0,338	20,518	2,377	0,347	0,027	1,648	4,259	0,346	99,964	1
10	43,532	53,892	0	2,85	0,573	0,025	0,017	0	0,047	0,048	0,046	101,03	1
11	43,496	54,132	0	2,814	0,584	0,028	0,011	0,038	0,046	0,06	0,043	101,252	1
12	43,486	53,702	0	2,816	0,627	0,025	0,002	0,006	0,048	0,079	0,015	100,806	1
13	10,164	0,139	0,019	0,523	71,939	0,008	0	15,682	0,023	0	0,066	98,563	1
14	10,147	0,154	0	0,515	71,956	0	0	15,175	0,032	0	0,13	98,109	1
15	10,206	0,142	0	0,514	72,024	0	0	15,592	0,001	0	0,099	98,578	1
16	24,076	0,039	0	0,386	62,014	0,005	0,008	15,351	0,003	0	0,324	102,206	1
17	23,96	0,094	0	0,354	62,135	0	0	15,394	0	0	0,394	102,331	1
18	24,04	0,084	0,002	0,378	61,461	0	0,025	15,586	0	0	0,304	101,88	1
19	19,708	41,648	0,024	0,378	3,02	6,901	0,419	0	11,755	15,272	0,061	99,186	1,2
20	19,693	41,365	0,005	0,428	3,067	6,785	0,475	0,013	11,588	15,369	0,064	98,852	1,2
21	19,918	40,838	0	0,44	3,05	6,731	0,371	0,021	11,437	15,119	0,061	97,986	1,2
22	69,563	0,623	0	28,819	0,183	0,043	0,003	0,013	0,09	0,161	0,018	99,516	1,2
23	69,499	0,689	0	28,88	0,194	0,043	0,007	0,033	0,079	0,154	0,002	99,58	1,2
24	69,236	0,508	0	28,906	0,24	0,051	0	0	0,037	0,106	0,027	99,111	1,2
25	21,278	0,134	0,197	0,558	69,832	0	0,02	8,821	0	0	0,062	100,902	1,2
26	19,806	0,066	0,32	0,585	70,124	0	0,019	8,851	0	0,006	0,051	99,828	1,2
27	21,585	0,022	0,211	0,561	69,937	0,029	0,027	8,91	0,01	0	0	101,292	1,2
28	10,012	0,125	0	0,54	75,504	0	0,01	11,8	0,015	0	0,05	98,056	1,2
29	9,949	0,154	0	0,55	75,098	0,003	0	12,299	0,015	0	0,027	98,095	1,2
30	10,071	0,133	0,005	0,544	75,144	0	0	11,999	0	0	0,041	97,937	1,2
31	24,352	0,061	0	0,387	65,426	0	0,023	11,183	0	0	0,446	101,878	1,2
32	24,259	0,031	0	0,376	65,677	0	0,026	11,2	0,005	0,013	0,373	101,96	1,2
33	24,154	0,055	0,005	0,392	65,006	0	0	11,439	0	0	0,341	101,392	1,2
34	20,733	42,048	0	0,36	6,029	6,461	0,016	0,034	8,875	16,494	0,025	101,075	2
35	20,928	41,962	0,001	0,339	6,193	6,315	0,023	0,016	8,771	16,491	0,013	101,052	2
36	20,75	41,745	0	0,329	6,049	6,404	0	0,031	8,704	16,407	0,062	100,481	2
37	10,054	0,151	0	0,545	76,589	0	0,013	11,13	0	0	0,069	98,551	2
38	10,085	0,114	0	0,558	76,206	0,038	0,014	11,131	0,001	0,006	0,047	98,2	2
39	9,985	0,112	0	0,591	75,515	0	0,003	12,102	0	0	0,116	98,424	2
40	23,872	0,043	0	0,374	65,967	0	0,018	11,296	0,008	0	0,25	101,828	2
41	24,006	0,063	0	0,375	65,431	0	0,004	11,272	0,012	0	0,28	101,443	2
42	24,043	0	0	0,382	66,047	0	0,025	11,37	0,011	0,013	0,277	102,168	2
43	20,775	42,076	0	0,325	6,019	6,415	0,019	0,031	8,769	16,54	0,009	100,978	2
44	20,849	42,01	0,027	0,321	6,055	6,419	0,019	0,022	8,888	16,449	0,015	101,074	2
45	20,715	42,358	0	0,321	6,092	6,367	0,014	0,005	8,776	16,704	0,057	101,409	2
46	9,954	0,175	0	0,523	75,717	0	0	11,456	0	0,01	0,073	97,908	3
47	10,184	0,252	0	0,52	76,416	0	0	11,478	0,007	0,009	0,036	98,902	3
48	10,144	0,088	0	0,516	75,947	0	0,001	11,838	0,005	0	0,067	98,606	3
49	24,258	0,138	0	0,374	65,733	0	0,003	11,481	0,022	0,012	0,39	102,411	3
50	24,188	0,09	0	0,369	65,883	0,005	0	11,412	0,012	0	0,36	102,319	3
51	24,149	0,05	0	0,38	65,392	0	0,001	11,548	0,008	0	0,339	101,867	3
52	28,77	41,392	0	0,404	17,288	2,013	0,31	0,076	3,183	3,79	0,51	97,736	3
53	29,128	41,647	0	0,423	17,234	1,972	0,264	0,019	3,106	3,789	0,405	97,987	3
54	29,381	41,645	0	0,403	16,881	1,982	0,3	0,018	3,178	3,799	0,427	98,014	3

B.2 Samples 4-5 & 7

Mass percen	Group : Si	Sample : 11	Page	1									
No.	Si	O	P	C	Mn	Mg	S	Fe	Al	Ca	Ti	Total	Comment
1	20.707	43.921	0.000	0.375	6.067	6.406	0.003	0.012	8.911	16.452	0.008	102.862	4
2	20.780	43.134	0.005	0.385	6.114	6.337	0.007	0.023	8.872	16.605	0.000	102.262	4
3	20.769	43.222	0.000	0.361	6.303	6.311	0.000	0.000	8.946	16.458	0.011	102.381	4
4	9.870	0.178	0.000	0.559	77.529	0.007	0.000	10.562	0.013	0.018	0.075	98.811	4
5	9.663	0.155	0.074	0.555	74.637	0.000	0.000	12.788	0.003	0.017	0.030	97.922	4
6	9.889	0.200	0.050	0.559	75.574	0.002	0.000	11.475	0.022	0.010	0.066	97.847	4
7	23.458	0.288	0.000	0.468	66.028	0.000	0.000	10.963	0.000	0.000	0.144	101.349	4
8	23.439	0.116	0.000	0.395	66.568	0.024	0.010	10.875	0.015	0.018	0.155	101.615	4
9	23.580	0.108	0.000	0.402	66.454	0.000	0.004	10.660	0.000	0.000	0.207	101.415	4
10	15.383	0.096	1.006	0.297	69.409	0.000	0.005	14.624	0.022	0.009	0.009	100.860	5
11	9.948	0.225	0.032	0.539	77.111	0.000	0.007	10.276	0.003	0.000	0.019	98.160	5
12	10.163	0.195	0.000	0.544	77.040	0.000	0.009	10.532	0.000	0.000	0.000	98.483	5
13	23.910	0.029	0.000	0.393	67.631	0.000	0.000	9.703	0.000	0.013	0.174	101.853	5
14	23.682	0.110	0.000	0.387	67.825	0.000	0.010	9.583	0.000	0.007	0.129	101.733	5
15	23.734	0.077	0.000	0.379	67.263	0.003	0.014	10.039	0.000	0.000	0.102	101.611	5
16	21.349	43.653	0.021	0.369	4.933	6.483	0.012	0.030	8.976	16.708	0.018	102.552	5
17	21.243	43.060	0.002	0.374	4.779	6.462	0.000	0.000	9.038	16.877	0.000	101.835	5
18	21.403	43.457	0.000	0.390	4.791	6.385	0.019	0.009	8.955	16.723	0.000	102.132	5
19	69.583	0.199	0.003	29.430	0.671	0.013	0.000	0.137	0.018	0.000	0.000	100.054	5
20	69.362	0.261	0.000	29.205	0.683	0.000	0.010	0.119	0.000	0.000	0.000	99.640	5
21	69.805	0.203	0.000	28.548	0.754	0.015	0.017	0.156	0.000	0.000	0.000	99.498	5
22	21.101	42.538	0.014	0.359	5.470	6.120	0.019	0.025	8.755	16.736	0.479	101.616	7
23	21.111	42.313	0.000	0.363	5.485	6.204	0.004	0.000	8.703	16.694	0.448	101.325	7
24	21.047	42.520	0.000	0.353	5.535	6.125	0.000	0.000	8.788	16.744	0.486	101.598	7
25	24.203	0.065	0.000	0.392	67.052	0.000	0.000	9.035	0.000	0.008	0.865	101.620	7
26	24.010	0.078	0.000	0.384	67.407	0.005	0.025	9.193	0.000	0.000	0.718	101.820	7
27	24.047	0.023	0.000	0.401	67.771	0.000	0.016	9.299	0.013	0.000	0.598	102.168	7
28	35.101	0.071	0.000	0.417	54.010	0.000	0.004	14.133	0.015	0.009	0.014	103.774	7
29	34.671	0.070	0.015	0.417	53.666	0.019	0.003	13.907	0.009	0.000	0.011	102.788	7
30	35.124	0.052	0.000	0.408	53.756	0.000	0.000	13.810	0.000	0.000	0.017	103.167	7
31	70.270	0.125	0.000	27.959	1.134	0.000	0.000	0.202	0.000	0.000	0.088	99.778	7
32	70.527	0.143	0.012	27.805	0.986	0.000	0.000	0.158	0.000	0.019	0.000	99.650	7
33	70.515	0.152	0.005	28.296	1.017	0.000	0.002	0.160	0.005	0.000	0.061	100.213	7
34	0.224	0.869	0.000	19.816	2.410	0.000	0.006	0.065	0.003	0.006	77.825	101.224	7
35	0.185	0.822	0.000	19.636	5.285	0.000	0.014	0.192	0.000	0.009	75.105	101.248	7
36	0.147	1.381	0.006	20.381	1.782	0.000	0.000	0.073	0.014	0.000	77.726	101.510	7
Minimum	0.147	0.023	0.000	0.297	0.671	0.000	0.000	0.000	0.000	0.000	0.000	97.847	
Maximum	70.527	43.921	1.006	29.430	77.529	6.483	0.025	14.624	9.038	16.877	77.825	103.774	
Average	27.611	10.947	0.035	6.731	35.581	1.581	0.006	5.634	2.225	4.171	6.544	101.066	
Sigma	21.005	18.825	0.167	11.285	32.931	2.773	0.007	5.782	3.899	7.317	21.514	1.515	

B.3 Samples 6, 8-10

Mass percen	Group : Si	Sample : 14	Page	1									
No.	Si	O	P	C	Mn	Mg	S	Fe	Al	Ca	Ti	Total	Comment
1	21.690	40.242	0.000	0.284	6.108	6.198	0.003	0.011	8.584	16.350	0.327	99.797	6
2	21.748	44.146	0.008	0.308	6.236	6.224	0.017	0.015	8.725	16.312	0.350	104.089	6
3	21.837	44.460	0.000	0.295	5.953	6.233	0.014	0.002	8.802	16.554	0.306	104.456	6
4	0.304	6.516	0.000	18.215	0.913	0.111	0.000	0.084	0.131	0.931	78.229	105.434	6
5	0.236	6.672	0.002	18.645	0.866	0.096	0.000	0.062	0.100	0.794	77.697	105.170	6
6	1.687	6.197	0.003	19.895	1.237	0.456	0.000	0.048	0.709	1.928	73.999	106.159	6
7	9.644	0.193	0.110	0.757	80.248	0.066	0.011	5.006	0.035	0.133	0.191	96.394	6
8	13.536	0.212	0.201	0.796	76.928	0.027	0.000	5.088	0.065	0.098	0.134	97.085	6
9	13.624	0.172	0.116	0.685	76.236	0.011	0.000	5.383	0.069	0.169	0.664	97.129	6
10	9.687	0.177	0.039	0.525	76.888	0.011	0.018	10.983	0.054	0.000	0.093	98.475	6
11	9.604	0.190	0.000	0.528	77.877	0.000	0.003	10.524	0.029	0.000	0.092	98.847	6
12	9.834	0.090	0.000	0.481	77.007	0.037	0.000	10.837	0.019	0.011	0.112	98.428	6
13	23.288	0.041	0.000	0.367	66.100	0.000	0.000	10.793	0.033	0.000	0.690	101.312	6
14	23.486	0.119	0.000	0.446	66.447	0.023	0.000	10.647	0.014	0.002	0.620	101.804	6
15	23.515	0.021	0.000	0.254	66.436	0.000	0.000	10.728	0.026	0.000	0.577	101.557	6
16	22.369	40.897	0.030	0.342	5.543	6.068	0.000	0.034	8.896	16.736	0.196	101.111	6
17	21.876	39.815	0.000	0.337	5.897	6.290	0.008	0.069	8.844	16.568	0.359	100.063	6
18	21.706	40.287	0.000	0.393	6.027	6.205	0.007	0.071	8.841	16.782	0.393	100.712	6
19	22.102	40.681	0.014	0.327	5.243	6.154	0.018	0.000	8.943	16.759	0.287	100.528	6
20	21.615	39.979	0.008	0.290	6.365	6.186	0.000	0.000	8.874	16.468	0.423	100.208	6
21	21.597	39.792	0.000	0.321	6.428	6.082	0.011	0.000	8.807	16.413	0.419	99.870	6
22	36.530	43.229	0.003	0.385	4.455	1.778	0.217	0.009	3.480	5.391	0.164	95.641	8
23	36.633	43.106	0.000	0.395	4.405	1.781	0.202	0.000	3.467	5.202	0.096	95.287	8
24	36.512	43.792	0.008	2.555	4.464	1.841	0.188	0.000	3.514	5.383	0.165	98.422	8
25	23.754	0.079	0.000	2.022	68.521	0.000	0.000	9.377	0.000	0.000	0.360	104.113	8
26	23.674	0.049	0.033	2.026	68.739	0.000	0.016	9.220	0.000	0.000	0.434	104.191	8
27	23.879	0.074	0.023	0.300	68.181	0.000	0.007	9.408	0.000	0.000	0.456	102.328	8
28	34.068	0.099	0.000	0.346	55.279	0.015	0.000	12.689	0.000	0.002	0.038	102.536	8
29	34.109	0.071	0.000	0.348	55.320	0.003	0.000	12.582	0.000	0.002	0.026	102.461	8
30	34.047	0.129	0.000	0.341	55.083	0.007	0.003	12.790	0.003	0.000	0.008	102.411	8
31	35.963	43.345	0.003	0.582	2.036	2.044	0.033	0.060	3.903	7.442	0.106	95.517	8
32	36.124	43.557	0.000	0.697	1.700	1.914	0.036	0.022	4.025	7.071	0.042	95.188	8
33	36.241	43.469	0.000	0.926	1.647	1.882	0.027	0.010	4.056	6.854	0.085	95.197	8
34	68.614	0.254	0.010	5.065	0.142	0.015	0.019	0.000	0.025	0.023	0.000	74.167	8
35	68.948	0.241	0.002	5.131	0.188	0.000	0.000	0.011	0.022	0.001	0.000	74.544	8
36	68.691	0.463	0.003	5.049	0.549	0.013	0.000	0.124	0.002	0.010	0.001	74.905	8
37	23.855	0.046	0.000	0.325	67.874	0.000	0.036	9.362	0.023	0.025	0.612	102.158	8
38	23.869	0.040	0.000	0.324	67.430	0.000	0.000	9.539	0.000	0.000	0.441	101.643	8
39	23.629	0.019	0.020	0.318	67.582	0.011	0.012	9.485	0.010	0.000	0.631	101.717	8
40	34.700	0.076	0.000	0.338	55.062	0.000	0.018	13.060	0.000	0.000	0.000	103.254	8
41	34.542	0.048	0.000	0.328	55.723	0.021	0.000	12.633	0.000	0.000	0.000	103.295	8
42	34.528	0.114	0.000	0.333	55.338	0.013	0.025	13.149	0.000	0.000	0.000	103.500	8
43	9.921	0.291	0.039	0.579	76.956	0.002	0.005	11.145	0.004	0.000	0.053	98.995	9
44	9.762	0.168	0.000	0.505	77.836	0.000	0.000	10.886	0.013	0.000	0.051	99.221	9
45	9.699	0.075	0.000	0.504	77.153	0.000	0.000	11.026	0.008	0.010	0.131	98.606	9
46	23.003	0.000	0.000	0.339	66.539	0.005	0.000	11.483	0.022	0.000	0.298	101.689	9
47	22.771	0.045	0.000	0.370	66.720	0.018	0.000	10.932	0.008	0.000	0.128	100.992	9
48	23.349	0.032	0.000	0.374	66.313	0.000	0.013	11.310	0.016	0.005	0.409	101.821	9
49	0.466	0.743	0.000	19.071	8.288	0.000	0.008	0.202	0.016	0.000	71.046	99.840	9
50	0.349	0.691	0.000	18.742	10.263	0.001	0.004	0.302	0.000	0.013	69.579	99.944	9
51	0.640	0.514	0.000	19.150	9.969	0.000	0.000	0.309	0.010	0.013	70.204	100.809	9
52	70.207	0.187	0.000	27.291	1.192	0.000	0.000	0.210	0.001	0.010	0.225	99.323	9
53	70.540	0.203	0.003	26.983	1.303	0.005	0.000	0.216	0.030	0.012	0.076	99.371	9
54	70.764	0.183	0.000	27.209	1.399	0.005	0.008	0.289	0.039	0.000	0.079	99.975	9
55	21.841	38.494	0.000	0.314	4.882	6.309	0.011	0.040	8.963	17.299	0.312	98.465	9
56	21.953	38.452	0.000	0.323	4.861	6.212	0.009	0.000	9.016	17.514	0.288	98.628	9
57	22.013	38.422	0.012	0.300	4.812	6.309	0.000	0.004	8.985	17.253	0.288	98.398	9
58	23.016	40.157	0.000	0.391	2.709	6.378	0.000	0.050	9.027	17.259	0.260	99.247	10
59	22.810	39.922	0.000	0.357	3.044	6.338	0.013	0.015	8.993	17.176	0.345	99.013	10
60	22.904	40.165	0.000	0.413	2.972	6.168	0.003	0.007	9.055	17.002	0.236	98.925	10
61	22.410	39.988	0.017	0.390	3.996	6.173	0.003	0.000	8.987	17.015	0.295	99.274	10
62	22.586	39.783	0.005	0.303	3.936	6.289	0.000	0.000	9.003	16.843	0.303	99.051	10
63	22.413	40.573	0.000	0.408	3.936	6.249	0.027	0.001	8.902	16.908	0.335	99.752	10
64	23.256	0.041	0.000	0.333	68.254	0.007	0.004	9.704	0.001	0.017	0.279	101.896	10
65	23.183	0.076	0.000	0.352	67.716	0.002	0.008	8.989	0.003	0.001	0.766	101.096	10
66	23.365	0.000	0.020	0.326	67.807	0.026	0.000	8.900	0.000	0.019	0.796	101.259	10
67	33.605	0.135	0.028	0.362	54.029	0.000	0.015	14.207	0.008	0.000	0.000	102.389	10
68	33.734	0.103	0.000	0.371	54.098	0.000	0.024	14.101	0.020	0.000	0.000	102.451	10
69	33.748	0.062	0.000	0.405	53.667	0.000	0.000	14.367	0.000	0.000	0.000	102.249	10
70	0.283	4.084	0.007	18.046	1.067	0.029	0.000	0.129	0.024	0.031	78.642	102.342	10
71	0.298	3.699	0.000	18.004	1.092	0.009	0.007	0.195	0.032	0.034	78.648	102.018	10
72	0.268	3.523	0.001	18.285	0.960	0.000	0.000	0.157	0.013	0.037	78.668	101.912	10
73	69.474	0.286	0.015	28.733	0.368	0.006	0.005	0.076	0.007	0.013	0.037	99.020	10
74	69.501	0.289	0.003	29.066	0.371	0.000	0.000	0.091	0.000	0.023	0.014	99.358	10
75	69.577	0.251	0.016	28.709	0.512	0.000	0.002	0.127	0.008	0.005	0.054	99.261	10
Minimum	0.236	0.000	0.000	0.254	0.142	0.000	0.000	0.000	0.000	0.000	0.000	74.167	
Maximum	70.764	44.460	0.201	29.066	80.248	6.378	0.217	14.367	9.055	17.514	78.668	106.159	
Average	26.688	13.664	0.011	5.066	31.330	1.658	0.015	4.712	2.458	4.599	9.236	99.436	
Sigma	18.991	19.039	0.030	9.024	32.131	2.633	0.040	5.490	3.782	7.134	24.555	5.661	

B.4 Samples 12-15

Mass percen Group : Si Sample : 24I Page 1

No,	Si	O	P	C	Mn	Mg	S	Fe	Al	Ca	Ti	Total	Comment
1	20,551	36,722	0	0,304	14,291	1,213	0	0,061	7,861	13,185	2,177	96,365	12
2	20,48	36,517	0	0,309	14,222	1,488	0,014	0,075	7,757	13,207	2,097	96,166	12
3	20,417	36,632	0	0,296	14,588	1,183	0,027	0,058	8,04	12,989	1,952	96,182	12
4	20,73	37,449	0,003	0,31	6,048	6,512	0	0,006	7,884	15,002	2,997	96,941	12
5	20,78	37,876	0,042	0,316	5,881	6,556	0,007	0,012	7,892	14,988	2,948	97,298	12
6	20,729	37,917	0,011	0,33	6,064	6,693	0,023	0,018	7,806	15,038	3,096	97,725	12
7	0,284	6,767	0	17,514	0,449	0,064	0,004	0,061	0,098	0,461	75,691	101,393	12
8	0,431	5,956	0,001	17,722	0,425	0,095	0,031	0,06	0,15	0,635	75,669	101,175	12
9	0,289	6,243	0,025	18,836	0,465	0,052	0	0,103	0,087	0,346	75,481	101,927	12
10	9,68	0,279	0	0,54	77,528	0,021	0,008	12,081	0	0,011	0,049	100,197	12
11	9,479	0,269	0	0,535	77,315	0	0,003	12,294	0	0	0,033	99,928	12
12	9,44	0,25	0	0,535	77,568	0	0,022	12,474	0	0	0,054	100,343	12
13	22,249	0,017	0,003	0,358	66,512	0,017	0	12,764	0,023	0	0,168	102,111	12
14	22,599	0,061	0	0,361	66,695	0,015	0,015	12,148	0,016	0	0,35	102,26	12
15	22,558	0,02	0,012	0,359	67,009	0	0	12,202	0,001	0,021	0,309	102,491	12
16	22,897	0,036	0	0,336	66,971	0	0,008	9,833	0	0	1,934	102,015	13
17	22,958	0,091	0	0,341	67,498	0	0	10,169	0	0,002	1,797	102,856	13
18	22,94	0,071	0	0,33	67,977	0,02	0	10,235	0	0	1,105	102,678	13
19	32,915	0,1	0	0,341	55,183	0,017	0,001	14,228	0,018	0,009	0,034	102,846	13
20	32,634	0,082	0	0,345	55,513	0	0,008	14,226	0,025	0	0,057	102,89	13
21	32,933	0,073	0	0,353	54,8	0	0,016	14,599	0,026	0	0,047	102,847	13
22	0,15	1,01	0,009	19,957	1,277	0	0	0,135	0	0,008	77,329	99,875	13
23	0,208	0,713	0,002	19,959	1,774	0	0	0,128	0,005	0	76,441	99,23	13
24	0,136	0,898	0	19,798	1,141	0,012	0	0,143	0,021	0,003	77,407	99,559	13
25	21,479	37,475	0	0,319	9,333	2,661	0,024	0,031	7,761	12,888	3,55	95,521	13
26	21,273	37,396	0	0,318	9,445	2,455	0,019	0,008	8,67	12,765	2,924	95,273	13
27	21,956	37,085	0,015	0,326	9,895	1,483	0,009	0,029	8,62	12,565	3,161	95,144	13
28	20,916	36,856	0,014	0,309	6,123	6,832	0,007	0,017	6,387	14,993	3,978	96,432	13
29	19,967	36,641	0	0,315	4,137	6,619	0	0	6,393	14,929	6,093	95,094	13
30	19,696	37,02	0,008	0,307	3,977	6,141	0	0,027	7,361	15,262	6,854	96,653	13
31	9,768	0,58	0	0,57	78,016	0,012	0,001	10,79	0	0	0,058	99,795	14
32	9,845	0,456	0	0,554	78,343	0	0	10,583	0	0	0,065	99,846	14
33	9,788	1,038	0	0,629	77,328	0	0	10,974	0,005	0,012	0,066	99,84	14
34	21,933	0,09	0	0,356	68,482	0,003	0,014	10,629	0	0	0,249	101,756	14
35	21,992	0,047	0	0,358	68,258	0	0,008	10,521	0,003	0	0,23	101,417	14
36	22,046	0,093	0	0,356	68,642	0	0,026	10,56	0	0	0,196	101,919	14
37	0,274	5,355	0,004	17,813	0,799	0,06	0,002	0,094	0,068	0,559	76,161	101,189	14
38	0,256	5,109	0,012	17,789	0,893	0,036	0	0,143	0,089	0,511	76,028	100,866	14
39	0,226	6,068	0	16,955	1,291	0,071	0	0,219	0,135	0,152	75,622	100,739	14
40	23,811	39,067	0	0,349	4,589	5,096	0,007	0,004	8,388	15,007	0,259	96,577	14
41	23,976	39,004	0,001	0,512	4,518	5,109	0,003	0,025	8,331	14,861	0,158	96,498	14
42	23,558	39,067	0,003	0,394	5,178	5,034	0,009	0	8,258	14,801	0,532	96,834	14
43	21,395	36,539	0	0,562	8,93	4,967	0,016	0,032	8,011	14,712	1,004	96,168	15
44	21,596	36,647	0	0,4	8,955	4,852	0,015	0,053	8,079	14,688	0,943	96,228	15
45	21,552	36,224	0,01	0,394	9,406	4,576	0,004	0,023	8,124	15,003	0,983	96,299	15
46	21,693	36,713	0,004	0,503	7,051	6,669	0,001	0,022	7,989	14,847	1,289	96,781	15
47	21,359	34,421	0,023	0,909	6,546	7,131	0,045	0,014	7,691	14,238	1,66	94,037	15
48	21,616	36,753	0	0,378	6,559	7,075	0	0,002	7,803	14,448	1,528	96,162	15
49	0,786	6,924	0,018	17,214	0,772	0,194	0,003	0	0,308	0,824	74,411	101,454	15
50	3,52	10,222	0	16,501	2,331	0,431	0,011	0,034	0,715	1,626	69,229	104,62	15
51	0,431	6,352	0	17,333	0,878	0,097	0,003	0,025	0,169	0,54	75,655	101,483	15
52	9,874	0,411	0	0,553	78,763	0	0,005	11,971	0	0,007	0,055	101,639	15
53	15,854	0,172	0,277	0,393	69,95	0,01	0,029	17,478	0,015	0	0,022	104,2	15
54	16,068	0,103	0,235	0,294	69,935	0,005	0,012	17,803	0	0,014	0	104,469	15
55	23,185	0,068	0	0,354	67,831	0	0,023	13,044	0	0,008	0,2	104,713	15
56	23,057	0,059	0	0,362	67,366	0	0,008	13,183	0,011	0	0,186	104,232	15
57	23,074	0,112	0	0,366	67,809	0	0,008	13,283	0,001	0,015	0,083	104,751	15
Minimum	0,136	0,017	0	0,294	0,425	0	0	0	0	0	0	94,037	
Maximum	32,933	39,067	0,277	19,959	78,763	7,131	0,045	17,803	8,67	15,262	77,407	104,751	
Average	16,251	14,846	0,013	4,13	32,272	1,782	0,009	5,258	2,931	5,372	16,889	99,753	
Sigma	9,595	17,342	0,048	7,307	32,272	2,639	0,01	6,309	3,816	6,911	30,546	3,047	

B.5 Samples 16-19

Mass percen Group : Si Sample : 24I Page 1

No.	Si	O	P	C	Mn	Mg	S	Fe	Al	Ca	Ti	Total	Comment
58	21,013	35,447	0	0,517	11,334	3,78	0,004	0,022	7,556	13,859	1,89	95,422	16
59	20,862	35,275	0	0,508	12,849	3,1	0,011	0,023	7,513	13,617	1,827	95,585	16
60	20,889	35,62	0,014	0,522	12,168	3,365	0	0,032	7,485	13,708	1,895	95,698	16
61	21,126	36,333	0	0,506	5,961	6,855	0	0,016	7,637	14,785	3,1	96,319	16
62	21,165	35,926	0,008	0,513	6,07	6,869	0,013	0,035	7,7	14,678	2,808	95,785	16
63	20,997	36,267	0	0,511	5,917	6,876	0	0,032	7,487	14,565	3,35	96,002	16
64	0,27	6,349	0,004	16,949	0,733	0,059	0	0,076	0,093	0,642	76,277	101,452	16
65	0,198	6,294	0,017	16,449	0,889	0,079	0	0,123	0,085	0,356	76,193	100,683	16
66	0,76	6,835	0,004	16,896	0,762	0,288	0	0,072	0,435	1,384	72,138	99,574	16
67	15,981	0,18	0,282	0,423	68,299	0	0	18,333	0	0,009	0,056	103,563	16
68	9,737	0,398	0	0,658	77,187	0	0	12,536	0	0,014	0,07	100,6	16
69	15,896	0,146	0,272	0,41	68,523	0	0,027	18,29	0,017	0,012	0,036	103,629	16
70	22,898	0,162	0	0,493	65,992	0	0	13,35	0	0,006	0,214	103,115	16
71	22,447	0,137	0	0,477	66,364	0	0	13,386	0,025	0	0,19	103,026	16
72	22,245	0,137	0	0,469	66,642	0	0,012	13,493	0,021	0,001	0,221	103,241	16
73	20,808	36,051	0	0,448	12,417	1,694	0,028	0,043	8,222	12,388	2,987	95,086	17
74	20,761	36,435	0	0,459	12,392	1,774	0	0,044	8,312	12,492	3,19	95,859	17
75	20,718	36,185	0,004	0,446	13,181	1,666	0,012	0,031	8,263	12,243	2,802	95,551	17
76	19,685	36,354	0	0,459	4,32	6,068	0,026	0	7,439	15,118	6,276	95,745	17
77	19,68	36,21	0	0,46	3,925	6,056	0	0,009	7,563	15,147	6,265	95,315	17
78	19,901	36,804	0,007	0,452	5,196	5,867	0,004	0,044	7,31	15,033	6,171	96,789	17
79	0,287	6,67	0,002	16,982	0,506	0,033	0	0,011	0,108	0,452	76,802	101,853	17
80	0,292	6,23	0	17,016	0,435	0,064	0	0,011	0,086	0,343	77,109	101,586	17
81	0,316	6,839	0,007	17	0,319	0,066	0	0,094	0,111	0,452	77,07	102,274	17
82	65,226	0,834	0	29,623	0,315	0,017	0	0,048	0,024	0,116	0,102	96,305	17
83	65,18	0,755	0,002	29,672	0,368	0,015	0	0,071	0,027	0,059	0,052	96,201	17
84	65,232	0,834	0,03	29,318	0,555	0,025	0,029	0,112	0,031	0,083	0,052	96,301	17
85	23,163	0,154	0	0,483	67,067	0	0,021	9,907	0,015	0,01	1,778	102,598	17
86	23,42	0,237	0	0,465	67,671	0,014	0,003	11,753	0	0	0,41	103,973	17
87	23,323	0,182	0	0,487	67,146	0	0	9,928	0,02	0	1,7	102,786	17
88	33,861	0,186	0,01	0,517	54,188	0,003	0,015	15,666	0	0	0,018	104,464	17
89	33,88	0,18	0,014	0,521	53,893	0	0	15,718	0	0	0,041	104,247	17
90	33,985	0,174	0	0,529	53,74	0	0	15,946	0	0	0,003	104,377	17
91	22,562	38,443	0	0,496	4,781	5,27	0,024	0,044	8,854	16,073	0,395	96,942	18
92	22,575	37,629	0,003	0,485	4,833	5,372	0,01	0,013	8,811	15,882	0,399	96,012	18
93	22,65	37,557	0	0,457	4,842	5,263	0	0,026	8,749	15,39	0,397	95,331	18
94	0,178	2,206	0,009	19,195	1,527	0,008	0	0,147	0,028	0,076	75,962	99,336	18
95	0,194	1,537	0	20,059	2,568	0,003	0,016	0,191	0,028	0,111	75,186	99,893	18
96	0,156	1,332	0	19,665	2,316	0	0	0,232	0	0	74,754	98,455	18
97	66,505	0,332	0	29,269	0,597	0	0	0,135	0	0,015	0,118	96,971	18
98	66,47	0,385	0,012	29,295	0,543	0	0	0,08	0,014	0	0,193	96,992	18
99	66,333	0,409	0	29,352	0,473	0	0,003	0,101	0	0,007	0,053	96,731	18
100	22,948	0,173	0	0,461	69,136	0	0	9,644	0,019	0,02	0,474	102,875	18
101	22,863	0,149	0	0,465	69,155	0,007	0,016	9,644	0	0	0,392	102,691	18
102	22,526	0,098	0,018	0,458	69,154	0	0	9,644	0	0,009	0,302	102,209	18
103	20,711	35,821	0,031	0,393	11,271	1,4	0	0,025	8,149	11,934	4,046	93,781	19
104	20,821	35,893	0	0,367	11,477	1,356	0,011	0,031	8,244	11,778	4,183	94,161	19
105	20,454	36,024	0,058	0,419	11,17	2,097	0,001	0,061	7,829	11,983	4,233	94,329	19
106	19,569	36,49	0	0,458	4,345	6,197	0,017	0,022	7,542	15,114	6,128	95,882	19
107	19,623	37,309	0	0,466	4,29	6,433	0,001	0,02	7,607	15,282	5,83	96,861	19
108	19,971	37,147	0,02	0,478	4,635	6,241	0,004	0	7,4	15,014	5,543	96,453	19
109	0,329	5,325	0	17,55	1,037	0,015	0,011	0,214	0,034	0,159	76,066	100,74	19
110	0,327	5,759	0	17,602	0,708	0	0	0,106	0,06	0,311	75,868	100,741	19
111	0,223	2,068	0	20,053	1,388	0	0,024	0,252	0,004	0,012	76,342	100,366	19
112	66,681	0,426	0	30,784	0,59	0,002	0,008	0,138	0,004	0,008	0,023	98,664	19
113	66,469	0,443	0,023	30,502	0,617	0	0,002	0,145	0	0,011	0,036	98,248	19
114	66,425	0,346	0,029	29,831	0,748	0	0	0,191	0	0	0,017	97,587	19
115	23,042	0,205	0	0,52	66,33	0,004	0	10,367	0,007	0	1,405	101,88	19
116	23,213	0,173	0	0,514	66,377	0,014	0,007	10,682	0,018	0,005	1,292	102,295	19
117	23,026	0,229	0	0,522	66,394	0	0	10,235	0,01	0,008	1,454	101,878	19
118	33,746	0,178	0	0,556	54,474	0	0,007	14,869	0,002	0,02	0	103,852	19
119	33,041	0,15	0	0,535	53,864	0,009	0,011	15,262	0,004	0,006	0,003	102,885	19
120	33,856	0,364	0	0,45	54,397	0,055	0,007	14,896	0,008	0	0	104,033	19

Minimum	0.156	0.098	0.000	0.367	0.315	0.000	0.000	0.000	0.000	0.000	0.000	93.781
Maximum	66.681	38.443	0.282	30.784	77.187	6.876	0.029	18.333	8.854	16.073	77.109	104.464
Average	24.662	13.197	0.014	7.989	24.307	1.498	0.006	4.392	2.651	4.775	15.781	99.271
Sigma	19.589	16.685	0.049	11.244	28.855	2.421	0.009	6.370	3.745	6.698	29.417	3.336

C Mass Balance Calculations

C.1 Slag calculation using Ca

		IN		OUT			
Experiment	Slag type	Slag [g]	Ca [%] (slag)	Ca [%] (slag)	Slag [g]	Slag diff (out-in) [g]	Slag increase [%]
2	1	47,35	16,91	16,51	48,50	1,15	2,42
4	1	45,89	16,91	16,51	47,00	1,11	2,42
5	1	37,84	16,91	16,77	38,16	0,32	0,83
6	2	35,45	16,06	16,55	34,40	-1,05	-2,96
7	2	37,41	16,06	16,72	35,93	-1,48	-3,95
9	2	34,92	16,06	17,36	32,31	-2,61	-7,49
10	2	34,58	16,06	16,92	32,82	-1,76	-5,08
12	3	35,5	17,9	14	45,39	9,89	27,86
13	3	34,72	17,9	13,75	45,20	10,48	30,18
14	3	34,78	17,9	14,89	41,81	7,03	20,21
15	3	34,41	17,9	14,7	41,90	7,49	21,77
16	3	35,21	17,9	14,2	44,38	9,17	26,06
17	3	34,92	17,9	13,75	45,46	10,54	30,18
18	2	20,62	19,73	15,8	25,75	5,13	24,87
19	3	36,19	17,9	13,5	47,99	11,80	32,59

C.2 Slag calculation using Al

		IN		OUT			
Experiment	Slag type	Slag [g]	Al [%] (slag)	Al [%] (slag)	Slag [g]	Slag diff (out-in) [g]	Slag increase [%]
2	1	47,35	9,37	8,8	50,42	3,07	6,48
4	1	45,89	9,37	8,91	48,26	2,37	5,16
5	1	37,84	9,37	8,99	39,44	1,60	4,23
6	2	35,45	9,53	8,81	38,35	2,90	8,17
7	2	37,41	9,53	8,75	40,74	3,33	8,91
9	2	34,92	9,53	8,99	37,02	2,10	6,01
10	2	34,58	9,53	8,96	36,78	2,20	6,36
12	3	35,5	8,5	7,88	38,29	2,79	7,87
13	3	34,72	8,5	7,9	37,36	2,64	7,59
14	3	34,78	8,5	8,33	35,49	0,71	2,04
15	3	34,41	8,5	7,95	36,79	2,38	6,92
16	3	35,21	8,5	7,8	38,37	3,16	8,97
17	3	34,92	8,5	7,85	37,81	2,89	8,28
18	2	20,62	9,53	8,8	22,33	1,71	8,30
19	3	36,19	8,5	7,8	39,44	3,25	8,97

C.3 Slag calculation using Mg

		IN		OUT			
Experiment	Slag type	Slag [g]	Mg [%] (slag)	Mg [%] (slag)	Slag [g]	Slag diff (out-in) [g]	Slag increase [%]
2	1	47,35	4,13	6,4	30,56	-16,79	-35,47
4	1	45,89	4,13	6,35	29,85	-16,04	-34,96
5	1	37,84	4,13	6,44	24,27	-13,57	-35,87
6	2	35,45	4,26	6,18	24,44	-11,01	-31,07
7	2	37,41	4,26	6,15	25,91	-11,50	-30,73
9	2	34,92	4,26	6,28	23,69	-11,23	-32,17
10	2	34,58	4,26	6,24	23,61	-10,97	-31,73
12	3	35,5	3,72	3,1	42,60	7,10	20,00
13	3	34,72	3,72	3,64	35,48	0,76	2,20
14	3	34,78	3,72	5,08	25,47	-9,31	-26,77
15	3	34,41	3,72	5,52	23,19	-11,22	-32,61
16	3	35,21	3,72	5,15	25,43	-9,78	-27,77
17	3	34,92	3,72	3,85	33,74	-1,18	-3,38
18	2	20,62	4,26	5,3	16,57	-4,05	-19,62
19	3	36,19	3,72	3,95	34,08	-2,11	-5,82

C.4 Comparison of slag calculations

	Ca		Al		Mg	
Experiment	Slag diff (out-in) [g]	Slag increase [%]	Slag diff (out-in) [g]	Slag increase [%]	Slag diff (out-in) [g]	Slag increase [%]
2	1,1	2,4	3,1	6,5	-16,8	-35,5
4	1,1	2,4	2,4	5,2	-16,0	-35,0
5	0,3	0,8	1,6	4,2	-13,6	-35,9
6	-1,0	-3,0	2,9	8,2	-11,0	-31,1
7	-1,5	-3,9	3,3	8,9	-11,5	-30,7
9	-2,6	-7,5	2,1	6,0	-11,2	-32,2
10	-1,8	-5,1	2,2	6,4	-11,0	-31,7
12	9,9	27,9	2,8	7,9	7,1	20,0
13	10,5	30,2	2,6	7,6	0,8	2,2
14	7,0	20,2	0,7	2,0	-9,3	-26,8
15	7,5	21,8	2,4	6,9	-11,2	-32,6
16	9,2	26,1	3,2	9,0	-9,8	-27,8
17	10,5	30,2	2,9	8,3	-1,2	-3,4
18	5,1	24,9	1,7	8,3	-4,0	-19,6
19	11,8	32,6	3,2	9,0	-2,1	-5,8

C.5 Metal calculation using Mn

	In						
Experiment	Slag amount [g]	%Mn in slag	Mn from slag [g]	Alloy amount [g]	%Mn in alloy	Mn from alloy [g]	Total Mn in [g]
2	47,35	7,33	3,47	10,33	65,37	6,75	10,22
4	45,89	7,33	3,36	10,43	65,37	6,82	10,18
5	37,84	7,33	2,77	7,7	58,74	4,52	7,30
6	35,45	7,24	2,57	7,89	65,37	5,16	7,72
7	37,41	7,24	2,71	7,51	58,74	4,41	7,12
9	34,92	7,24	2,53	10,16	65,37	6,64	9,17
10	34,58	7,24	2,50	9,75	58,74	5,73	8,23
12	35,5	6,6	2,34	7,75	65,37	5,07	7,41
13	34,72	6,6	2,29	7,75	58,74	4,55	6,84
14	34,78	6,6	2,30	7,75	58,74	4,55	6,85
15	34,41	6,6	2,27	7,8	65,37	5,10	7,37
16	35,21	6,6	2,32	7,85	65,37	5,13	7,46
17	34,92	6,6	2,30	7,72	58,74	4,53	6,84
18	20,62	7,24	1,49	4,46	58,74	2,62	4,11
19	36,19	6,60	2,39	7,63	58,74	4,48	6,87

			Out					
Slag amount [g]	%Mn in slag	Mn in slag [g]	Alloy amount [g]	%Mn in alloy	Mn in alloy [g]	Total Mn out [g]	Alloy diff (out-in) [g]	Alloy increase [%]
50,42	6,07	3,06	9,99	71,7	7,16	10,22	-0,34	-3,25
48,26	6,16	2,97	10,24	70,4	7,21	10,18	-0,19	-1,79
39,44	4,83	1,90	7,93	68,0	5,39	7,30	0,23	2,99
38,35	5,98	2,29	7,63	71,1	5,43	7,72	-0,26	-3,24
40,74	5,5	2,24	7,39	66,1	4,88	7,12	-0,12	-1,64
37,02	4,85	1,80	10,51	70,2	7,37	9,17	0,35	3,41
36,78	3,96	1,46	10,16	66,7	6,77	8,23	0,41	4,22
38,29	11,58	4,43	4,28	69,5	2,97	7,41	-3,47	-44,79
37,36	7,96	2,97	6,06	63,9	3,87	6,84	-1,69	-21,86
35,49	4,76	1,69	7,23	71,4	5,16	6,85	-0,52	-6,76
36,79	8,31	3,06	6,19	69,7	4,31	7,37	-1,61	-20,68
38,37	9,1	3,49	5,77	68,7	3,96	7,46	-2,08	-26,48
37,81	8,6	3,25	5,43	66,1	3,59	6,84	-2,29	-29,69
22,33	4,8	1,07	4,40	69,10	3,04	4,11	-0,06	-1,33
39,44	8,35	3,29	5,69	62,9	3,58	6,87	-1,94	-25,40
Based on slag calculation using Al								

C.6 Metal calculation using Fe

	In						
Experiment	Slag amount [g]	%Fe in slag	Fe from slag [g]	Alloy amount [g]	%Fe in alloy	Fe from alloy [g]	Total Fe in [g]
2	47,35	0,00	0,00	10,33	11,92	1,23	1,23
4	45,89	0,00	0,00	10,43	11,92	1,24	1,24
5	37,84	0,00	0,00	7,7	10,33	0,80	0,80
6	35,45	0	0,00	7,89	11,92	0,94	0,94
7	37,41	0	0,00	7,51	10,33	0,78	0,78
9	34,92	0	0,00	10,16	11,92	1,21	1,21
10	34,58	0	0,00	9,75	10,33	1,01	1,01
12	35,5	0	0,00	7,75	11,92	0,92	0,92
13	34,72	0	0,00	7,75	10,33	0,80	0,80
14	34,78	0	0,00	7,75	10,33	0,80	0,80
15	34,41	0	0,00	7,8	11,92	0,93	0,93
16	35,21	0	0,00	7,85	11,92	0,94	0,94
17	34,92	0	0,00	7,72	10,33	0,80	0,80
18	20,62	0	0	4,46	10,33	0,46	0,46
19	36,19	0	0	7,63	10,33	0,79	0,79

			Out				Difference	
Slag amount [g]	%Fe in slag	Fe in slag [g]	Alloy amount [g]	%Fe in alloy	Fe in alloy [g]	Total Fe out [g]	Alloy diff (out-in) [g]	Alloy increase [%]
50,42	0,02	0,00	10,81	11,4	1,23	1,23	0,48	4,62
48,26	0,01	0,00	11,10	11,2	1,24	1,24	0,67	6,40
39,44	0,01	0,00	8,00	9,9	0,79	0,80	0,30	3,86
38,35	0,02	0,00	8,75	10,7	0,94	0,94	0,86	10,90
40,74	0,01	0,00	7,99	9,7	0,77	0,78	0,48	6,41
37,02	0,01	0,00	10,81	11,2	1,21	1,21	0,65	6,43
36,78	0	0,00	10,44	9,7	1,01	1,01	0,69	7,05
38,29	0,03	0,00	7,48	12,3	0,92	0,92	-0,27	-3,47
37,36	0,01	0,00	7,04	11,3	0,80	0,80	-0,71	-9,15
35,49	0,01	0,00	7,49	10,6	0,80	0,80	-0,26	-3,31
36,79	0,02	0,00	6,56	14,2	0,93	0,93	-1,24	-15,92
38,37	0	0,00	6,32	14,8	0,94	0,94	-1,53	-19,51
37,81	0	0,00	7,25	11,0	0,80	0,80	-0,47	-6,10
22,33	0	0,00	4,80	9,6	0,46	0,46	0,34	7,60
39,44	0	0,00	6,70	11,8	0,79	0,79	-0,93	-12,13
Based on slag calculation using Al								

C.7 Comparison of metal calculations

	Mn		Fe	
Experiment	Alloy diff (out-in) [g]	Alloy increase [%]	Alloy diff (out-in) [g]	Alloy increase [%]
2	-0,3	-3,2	0,5	4,6
4	-0,2	-1,8	0,7	6,4
5	0,2	3,0	0,3	3,9
6	-0,3	-3,2	0,9	10,9
7	-0,1	-1,6	0,5	6,4
9	0,3	3,4	0,7	6,4
10	0,4	4,2	0,7	7,0
12	-3,5	-44,8	-0,3	-3,5
13	-1,7	-21,9	-0,7	-9,2
14	-0,5	-6,8	-0,3	-3,3
15	-1,6	-20,7	-1,2	-15,9
16	-2,1	-26,5	-1,5	-19,5
17	-2,3	-29,7	-0,5	-6,1
18	-0,1	-1,3	0,3	7,6
19	-1,9	-25,4	-0,9	-12,1

C.8 Mass balance, Ti

	IN						
Experiment	**Ti in slag [%]**	**Slag [g]**	**Ti in slag [g]**	**Ti in alloy [%]**	**Alloy [g]**	**Ti in alloy [g]**	**Total Ti [g]**
6	0,55	35,45	0,19	0,25	7,89	0,02	0,21
7	0,55	37,41	0,21	0,26	7,51	0,02	0,23
9	0,55	34,92	0,19	0,25	10,16	0,03	0,22
10	0,55	34,58	0,19	0,26	9,75	0,03	0,22
12	5,77	35,5	2,05	0,25	7,75	0,02	2,07
13	5,77	34,72	2,00	0,26	7,75	0,02	2,02
14	5,77	34,78	2,01	0,26	7,75	0,02	2,03
15	5,77	34,41	1,99	0,25	7,8	0,02	2,00
16	5,77	35,21	2,03	0,25	7,85	0,02	2,05
17	5,77	34,92	2,01	0,26	7,72	0,02	2,03
18	0,55	20,62	0,11	0,26	4,46	0,01	0,13
19	5,77	36,19	2,09	0,26	7,63	0,02	2,11

				OUT					
Ti in slag [%]	**Slag [g]**	**Ti in slag [g]**	**% of total Ti to slag**	**Ti in alloy [%]**	**Alloy [g]**	**Ti in alloy [g]**	**% of total Ti to alloy**	**Total Ti [g]**	**Ti in alloy+slag [g]**
0,34	38,35	0,13	60,73	0,4	8,75	0,03	16,13	0,21	0,17
0,47	40,74	0,19	85,01	0,7	7,99	0,05	23,34	0,23	0,24
0,3	37,02	0,11	51,07	0,2	10,81	0,02	10,46	0,22	0,13
0,31	36,78	0,11	52,90	0,6	10,44	0,06	27,04	0,22	0,17
2,39	38,29	0,92	44,26	0,2	7,48	0,02	0,78	2,07	0,93
4,02	37,36	1,50	74,22	1,2	7,04	0,08	4,03	2,02	1,58
0,32	35,49	0,11	5,60	0,2	7,49	0,01	0,65	2,03	0,13
1,15	36,79	0,42	21,10	0,1	6,56	0,01	0,34	2,00	0,43
2,5	38,37	0,96	46,76	0,1	6,32	0,01	0,42	2,05	0,97
4,6	37,81	1,74	85,47	1,2	7,25	0,09	4,21	2,03	1,82
0,4	22,33	0,09	71,45	0,4	4,80	0,02	15,36	0,13	0,11
5	39,44	1,97	93,54	1,0	6,70	0,07	3,13	2,11	2,04

(From alloy calculation using Fe)

Ti for carbide/oxide [g]	**% of total Ti for TiC**	**Ti in carbide [%]**	**Ti-C [g]**
0,06	25,83	76,64	0,07
-0,01	-6,62	76,89	-0,02
0,09	39,95	70,28	0,12
0,07	34,74	78,65	0,10
1,14	55,16	75,61	1,51
0,47	23,11	77,06	0,61
1,90	93,88	75,94	2,51
1,58	78,58	73,1	2,16
1,08	52,78	74,9	1,45
0,26	12,59	77	0,33
0,02	17,18	75,3	0,03
0,09	4,49	76,1	0,12

C.9 Mass balance, Si

	IN						
Experiment	Si in slag [%]	Slag [g]	Si in slag [g]	Si in alloy [%]	Alloy [g]	Si in alloy [g]	Total Si [g]
2	19,8	47,4	9,4	19,7	10,3	2,0	11,4
4	19,8	45,9	9,1	19,7	10,4	2,1	11,1
5	19,8	37,8	7,5	29,4	7,7	2,3	9,8
6	19,7	35,5	7,0	19,7	7,9	1,6	8,5
7	19,7	37,4	7,4	29,4	7,5	2,2	9,6
9	19,7	34,9	6,9	19,7	10,2	2,0	8,9
10	19,7	34,6	6,8	29,4	9,8	2,9	9,7
12	17,9	35,5	6,4	19,7	7,8	1,5	7,9
13	17,9	34,7	6,2	29,4	7,8	2,3	8,5
14	17,9	34,8	6,2	29,4	7,8	2,3	8,5
15	17,9	34,4	6,2	19,7	7,8	1,5	7,7
16	17,9	35,2	6,3	19,7	7,9	1,5	7,8
17	17,9	34,9	6,3	29,4	7,7	2,3	8,5
18	19,7	20,6	4,1	29,4	4,5	1,3	5,4
19	17,9	36,2	6,5	29,4	7,6	2,2	8,7

				OUT					
Si in slag [%]	Slag [g]	Si in slag [g]	of total Si to sl	Si in alloy [%]	Alloy [g]	Si in alloy [g]	f total Si to al	Total Si [g]	in alloy+slag
20,8	50,4	10,5	92,0	16,0	10,81	1,7	15,2	11,4	12,2
20,8	48,3	10,0	90,2	17,7	11,10	2,0	17,6	11,1	12,0
21,3	39,4	8,4	86,1	23,1	8,00	1,8	18,9	9,8	10,2
21,8	38,3	8,4	97,8	17,4	8,75	1,5	17,8	8,5	9,9
21,1	40,7	8,6	89,6	25,2	7,99	2,0	21,0	9,6	10,6
21,9	37,0	8,1	91,2	18,5	10,81	2,0	22,5	8,9	10,1
22,7	36,8	8,3	86,1	24,2	10,44	2,5	26,1	9,7	10,9
20,7	38,3	7,9	100,6	19,1	7,48	1,4	18,1	7,9	9,4
20,3	37,4	7,6	89,3	25,8	7,04	1,8	21,4	8,5	9,4
23,8	35,5	8,4	99,3	18,2	7,49	1,4	16,0	8,5	9,8
21,5	36,8	7,9	102,8	19,5	6,56	1,3	16,6	7,7	9,2
21,0	38,4	8,1	102,7	18,5	6,32	1,2	14,9	7,8	9,2
20,0	37,8	7,6	88,7	24,3	7,25	1,8	20,6	8,5	9,3
22,6	22,3	5,0	93,8	22,8	4,80	1,1	20,3	5,4	6,1
19,9	39,4	7,8	90,0	26,1	6,70	1,7	20,1	8,7	9,6

From alloy calc using Fe

Si for carbide [g]	% of total Si	Si in carbide [%]	SiC [g]
-0,8	-7,1		
-0,9	-7,8		
-0,5	-5,0	69,6	-0,71
-1,3	-15,6		
-1,0	-10,6	70,4	-1,45
-1,2	-13,7	70,5	-1,73
-1,2	-12,2	69,5	-1,70
-1,5	-18,8		
-0,9	-10,6		
-1,3	-15,3		
-1,5	-19,5		
-1,4	-17,6		
-0,8	-9,4	65,2	-1,22
-0,8	-14,1	66,4	-1,14
-0,9	-10,0	66,5	-1,31

D Procedure For The Furnaces

D.1 Procedure for the thermogravimetric furnace

Getting started

1. Open the furnace by unscrewing the bolts and using the lever. Mount the graphite crucible on the Mo-wire by using the hook inside the furnace. Check if both thermocouples are in the right position according to experimental parameters and temperature gradient. Close the furnace tightly by using the lever and then fasten the bolts
2. Make sure the bottom out-let gas valve is closed, turn on the pump and open the pump valve to vacuum the furnace. Check the pressure until it is below approximately 4 mbar, then close the pump valve and stop the pump
3. Check the argon gas tank prior to use. Input Ar gas by using the master switch (without flow controller). Check the pressure inside the furnace; when the pressure is approximately 700mbar, close the Ar gas master switch
4. Open pump valve again and vacuum the furnace by turning on the pump. Repeat procedures 3-4 at least 3 times to get rid of any excess air in the furnace

Furnace

5. When the vacuum cleaning is done, fill the furnace with Ar gas until the pressure is approximately 1050 mbar. Check that the ventilation glass tubes contain mineral oil. Close the Ar gas by using the master switch and open the out-let gas valve. Check that the excess Ar gas passes through the ventilation by seeing bubbles in the glass tube. By using the Ar gas controller, set the gas flow to 0.5 l/min and open the black flow switch. Check that the Ar gas controller is showing a steady flow of 0.5 l/min
6. Turn on the cooling water: make sure to turn on switch 1 (water out) and then switch 2 (water in) to avoid overpressure in the cooling system. If the water is working correctly, you can check a green light on the furnace temperature display
7. Turn on the power.
8. Activate the software on the computer associated to the furnace.
9. Check that the thermocouple types are according to the specified experiment procedures (usually, S-type for wall and B-type for crucible)
10. Input temperature profile according to experiment. Note that the “working temperature” and “crucible temperature” have a significant temperature difference, approximately 300°C. Adjust the “working temperature” according to temperature profile. Make sure to input the weight of the sample and reset the scale settings to zero. If everything is set and OK, click “Program run” to start the furnace

D.2 Procedure for the induction furnace

Operating instructions

Blue induction furnace, E-K013

NOTE: The furnace should not be used without proper training.
Furnace parts and modules which are mentioned in these instructions refer to Figure 1.

Before starting: Check that there is a sufficient amount of Argon in the gas bottle. Should be more than 50 bar. Also check that mica sheet and graphite wool are available. Check that the furnace has been cleaned (should be performed by last user of the furnace), and make sure that it is sufficiently cold after the previous run. Turn on "mech pump" to start the vacuum pump; the pump may be switched on during the whole operation run. Start the ventilation by pressing the ON button on ventilation cabinet, next to the exit door.

If necessary, the furnace can be vacuumed several times before the crucible is inserted to ensure extra purity in the furnace atmosphere.

Opening furnace: Be sure that the crucible is cold enough to avoid unwanted oxidation of crucible or other parts. Be careful when reaching inside the furnace or touching the crucible; the crucible stays hot for a long time! Open the four screws which hold the door in. Until there is atmospheric pressure, the door will stay closed. Turn the valve "Valve 1" carefully to let gas in. The more it is opened, the more flow and this may cause dust in the furnace if it has not been well cleaned. When "Pressure gauge 01" has reached zero, the door will open.

Applying vacuum: Check that "Valve 1" is closed, and open the switch "rough valve". The value of "Pressure gauge 01" should now decrease approx. 0.1 bar each 5 seconds; possibly slowing a little towards the end. When "Pressure gauge 01" reads 1 bar, watch "Pressure gauge 02" (Marked TC1) to monitor the pressure. The lowest pressure possible on this furnace is normally $1.3 \cdot 10^{-3}$ mbar. Reaching minimum pressure normally takes more than 20 minutes. When the desired pressure has been reached, close "rough valve".

Inserting Argon gas: Open the outlet from the Argon bottle. Then open the "backfill valve". Turn the manometer on the left hand side several turns to the left, to let argon into the furnace. Watch "Pressure gauge 01" to monitor the flow of gas. Then, close "backfill valve" and turn the manometer to the right. Close the outlet from the Argon bottle.

Preparing and inserting crucible: Check that the circular brick is in place in the lower part of the coil. Arrange a piece of graphite wool which fits the side wall of the crucible. The graphite wool should overlap itself. Note: If the crucible content is to be poured out when molten, it is important that the crucible stays inside the copper coil. To ensure that it is stuck, make a larger overlap of graphite wool (this also depends on the crucible diameter). Cut a circular piece with the same diameter as the crucible. Also cut a piece of mica sheet, sufficient to surround the graphite wool and overlap a little. The mica should be approx. 1 cm higher than the graphite wool for heat protection of the upper part of the coil. Wrap graphite wool and mica sheet tightly around the crucible. Place the circular graphite wool piece under the crucible from beneath. Carefully insert the crucible into the copper coil, making sure that it is gripped tightly enough so that neither the crucible nor the wool moves out of place.

Applying voltage: Be sure that the desired vacuum is reached and that the crucible is properly installed. On the power cabinet, check that the power level switch is at minimum (turned to the left until it stops). Turn on the cooling water on the wall behind the furnace. The lamp "Cooling water low" should then automatically switch off; if not, there is a cooling water failure and the furnace must not be started. Turn the main power switch of the voltage cabinet to ON. Press "ein" on the power cabinet. Turn the power level switch to the right, and watch the kW scale above it to read the power. Depending on the crucible contents, the wear of the crucible, etc., the power can then be increased carefully. Good experience has been made with a starting power level of 2.5 kW. Typical range necessary for achieveing 1600-1700 C is 2.5 - 7 kW, increasing slowest in the beginning.

End procedure: Turn the power level down to minimum. The power may also be turned gradually down if desired. Shut off the power by pressing "aus" on the power cabinet. Then set the main power switch to OFF. After sufficient cooling, follow the procedure above to open the furnace. When the crucible has been removed, close the door and apply vacuum until "Pressure gauge 01" reaches approx. 1.0. Then insert argon until "Pressure gauge 01" reaches approx. 0.4. When 2 hours have passed after the power was shut off, shut off the cooling water. The lamp "Cooling water low" should then automatically switch on. Turn the ventilation to OFF. Close "mech pump".

Figure 67: Operating instructions for the induction furnace [Krystad, 2011]

E JEOL JXA-8500F EPMA product information

JEOL JXA-8500F Electron Probe Micro analyzer (EPMA)

The **JXA-8500F** is a high performance thermal field emission electron probe micro analyzer combining high SEM resolution with high quality X-ray analysis of submicron areas. The JEOL JXA-8500F instrument is equipped with 5 wavelength dispersive X-ray spectrometers (WDS) and an energy dispersive X-ray spectrometer (EDS). This combination can simultaneously analyse 5 elements WDS + 16 elements EDS plus collect image signals from backscatter and secondary electron detectors.

The use of WDS (wavelength dispersive X-ray spectrometer), high probe current and small probe diameter, the **JXA-8500F** is capable of extreme elemental analysis of sub-micron areas:

- High detection sensitivity for trace elements
- High accuracy of quantitative analysis
- High resolving power for adjacent X-ray spectra
- High accuracy of light elements analysis

The system is highly automated and controlled by a powerful SUN workstation system.

JXA-8500F Hyperprobe

JEOL (SKANDINAVISKA) AB
http://www.jeol.se

Specifications:

- Spectrometers: 5 WDS, 1 EDS
- Acc.Voltage: 1 to 30 kV (0.1 kV steps)
- Magnification: 40 to 300.000X
- Stage speed max: 15 mm/s
- Probe current: $1x10^{-11}$ to $5x10^{-7}$ A
- Current stability: ±0.5%/h (FEG)

- **Detectable element range :**
  - 4^{Be} to 92^{U}
- **Detectable wavelength range :**
  - 0.087 to 9.3 nm
- **Secondary electron image resolution (SEI):**
  - 3.0 nm (WD11mm, 30 kV)
- **Backscattered electron image (BEI) :**
  - Topo and composition image
- **Specimen Stage :**
  - High Precision stage (HPSS)
  - X 90 mm
  - Y 90 mm
  - Z 7.5 mm
- **Specimen size :**
  - 100 X 100 X 10 mmH
  - 36 mm dia. X 4 pcs X 20 mmH
  - 25.5 mm dia X 9 pcs X 20 mmH
  - Slide glass spec. holder X 4 pcs

F Risk analysis

Risikovurdering.pdf

Endelig resultat

Hjelp

I tabellen under er hver uønsket hendelse merket med det endelige resultatet av risikovurderingen.

Konsekvensområde	Resultat	Resultat etter tiltak
Farekilde: Blue furnace / E-K013 Berg Building [52722]		
Uønsket hendelse: Argon [63329]		
Helse	Akseptabel risiko	
Uønsket hendelse: Argon [71372]		
Helse	Akseptabel risiko	
Uønsket hendelse: Electrical wires / tubes [63332]		
Helse	Risiko må vurderes	
Uønsket hendelse: Electrical wires / tubes [71375]		
Helse	Risiko må vurderes	
Uønsket hendelse: Ethanol [63330]		
Helse	Akseptabel risiko	
Uønsket hendelse: Ethanol [71373]		
Helse	Akseptabel risiko	
Uønsket hendelse: Harmix 5 (5% Hydrogen, rest Argon) [63331]		
Helse	Akseptabel risiko	
Materielle verdier	Akseptabel risiko	
Uønsket hendelse: Harmix 5 (5% Hydrogen, rest Argon) [71374]		
Helse	Akseptabel risiko	
Materielle verdier	Akseptabel risiko	
Uønsket hendelse: High temperature equipment [63333]		
Helse	Risiko må vurderes	
Uønsket hendelse: High temperature equipment [71376]		

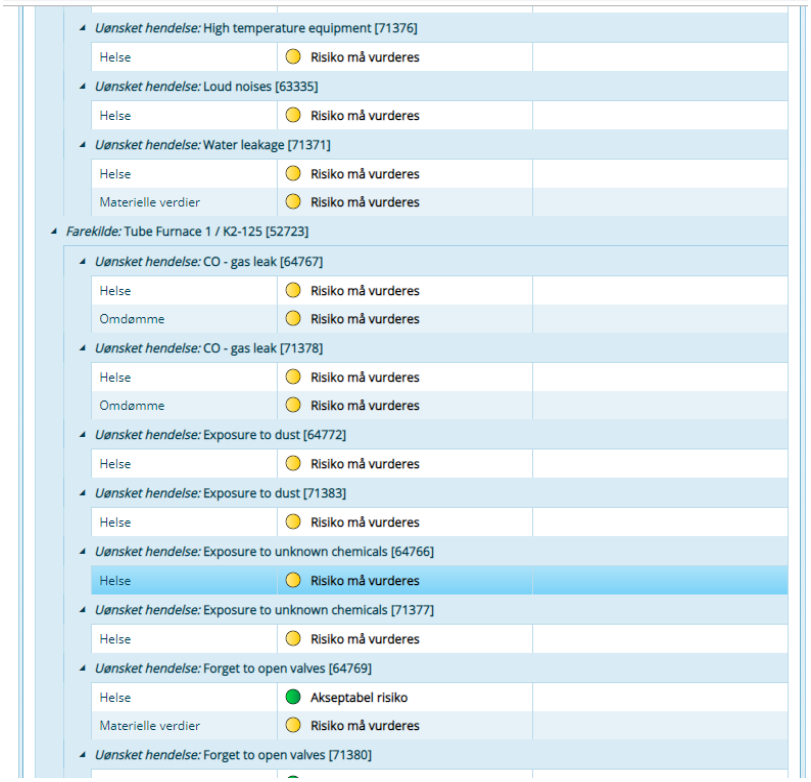
Uønsket hendelse: High temperature equipment [71376]
Helse
Risiko må vurderes
Uønsket hendelse: Loud noises [63335]
Helse
Risiko må vurderes
Uønsket hendelse: Water leakage [71371]
Helse
Risiko må vurderes
Materielle verdier
Risiko må vurderes
Farekilde: Tube Furnace 1 / K2-125 [52723]
Uønsket hendelse: CO - gas leak [64767]
Helse
Risiko må vurderes
Omdømme
Risiko må vurderes
Uønsket hendelse: CO - gas leak [71378]
Helse
Risiko må vurderes
Omdømme
Risiko må vurderes
Uønsket hendelse: Exposure to dust [64772]
Helse
Risiko må vurderes
Uønsket hendelse: Exposure to dust [71383]
Helse
Risiko må vurderes
Uønsket hendelse: Exposure to unknown chemicals [64766]
Helse
Risiko må vurderes
Uønsket hendelse: Exposure to unknown chemicals [71377]
Helse
Risiko må vurderes
Uønsket hendelse: Forget to open valves [64769]
Helse
Akseptabel risiko
Materielle verdier
Risiko må vurderes
Uønsket hendelse: Forget to open valves [71380]


Helse
Risiko må vurderes
Uønsket hendelse: Forget to open valves [64769]
Helse
Akseptabel risiko
Materielle verdier
Risiko må vurderes
Uønsket hendelse: Forget to open valves [71380]
Helse
Akseptabel risiko
Materielle verdier
Risiko må vurderes
Uønsket hendelse: Forget water cooling [64768]
Materielle verdier
Risiko må vurderes
Uønsket hendelse: Forget water cooling [71379]
Materielle verdier
Risiko må vurderes
Uønsket hendelse: Hot crucible / equipment [64770]
Helse
Akseptabel risiko
Materielle verdier
Akseptabel risiko
Uønsket hendelse: Hot crucible / equipment [71381]
Helse
Akseptabel risiko
Materielle verdier
Akseptabel risiko
Uønsket hendelse: Waste handling [64771]
Helse
Akseptabel risiko
Materielle verdier
Akseptabel risiko
Uønsket hendelse: Waste handling [71382]
Helse
Akseptabel risiko
Materielle verdier
Akseptabel risiko

Endelige vurderinger (må fylles ut før lukking) *

Fyll ut begrunnelser og kommentarer til restrisiko, samt om usikkerhet ved vurderingen (f.eks. om den er av generell art, om vurderingen er basert på få personer etc.).

In general, the risks of using the various equipment is well documented, and relevant training has been given. The activities are considered safe, as long as relevant equipment is used, protective gear is worn, and procedures are followed. Extra caution has been given to CO-gas leakage. In the beginning, an experienced engineer assisted in the use of the equipment. An experienced engineer was always nearby or available by phone. The induction furnace should never be left alone. Operating hours were always during the day when people were around.
Approved by Ivar Andre Ødegård.

Sigurd Johannes Slåtsve Øvrelid

Carbides in Manganese Furnaces

NTNU
Kunnskap for en bedre verden